**Title**
Bacterial Interactions with the Ocular Surface



**Author**
Wan, Stephanie Janelle

**Publication Date**
2019

Peer reviewed|Thesis/dissertation

# Bacterial Interactions with the Ocular Surface

by

Stephanie J Wan

A dissertation submitted in partial satisfaction of the

requirements for the degree of

Doctor of Philosophy

in

Vision Science

in the

Graduate Division

of the

University of California, Berkeley

Committee in charge:

Professor Suzanne Fleiszig, Chair
Professor Nancy McNamara
Professor Michi Taga

Spring 2019

Bacterial Interactions with the Ocular Surface

**Abstract**

Bacterial Interactions with the Ocular Surface

by

Stephanie J Wan

Doctor of Philosophy in Vision Science

University of California, Berkeley

Professor Suzanne Fleiszig, Chair

Bacterial keratitis is a devastating, sight-threatening infection of the cornea. However, in order to truly grasp how bacterial keratitis ensues, it is first imperative to understand how the healthy eye is maintained. Only then can we truly decipher the intricacies of how a cornea becomes susceptible to potentially dangerous microorganisms.

Bacteria surround us and inhabit almost every niche in our environment and on our bodies. Thus, the question arose: are bacteria present on the ocular surface, and if so, what role do they play in maintaining health? This is the first question I sought to address in my dissertation. I used bacterial labeling techniques to be able to identify live microbes and gain a spatial understanding of the bacteria on the mouse ocular surface. Interestingly, I found that live bacteria are rarely present on the cornea. This was in stark contrast to the conjunctiva, which does host bacterial inhabitants, including long filamentous bacteria. The cornea's ability to prevent a microbiome is dependent on IL-1R and MyD88 signaling, an important finding to demonstrate the role of this pathway during homeostasis and not just as a response to pathogens.

It is fortunate that the cornea is an expert at preventing bacterial colonization considering that it is constantly exposed to the environment and all of the surrounding microbes. Thus, I wanted to gain a further understanding of how the cornea prevents a microbiome on its surface. Tear fluid has previously been shown to be an important factor towards bacterial defense of the ocular surface. Several constituents that make up basal tears are antimicrobial and impede bacterial virulence. One such component is DMBT1, a glycoprotein that inhibits bacterial twitching. Twitching motility is a surface movement important for epithelial traversal and virulence. How DMBT1 inhibits *Pseudomonas aeruginosa* twitching, a common cause of contact lens related corneal infections, was investigated. It was found that N-glycosylation of DMBT1 contributes to this defense mechanism.

The cornea is the most innervated tissue in the body. Not only are nerves important for sensory transduction, but they also can have immunomodulatory roles. The contributions of sensory nerves in regard to corneal defense has previously not been explored. Thus, I sought to unravel the role of polymodal nociceptors, TRPA1 and TRPV1, in corneal defense against bacteria. I found that these neuronally expressed ion channels contribute to preventing bacterial

colonization on the cornea and communicate with immune cells when the healthy cornea is challenged with *P. aeruginosa*.

After exploring several factors involved in keeping the cornea free of bacteria, I next wanted to gain a better understanding of how common ocular modulations affect its ability to withstand bacteria. First, I explored the impact of dry eye disease, a common debilitating disease with an unknown pathogenesis, on susceptibility to bacterial adhesion. Dry eye disease is associated with a myriad of factors that hinder corneal defense such as altered tear film composition, reduction of antimicrobial peptides, and poor epithelial integrity. I used an experimentally induced mouse model of dry eye disease and determined if environmental bacteria could colonize the corneas. Interestingly, I found that dry eye disease did not increase susceptibility to bacterial colonization on the cornea and no changes occurred on the conjunctiva. Thus, local bacteria on the ocular surface are unlikely to play a role in the pathogenesis of dry eye disease and induction of the disease does not hamper the ability of the cornea to ward off unwanted inhabitants.

Finally, the effects of contact lens wear on the cornea was studied. Progress to decipher how a contact lens alters the corneal environment and any implications this may have, has previously been hindered by limitations of human studies and a lack of animal models. Our lab developed a silicon-hydrogel contact lens to fit on mice that mimics a human lens wearer. We found that a contact lens on a healthy cornea initiates a parainflammatory response observed as an infiltration of dendritic cells at 24 h after lens wear and an influx of neutrophils after 5 days of lens wear. Interestingly, this increase in immune cells in the cornea did not disrupt the macroscopic morphology and the cornea remained clear. Colonization of environmental bacteria on the contact lens was also detected. This understanding of how the lens affects the healthy cornea is imperative to grasp what is being altered that increases susceptibility to bacterial keratitis.

Overall, this dissertation focuses on bacterial interactions with the ocular surface. First, I determined that the cornea does not host a microbiome. Several factors contribute to keeping the cornea free of bacteria including tear fluid, and glycoprotein DMBT1, IL-1R and MyD88 dependent signaling, and polymodal nociceptors. Dry eye disease does not increase the susceptibility to bacterial colonization but contact lens wear is associated with bacterial adhesion. Whether these bacteria on the lens contribute to the infiltration of immune cells observed with lens wear remains to be understood. The results from this dissertation increases our general understanding of how the ocular surface maintains health and prevents bacterial colonization. Studies also give insights into mechanisms impacted by lens wear that may contribute to the increased risk of bacterial keratitis.

To Ben Kirby

This dissertation is dedicated to my soon-to-be husband Ben Kirby. Thank you for always believing in me and providing the unending support to let me pursue my own passions and dreams. I am truly grateful for your constant love and confidence, and for being by my side throughout this process.

# Contents

# List of Figures

# List of Tables

## Acknowledgments

They say it takes a village to raise a child, I would say it also takes a village to complete a PhD. There are numerous people who played a vital role in supporting and helping me complete my graduate studies. I am eternally grateful and thankful to have had a wonderful graduate experience with an amazing support team.

I would first like to thank my mentor, Dr. Suzanne Fleiszig. From the first day I met you, walking into your office thinking of applying to the Infectious Diseases and Immunology program, you have been my number one advocate. I am so grateful to have been convinced to switch my application to the Vision Science program where I was given the opportunity to have a fantastic multidisciplinary education. Thank you for taking me into your lab where I have been able to learn a multitude of technical skills from various fields, learned to develop methods, become a critical thinker, and learned to always remember to look at the big picture. Your ability to appreciate an unexpected (or even unwanted) result and see the positive and exciting side of it is something I will always carry with me and try to emulate. I am thankful that you allowed me to be an independent worker and learn from my colleagues but also always knew you were always available if I ever needed help.

I would also like to thank my co-PI Dr. David Evans. I am still in constant awe of your never-ending span of knowledge. On a technical level I learned a great deal from you about a proper control and the importance of details. I am grateful for your sense of humor and ability to not take things too seriously during stressful moments.

To all of my lab mates throughout the years, I never would have finished if it weren't for my wonderful colleagues who taught me the intricacies of how to be a scientist. Thank you to Matteo, Abby, Aaron, Vince, Jianfang, Melinda and Hart. I learned so many techniques from all of you and your scientific wisdom and advice has been invaluable. Thank you for making the Fleisizg lab a wonderful community and great place to come to work each day. A special thank you to Aaron for first showing me the ropes when I first came to the Fleiszig lab and for being the initial instigator of the ocular microbiome project.

A big thank you to my friend and cohort-mate, Natalie. You have been my constant emotional support throughout the years and one of the biggest reasons why graduate school has been so fun! Thanks for being so organized and always keeping me on track!

I would also like to thank the Vision Science program and administrative staff that help run this program and give graduate students the support and education to be successful. Thank you to my qualifying committee, Dr. Lu Chen, Dr. John Flanagan, Dr. Nancy McNamara, and Dr. John Taylor. Thank you also especially to my thesis committee, Dr. Nancy McNamara and Dr. Michi Taga for taking the time out of your busy schedules to meet with me and give me scientific guidance that made this dissertation possible!

I am incredibly thankful to all of my friends and family. It is with all of your support and love that I am able to be the person I am today. I am especially thankful for my amazing family who always have been my biggest fans. Especially to my parents who instilled a deep sense of curiosity in me and for your endless support. It is with your guidance and encouragement that I was able to develop a love for biology and have the incredible opportunities that ultimately led me to

Berkeley. Thank to my sister Alison! You have been my number one supporter since day 1 and am I so incredibly thankful to have you by my side! Thank you to Javier and my adorable niece Madalyn for letting me take Alison's attention whenever I need it and being the best additions to the family! And a huge shout out to my fiancé Ben. You have been my daily supporter and always believed in me and pushed me to the best I can be. Thank you for always letting me follow my dreams.

# Chapter 1

# Introduction

Microbes are present in every niche and corner of the earth where scientists have looked. The last few decades have brought an immense amount of research demonstrating the importance of the microbial world. Not only are microbial ecosystems essential for global sustainability (i.e. providing nitrogen in soil or the breakdown of pollutants), but it is becoming increasing clear that microbes on and in the human body play a vital role in maintaining health. In 2008, the NIH initiated the Human Microbiome Project (HMP) with the goal of characterizing these microbial communities associated with the human body and to examine their role in health and disease (Turnbaugh et al., 2007). However, whether the ocular surface hosted a microbiome, and the impact on health, was not investigated. Furthermore, several claims kept popping up ensuring that similar to other tissues, the ocular surface also hosted bacteria, yet this was never proven. Given, the ability of the eye to defend against large amounts of pathogenic bacteria, these notions also seemed unlikely. The implications for understanding the interactions of environmental bacteria with the ocular surface are vast. This allows us a greater understanding of how the healthy eye protects itself from insult and whether other bacteria contribute to the normal homeostasis of the ocular surface as in other mucosal tissues. Only then can we truly discover what is going wrong during incidences of disease such as infection, dry eye, or contact lens-related complications.

My dissertation first focuses on determining whether the murine cornea has a bacterial microbiome utilizing imaging techniques in order to visualize bacteria present. I then investigate defenses of the ocular surface to prevent bacterial colonization including MyD88 dependent signaling, DMBT1, a glycoprotein present in tear fluid as well as TRPA1 and TRPV1 ion channels. Finally, I determine how altered states of the ocular surface, including dry eye disease and contact lens wear impacts the ability for environmental bacteria to inhabit the eye.

## 1.1 Anatomy of the Ocular Surface

To investigate whether the ocular surface hosts a live, stable microbiome, it is imperative to first understand the composition of this critical structure. Here, we will divide the ocular surface

into two distinct but neighboring tissues: the cornea and the conjunctiva (Figure 1.1).

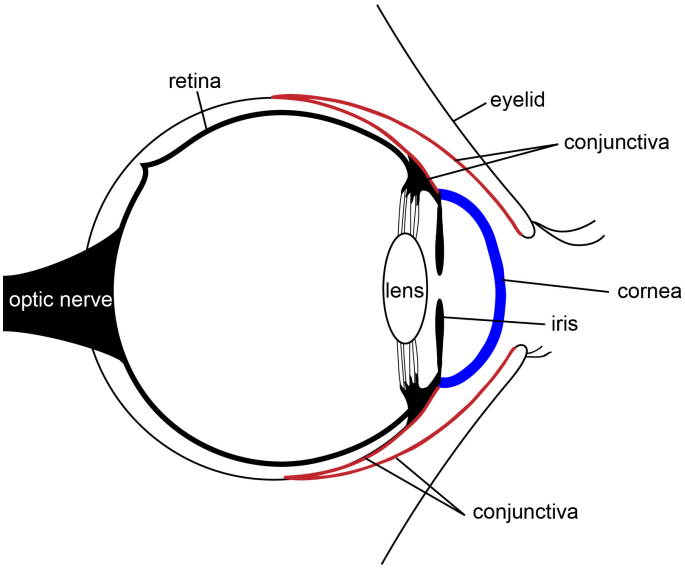


**Figure 1.1:** Cross section of the eye. Cornea is highlighted in blue while conjunctiva is in red.

### 1.1.1 Cornea

The cornea is a transparent avascular connective tissue with two major functions: 1) provide most of the refraction of the eye and 2) be the first barrier to the outside world. In my dissertation, I am interested in the second function of the cornea. However, in order for vision to occur, the cornea must be transparent to allow light to pass through the eye. As a result, there are no blood vessels in the cornea and the aqueous humor and tear film provide nutrients to the cornea (Forrester et al., 2015; MD and MD, 2011). It is also one of the most highly innervated tissues in the body (Belmonte et al., 2017). The cornea is composed of 5 organized layers: epithelium, bowman's layer, stroma, descemet's membrane and endothelium (Figure 1.2).

The epithelium is the outermost layer made up of five to seven cellular layers making it 50-60 $\mu$M thick. The cell layers are made up of stratified, squamous, non-keratinized cells that are held together by tight junctions, desmosomes, and gap junctions (Forrester et al., 2015; Knop and Knop, 2007; MD and MD, 2011). The most superficial layers are flat, polygonal cells with microvilli coved by the glycocalyx. This glycoprotein-polysaccharide layer covers cell membranes and helps with cell-cell recognition, intercellular adhesions, identification of own healthy cells, and stabilization of the precorneal tear film layer (Forrester et al., 2015; Mantelli and Argüeso, 2008; MD and MD, 2011). Beneath the superficial layer are wing cells that are 2-3 cells thick. Next is the basal layer, the deepest layer of the epithelium consisting of a single layer of columnar epithelium cells that are about 20 $\mu$M tall. The basal layer is attached to the basement membrane by hemidesmosomes and helps prevent the epithelium from detaching from the underlying corneal layers. These are the only epithelial cells capable of mitosis and are the source of wing and superficial cells. Epithelium stem cells are located in the limbal basal epithelium. These

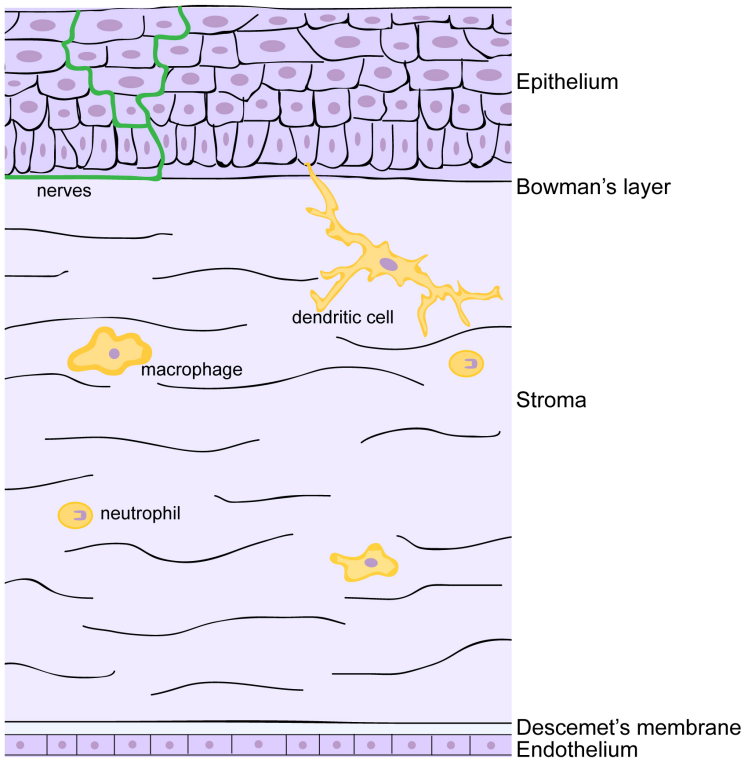


**Figure 1.2:** Schematic of the cornea. The 5 organized corneal layers are demonstrated here as well as the presence of few immune cells and sensory nerves coming up into the epithelium.

new corneal cells migrate to the central cornea and differentiate to transient cells capable of limited cell division. The corneal epithelium continually goes through apoptosis and a complete turnover occurs about every seven days (MD and MD, 2011).

Bowman's layer lies underneath the epithelium but is a not a true membrane. It is made up of randomly arranged collagen that is 8-12 $\mu$M thick. Bowman's layer is actually part of the stroma and helps maintain corneal shape. It does not regenerate, thus if it is disrupted scarring can occur (MD and MD, 2011).

The majority of the cornea is made up of the stroma consisting of 200-250 of 2 $\mu$M layers of collagen lamellae. The stroma helps maintain the transparency of the cornea due to the regular spacing of the collagen fibers, which are surrounded by proteoglycans that help regulate the hydration (Forrester et al., 2015; MD and MD, 2011). Keratocytes are the major cell type of the stroma. They maintain the extracellular matrix by synthesizing collagen, glycosaminogycans (GAGs) and matrix metalloproteinases (MMPs). The transparency of the cornea is highly dependent on the organization and regular spacing of the collagen fibers (Forrester et al., 2015).

Between the endothelium and stroma lies a thick basement membrane (8-10 $\mu$M) known as descemet's membrane. It consists of a posterior layer secreted mainly by endothelial cells and an anterior layer of collagen and proteoglycans (Forrester et al., 2015).

The endothelium is the back layer of the cornea and is a single layer of hexagonal cells, about 4 $\mu$M thick. The adjacent cells share extensive interdigitations, gap junctions, and tight junctions.

The lateral membrane contains several Na+, K+-ATPase pump sites. These pumps, along with carbonic anhydrase are critical ion transport system that produce a net flux of ions from the stroma to the aqueous humor that helps maintain the cornea in a relatively deturgesced state (Forrester et al., 2015; MD and MD, 2011). Endothelial cells have no mitotic activity and so cell density decreases with age. As cells are lost, those remaining fill out but this contributes to a loss of transparency.

### 1.1.2 Conjunctiva

The conjunctiva is a thick transparent mucous membrane consisting of 3 parts. The palpebral conjunctiva lines the inner surface of the eyelids, the forniceal conjunctiva creates a "cul de sac" where it folds up to cover the sclera creating the bulbar conjunctiva that covers the globe of the eye (Forrester et al., 2015). This arrangement allows the eyelids and globe to move independently from each other.

Conjunctival epithelium transitions from keratinized squamous epithelium of the epidermis to nonkeratinised squamous epithelium at the lid margin (Forrester et al., 2015). The conjunctival epithelium varies depending on location. The marginal conjunctiva consists of 5 layers of layered non-keratinised stratified squamous epithelium with the most superficial layer being squamous cells, the middle three layers being polyhedral and the deepest layer cylindrical. The palpebral epithelium consists of 2 layers of stratified cuboidal epithelium and the fornix and bulbar epithelium has 3 layers epithelium. (Forrester et al., 2015; Gillan, 2008). One of the most important features of the conjunctiva are goblet cells. Goblet cells are mucin secreting cells that populate the conjunctival epithelium either singly or in clusters (Gillan, 2008; Mantelli and Argüeso, 2008). The mucin layer is important to maintain ocular surface integrity as it protects the epithelial cells and it interacts with the tear film layer to ensure stability.

The conjunctival epithelium sits on top of a connective tissue layer called the substantia propria (Forrester et al., 2015) (Figure 1.3). This layer consists of a superficial lymphoid layer and a deeper fibrous layer. The lymphoid layer hosts several lymphocytes, primarily T cells and some B cells. Mast cells also populate the lymphoid layer which play a large role in allergic conjunctivitis. The fibrous layer contains the vessels and nerves that innervate the conjunctiva (Forrester et al., 2015). The muscular, medial palpebral and lacrimal branches of the ophthalmic artery supply the conjunctiva. Blood vessels are visible underneath the bulbar conjunctiva as it is an extremely thin tissue. Conjunctival sensory nerves are derived from the ophthalmic branch of the trigeminal nerve.

### 1.1.3 Differences in Mouse Model

The cornea and conjunctiva are very similar in the mouse compared to a human allowing the mouse to be a great model for ocular surface research. The main difference is the obvious size disparity. Additionally, the mouse cornea takes up a larger proportion of the ocular surface and does not have a bowman's layer equivalent. Mice also have a nictitating membrane which is a translucent fold of the conjunctiva that acts like a third eyelid. The plica semilunaris on

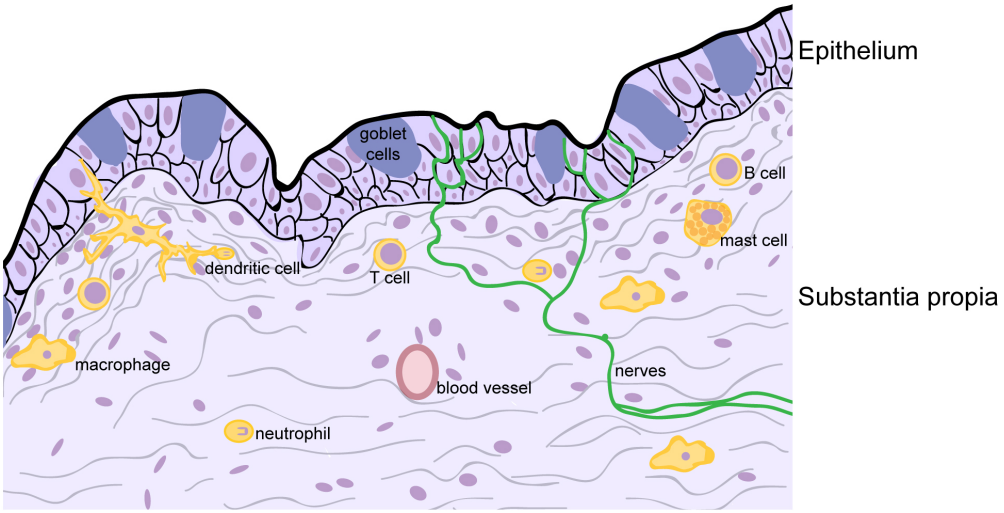


**Figure 1.3:** Schematic of the conjunctiva. The two conjunctival layers, epithelium and substantia propia are shown here. The irregularity and abundance of cells in the conjunctiva vastly differ from the cornea.

the medial side of a human eye is the counterpart to the nictitating membrane (2011). Few proteins also differ among the mouse and human ocular surface. While the human cornea and conjunctiva express both MUC1 and MUC16, the mouse expresses MUC16 only at the conjunctiva (Shirai et al., 2014). The human ocular surface is also known to express Toll-like Receptors (TRL) 1-10 but the mouse lacks TLR10 and also expresses TLRs 11-13 (Kumar and Yu, 2006; Pearlman et al., 2008).

## 1.2 Innate Defenses of the Ocular Surface

The eye is exposed to the outside world and as a result it is constantly barraged with debris, pathogens, and allergens. It has therefore developed a complex system of mechanical, anatomical and immunological defense mechanisms to protect and guard itself against a possibility of losing vision. Here, I will focus on immediate defenses against bacterial colonization and adherence, with an emphasis on the cornea.

### 1.2.1 Eyelids

The eyelids provide a physical barrier to the outside environment. Due to the dense innervation of the cornea, even small specks of dust can cause pain and irritation leading to closing the eyelids and blinking. These actions block out further influx of debris and blinking wipes the ocular surface of any unwanted contaminants. Further, blinking helps to distribute the tear film evenly over the ocular surface which also has a protective role discussed below (Holly, 1973).

### 1.2.2 Tears

The overlying tear fluid plays a major role in protecting the ocular surface epithelium. Tears are involved in the flushing action to remove foreign particles and it also has direct antimicrobial properties (Akpek and Gottsch, 2003; Fleiszig et al., 2003; McClellan, 1997) (Fig 1.4). Some of the major components are listed below:

**Table 1.1:** Major components and antimicrobial activity of tear fluid.

| Protein | Function |
|---|---|
| **Lysozyme** | Makes up 40% of tear proteins, disrupts cell wall of microbes |
| **IgA** | Prevents bacterial attachment |
| **Lactoferrin** | Deprives bacteria of nutritionally essential iron |
| **Betalysin** | Lyses bacterial cell walls |
| **Lipocalin** | Deprives microbes of essential nutrients |
| **Mucin** | Prevents bacterial attachment and traps microbes |
| **Defensins** | Inhibits pathogen growth |
| **SP-D** | Prevents bacterial attachment and promotes clearance |

Human tear fluid has also been shown to inhibit bacterial growth independent of antimicrobial activity. For example, *P. aeruginosa* grown in the presence of cells was significantly hindered when tears were added to the sample compared to growth in MEM (Fleiszig et al., 2003). A follow-up study also demonstrated the protective effects of human tear fluid against bacterial invasion and colonization. Results showed that tear fluid significantly reduced bacterial colonization of the cornea at 1 hour after the mouse cornea was scratched and allowed to heal for 6 hours (Kwong et al., 2007). It has also been established that human tear fluid acts directly on epithelial cells to enhance resistance to bacteria. Pretreatment with tear fluid on human corneal epithelial cells upregulated stress response factors NF- $\kappa$B and AP-1 suggesting that tears prime innate defense pathways (Mun et al., 2011). A recent publication in our lab has also found the DMBT-1, a protein in tear fluid prevents bacteria from twitching, inhibiting its virulence (Li et al., 2017).

### 1.2.3 Epithelium

The epithelium has also been shown to be a formidable barrier to microbes. In fact, in order to reliably induce an infection, researchers have relied on the scratch model prior to inoculation in order to bypass the epithelium entirely. Several factors of the epithelium contribute to its impressive defense system.

#### 1.2.3.1 Mucins

Epithelial mucins are thought to be an important contributor to preventing bacterial adherence (Evans and Fleiszig, 2013; Jolly et al., 2017). Mucins are high molecular weight glycoproteins characterized by extensive O-glycosylation. Both cell surface associated mucins and gel-forming

secreted mucins are expressed at the ocular surface (Mantelli and Argüeso, 2008). Corneal and conjunctival epithelia are known to express three membrane spanning associated mucins: MUC1 and MUC16 are detected on both the cornea and conjunctiva, and MUC4 is expressed only at the conjunctiva. These mucins have been found to be concentrated on the tips of apical cells and form the dense glycocalyx which prevents microbes from gaining access to host membranes (Figure 1.4). Conjunctival goblet cells also produce secretory gel-forming MUC5AC which facilitates in trapping debris and clearance from the ocular surface.

#### 1.2.3.2 Junctional Complexes

In addition to the glycocalyx, additional barrier function is present in the ocular surface epithelium due to intracellular junctions. In general, compared to the cornea, the conjunctiva has poor barrier function (Kinoshita et al., 2001). In the cornea, four different junctional complexes have been identified that occur at different layers within the epithelium (Mantelli and Argüeso, 2008). The most superficial layer contains tight junctions, which provide the greatest resistance to penetration. Tight junctions prevent the diffusion of molecules through the paracellular pathway by sealing the intercellular space through a network of transmembrane proteins that essentially sow adjacent cells together (Figure 1.4). Desmosomes in the wing cell layers, adherens junctions and hemidesmosomes in the basal cells also help provide structural integrity and cell adhesions (Tsubota et al., 2002).

#### 1.2.3.3 Interleukin 1 Receptor (IL-1R) and Toll-like Receptor (TLR) Signaling

The Toll/IL-1 Receptor family are important immune receptors present in the eye that can respond quickly to bacterial challenge (Pearlman et al., 2008; Redfern and McDermott, 2010) (Figure 1.4). Both are transmembrane proteins that share similar structural and functional properties. TLRs recognize conserved microbial components (pathogen-associated molecular patterns, PAMPs). PAMPs make ideal targets because they are produced only by microbes and thus the host cells can distinguish between self and non-self. PAMPs are essential for microbial survival so patterns are not subject to high mutation rates, and they do not have much variability, thus a limited number of PRRs are needed. In total, 13 TLRs have been identified: TLR1-9 are common to both mouse and human, TLR-10 is only found in humans and TLRs11-13 are only found in mice. IL-1Rs respond to pro-inflammatory cytokines produced and released in response to bacterial and viral pathogens. Toll/IL-1 receptors differ in their extracellular domains (TLRs are made up of leucine-rich repeats while IL-1Rs are made up of immunoglobulin-like domains) but share a common cytoplasmic motif, the Toll-IL-1 receptor (TIR) domain which is required for signal transduction (Martin and Wesche, 2002). Myeloid differentiation factor 88 (MyD88) is a common adaptor molecule that is recruited by TIR through a series of signaling events leading to NF-kB or AP-1 translocation to the nuclease and the upregulation of proinflammatory cytokines and chemokines (Kumar and Yu, 2006; Pearlman et al., 2008). MyD88-independent signaling pathways can also occur such as through the MyD88-Like adapter protein (Mal) (Martin and Wesche, 2002).

#### 1.2.3.4 Antimicrobial Peptides (AMPs)

Additionally, the cornea and conjunctiva express antimicrobial peptides, which have broad-spectrum activity against bacteria (McDermott, 2009; McNamara et al., 1999) (Figure 1.4). AMPs are small peptides, less than 50 amino acids, that carry an overall positive charge. AMPs are divided into two major categories: defensins and cathelicidins. Defensins are further divided into alpha, most of which have been found in neutrophils known as human neutrophil peptides (HNP) 1-4, and beta, primarily expressed in epithelial tissues and named human $\beta$-defensin (HMD) 1-4. Humans are known to only express one cathelicidin: LL-37, which was initially isolated from neutrophils but now known to be expressed by other immune cells and epithelia (McDermott, 2009). Because bacteria are negatively charged, the positively charged AMPs can detect these foreign invaders. The initial electrostatic interaction disrupts the microbial cell membrane leading to permeabilization, loss of intracellular components and finally death. There are several models as to how the interaction between AMPs and microbes occur but in general, the AMPs interact with the surface membrane of the bacteria and orient themselves so that the hydrophobic portion is towards the membrane lipids and the hydrophilic region faces the polar heads groups of the phospholipids. At a threshold concentration, the lipid bilayer curvature is disrupted and the membrane is permeated (McDermott, 2009).

Both alpha and beta-defensins have been detected at the ocular surface. The primary source of alpha-defensins are infiltrating neutrophils. They also have been found in normal tear film. HBD-1 is constitutively expressed by both corneal and conjunctival epithelia. HBD-2 on the other hand is variably expressed but is known to be induced by both Gram-negative and Gram-positive bacterial products (McDermott, 2009; McDermott et al., 2003; McNamara et al., 1999). It is mainly mediated by the activation of TLRs. LL-37 is also expressed by both corneal and conjunctival epithelial cells . It is a major component of neutrophil granules and has been shown to increase expression in response to injury and bacterial challenge with *P. aeruginosa* and *S. aureus*. HBD-3 is also known to be expressed at the ocular surface (McDermott, 2009; McDermott et al., 2003). Several animal studies support the role of AMPs including animal gene knock out studies that show delayed bacterial clearance and increased susceptibility to bacterial keratitis (Augustin et al., 2011; Huang et al., 2007; Tam et al., 2012). Pretreatment with TLRs have also been shown to upregulated AMPs leading to a more rapid bacterial clearance (Redfern et al., 2011).

Corneal epithelial cells also express other antimicrobial compounds. Systematic fractionation of human corneal epithelial cells combined with mass spectrometry revealed a series of glycine-rich C-terminal peptides of human cytokeratin 6A (Tam et al., 2012). This keratin-derived antimicrobial peptide (KDAMP) has been shown to have bactericidal activity against *P. aeruginosa*. Additionally, knockdown of its expression in mice resulted in increased *P. aeruginosa* adherence to mice corneas *ex vivo* by 5-fold. It was also shown to be effective against *E. coli, S. aureus,* and *S. epidermidis* and that it's bactericidal activity involves bacterial cell wall disruption.

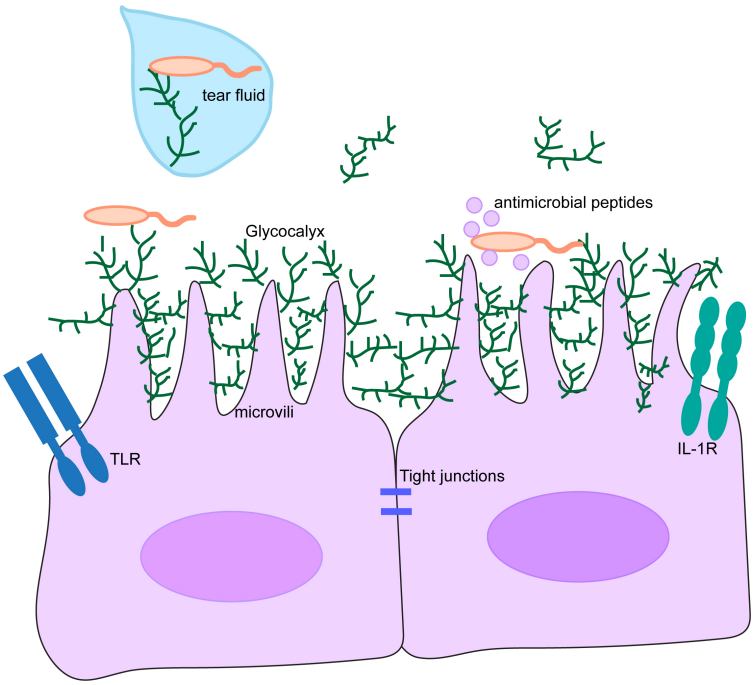


**Figure 1.4:** Epithelial defenses against bacteria. Tear fluid, microvilli, mucins, tight junctions, TLRs/IL-1Rs, and antimicrobial peptides all contribute to keeping bacteria from colonizing and infecting the cornea.

#### 1.2.3.5 Resident Immune Cells

The cornea is considered to be an immune-privileged site meaning that it is tolerant of antigens and does not normally elicit an inflammatory response. This is critical to protect the clarity of the cornea and to ensure that small attacks do not lead to sight-threating reactions. While it was once thought that this was due to the cornea being devoid of immune cells, more and more research is revealing the presence of resident cells present in the corneal epithelium and stroma. For example, the peripheral and even central cornea have been found to host antigen-presenting cells, including dendritic cells, in the epithelium and stroma (Hamrah et al., 2002; Metruccio et al., 2017). Additionally, few macrophages and neutrophils have also been identified to be present in the healthy cornea (Hamrah et al., 2003; Metruccio et al., 2018) and thought to be important for immune surveillance and protection. However, resident corneal immune cells are often described to be immature and present in much less abundance compared to other mucosal tissues. Interestingly, the closed eye (i.e. during sleep) has been linked to an increase in neutrophils and pro-inflammatory factors that help to attack and clear microbes (Knop and Knop, 2007). Overall, these studies suggest that the cornea is capable of antigen presentation and mounting an inflammatory response, but perhaps at a different level than what is normally considered to be inflammatory.

#### 1.2.3.6 Nerves

The cornea is the most innervated tissue in the body. It is supplied by the ophthalmic division of the trigeminal nerve and terminates as free nerve endings in the epithelium (Cruzat et al., 2010; Laura Oliveira-soto, 2001; Shaheen et al., 2014). Nerve bundles enter the peripheral mid-stroma in a radial pattern and branch into smaller divisions, increasing in nerve density while decreasing in nerve diameter as they move anteriorly (Shaheen et al., 2014). The peripheral stromal nerves give rise to the subbasal nerve plexus which provides the nociceptive nerve fibers innervating the corneal epithelium that respond to mechanical, thermal, and chemical stimuli (Shaheen et al., 2014).

Majority of the nerve fibers (70%) in the corneal epithelium are polymodal, meaning they respond to a variety of stimuli (Belmonte et al., 2017; Shaheen et al., 2014). Transient receptor potential (TRP) cation channels, most notably TRPV1 and TRPA1 play important roles for sensory transduction as polymodal nociceptors in the cornea (Belmonte et al., 2017). It is also controversial whether TRPA1 and TRPV1 expression restricted to nerve fibers or if they are also expressed in epithelial and immune cells in the cornea (Belmonte et al., 2017).

Increasing evidence supports the notion that the immune and nervous systems are intimately intertwined and play an important role in ocular surface homeostasis. For example, nociceptors in the cornea releases neuropeptides substance P and CCRP in response to tissue injury which helps initiate and amplify an inflammatory reaction (Belmonte et al., 2017). An increase in number of resident and infiltrating immune cells during microbial infection in the cornea is also correlated with reduced subbasal nerves in the central cornea suggesting a causal relationship (Cruzat et al., 2011). Interestingly, TRP channels have also been found to respond specifically to microbial ligands in tissues (Chiu et al., 2013; Pinho-Ribeiro et al., 2017). Nociceptor's ability to respond within milliseconds, makes them ideally suited to be a first line of defense against pathogens. Additionally, several immune cells, including dendritic cells, neutrophils macrophages and T cells express receptors for neuromodulators allowing them to respond to nociceptor signaling (Pinho-Ribeiro et al., 2018). In my dissertation, I focused on the role of TRPA1 and TRPV1 in corneal defense against bacterial colonization.

## 1.3 Ocular Surface Microbiome

While it was once thought that microbes outnumber human cells by a factor of 10, it has recently been challenged to be closer to a 1:1 ratio (Sender et al., 2016). Exact figures and numbers of individual microbes present may be contested, but it is clear that these microorganisms play a critical role in our everyday lives. Humans (and animals) have a symbiotic relationship with microbes and it is thought that they have been a part of our evolution. Microbes can extract vitamins and nutrients that otherwise would be inaccessible to humans, influence and help keep our immune system in balance, prevent foreign pathogens from colonization, and perhaps even impact human behavior (Turnbaugh et al., 2007). It is important to note that microbiomes

include a collection of all microorganisms (eukaryotes, archaea, bacteria, and viruses) but in my dissertation, I focused on bacteria.

### 1.3.1 Microbiome Methods

Perhaps the most straightforward approach used to investigate microbiomes is to culture microorganisms from a sample of interest. Swabs of various bodily sites or substances (skin, feces, saliva, etc.) can easily be taken and plated on various media containing nutrients to facilitate microbial growth. Oxygen content, nutrients, temperature, and pH can easily be manipulated. However, it is now known that standard laboratory culture techniques do not allow for the growth of all bacteria. In fact, it is thought that over 99% of the bacteria kingdom cannot be culture using these standard methods (Epstein, 2013).

With the advent of molecular technologies, high-throughput culture-independent techniques have been developed to overcome this obstacle. The gold standard for analyzing microbial communities has recently been sequencing the 16S ribosomal (rRNA) gene (Turnbaugh et al., 2007). This gene is highly conserved in the bacteria kingdom. Additionally, the presence of variable regions allows for the identification of specific bacteria present down to the species level. These methods have revealed more diverse microbial communities present than originally thought. However, this method still has several limitations. Contamination is a significant concern, particularly when a sample has a low amount of biomass. Additionally, sequencing errors and difficulties in assessing operational taxonomic units (OTUs) are other challenges. A study performed in 2015 explored the accuracy and reliability of utilizing 16S rRNA gene sequencing. A control sample in which only four known species were present resulted in the identification of 13 species with this method (Poretsky et al., 2014) exposing that 16S rRNA gene sequencing methods can artificially increase the apparent diversity in a community.

Fluorescent in situ hybridization is also a common method used by many researchers to investigate spatial relationships in a microbial community. It is common to use a universal probe against the 16S rRNA bacterial gene in order to identify and visualize bacteria interacting with host tissue. Recently, laboratories are also utilizing probes against specific genus of bacteria (Mark Welch et al., 2016). However, one must know the specific species present in the sample under investigation in order to utilize these probes efficiently.

While 16S rRNA sequencing and FISH labeling have opened our eyes to the diversity and abundance of microbes in a community, both methods detect bacterial nucleic acids. Bacterial DNA is ubiquitous in our environment and is known to have a half-life of over 521 years (Allentoft et al., 2012). Therefore, using these methods, we do not know for certain if the bacterial DNA identified is from a viable organism or rather is the debris from a past bug.

### 1.3.2 Ocular Surface Microbiome

When it comes to the ocular surface, studies have only been done on the conjunctiva, mainly due to the fact that taking a sample from a human conjunctiva is much more amenable than the cornea. Culture results have shown infrequent and variable levels of bacteria (Fleiszig and Efron,

1992; Willcox, 2013). However, when bacteria are cultured they are most commonly identified as *Corynebacterium, Propionibacterium*, and Coagulase Negative *Staphylococci* species. 16S rRNA sequencing studies have shown a much more diverse amount of bacteria present on the human conjunctiva compared to culture studies. The most conservative of estimates predicts 42 different genera (Doan et al., 2016). However, the most commonly identified bacteria are similar to culture results suggesting that inhabitants of these species are likely present on the conjunctiva. Overall, it is generally agreed upon that the conjunctiva has much fewer bacteria present than other bodily sites. One study approximates that there are about 0.06 bacterium per human cell in the conjunctiva compared to 16 bacteria per human cell in the skin (Doan et al., 2016). Not only do these bacteria exist on the conjunctiva but it also been shown that they can have a functional role. One study showed that *Corynebacterium* present on the conjunctiva illicit an inteleukin-17 response through $\gamma\ \delta$ T cells which has a protective effect against corneal infection (St Leger et al., 2017). However, whether any bacteria exist on the cornea, previously was not explored.

On the one hand, we know that microbes colonize nearly every exposed tissue and considering that the eye is constantly in contact with the environment, it is plausible that bacteria also inhabit the cornea. However, we also know that the ocular surface has a complex system of defenses to protect it from the outside world. The first portion of my dissertation set out to answer and clarify whether the ocular surface hosts a microbiome. After I determined that the mouse cornea does not host resident bacteria, I went on to understand how the cornea prevents bacterial adhesion and colonization. I found that this was dependent on IL-1R/MyD88 signaling. I also looked at the role of nerves and nociceptors in bacterial defense against the bacterial colonization as well DMBT1, a glycoprotein in tear fluid. Finally, I sought to determine if altered states such as contact lens wear or dry eye disease impacts the corneal environment to allow colonization of bacteria.

# Chapter 2

# IL-1R and MyD88 contribute to the absence of a bacterial microbiome on the healthy murine cornea

## 2.1 Abstract

This Chapter is a full reprint of Wan et al., *Frontiers in Microbiology* (2018), in which I was a primary author. The work is included with permission from all authors.

**Relevant Publication:**
Wan SJ, Sullivan AB, Shieh P, Metruccio MME, Evans DJ, Bertozzi CR and Fleiszig SMJ (2018) IL-1R and MyD88 Contribute to the Absence of a Bacterial Microbiome on the Healthy Murine Cornea. Front. Microbiol. 9:1117.

Microbial communities are important for the health of mucosal tissues. Traditional culture and gene sequencing have demonstrated bacterial populations on the conjunctiva. However, it remains unclear if the cornea, a transparent tissue critical for vision, also hosts a microbiome. Corneas of wild-type, IL-1R (-/-) and MyD88 (-/-) C57BL/6 mice were imaged after labeling with alkyne-functionalized D-alanine (alkDala), a probe that only incorporates into the peptidoglycan of metabolically active bacteria. Fluorescence in situ hybridization (FISH) was also used to detect viable bacteria. AlkDala labeling was rarely observed on healthy corneas. In contrast, adjacent conjunctivae harbored filamentous alkDala-positive forms, that also labeled with DMN-Tre, a Corynebacterineae-specific probe. FISH confirmed the absence of viable bacteria on healthy corneas, which also cleared deliberately inoculated bacteria within 24 h. Differing from wild-type, both IL-1R (-/-) and MyD88 (-/-) corneas harbored numerous alkDala-labeled bacteria, a result abrogated by topical antibiotics. IL-1R (-/-) corneas were impermeable to fluorescein suggesting that bacterial colonization did not reflect decreased epithelial integrity. Thus, in contrast to the conjunctiva and other mucosal surfaces, healthy murine corneas host very few

viable bacteria, and this constitutive state requires the IL-1R and MyD88. While this study cannot exclude the presence of fungi, viruses, or non-viable or dormant bacteria, the data suggest that healthy murine corneas do not host a resident viable bacterial community, or microbiome, the absence of which could have important implications for understanding the homeostasis of this tissue.

## 2.2 Introduction

Diverse communities of resident microorganisms on host tissues (microbiomes) play important roles in maintaining health and development of a functional immune system (Turnbaugh et al., 2007; Consortium, 2012; Gevers et al., 2012; Thaiss et al., 2016; Blacher et al., 2017). Furthermore, it is becoming increasingly evident that alterations in abundance and diversity of these bacterial constituents are associated with inflammation and disease (Frank et al., 2007; Koeth et al., 2013; Scher et al., 2013; Corrêa et al., 2017; Halfvarson et al., 2017). Much work has been done to decipher the role of microorganisms within the nasal and respiratory tract, oral cavity, urogenital tract, gut and skin (Gillan, 2008; Grice et al., 2009; Ravel et al., 2011; Consortium, 2012; Liu et al., 2015; Mark-Welch et al., 2016). However, the location and role of bacteria that normally colonize the ocular surface, and the implications for ocular health and immunity, is only beginning to be appreciated (Doan et al., 2016; Kugadas et al., 2016). Standard microbiological culture methods and molecular techniques have both been used to demonstrate a conjunctival microbiome. Culture methods revealed small numbers and infrequent growth of bacteria on the human conjunctiva, typically ~100 or less colony-forming units (CFU) per swab (Fleiszig and Efron, 1992; Willcox, 2013). However, 16S rRNA gene sequencing suggested far more bacterial genera were present on the conjunctiva than indicated by culture results (Graham et al., 2007; Dong et al., 2011; Doan et al., 2016; Ozkan et al., 2017). Still, significantly fewer bacteria are thought to inhabit the conjunctiva compared to other mucosal surfaces, e.g., ~0.06 bacteria per cell in the human conjunctiva versus 12 and 16 bacteria per cell in the oral cavity or on the skin, respectively (Doan et al., 2016).

Culture and sequencing methodologies used to demonstrate conjunctival microflora each have limitations. Nucleic acid sequencing does not equate to viable bacteria, and is therefore prone to false-positive results, while culture methods can miss viable microbes, e.g., bacteria with fastidious nutritional requirements or those undergoing stress responses, thereby prone to false-negative results (Oliver, 2005; Epstein, 2013; Kawai et al., 2015). Moreover, the lower biomass at the ocular surface can also lead to false-positive results due to contaminants from the environment or reagents (Schabereiter-Gurtner et al., 2001; Salter et al., 2014). Importantly, neither culture nor sequencing provides spatial information on bacterial location at the ocular surface. To that end, scientific publications often do not appear to distinguish the cornea from conjunctiva in reporting the “ocular surface” microbiome (Dong et al., 2011; Lu and Liu, 2016; Ozkan et al., 2017). Thus, our understanding of the bacterial landscape on the eye remains unresolved.

The cornea of the ocular surface is critical to vision, and unusual among body surfaces in its remarkable resistance to infection. The cornea is protected against colonization by pathogenic bacteria by multiple defenses which were originally thought to be due to blinking, and the antimicrobial and aggregative components of tear fluid (Masinick et al., 1997; Kwong et al., 2007; Evans and Fleiszig, 2013). It is now known that tear fluid plays much more complex roles and that epithelial- expressed mucins, tight junctions and antimicrobial peptides are also involved (McNamara et al., 1999; Yi et al., 2000; Blalock et al., 2007; Kwong et al., 2007; Augustin et al., 2011; Mun et al., 2011; Tam et al., 2012; Evans and Fleiszig, 2013; Li et al., 2017).

Indeed, the opportunistic bacterial pathogen *Pseudomonas aeruginosa* will not colonize the healthy corneal surface. Susceptibility to bacterial adhesion requires the introduction of some form of compromise to the surface epithelium (Alarcon et al., 2011) or to innate defenses such as MyD88-deficiency (Tam et al., 2011). Deliberate inoculation of healthy corneas with *P. aeruginosa* results in rapid clearance of the bacteria without colonization or pathology (Mun et al., 2009; Augustin et al., 2011). Thus, the murine cornea appears inhospitable to *P. aeruginosa*, a bacterium unusual in its capacity to survive in a diverse array of conditions. This could have led to an assumption among some researchers in the field that the cornea is inhospitable to bacteria in general, albeit a notion not actually proven.

The aim of this study was to determine if the healthy mouse cornea hosts a resident bacterial microbiome, and whether it is able to clear other deliberately inoculated bacteria as effectively as *P. aeruginosa*. We utilized a novel approach to overcome obstacles and limitations of traditional culture and sequencing methodologies. An alkDala probe was used to label only viable, metabolically active, bacteria *in situ*. This reagent utilizes the ability of peptidoglycan metabolic enzymes to take up natural and unnatural D-amino acid substrates to insert into the stem peptides of cell wall peptidoglycan if bacteria are metabolically active (Siegrist et al., 2013, 2015; Shieh et al., 2014). Bacteria that have incorporated the probe are then detected using an azide- fluorophore via copper-catalyzed click chemistry, and imaged by fluorescence microscopy (Siegrist et al., 2013). AlkDala labeling has previously only been used to label bacteria *in vitro* (Siegrist et al., 2013, 2015; Shieh et al., 2014). FISH of a universal 16S rRNA gene probe was also used to detect viable bacteria for which peptidoglycan metabolism was absent, inactive, or at a very low level (Vaishnava et al., 2011; Mark-Welch et al., 2016). Results showed that healthy murine corneas are broadly inhospitable to bacteria, a constitutive state requiring the IL-1R and MyD88, and that consequently they lack a resident viable bacterial community, or microbiome.

## 2.3 Experimental Procedures

### 2.3.1 Bacterial Strains

*Pseudomonas aeruginosa* (strain PAO1), *Staphylococcus aureus* (isolated from a human corneal infection), and a Coagulase- negative *Staphylococcus* (CNS) species (sp.) isolated from a mouse eyelid (this laboratory) were used in the clearance experiments. CNS sp. were confirmed using standard biochemical diagnostic tests. *P. aeruginosa* strain PAO1 expressing d-Tomato on

plasmid p67T1 (PAO1-dtom) was used for experiments to validate bacterial labeling methods (Singer et al., 2010). Inocula were prepared from overnight cultures grown on TSA plates at 37°C for ~16 h before to a concentration of ~ $10^{10}$ or ~ $10^{11}$ CFU/mL. PAO1-dtom was grown on TSA supplemented with carbenicillin (400 $\mu$g/mL). Viable counts of bacterial suspensions were performed by serial dilution in PBS as needed (typically from $10^{-6}$ to $10^{-9}$) and plating in triplicate onto TSA plates, followed by incubation for ~18 h at 37°C to determine CFU.

### 2.3.2 Bacterial Isolation and Identification

To culture bacteria from the corneas of wild-type and IL- 1R (-/-) mice, the corneal epithelium was collected using the Algerbrush II, placed in 500 $\mu$L 0.25% Triton + PBS, then vortexed. An aliquot (100 $\mu$L) of lysate was inoculated onto TSA, blood agar, or chocolate agar and incubated at 37°C in aerobic and anaerobic conditions for up to 7 days. Isolated bacterial colonies were identified by direct colony PCR of the 16S ribosomal RNA gene using universal primers P11P (5' -GAGGAAGGTGGGGATGACGT-3') and P13P (5'-AGGCCCGGGAACGTATTCAC-3') (Widjojoatmodjo et al., 1994). Reaction mixes (50 $\mu$L) were set up as follows: 1X Q5 Reaction Buffer (New England BioLabs), 1X Q5 High GC Enhancer, 200 $\mu$M dNTPs, 0.5 $\mu$M Forward Primer, 0.5 $\mu$M Reverse Primer, and 0.02 U/$\mu$L Q5 High-Fidelity DNA Polymerase. A sterile toothpick was used to touch a bacterial colony on an agar plate and inserted directly into the PCR reaction tube. The reaction mixtures were subjected to the following thermal cycling sequence on a Bio-Rad Thermal Cycler: 98°C for 3 min followed by 30 cycles of 98°C for 10 sec, 63°C for 20 sec, 72°C for 45 s, followed by a final extension of 72°C for 2 min. Molecular grade water was included as a negative control, and a known strain of *P. aeruginosa* (PAO1) used as a positive control. Following amplification, samples were examined by electrophoresis in 1% agarose gels in 1× TBE buffer. Amplicons were purified using PureLink™ PCR Purification Kit (Invitrogen) and sequenced at the UC Berkeley DNA Sequencing Facility. Sequences obtained were identified using NIH BLAST Search Tool (https://blast.ncbi.nlm.nih.gov).

### 2.3.3 Mice

All procedures were carried out in accordance with a protocol approved by the Animal Care and Use Committee, University of California, Berkeley. Six to 12 weeks old male and female wild- type C57BL/6 mice (from Charles River or Jackson Laboratory), mT/mG knock-in mice (bred in house), IL-1R gene knockout (-/-) mice (bred in house), and MyD88 gene knockout (-/-) mice (bred in house) were used. Corneas of C57BL/6 mice have an area of ~5.3 mm$^2$. Both male and female mice contributed to the results since no differences were observed between them. Anesthesia was induced by intraperitoneal injection of ketamine (80–100 mg/Kg) and dexmedetomidine (0.25– 0.5 mg/Kg) before inoculation with bacterial suspensions (5 $\mu$L). At 1 h, or other times post-inoculation, the anesthetic antidote atipamezole (2.5–5 mg/Kg) was administered, and mice were allowed to recover with food and water. Mice were euthanized by intraperitoneal injection of ketamine (80–100 mg/Kg) and xylazine (5–10 mg/Kg) followed by

cervical dislocation. All experiments involved at least three animals per group and were repeated at least twice.

### 2.3.4 Ocular Clearance of Bacteria

Wild-type C57BL/6 mice (6–12 weeks) were used. After induction of anesthesia, 5 $\mu$L of bacterial inoculum containing ~$10^8$ or ~$10^4$ CFU was applied to the healthy ocular surface. At 24 and 72 h post-inoculation, tear fluid was collected from the ocular surface, and the numbers of viable bacteria determined. Tear fluid was collected by capillary action using a 30 $\mu$l glass capillary tube from the lateral canthus after 10 $\mu$l of PBS was added. The conjunctiva and cornea were then extracted and homogenized in 500 $\mu$l of PBS. Viable bacterial counts were determined by 10-fold serial dilution of the homogenates in PBS from $10^{-1}$ to $10^{-4}$ before plating in triplicate onto on TSA plates, followed by incubation for ~18 h at 37°C to determine CFU. In other experiments, whole eyes were enucleated and subject to FISH *ex vivo* after inoculation with bacteria as above.

### 2.3.5 AlkDala (Alkyne-Functionalized D-Alanine) Labeling

Labeling of live bacteria using an alkyne functionalized D-alanine (alkDala) biorthogonal probe (Siegrist et al., 2013; Shieh et al., 2014) was adapted for use on the murine ocular surface. Enucleated eyes were incubated in a solution of alkDala (10 mM) in Dulbecco's Modified Eagle Medium (DMEM) at 37°C for 2 h. In other experiments, eyes of IL-1R (-/-) and MyD88 (-/-) mice were first incubated in an antibiotic cocktail of gentamicin (300 $\mu$g/mL), ofloxacin (300 $\mu$g/mL) and vancomycin (5 mg/mL) in DMEM. After alkDala incubation, all eyes were transferred to pre-chilled 70% EtOH and fixed for 20 min at −20°C. After rinsing, eyes were permeabilized in PBS with Triton-X100 (0.5%) for 10 min with shaking at room temperature (RT), then washed 3 times for 5 min each in PBS with Triton-X100 (0.1%) and BSA (3%) with shaking at RT. Eyes were then transferred to the click-labeling cocktail [in PBS, TBTA (100 $\mu$M), CuSO4 (1 mM), sodium ascorbate (2 mM), 488 nm azide-fluorophore (10 $\mu$M), BSA (0.1 mg/mL)] for 1 h with shaking at RT.

### 2.3.6 Fluorescence *in Situ* Hybridization

Enucleated eyes were fixed in paraformaldehyde (2%) for 1 h with shaking at RT. Bacterial hybridization was performed using a universal 16S rRNA gene [Alexa488]- GCTGCCTCCCG-TAGGAGT -[Alexa488] (Eurofins Genomics) as previously described (Vaishnava et al., 2011; Mark-Welch et al., 2016). Briefly, fixed eyes were washed in 80% EtOH, 95% EtOH, and then PBS for 10 min each with shaking at RT. Eyes were then placed in a hybridization buffer solution [NaCl (0.9 M), Tris–HCl (20 mM, pH 7.2) and SDS (0.01%)] and incubated at 55°C for 30 min. The probe was added to final concentration of 100 nM and incubated at 55°C overnight. Eyes were then transferred to wash buffer solution [NaCl (0.9 M) and Tris–HCl (20 mM, pH 7.2)] and washed three times for 10 min each with shaking at RT.

### 2.3.7 DMN-Tre (4-*N,N*-Dimethylamino-1,8- Naphthalimide-Trehalose) Labeling

A DMN-Tre conjugate was used to label bacteria specific to the Corynebacterineae suborder (Kamariza et al., 2018) in conjunction with alkDala-labeling. Conjunctival tissue, aseptically obtained from healthy mouse eyes, was homogenized in 500 $\mu$L of DMEM then centrifuged at 14,000 × g for 2 min. Liquid was aspirated and the pellet suspended in alkDala (10 mM) and DMN-Tre (100 $\mu$M) in DMEM and incubated at 37°C for 2 h. Samples were processed as described above except that a 647 nm azide-fluorophore was used in the click-labeling cocktail. Then, 10 $\mu$L of conjunctival homogenate was spotted on microscope slide with coverslip on top. Conjunctival tissue pieces with alkDala (647 nm) and DMN-Tre (488 nm) fluorescent labels were imaged using a Nikon ECLIPS Ti microscope with a 60× oil-immersion objective.

### 2.3.8 Fluorescein Staining

Eyes were rinsed with PBS after the induction of anesthesia as described above. For wild-type mice, one eye was blotted with a Kimwipe™ tissue paper. Eyes of IL-1R (-/-) mice were not blotted. A drop (5 $\mu$L) of fluorescein solution (0.02%) was then added to the ocular surface, and corneal epithelial integrity examined using a slit lamp and confocal microscopy.

### 2.3.9 Antimicrobial Activity of Corneal Lysates

The antimicrobial activity of murine cornea epithelial lysates was assessed as previously described (Sullivan et al., 2015). Corneas of wild-type or IL-1R (-/-) mice were left untreated or exposed to 5 $\mu$l of *P. aeruginosa* antigens [supernatant of a PAO1 culture (Maltseva et al., 2007)] for 3 h. Corneas were extracted and homogenized in distilled water (two corneas per 350 $\mu$L of water) and centrifuged at 14,000 × g for 2 min to remove cell debris and stromal tissue. Crude lysates were confirmed to have equal protein concentration with a BCA (bicinchoninic acid) assay kit (Pierce Biotechnology, Inc., Thermo Fisher Scientific, Rockford, IL, United States). P. aeruginosa (~$10^6$ CFU/mL) in lysate or water were incubated in triplicate at 37°C with shaking for 3 h. Viable bacterial counts of samples were then determined by 10- fold serial dilution in PBS as described above, plating in triplicate onto MacConkey Agar, followed by incubation for ~18 h at 37°C to determine CFU. Percentage survival at 3 h was determined as follows: (viable counts from cell lysates at 3 h/viable counts from distilled water at 3 h) × 100%.

### 2.3.10 Confocal Microscopy

Murine eyeballs were imaged *ex vivo* as previously described (Tam et al., 2011). Briefly, eyes were fixed to a 12 mm glass coverslip with cyanoacrylate glue with cornea facing upward. The coverslip with eyeball was placed in a 47 mm Petri dish and filled with PBS to cover the eyeball completely. Confocal imaging was performed using an Olympus FV1000 confocal microscope [Olympus BX615Wi upright microscope with Olympus FluoView 1000 detection system equipped

with Laser Diodes (LD) 405, 440, 559, 635, and an Argon Laser 488/515]. The 488 nm laser (emission filter: 500–545 nm) was used for detection of bacteria labeled with alkDala or FISH, or corneas stained with fluorescein, the 559 nm laser (emission filter: 570–670 nm) used for detection of red-fluorescent bacteria (PAO1-dtom) or red fluorescent cell membranes, and the 635 nm laser used to obtain ocular surface reflectance (excitation and emission at same wavelength). Three or more randomly chosen fields of each eye (~0.04 $mm^2$) were imaged from the corneal surface through the entire epithelium in 1.0 $\mu$m steps as previously described (Tam et al., 2011). Three-dimensional images were reconstructed from z-stacks using IMARIS software (Bitplane). Images were compared to controls to determine threshold for each emission filter and held constant for all images. Bacteria were identified and quantified using the surface generation feature on IMARIS.

### 2.3.11 Statistical Analysis

Data were expressed as mean ± standard deviation (SD). Statistical significance of differences between means was determined using an unpaired Student's t-Test or Mann–Whitney U-test for two group comparisons. For three or more groups, the Kruskal–Wallis test was used with Dunnett's multiple comparison test for post hoc analysis. P-values < 0.05 were considered significant.

## 2.4 Results

### 2.4.1 AlkDala-labeling shows the absence of metabolically active bacteria on the murine cornea

To explore whether the cornea hosts a microbiome composed of viable bacteria we used alkDala, a reagent that incorporates into the peptidoglycan of any metabolically active bacterium. Bacteria that have taken up alkDala can then be detected with an azide- fluorophore attached via click chemistry (Figure 2.1A). Prior to use in the mouse eye, these reagents were tested for specificity and efficacy in the presence of host tissue. This was done first using cultured HeLa cells incubated with either *P. aeruginosa* strain PAO1 or *S. aureus* (clinical isolate). The results showed that viable bacteria, but not the inoculated HeLa cells, labeled with the reagents (Figure 2.1B). As expected, heat-killed bacteria or bacteria treated with D-alanine alone (i.e., no alkyne group) did not label (Figure 2.1B). Moreover, environmental fungi did not label with alkDala *in vitro* (Supplementary Figure S1). Next, we explored if the reagent is also able to detect live bacteria in the context of murine corneas. Eyeballs freshly excised from mice were incubated in ~$10^{11}$ CFU/mL of PAO1-dtom *ex vivo* for 5 h. As shown in Figure 2.1C, bacteria that attached to the corneal surface (visible via dtom), were also detectable by alkDala.

Having shown that alkDala can distinguish viable bacteria in the context of the eye, we next used it to explore if uninoculated wild-type murine corneas harbored viable bacteria. Three random fields were selected to count the number of visible bacterial forms, the size of each field

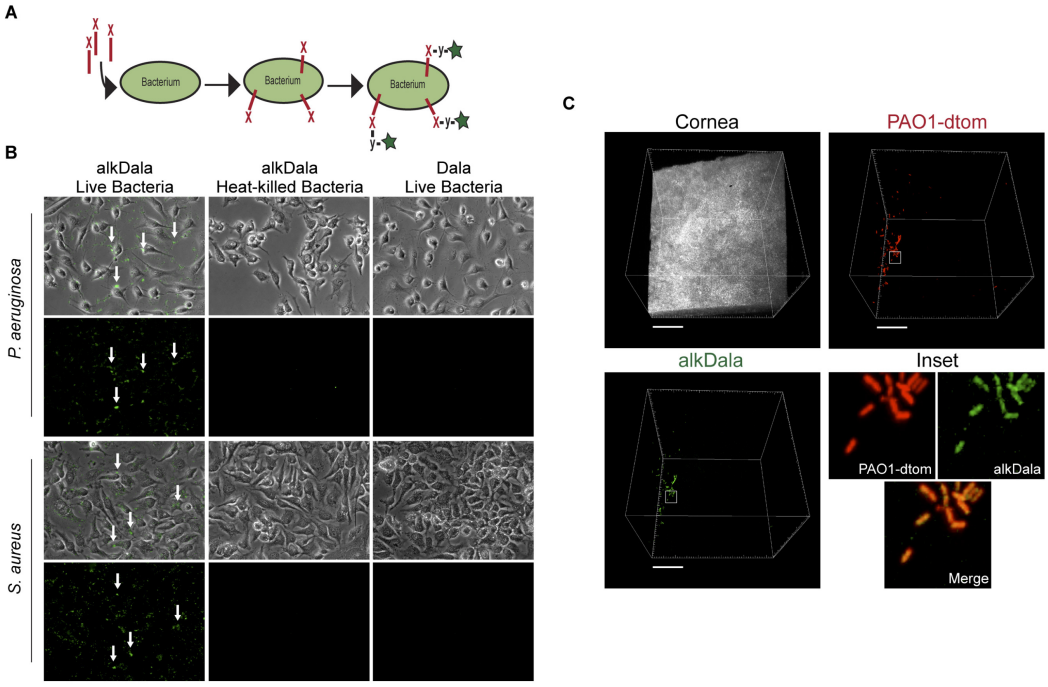


**Figure 2.1:** Alkyne-functionalized D-alanine (AlkDala) detects metabolically active bacteria inoculated onto cell culture and the murine cornea.(A) Schematic of alkDala (shown as a red X) labeling of bacteria. AlkDala is added to a bacterial suspension to allow incorporation into the cell wall peptidoglycan followed by a copper-catalyzed click-chemistry reaction with an azide-fluorophore (shown as a y-star symbol) to detect bacteria with incorporated probe. (B) AlkDala labeling was tested on *Pseudomonas aeruginosa* (PAO1) and *Staphylococcus aureus* (clinical isolate) in the presence of HeLa cells, and labeled all live bacteria (green, arrows) (Lower Left). Heat-killed bacteria were not detected (Lower Middle), nor were live bacteria detected if incubated with D-alanine without an attached alkyne (Lower Right). (Upper) show the phase-contrast images of respective fields. (C) To determine if bacteria on the murine ocular surface could be labeled with alkDala, whole eyeballs were incubated in ~$10^{11}$ CFU/mL of red fluorescent *P. aeruginosa* (PAO1-dtom) for 5 h, and then labeled using alkDala (green). The same fields of view are shown with different emission filters. Inset shows zoom of the white box with merge. Scale bar, 50 $\mu$m.

being ~0.04 $\mu m^2$. Very few alkDala-labeled bacteria were present on the healthy murine cornea (Figure 2.2A). In contrast, the conjunctiva displayed numerous alkDala-labeled forms (Figure 2.2B), supporting the existence of conjunctival- associated bacteria as previously reported by us, and others, using culture and sequencing methods (Fleiszig and Efron, 1992; Schabereiter-Gurtner et al., 2001; Graham et al., 2007; Dong et al., 2011; Doan et al., 2016). Surprisingly, the alkDala-labeled forms existed in long filamentous and tangled states, not previously reported (Figure 2.2B).

Use of D-alanine alone, without an alkyne, confirmed that fluorescent labeling was specific to alkyne incorporation into bacterial cell walls (Figure 2.3A). Furthermore, transgenic mice with red fluorescent cell membranes demonstrated that these alkDala-labeled forms were not host tissue, suggesting that these filamentous structures were microbial (Figure 2.3B).

We hypothesized that the filamentous forms belong to the *Corynebacterium* spp., which are known to inhabit the conjunctiva, and exist in filamentous forms in dental plaque (Mark-Welch et al., 2016; St Leger et al., 2017). To test this, a novel DMN-Tre labeling probe, specific

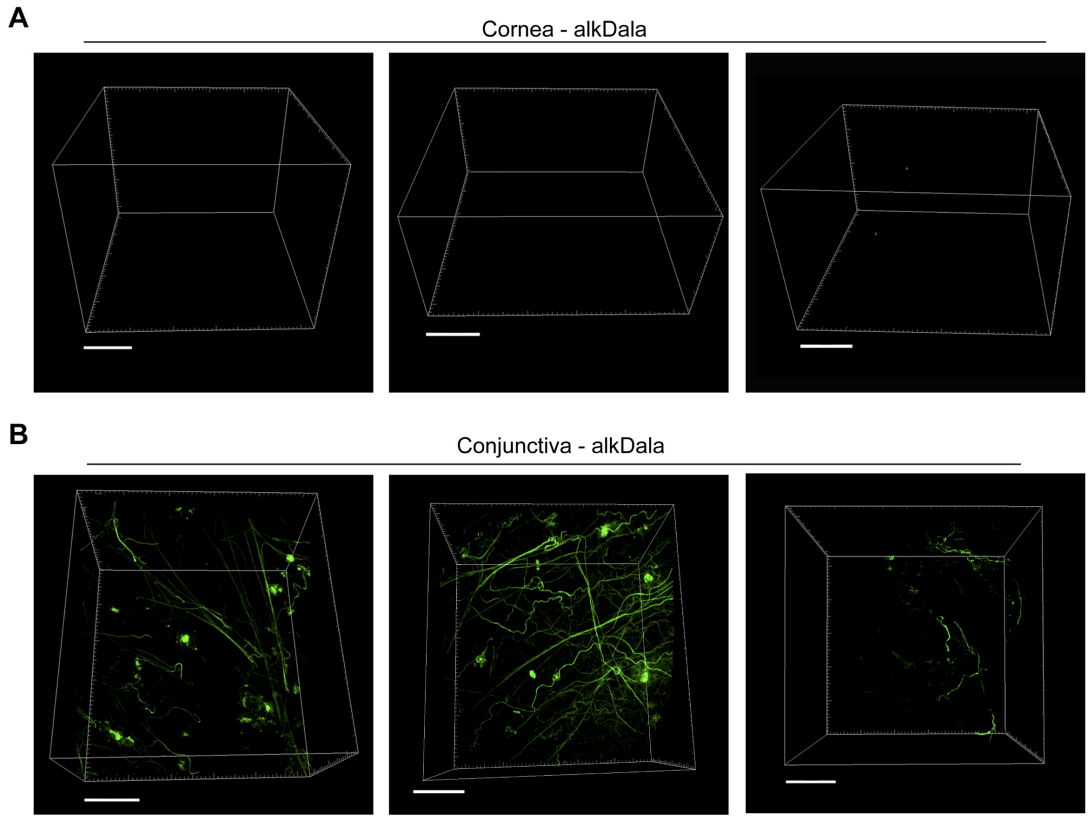


**Figure 2.2:** The healthy murine cornea is nearly devoid of viable bacteria. (A) AlkDala labeling revealed very few viable bacteria on the healthy corneas of C57BL/6 mice. Representative fields shown from four different labeled corneas (two male and two female mice). (B) AlkDala labeling of the conjunctiva of C57BL/6 mice revealed numerous viable bacteria, many in a filamentous form. Representative fields of view are shown from seven different eyes (three male and four female mice). Scale bars, 50 $\mu$m.

to the Corynebacterineae suborder, was used together with alkDala on murine conjunctival tissue. The DMN-Tre reagent metabolically incorporates into the outer mycomembrane of Corynebacterineae (includes *Mycobacterium* spp. and *Corynebacterium* spp.) as trehalose mycolates (Kamariza et al., 2018). The fluorescence signal is activated upon entry into the hydrophobic mycomembrane. Results showed that the alkDala-labeled filamentous forms (green) tangled in conjunctival tissue also labeled with DMN- Tre (red) (Figure 2.3C) suggesting that they belong to the Corynebacterineae.

### 2.4.2 FISH supports the absence of viable bacteria on healthy murine corneas

To account for the possibility of viable bacteria without peptidoglycan-metabolic processes, or for which peptidoglycan metabolism was inactive or at very low levels, we employed FISH using a universal 16S rRNA gene probe. Unlike alkDala, FISH does not require probe incorporation into bacterial cell wall peptidoglycan, allowing the detection of viable bacteria independently of

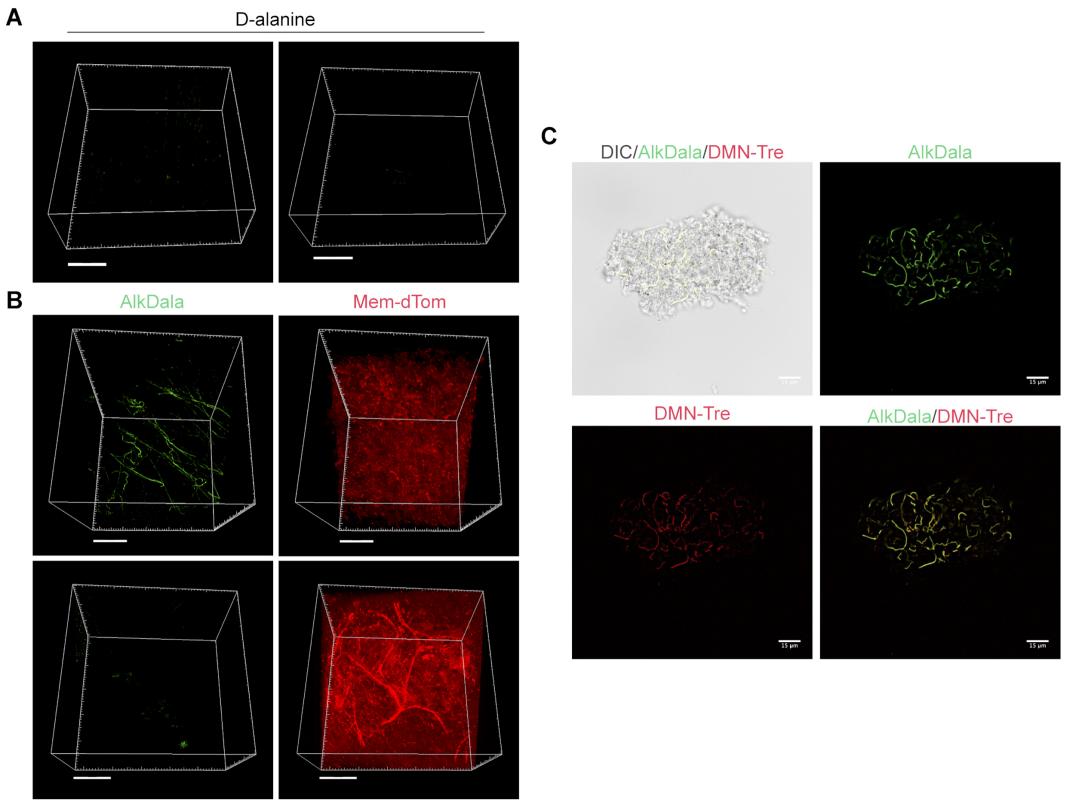


**Figure 2.3:** Filamentous structures identified on conjunctiva are not host tissue (A) Mouse eyes incubated in D-alanine, without an alkyne, resulted in no fluorescent labeling. (B) Wild-type transgenic mice with fluorescent red cell membranes mT/mG knock-in mice (Muzumdar et al., 2007) were used in conjunction with alkDala labeling to determine if the filaments identified on the conjunctiva colocalized with host tissue. Filamentous structures on the conjunctiva (Upper) did not colocalize with host cell membranes (denoted Mem-dtom). Conversely, when filament-like structures were present in host tissue, alkDala labeling was not present (Lower). Images shown on the left and right are of the same fields of view with different emission filters. (C) Imaging of murine conjunctival epithelial tissue shows that DMN-Tre, a probe specific for Corynebacterineae (red), labeled most of the same conjunctival forms as alkDala (green). All images are from the same field of view with different emission filters.

peptidoglycan metabolism. FISH labeling on the murine cornea was validated by incubating excised whole mouse eyes in ~$10^{11}$ CFU/mL of red fluorescent P. aeruginosa (PAO1-dtom) for 5 h *ex vivo*. After one PBS wash, bacteria remaining on the cornea were detected with FISH (green), and consistently colocalized with red fluorescent *P. aeruginosa* (Supplementary Figure S2).

Fluorescence *in situ* hybridization labeling was then applied to healthy wild-type mouse corneas. Results revealed very few bacterial forms were present on the murine cornea (Figure 2.4A), consistent with previous results with alkDala (Figure 2.2A) and suggesting that the cornea was free of viable bacteria. A comparison of quantitative alkDala-labeling (0.53 ± 0.76 bacteria/field of view, ~60 bacteria per cornea) with results obtained from FISH labeling (0.88 ± 0.35 bacteria/field of view, ~100 bacteria per cornea) revealed no significant difference between methods (Figure 2.4B, P = 0.40, Student's t-Test). Thus, on rare occasions that bacteria were detected on healthy murine corneas, they mostly existed in viable, metabolically active states.

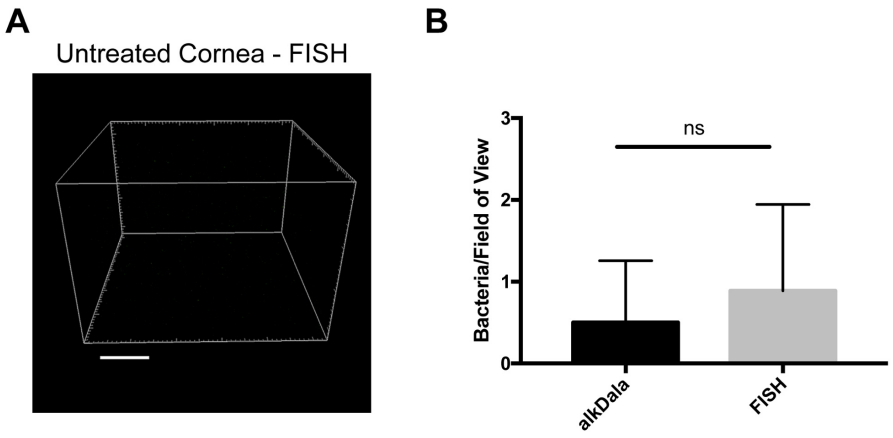


**Figure 2.4:** Fluorescence *in situ* hybridization (FISH) labeling confirms that healthy murine corneas are nearly devoid of viable bacteria. (A) FISH labeling confirmed C57BL/6 mouse corneas host very few viable bacteria. A representative field of view is shown from four different corneas (two male and two female mice).(B) Quantification of viable bacteria on healthy murine corneas using alkDala or FISH expressed as mean ± SD per field of view. One field of view is ~0.04 $mm^2$. ns = there was no significant difference between number of bacteria detected by either method (P = 0.40, Student's t-Test).

### 2.4.3 Murine corneas efficiently clear multiple species of inoculated bacteria

Previously we reported that *P. aeruginosa* was rapidly cleared from the healthy mouse cornea and tear fluid after deliberate inoculation (Mun et al., 2009). Here, we expanded those studies to determine if *P. aeruginosa, S. aureus,* or a murine eyelid commensal (CNS), could gain a foothold in any region of the murine ocular surface after inoculation (Figure 2.5). Thus, healthy wild-type animal eyes were inoculated in vivo with ~$10^8$ CFU bacteria, and the number of viable bacteria remaining at multiple locations examined after 24 h. Very few bacteria were recovered from the eyewash/tear fluid of eyes inoculated with the eyelid CNS commensal (~100 CFU, 6-log reduction compared to inoculum). Bacteria could not be recovered at all from the tear fluid of eyes inoculated with *S. aureus* or *P. aeruginosa.* Corneas and conjunctival tissue each harbored between ~$10^2$ to ~$10^3$ CFU culturable bacteria for all three species, representing a clearance rate of >99.99% of the original inoculum (Figure 2.5A). We next explored if the few bacteria remaining at 24 h could persist on the ocular surface for longer time periods. Thus, experiments were repeated using a 72 h time frame. At this later time point, bacteria were no longer detected in any of the eye washes, and negligible (~10 CFU) or no bacteria were detected on the cornea and conjunctiva (Figure 2.5B). In case the large inoculum used had activated innate defenses not otherwise involved, experiments were repeated again using a much smaller inoculum (~$10^4$ rather than ~$10^8$ CFU). The results revealed even fewer bacteria recovered after 24 h than were recovered after the larger inoculum (Figure 2.5C). No ocular pathology was observed in any of the experiments.

To determine if some additional remaining bacteria had escaped detection by transitioning into a non-culturable state, we also used the FISH label to detect viable bacterial forms. This was

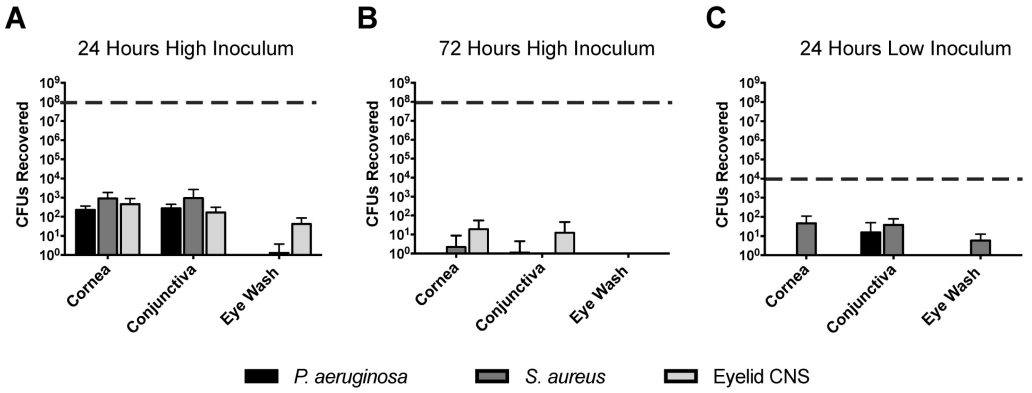


**Figure 2.5:** Bacterial clearance from the murine ocular surface. Eyes of C57BL/6 mice were inoculated *in vivo* with *P. aeruginosa, S. aureus,* or a CNS sp. previously isolated from a mouse eyelid, to determine if bacteria could persist on the ocular surface. Data was expressed as the mean ± SD of viable bacteria recovered from the cornea, conjunctiva, or eye wash (see section "Materials and Methods"). The dashed line represents initial inocula. (A) After 24 h, the vast majority of inoculated bacteria (~$10^8$ CFU) were cleared from the cornea, conjunctiva, and eye wash. (B) By 72 h (3 days), virtually all bacteria were cleared from the ocular surface. (C) A lower inoculum (~$10^4$ CFU) resulted in few remaining bacteria after 24 h. In each instance, $P < 0.05$ compared to the initial inoculum (Kruskal–Wallis test, with Dunnett's multiple comparison).

done 24 h after inoculation with ~$10^8$ CFU of *P. aeruginosa, S. aureus,* or CNS. In all instances, the number of bacterial forms visible on corneas using FISH was similar to numbers obtained by viable counts (Figure 2.6). These results further illustrate the in-hospitability of the corneal surface to bacterial colonization and show that bacterial clearance from the healthy corneal surface involves complete removal of bacterial forms, not simply neutralization of viable bacteria.

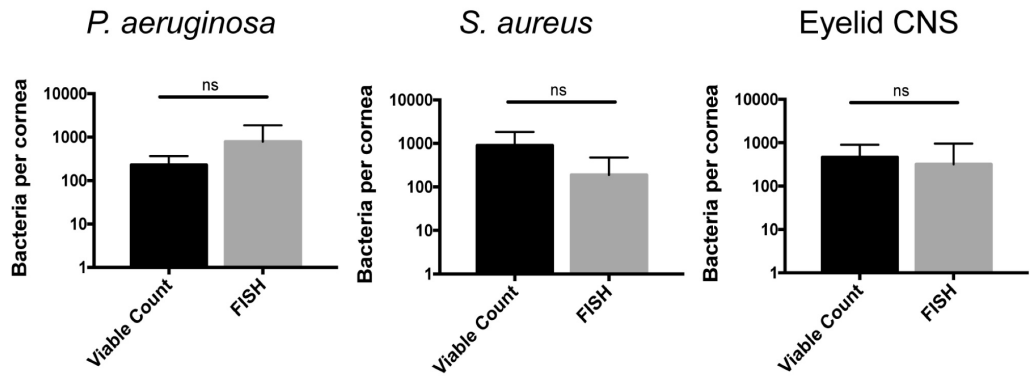


**Figure 2.6:** Number of bacteria detected per cornea using viable counts compared to FISH labeling at 24 h after uninjured mouse eyes were inoculated *in vivo* with ~$10^8$ CFU of *P. aeruginosa, S. aureus,* or CNS. Data were expressed as the mean ± SD of bacteria identified per cornea. ns = No significant difference was found between methods used ($P > 0.05$, Mann–Whitney U-test).

### 2.4.4 Corneas of IL-1R (-/-) and MyD88 (-/-) mice host metabolically active bacteria

Mucosal surfaces are normally colonized by a significant number of commensal microbes, which as an aggregate is termed a microbiome. The above results confirmed the notion that the healthy murine cornea differs in this respect by being virtually clear of viable bacteria. To begin to understand the mechanisms by which the cornea maintains this condition, we tested the hypothesis that innate immune defenses that normally detect and respond to microbes are required. Thus, we explored if the IL-1R was involved using knockout mice, given that it plays an integral role in regulation of innate immunity at mucosal surfaces, including the eye (Pearlman et al., 2008; McDermott, 2009). AlkDala labeling revealed that metabolically active bacteria were present on uninjured corneas of IL-1R (-/-) mice (Figure 2.7A). Since we had previously shown that MyD88 was critical for protecting the murine corneal epithelium against penetration by *P. aeruginosa* (Tam et al., 2011), and MyD88 is an important adaptor molecule for IL-1R signaling, MyD88 (-/-) corneas were also examined. AlkDala labeling revealed that uninjured corneas of MyD88 (-/-) mice also harbored metabolically active bacteria (Figure 2.7B). FISH showed similar numbers of bacteria to alkDala labeling confirming that most detected bacteria on IL-1R (-/-) and MyD88 (-/-) murine corneas were viable (Figure 2.7C). Comparison of bacterial numbers on IL-1R (-/-) mice (76.00 ± 152.19 bacteria/field of view, >10,000 CFU per cornea), MyD88 (-/-) mice (87.87 ± 81.29 bacteria/field of view), with wild-type (<1 bacteria/field of view) revealed significant increases in viable resident bacteria in each gene knockout mouse ($P < 0.05$ and $P < 0.01$ for IL-1R- and MyD88-gene knockout mice respectively, versus wild-type corneas, Kruskal–Wallis test with Dunn's multiple comparison) (Figure 2.7D). Antibiotic treatment reduced the number of alkDala-detected bacteria to wild-type levels for both IL-1R (-/-) and MyD88 (-/-) mice. For IL-1R (-/-) mice, antibiotics reduced bacterial numbers to 1.00 ± 1.00 bacteria/field of view, and for MyD88 (-/-) mice to 1.75 ± 1.75 bacteria/field of view ($P = 0.88$ and $P = 0.66$, respectively versus WT, Kruskal–Wallis test with Dunn's multiple comparison) (Figure 2.7D).

Next, we sought to determine which bacterial species inhabited the corneas of these immune-compromised mice. Corneal lysates of wild-type and IL-1R (-/-) mice were inoculated onto various agar media, and cultured bacteria identified by direct colony PCR of 16S rRNA (Table 2.1). Wild- type murine corneas revealed few, if any bacteria, consistent with previous results. Only one genus, *Streptococcus* spp. was identified in one of eight eyes with low bacterial numbers (7 CFU). In contrast, bacteria were isolated from seven of eight IL-1R (-/-) corneas with many more bacterial CFU compared to wild-type (Table 2.1). The most common bacteria identified were CNS spp. (five of eight eyes) and *Propionibacterium* (two of eight eyes). A *Bacillus* spp. was also identified in one eye (Table 2.1). It should be noted that the nature of the bacterial genera colonizing IL-1R (-/-) corneas will likely vary according to environment, e.g., differences between animal care facilities would likely affect culture results. Moreover, the limited number and diversity of bacteria isolated in the present study demonstrates the limitations of viable culture techniques and emphasizes the need for multiple methods when characterizing bacterial communities.

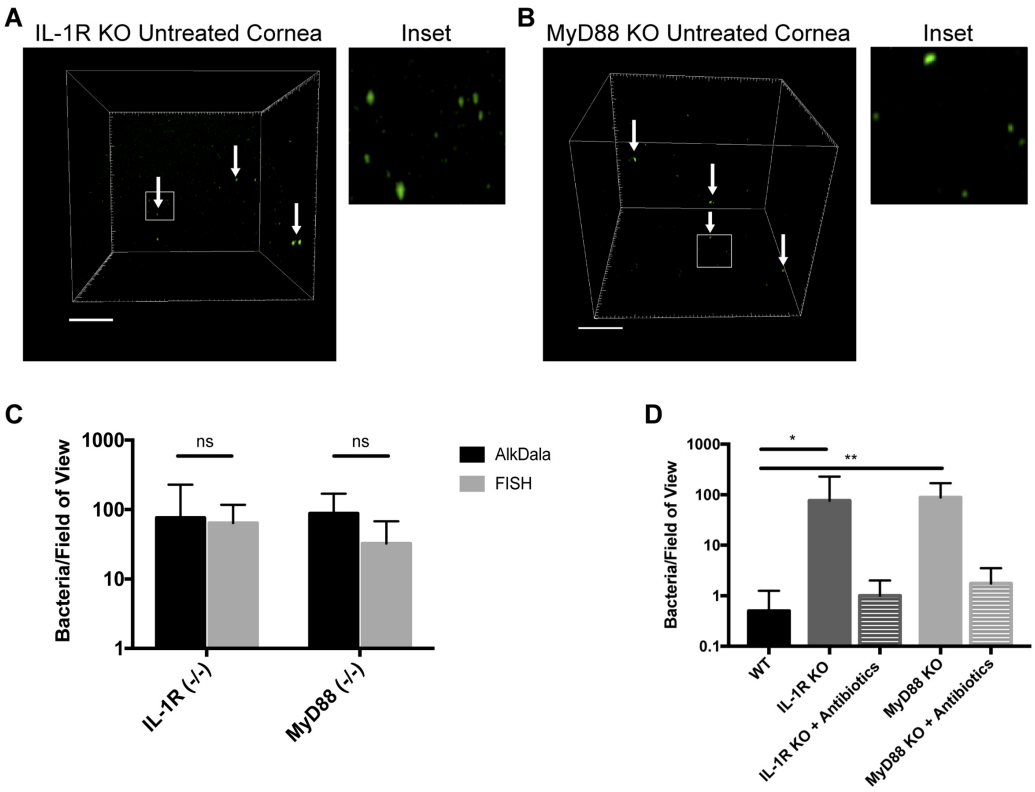


**Figure 2.7:** (A) AlkDala-labeling revealed many metabolically active bacteria (white arrows) on the corneas of uninjured IL-1R (-/-) mice. A representative field of view is shown from seven different corneas (three male and four female mice). (B) MyD88 (-/-) mouse corneas were also colonized with metabolically active bacteria. A representative field of view is shown from six different corneas (two male and four female mice). (C) AlkDala and FISH detected similar numbers of viable bacteria on Il-1R (-/-) or MyD88 (-/-) corneas (ns, not significant, Mann–Whitney U-test). (D) Quantification of viable bacteria detected per field of view using alkDala. Mean ± SD viable bacteria on the murine cornea was significantly higher in IL-1R (-/-) and MyD88 (-/-) mice versus wild-type, *P < 0.05, **P < 0.01 (Kruskal–Wallis test with Dunn's multiple comparison). Antibiotic treatment reduced bacterial detection to wild-type levels for IL-1R (-/-) and MyD88 (-/-) corneas (P = 0.88 and P = 0.66 versus wild-type, Kruskal–Wallis test with Dunn's multiple comparison). Scale bar, 50 $\mu$m.

### 2.4.5 IL-1R (-/-) corneas exhibit epithelial junction integrity but reduced antimicrobial activity

A potential mechanism for microbial colonization of corneas in knockout mice would be if there was disruption of epithelial tight junctions, which would reduce epithelial barrier function and loss of cell polarity, thereby enabling bacterial colonization of surface epithelial cells (Fleiszig et al., 1997; Alarcon et al., 2011; Tam et al., 2011). To explore that possibility, uninjured corneas of IL-1R (-/-) mice were treated with fluorescein, and compared to corneas of wild-type mice, either uninjured or blotted with a Kimwipe™ to induce superficial injury (Tam et al., 2011). While extensive fluorescein staining was observed in wild-type corneas after superficial injury, uninjured corneas of IL-1R (-/-) mice were similar to uninjured wild-type with little or no staining (Figure 2.8A), suggesting epithelial tight junctions were intact.

Previously, we showed that MyD88 (-/-) mouse corneas also resist corneal staining (Tam

**Table 2.1:** Bacteria identified on the corneas of wild-type and IL-1R (-/-) mice.

| | Wild-type | | IL-1R(-/-) | |
|---|---|---|---|---|
| | **CFUs/cornea** | **Bacteria** | **CFUs/cornea** | **Bacteria** |
| Eye 1 | 7 | *Streptococcus* spp. | 130 | *Staphylococcus* spp. (CNS) |
| Eye 2 | 0 | - | 354 | *Staphylococcus* spp. (CNS) |
| Eye 3 | 0 | - | 179 | *Staphylococcus* spp. (CNS) |
| Eye 4 | 0 | - | 257 | *Staphylococcus* spp. (CNS) |
| Eye 5 | 0 | - | 48 | *Bacillus* spp., *Staphylococcus* spp. (CNS) |
| Eye 6 | 0 | - | 3 | *Propionibacterium* spp. |
| Eye 7 | 0 | - | 13 | *Propionibacterium* spp. |
| Eye 8 | 0 | - | 0 | - |

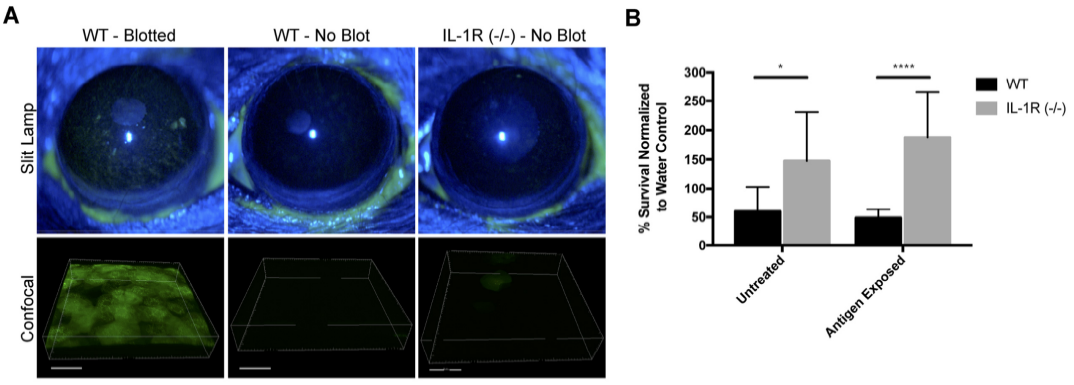


**Figure 2.8:** Uninjured IL-1R (-/-) murine corneas do not exhibit fluorescein staining, but show reduced antimicrobial activity. (A) After tissue paper blotting, wild-type (WT) corneas were susceptible to fluorescein staining suggesting the disruption of epithelial integrity. Non-blotted (uninjured) WT and IL-1R (-/-) corneas showed little or no fluorescein staining. (B) IL-1R (-/-) corneal epithelial lysates showed reduced antimicrobial activity against *P. aeruginosa* strain PAO1 compared to WT lysates. A similar result was obtained in a separate set of experiments in which corneas were exposed to bacterial antigens prior to lysate production. *P < 0.05, ****P < 0.0001 (Students t-Test).

et al., 2011), but that corneal lysates from these corneas have reduced antimicrobial activity compared to wild-type (Sullivan et al., 2015). Thus, we examined lysates of IL-1R (-/-) corneas and found that they too were significantly less antimicrobial (2.46-fold) against *P. aeruginosa* PAO1 compared to wild-type mice ($P < 0.05$, Student's t- Test) (Figure 2.8B). Prior exposure of the mouse corneas to bacterial antigens did not impact that outcome, with IL-1R (-/-) lysates remaining less antimicrobial (3.85-fold) than wild-type ($P < 0.0001$, Student's t-Test) (Figure 2.8B).

## 2.5 Discussion

The ocular surface is constantly exposed to a diverse array of microbes from the environment. In this study, we addressed the question of whether commensal bacteria can inhabit the cornea, similar to the conjunctiva and other mucosal tissues. To do this, we applied metabolic labeling of peptidoglycan using an alkDala probe to directly detect viable bacteria *in situ* using confocal imaging (Vaishnava et al., 2011; Siegrist et al., 2013). Used in conjunction with FISH to identify viable bacteria independently of peptidoglycan metabolism, alkDala has an advantage over traditional culture or 16S rRNA gene sequencing, which are indirect methods with potential for numerous false-negative and false-positive results, respectively. Our results show that the healthy murine cornea is generally inhospitable to bacteria, a condition that requires constitutive function of the IL-1R and MyD88. The results also suggest that, in contrast to the murine conjunctiva and other mucosal surfaces, the healthy murine cornea does not support a resident viable bacterial community (or microbiome).

Having ruled out a natural microbiome in wild-type mice, we explored if we could establish one through deliberate inoculation. We tested pathogens of both Gram-types, and a commensal from the mouse eyelid. These were each rapidly cleared from all regions of the ocular surface (cornea, conjunctiva, and tears), the timing dependent on the initial inoculum size, and the methods used ruled out the possibility that the bacteria had transitioned into a non-culturable viable state. These results also support the notion that the cornea is an inhospitable environment for bacteria.

The results showed that the gain of bacterial colonization in IL-1R and MyD88 (-/-) corneas did not correlate with a loss of barrier function to fluorescein, but was instead associated with a lack of antimicrobial activity in corneal lysates (Sullivan et al., 2015). Thus, local antimicrobial activity is a potential mechanism by which the wild-type cornea maintains its amicrobiomic status. Indeed, IL-1$\beta$ and toll-like receptor agonists are known to regulate the expression of various antimicrobial peptides, including human beta-defensin 2 (hBD2) and the cathelicidin LL-37, by human corneal epithelial cells (McDermott et al., 2003; Redfern et al., 2011). Possibly related, the murine equivalent of hBD2 (mBD3) is involved in the ocular surface clearance of *P. aeruginosa* after deliberate inoculation under healthy conditions (Augustin et al., 2011). Other potential mechanisms include ocular surface mucins, that can inhibit bacterial adhesion to the cornea (Fleiszig et al., 1994). While we recently showed that glycosylation patterns on the murine ocular surface can be dependent on IL-1R (Jolly et al., 2017), that was not the case for MyD88, and did not necessarily influence bacterial adhesion. Thus, any role for surface glycosylation in maintaining the amicrobiomic status of the cornea is likely to be complex. Our laboratory has also recently shown that uninjured IL-1R (-/-) mouse corneas were significantly more susceptible to *P. aeruginosa* adherence after challenge, and that protection of the cornea against *P. aeruginosa* adhesion involved IL-1R associated with both corneal epithelial cells and CD11C+ cells (Metruccio et al., 2017). Similar mechanisms may play a role in constitutively keeping the cornea free of a bacterial microbiome. It has also been shown that MyD88 (-/-) murine corneas exhibited reduced constitutive levels of cytokines, chemokines, and the matrix

metalloproteinase MMP-9 (Reins et al., 2017), which may also contribute to allowing bacteria to colonize the corneas of these mice. Thus, further studies will be needed to delineate factors downstream of IL-1R and MyD88 critical for constitutively keeping the healthy cornea free of resident bacteria under normal conditions.

Contrasting with the cornea, the conjunctiva appeared to be colonized by metabolically active bacteria. Conjunctival- associated alkDala-labeled bacteria appeared mostly as filamentous forms. Controls determined that this labeling was specific to alkDala, and that the filamentous structures did not co-localize with host structures, suggesting that they were indeed microbial. Subsequent imaging experiments showed that DMN-Tre, a probe specific for Corynebacterineae (e.g., a bacterial suborder including *Mycobacterium* and *Corynebacterium* spp.) labeled the same conjunctival filamentous forms as alkDala providing more evidence of their identity. This result was perhaps not surprising since the human conjunctiva is well known to support CNS spp., *Corynebacterium* spp., and *Propionibacterium* spp. (Turnbaugh et al., 2007; Dong et al., 2011; Doan et al., 2016). Moreover, in mice, resident conjunctival-associated bacterial flora contribute to protective ocular immune responses via IL-1$\beta$-dependent mechanisms, and local antibiotic treatment reduces corneal immune responses to *P. aeruginosa* infection after scarification injury (Kugadas et al., 2016). Another recent study, using a similar infection model, also implicated resident conjunctival *Corynebacterium mastitidis* in protecting murine corneas from *Candida albicans* and *P. aeruginosa* via IL-17-driven mucosal immune responses (St Leger et al., 2017). In our study, we detected the filamentous bacterial forms on the conjunctiva of mice obtained from both Charles River and Jackson Laboratory. However, we were unable to culture these filamentous bacteria from the conjunctiva of mice used in our study, nor identify *C. mastitidis* from the conjunctiva of mice from Jackson Laboratory, or from other mice in our facility. Further studies will be needed to identify the filamentous bacterial forms and determine their role in ocular surface homeostasis or immune responses.

Many different types of bacteria, including *Corynebacterium* spp., become filamentous when encountering stressful environments, such as in the presence of antibiotics or low nutrients (Wright et al., 1988; Justice et al., 2006, 2008). Possibly, adoption of this morphology represents a deliberate strategy to avoid removal from the ocular surface. For example, filamentation can be used by bacteria to avoid phagocytosis (Horvath et al., 2011). The conjunctiva is not the only place where filamentous bacteria have been identified. Indeed, filamentous *Corynebacterium* spp. are a part of dental plaque and segmented filamentous bacteria (SFB) are commensal inhabitants of the gut (Farkas et al., 2015; Schnupf et al., 2015; Mark-Welch et al., 2016). Unlike other commensals in the gut, SFB are the only bacteria that directly interact with epithelial cells and have been shown to play an important role in modulating the host immune system (Talham et al., 1999; Vaishnava et al., 2011; Farkas et al., 2015). Some bacteria respond to adverse environmental conditions by entering into a physiological state in which they remain viable, but are not culturable using standard laboratory methods (Oliver, 2010). These are referred to as VBNCs. Since VBNCs retain metabolic activity (Ramamurthy et al., 2014), they would be expected to label with the universal 16S rRNA gene probe used for FISH in our study. While further VBNC-specific detection methodologies would be needed to conclusively exclude VBNCs, our data suggest that they are not present on the healthy murine cornea.

A *caveat* to the present study, is that we cannot exclude the presence of fungi, viruses, or non-viable bacteria on the corneal surface since alkDala did not label these microbes in our studies. Moreover, FISH may not have detected non- viable or dormant bacteria, e.g., if ribosome content was low. Nevertheless, the results of this study support the conclusion that the healthy murine cornea contrasts with the conjunctiva in lacking a resident viable bacterial microbiome. Demonstrating that healthy murine corneas do not host a resident viable bacterial community, commonly present on the conjunctiva, or that are part of other microbiomes, addresses a long-standing knowledge gap in the field, and provides a foundation for a better understanding of corneal homeostasis and disease pathogenesis at the ocular surface. The details of how MyD88 and IL-1R constitutively modulate the absence of a bacterial microbiome on the cornea, and how this is impacted by the environment at the ocular surface, remain to be determined.

## 2.6 Acknowledgements

Our thanks to Dr. John Singer (The University of Maine) for the plasmid construct p67T1 (dTomato), Dr. Greg Barton (University of California, Berkeley) for the gene knockout mice, Dr. Arne Rietsch (Case Western Reserve University) and Dr. Dara Frank (Medical College of Wisconsin) for the *P. aeruginosa* strains and plasmid constructs, and the UC Berkeley DNA Sequencing Facility. This work was supported by the National Institutes of Health; EY011211 (SF), EY007043 (UC Berkeley Vision Science Training Grant), and GM058867 (CB). //

## 2.7 Supplementary Material

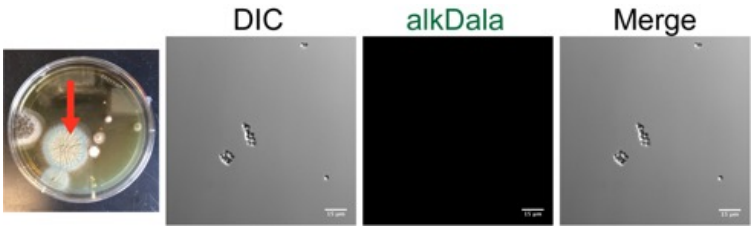


**Figure 2.9:** Supplementary Figure 1. AlkDala labeling was performed on environmental fungi (a mold, red arrow) grown on Sabouraud Dextrose agar. No labeling occurred demonstrating that alkDala is specific to bacteria. Same field of view is shown with different emission filters.

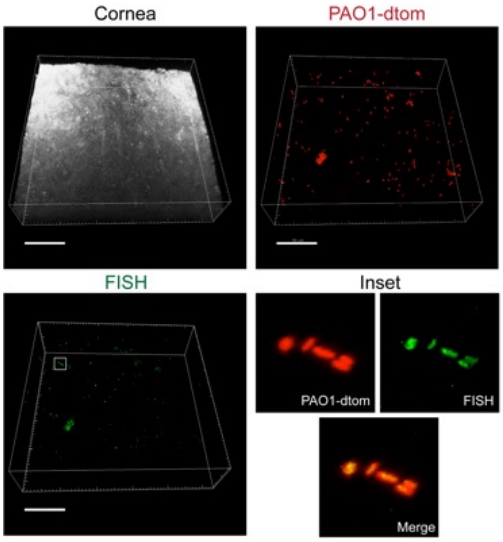


**Figure 2.10:** Supplementary Figure 2. Red-fluorescent *P. aeruginosa* were inoculated onto mouse eyes *ex vivo* for 5 h, and bacteria detected by FISH using a broad-range 16S rRNA gene probe (green). Images are from the same field of view with different emission filters shown. Inset shows zoom of the white box with merge. Scale bar, 50 $\mu$M.

# Chapter 3

# N-glycosylation of the salivary glycoprotein DMBT1 is involved in mediating its inhibition of *Pseudomonas aeruginosa* twitching motility

## 3.1 Abstract

By its scavenging capacity, mucosal fluid glycoprotein DMBT1 helps defend surface epithelia against microbial pathogens. Previously, we showed DMBT1 inhibited *Pseudomonas aeruginosa* twitching motility, a pilus-mediated mechanism of surface movement that contributes to epithelial traversal and virulence. Salivary DMBT1 also bound *P. aeruginosa* pili suggesting an involvement in twitching inhibition. Here, purified salivary DMBT1 was used to study mechanisms involved. Heat-denatured DMBT1 did not inhibit twitching motility and showed reduced pili binding (by ~40%). Lys-C digestion of native DMBT1 to remove and cleave the C-terminal (aa 1813-2413), followed by size-exclusion chromatography, showed only high-Mw fractions retained twitching inhibition. That suggested involvement of the N-terminal (aa 1-1812) containing repeated Scavenger Receptor Cysteine Rich (SRCR) domains with glycosylated SRCR-Interspersed Domains (SIDs). However, individual or pooled consensus-sequence-based peptides (SRCRPs 1 to 7) of the SRCR domains had no effect, and did not bind pili; neither did recombinant DMBT1 (aa 1-220) nor CD163, another SRCR-rich glycoprotein. Enzymatic de-N-glycosylation of DMBT1, but not de-O-glycosylation, significantly reduced the inhibition of twitching motility (by ~57% for colony size), without reducing pili binding. Thus, DMBT1 inhibition of *P. aeruginosa* twitching motility involves its N-glycosylation, but does not involve SRCR domain sequences that bind numerous other bacteria.

## 3.2 Introduction

DMBT1 (Deleted in Malignant Brain Tumors 1) is a 340 kDa glycoprotein that was first isolated from saliva and is involved in mucosal innate immunity (Madsen et al., 2010). It belongs to the highly conserved Scavenger Receptor Cysteine-Rich (SRCR) protein superfamily (Ligtenberg, 2010). From the N-terminal, DMBT1 contains 13 highly homologous SRCR domains separated by SIDs (SRCR-interspersed domains). A 14th SRCR domain is separated from the other 13 by a CUB (C1r/C1s Uegf Bmp1) domain, another of which separates the 14th domain from the ZP (zona pellucida) domain that forms the C-terminal (Bikker et al., 2002; Holmskov et al., 1999). DMBT1 salivary agglutinin (DMBT1$^{SAG}$) has extensively been shown to interact and agglutinate several Gram-positive and Gram-negative bacteria, except for *Pseudomonas aeruginosa* (Brittan and Nobbs, 2015; Hartshorn et al., 2006; Kukita et al., 2013; Ligtenberg et al.; Prakobphol et al., 2000). Similarly, tear fluid DMBT1 was also shown to bind *Staphylococcus aureus*, but not *P. aeruginosa* (Jumblatt et al., 2006).

DMBT1 is expressed in multiple tissues and body fluids and can undergo modifications that affect its function at specific sites (Jumblatt et al., 2006; Madsen et al., 2010). Indeed, there are different human DMBT1 alleles within the population and different isoforms in various tissues due to alternative splicing and post-translational modifications (Ligtenberg et al.; 2010; Madsen et al., 2010; Polley et al., 2015) (Bikker et al., 2017). In salivary-derived DMBT1$^{SAG}$, ~25% of the molecular mass is due to glycosylation (~10 % for N-glycosylation, and ~15% for O-glycosylation) (Holmskov et al., 1997; Oho et al., 1998). Previously, we showed that tear fluid DMBT1, and DMBT1 purified from saliva, play a protective role for mucosal tissues by inhibiting twitching motility of *P. aeruginosa* (Li et al., 2017). In that study, it was also shown that DMBT1 could bind extracted pili suggesting the involvement of pilus interaction in twitching inhibition.

Bacterial twitching motility is a surface-associated movement commonly used by Gram-negative bacteria driven by extension and retraction of Type IV pili (T4P) (Mattick, 2003). In *P. aeruginosa*, the T4P is a polymer predominately made up by the PilA subunit (Leighton et al., 2015). Extension and retraction, required for movement, is powered by ATPases PilB, PilU, and PilT (Persat et al., 2015). In previous studies, we showed that *P. aeruginosa* twitching mutants were defective in host cell exit after cell invasion, exhibited impaired traversal of corneal epithelia *in vitro* (Alarcon et al., 2009), and showed reduced virulence in the injured murine cornea (Zolfaghar et al., 2003). Consistent with those results, in the study above (Li et al., 2017), purified DMBT1 inhibited *P. aeruginosa* from traversing multi-layered cultured epithelial cells *in vitro*, and reduced *P. aeruginosa* virulence in a murine model of corneal infection.

Given the importance of twitching motility for *P. aeruginosa* virulence (Zolfaghar et al., 2003), we sought to further understand mechanisms by which DMBT1 inhibits twitching motility and the relationship to pilus binding. Here, we report structure-function studies using purified salivary DMBT1 (DMBT1$^{SAG}$), enzymatically digested fragments as well as synthetic peptides aimed at identifying molecular domains and characteristics involved mediating this host defense.

## 3.3 Experimental Procedures

### 3.3.1 Bacterial Strains and Culture Conditions

*P. aeruginosa strains* PAO1 was grown on tryptic soy agar (TSA) plates at 37°C for 16 h to obtain "lawn" cultures. A pilin mutant, PAO1-pilA::Tn (Jacobs et al., 2003), that does not express pili and thus lacks twitching motility, was grown on TSA with 60 $\mu$g/mL tetracycline, and was used as a negative control. For twitching motility assays, bacteria were grown on twitching motility Gellan Gum media (TMGG, 0.8 g gellan gum, 0.4 g tryptone, 0.2 g yeast extract, 0.2 g NaCl, 0.1 g MgSO4·7H2O, in 100 mL H2O) at 37°C in a humidified chamber for different times as specified in the results. *Streptococcus pyogenes* (ATCC19615) was grown in Brain and Heart Infusion (BHI) broth at 37°C overnight and used for DMBT1 purification (below).

### 3.3.2 Purification of DMBT1 from Human Saliva

Human saliva was obtained from 4 healthy volunteers under a protocol approved by the Committee for the Protection of Human Subjects, University of California, Berkeley and clarified by centrifugation at 3,800 x g for 10 min. Purification of DMBT1 from saliva was performed as described previously (Kukita et al., 2013; Loimaranta et al., 2005). Briefly, clarified saliva was diluted 50% with PBS. *Streptococcus pyogenes* was incubated in BHI broth overnight at 37°C, collected by centrifugation at 3,800 x g for 5 min, and washed three times with PBS. Bacterial concentration was adjusted to ~5 x$10^9$ CFU/mL. Equal volumes of bacterial suspension and diluted saliva were then mixed and incubated at 37°C for 60 min. Bacterial cells were collected again by centrifugation at 3,800 x g for 5 min, and washed three times with PBS. PBS (1.5 mL) containing 5 mM EDTA was then used to release bound protein at room temperature for 5 min. The bacterial culture was centrifuged at 15,000 x g for 5 min, the supernatant filtered using a 0.22 $\mu$m filter, and then dialyzed (Slide-A-Lyzer dialysis cassettes, Thermo Fisher, NY) against PBS at 4°C overnight. Dialyzed eluate was subjected to gel filtration chromatography on a Superose 6 10/300 GL column (GE Healthcare, CA) equilibrated in PBS (pH 7.4). The eluate at void volume was collected and used as purified DMBT1 from saliva. DMBT1 concentration was measured using a micro BCA protein assay kit (Thermo Scientific, IL, USA).

### 3.3.3 Twitching Motility Assays

Twitching motility was measured using a method modified from the microscope slide assay described previously (Turnbull and Whitchurch, 2014). Bacteria were grown on TSA plates (supplemented with tetracycline if needed) at 37°C for 16 h. Twitching motility Gellan Gum media was dried for 20 min in a sterile airflow (BSL2 Biosafety Cabinet) before use, and then 5 $\mu$L of DMBT1, PBS or other solution was dropped onto the twitching media until completely absorbed. Bacteria grown on TSA were collected, and mixed using a plastic inoculation loop and subsequently inoculated onto the twitching media using a sterile toothpick to achieve a tip-sized inoculum. A glass coverslip was gently placed onto the twitching media to create an "interstitial"

space. The slides were then incubated at 37°C for 4 h unless otherwise stated. After incubation, 5 min time-lapse videos were captured at 10 s intervals via differential interference contrast (DIC) microscopy using a Nikon ECLIPS Ti microscope with a 60 oil-immersion objective at 37°C.

### 3.3.4 Quantification of Twitching Motility

Twitching velocity was measured as the twitching distance of the colony leading edge divided by time as previously described (Li et al., 2017). The bacterial distance traveled in a 5 min video was measured from location in the first slide (Frame 1) to location in the last slide (Frame 31) using ImageJ. Different treatment groups for bacteria were performed in triplicate and ten bacteria were tracked in each video.

### 3.3.5 Dot-immunoblotting to Test Pili Binding to DMBT1 or Other Solutions

To prepare an extract of pili, a suspension of P. aeruginosa PAO1 in PBS was prepared to an $OD_{600}$ of ~10. The suspension was vortexed for 3 min, centrifuged at 15,000 x g for 20 min, and the supernatant collected. $MgCl_2$ solution (1 M) was added to the supernatant to a final concentration of 100 mM, and the supernatant placed at 4°C overnight. After centrifugation at 15,000 x g for 20 min, the pellet was resuspended in PBS (500 $\mu$l) to form a pili-containing extract. The same method was used to prepare a negative control extract of PAO1-pilA::Tn. For dot-immunoblot assays, 2 $\mu$L of DMBT1 in PBS (400 ng/$\mu$L and serial dilutions in PBS) were spotted onto a nitrocellulose membrane (0.2 $\mu$m pore-size, BioRad), along with a PBS control, the pili containing extract from PAO1 (positive control), and the extract from the pilA mutant (negative control). Positive and negative controls were prepared by diluting the respective extracts by 1 in 500 in PBS. After the membrane was dry, it was blocked with 5% BSA for 1 h at room temperature, then washed with PBS for 5 min. The membrane was then incubated with the original (undiluted) pili-containing extract of PAO1 for 40 min at room temperature, then washed 5 times with PBS. Membranes were then probed with anti-PilA primary antibody (1:5000) and Goat anti-Rabbit HRP-conjugated secondary antibody (1:5000). Dot intensity was measured using AlphaView FluoChem HD2 software.

### 3.3.6 Digestion of DMBT1 by Lys-C

Endoproteinase Lys-C (New England BioLabs) was used to digest the carboxyl side of lysine residues of DMBT1 under native conditions according to the manufacturer's instructions. Then, 50 $\mu$L of purified DMBT1 (200 ng/$\mu$L) was incubated with 10 $\mu$L of the Lys-C digestion solution (100 ng/$\mu$L), 10 $\mu$L of PBS, and 2 $\mu$L of Lys-C solution (20 mM Tris-HCL buffer, pH 8.0) at 37°C for 16 h. The sample was separated by size exclusion chromatography on an AKTAmicro system using Superose 6 10/300 GL column (GE Healthcare) with elution in PBS (pH 7.4). To minimize peak broadening, short lengths of 0.15 mm i. d. tubing were used between the injection valve and the fraction collector. Digested DMBT1 was injected onto the column, and fractions of 250

$\mu$L were collected. Protein was detected by UV absorbance at 280 nm. Eluted fractions were pooled according to protein peaks and concentrated using a $\mu$3 kDa cut-off filter (Millipore). Effects on *P. aeruginosa* twitching motility were assessed as described above.

### 3.3.7 SRCR Peptides

Based on the amino acid sequence of DMBT1, a series of individual SRCR domain peptides (SRCRP 1 through 7 were custom-synthesized as previously described (Bikker et al., 2002). Peptides were diluted to 200 $\mu$g/mL in TBS with 10 mM calcium chloride and effects on bacterial twitching motility were tested as described above.

### 3.3.8 Agglutination Assay

Agglutination assays were performed as previously described (Bikker et al., 2002). *S. pyogenes* and *P. aeruginosa* (PAO1) were suspended in TTC (Tris-Buffered Saline containing 0.1% Tween 20 and 1 mM $Ca^{2+}$) to a concentration of ~5 x $10^8$ CFU/mL. Then, 150 $\mu$L of bacteria were mixed with 150 $\mu$L of SRCRP2 solution (200 $\mu$g/mL in Tris-Buffered Saline [TBS] with 10 mM $Ca^{2+}$) in a 96-well plate then incubated for 2 h at 37°C. After agglutination, 10 $\mu$L of the bacteria were transferred on a microscope slide. Bacteria were heat-fixed then stained with crystal violet solution and examined with light microscopy. Buffer alone (TBS with 10 mM $Ca^{2+}$) and purified DMBT1 (200 $\mu$g/mL) were used as controls.

### 3.3.9 Recombinant CD163

Human recombinant CellExp™ CD163 was obtained from BioVision, Inc. (Milpitas, CA, USA). The recombinant protein has a reported Mw of 135-140 kDa due to glycosylation. For use in experiments, CD163 was resuspended in PBS to a final concentration of 200 ng/$\mu$L. Effects on *P. aeruginosa* twitching motility were tested as above.

### 3.3.10 Enzymatic Deglycosylation

A deglycosylation enzyme mix (Biolabs) was used to digest DMBT1 under native conditions. For each enzyme (PNGase F, O-Glycosidase, Neuraminidase, $\beta$1-4 Galactosidase, $\beta$-N-acetylglycosaminidase), 5 $\mu$L was used to make the enzyme mix and incubated with 20 $\mu$L of purified DMBT1 (250 ng/$\mu$L) at 37°C for 48 h. For complex de-O-glycosylation, 25 $\mu$L of purified DMBT1 (200 ng/$\mu$L) was incubated with 10X glycobuffer 2 (2 $\mu$L), enzyme mix (Neuraminidase, $\beta$1-4 Galactosidase, $\beta$-N-acetylglucosaminidase, and O-Glycosidase) (5 $\mu$L each) at 37°C for 2 h. To remove N-linked glycans, 15 $\mu$L of purified DMBT1 (200 ng/$\mu$L) was incubated with 10X glycobuffer 2 (3 $\mu$L), PNGase F (5 $\mu$L) and H2O (7 $\mu$L) at 37°C for 48 h.

### 3.3.11 Statistical Analysis

Data were expressed as a mean ± standard error of mean (SEM) unless otherwise stated. The significance of differences between multiple groups was assessed using a two-way ANOVA with Tukey's multiple comparisons for post-hoc analysis, or using a one-way ANOVA with Tukey's or Dunnett's multiple comparisons. The Kruskal-Wallis test with Dunn's multiple comparisons was used for nonparametric data. P values of less than 0.05 were considered significant.

## 3.4 Results

### 3.4.1 DMBT1 inhibition of *P. aeruginosa* twitching motility is lost and pili binding reduced after heat denaturation

Previously, we showed that DMBT1 purified from human saliva inhibited *P. aeruginosa* (PAO1) twitching motility and could also bind to extracted pili (Li et al., 2017). To determine if these activities were heat-stable, purified salivary glycoprotein DMBT1 was boiled for 10 min at 95°C. This protein-denaturing treatment abrogated DMBT1 inhibition of twitching motility (as measured by twitching velocity) (Figure 3.1A) suggesting that glycoprotein conformation is important for this activity. Furthermore, the anti-PilA dot-blot and its quantification showed that boiled DMBT1 exhibited reduced ability to bind extracted pili (~40%) compared to untreated DMBT1 (Figure 3.1B, C). Although the reduction of pili binding after heat denaturation was not statistically significant, the data suggest that DMBT1 binding to pilin is optimal in its native conformation.

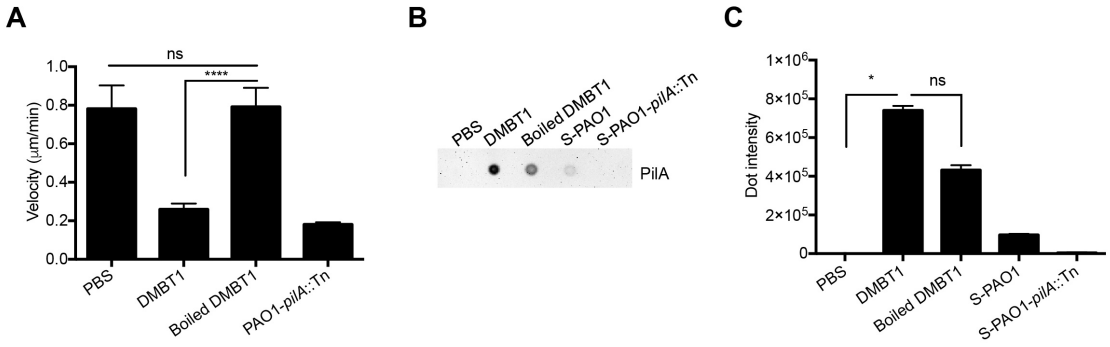


**Figure 3.1:** Boiled DMBT1 does not inhibit *P. aeruginosa* twitching motility. DMBT1 (100 ng/$\mu$L) was heated at 95°C for 10 min to denature the protein. (A) Boiled DMBT1 lost inhibitory activity against *P. aeruginosa* PAO1 twitching velocity. Data are shown as the mean ± SEM per sample from three independent experiments. One-way ANOVA with Tukey's post-hoc analysis, ****, P < 0.0001; ns, not significant. (B) Dot-immunoblot assay using anti-PilA antibody to show binding of PAO1 pili to DMBT1 or boiled DMBT1 after 40 min incubation with a pili-containing extract from PAO1. Diluted pili extracts from PAO1 (S-PAO1) or similarly diluted extracts from its pilA mutant (S-PAO1-pilA::Tn) served as controls (see Methods), along with PBS alone. A representative experiment of two independent experiments is shown. (C) Quantification of dot-intensity from the dot-immunoblot assay shown in panel B. Data are shown as the mean ± SEM of triplicate measurements from each sample. Kruskal-Wallis test with Dunn's multiple comparisons, *, P < 0.05; ns, not significant.

### 3.4.2 Lys-C endoproteinase digestion of DMBT1 does not abolish inhibition of twitching motility

To further investigate the role of different DMBT1 domains in the inhibition of *P. aeruginosa* twitching motility, purified salivary DMBT1 was enzymatically digested with Lys-C, an endoproteinase. Others have shown that DMBT1 contains 10 lysine residues located in the C-terminal region (Bikker et al., 2002). As such, Lys-C digestion should produce a large fragment containing the majority of SRCR domains and SRCR Interspersed Domains (SIDs) in addition to several smaller fragments (Figure 3.2A). Lys-C digested DMBT1 inhibited *P. aeruginosa* twitching motility as effectively as the native purified glycoprotein (Figure 3.2B). Size exclusion chromatography of Lys-C digested DMBT1 under native buffer conditions showed an expected pattern of fractionation (Figure 3.2C). Each Lys-C digested DMBT1 fraction obtained under native buffer conditions was tested for inhibition of *P. aeruginosa* twitching motility. Only Fraction 1, expected to contain fragments of combined high molecular-weight SRCR/SID domains (aa 1-1812), along with intact DMBT1, inhibited bacterial twitching motility (Figure 3.2D), suggesting that the SRCR/SID components of DMBT1 were required, and showing that smaller fragments of the C-terminal region produced by Lys-C digestion were ineffective.

### 3.4.3 Evaluation of DMBT1 SRCR domains, its N-terminal peptide, and CD163

Fraction 1 of Lys-C digested DMBT1 should have contained high-molecular weight fragments consisting of combined multiple SRCR/SID domains (aa 1-1812). Thus, a series of custom-synthesized peptides (SRCRP) spanning the consensus sequence of the DMBT1 SRCR domains (Bikker et al., 2002) were tested. Indeed, SRCRP2 has previously been shown to be involved in bacterial binding (Bikker et al., 2002). However, each of the individual SRCR consensus-based peptides tested (SRCRPs 1-7) had no effect on *P. aeruginosa* twitching motility (Figure 3.3A, B), and no inhibition was observed when these peptides were pooled (Figure 3.3A, B). It was also confirmed that (pooled) SRCR peptides (1-7) did not bind pili (Figure 3.3C). A control experiment confirmed previous findings that SRCRP2 caused agglutination/aggregation of *Streptococcus* spp. (shown here using *Streptococcus pyogenes*) (Bikker et al., 2002), but not *P. aeruginosa* (Figure 3.3D). As we have shown previously, (Li et al., 2017) purified salivary DMBT1 inhibited *P. aeruginosa* twitching motility (Figure 3.3A, B), but did not cause bacterial agglutination/aggregation (Figure 3,3D). Thus, exposing *P. aeruginosa* to the consensus sequence of the DMBT1 SRCR domains (albeit in fragments) was insufficient to inhibit twitching motility, or to bind extracted pili, supporting our previous hypothesis (Li et al., 2017) that DMBT1 inhibition of *P. aeruginosa* twitching motility involves a different type of bacterial cell interaction than shown for other bacterial species (Bikker et al., 2002).

Since Fraction 1 of Lys-C digested DMBT1 would also contain the N-terminal region (albeit as part of a large fragment containing multiple SRCRs/SIDs), a recombinant truncated peptide consisting of the N-terminal domain of DMBT1 (Met1-Ser 220) (Figure 3.4A) was tested. However,

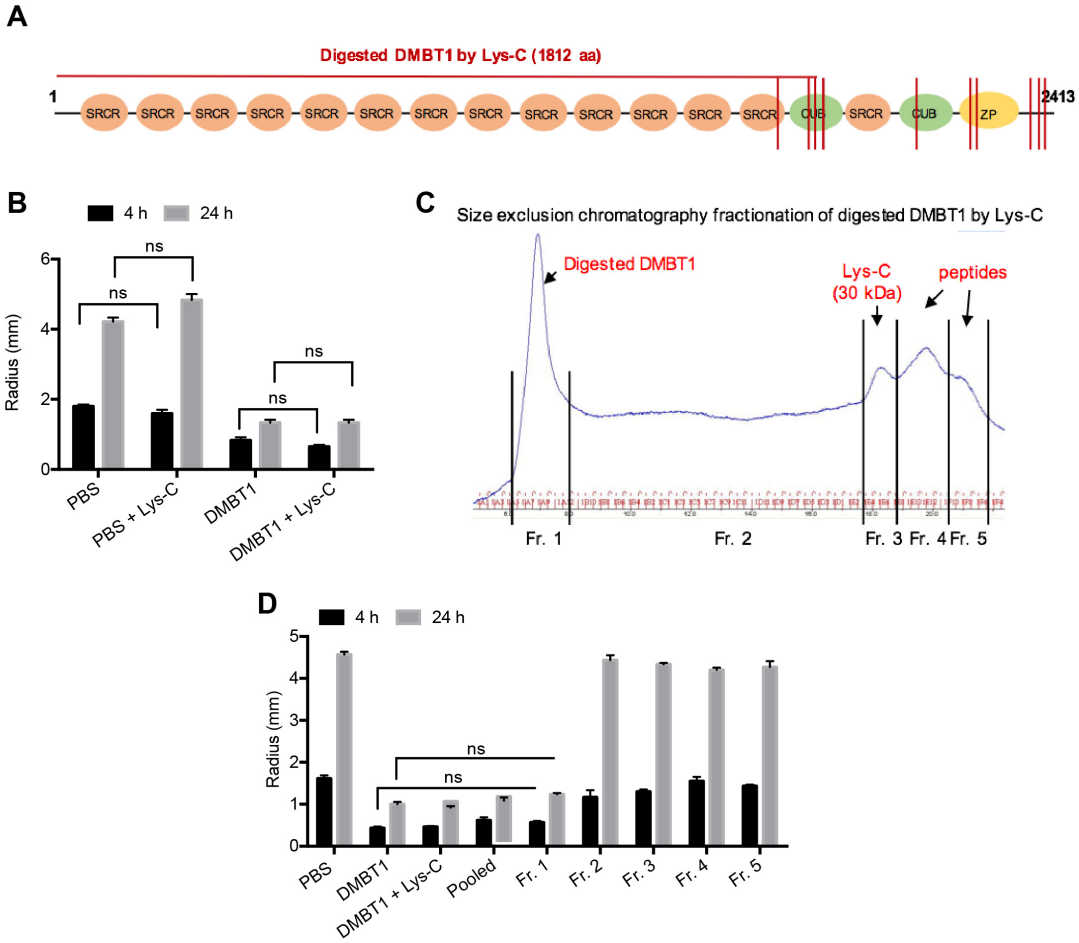


**Figure 3.2:** DMBT1 digested by Lys-C under native conditions inhibits *P. aeruginosa* twitching motility. (A) Schematic representation of human salivary DMBT1 with 14 scavenger receptor cysteine-rich (SRCR) domains, 2 CUB domains, and the Zona Pellucida (ZP) domain, showing endoproteinase Lys-C cleavage sites (red lines). (B) Effect of Lys-C digested DMBT1 (100 ng/$\mu$L) versus a DMBT1 control on colony size of P. aeruginosa strain PAO1 after 4 h and 24 h incubation Two-way ANOVA with Tukey's multiple comparisons, ns, not significant. (C) Size exclusion chromatography separation of Lys-C digested DMBT1. Fraction 1 contains high molecular-weight fragments (including aa 1-1812). (D) Colony size of *P. aeruginosa* after 4 h and 24 h incubation in different fractions of Lys-C digested DMBT1. Only fraction 1 inhibited *P. aeruginosa* twitching motility, similar to DMBT1. Two-way ANOVA with Tukey's multiple comparisons, ns, not significant.

this recombinant N-terminal peptide had no effect on twitching motility (Figure 3.4B), and did not bind pili (Figure 3.4C).

CD163 was also tested for inhibition since it is a member of the SRCR-superfamily (Figure 3.5A). Moreover, this plasma membrane glycoprotein is expressed on monocytes and macrophages and functions as a receptor for bacteria, resulting in the expression of proinflammatory cytokines (Fabriek et al., 2009). However, results showed that recombinant human CD163 had no effect on *P. aeruginosa* twitching motility (Figure 3.5B, C), despite considerable similarities in structure, i.e. multiple SRCR/SID regions, to DMBT1.

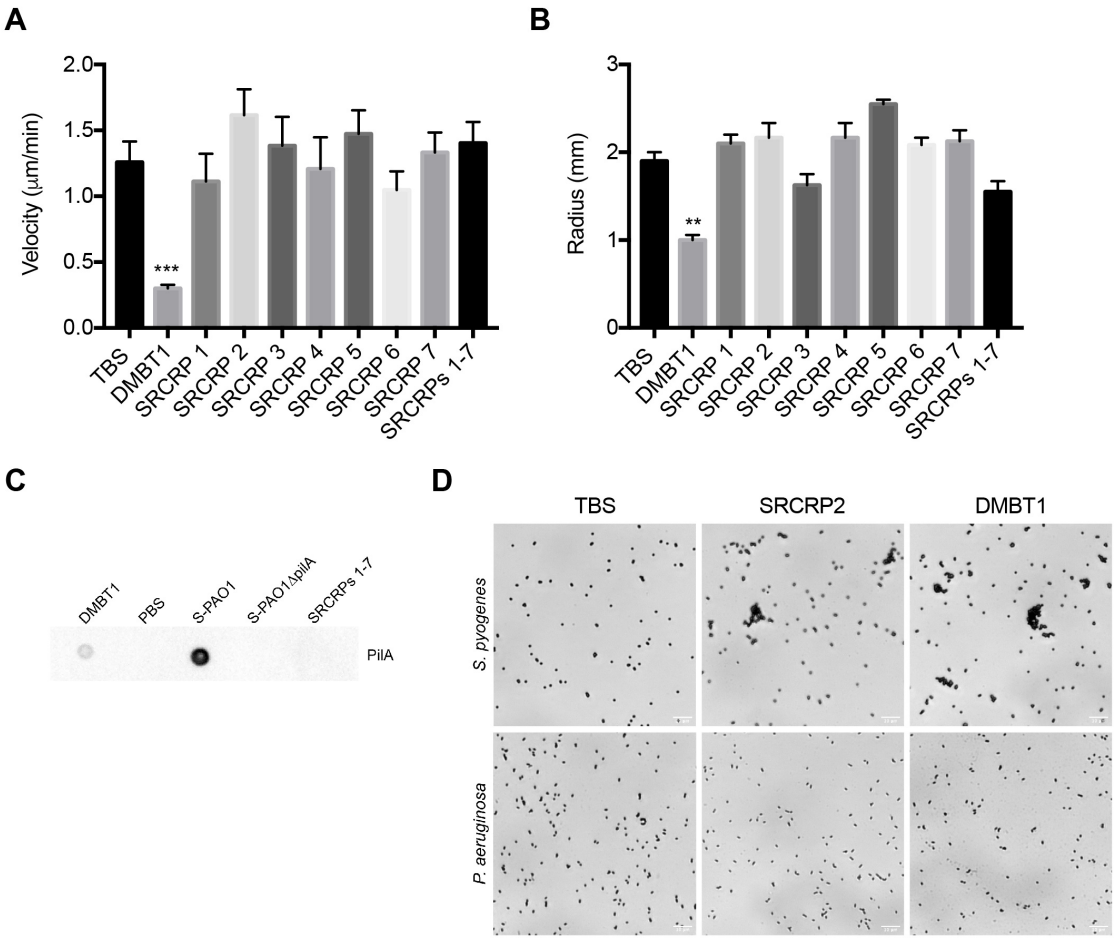


**Figure 3.3:** Effect of conserved peptides SCRCP 1-7 (200 ng/$\mu$L diluted in TBS with 10 mM $CaCl_2$) on (A) twitching velocity, and (B) colony size, of *P. aeruginosa* strain PAO1 after 4 h. Data are shown as the mean ± SEM. Experiments were performed in triplicate and significance determined using one-way ANOVA with Dunnett's multiple comparisons test. ***, P < 0.001, **, P < 0.01. None of the peptides showed a significant difference versus the TBS control. (C) Dot-immunoblot assay using anti-PilA antibody shows the binding of PAO1 pili to DMBT1, but not to pooled SRCRPs 1-7. Diluted pili extracts from PAO1 (S-PAO1) or those from its pilA mutant (S-PAO1-pilA::Tn) and PBS were used as controls. (D) Agglutination assay showing that purified salivary DMBT1, and the custom-made consensus peptide SRCRP2, agglutinate/aggregate *Streptococcus pyogenes* (upper panels) as previously shown (Bikker et al., 2002) , but not *P. aeruginosa* (lower panels), versus TBS controls.

### 3.4.4 N-glycosylation of DMBT1 is important for its inhibition of *P. aeruginosa* twitching motility

Having established that inhibition of twitching motility resided in high molecular-weight fractions of Lys-C digested DMBT1 containing the N-terminal region and combined SRCR/SID domains (aa 1-1812), but without finding activity on individual SRCR peptides of DMBT1 or proteins with similar SRCR composition, we studied if post-translational modifications were involved. Since DMBT1 is a highly-glycosylated protein (Holmskov et al., 1999), we postulated that glycosylation was involved in twitching inhibition. To test this, DMBT1 was digested by a deglycosylation enzyme mix containing N-glycosidase PNGase F, O-glycosidase, neuraminidase,

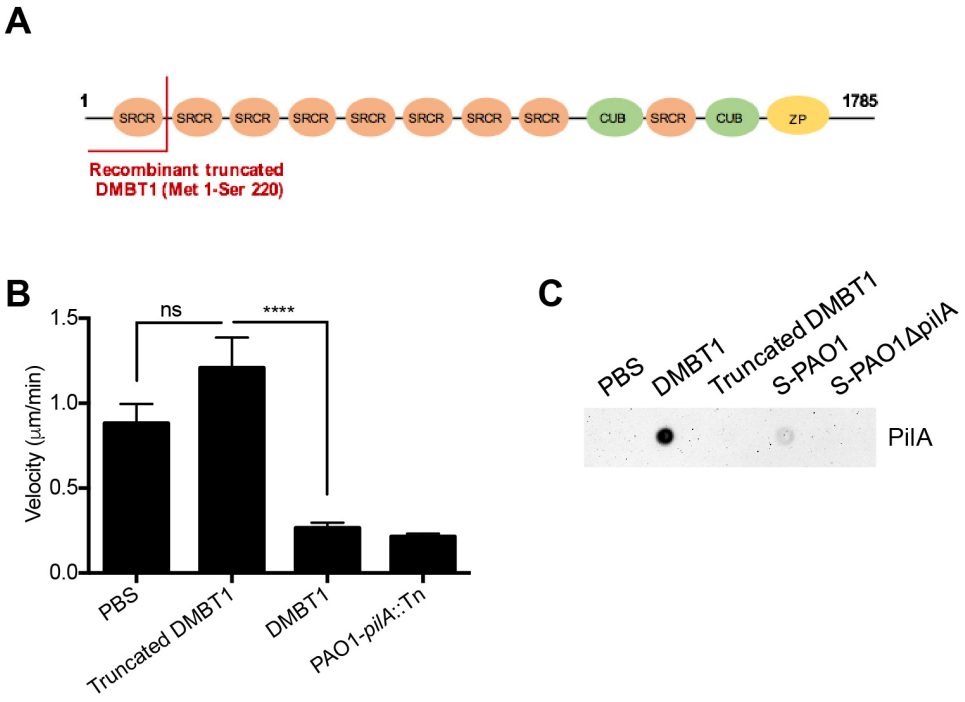


**Figure 3.4:** Recombinant DMBT1 (Met 1-Ser 220) has no effect on *P. aeruginosa* twitching motility. (A) Schematic representation of recombinant truncated human DMBT1 (NP_004397.2) (Met 1-Ser 220) shown in the primary sequence of DMBT1 with 9 scavenger receptor cysteine-rich (SRCR) domains, 2 CUB domains and Zona pellucida (ZP) domain. (B) Effect of truncated DMBT1 (100 ng/$\mu$L) on twitching velocity of *P. aeruginosa* strain PAO1 after 4 h. PAO1-pilA::Tn served as a negative control. One-way ANOVA with Tukey's multiple comparisons test, ****, $P < 0.0001$. (C) Dot-immunoblot assay using anti-PilA antibody shows binding of extracted PAO1 pili to DMBT1, but not truncated DMBT1. Pili extracts from PAO1 (S-PAO1), extracts from the pilA mutant (S-PAO1-pilA::Tn), both diluted 1 in 500 in PBS were used as controls, along with PBS alone.

exoglycosidase $\beta$1-4 galactosidase, and $\beta$-N-acetylglucosaminidase under native conditions to remove all N-linked and simple O-linked glycans, as well as some complex O-linked glycans (see Methods). After deglycosylation, DMBT1 showed significantly reduced inhibition activity of *P. aeruginosa* twitching motility compared to native DMBT1 controls, as measured by twitching velocity ($P < 0.001$, Figure 3.6A) and colony size ($P < 0.001$ at 24 h, Figure 3.6B). Examination of colony size data at 24 h indicated that full O- and N deglycosylation of DMBT1 reduced its ability to inhibit twitching motility by ~41 % (Figure 3.6B). However, deglycosylated DMBT1 still bound to pili as shown by dot-immunoblot assay (Figure 3.6C, D). These results suggest that the glycosylation of DMBT1 is involved in the inhibition of *P. aeruginosa* twitching motility. However, observation that reduced DMBT1-mediated twitching inhibition did not correlate with any reduction in pili binding suggests that additional (or other) mechanisms may be involved.

We next explored if the type of DMBT1 glycosylation linkage was important by selectively targeting O-linked versus N-linked moieties. The involvement of O-glycosylation in DMBT1 inhibition of twitching activity was studied with an O-glycan targeted enzyme mix (O-glycosidase, neuraminidase, exoglycosidase $\beta$1-4 galactosidase, and $\beta$-N-acetylglucosaminidase) under native conditions. No significant difference was found between DMBT1 and de-O-glycosylated

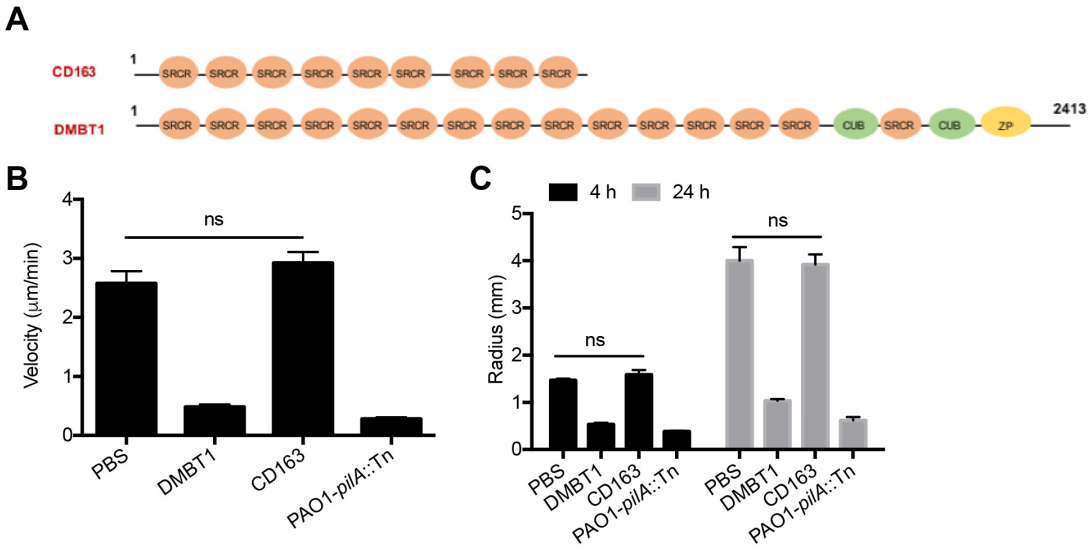


**Figure 3.5:** Glycoprotein CD163 does not inhibit *P. aeruginosa* PAO1 twitching motility. (A) Schematic representation of CD163 as expressed in HEK 293 cells (BioVision, Inc.) compared to human salivary DMBT1. (B) Effect of CD163 (200 ng/$\mu$L) on twitching velocity of *P. aeruginosa* PAO1 after 4 h treatment (One-way ANOVA with Tukey's multiple comparisons, ns, not significant), and (C) on colony size after 4 h and 24 h. PAO1-pilA::Tn served as a negative control. Significance determined using two-way ANOVA with Tukey's multiple comparisons, ns, not significant.

DMBT1 on twitching inhibition (Figure 3.7 A, B). The same results were obtained using longer incubation times with bacteria (from 24 to 48 h), and/or higher concentrations of deglycosylation enzymes (data not shown). According to the manufacturer's (Biolabs) documentation, this combination of enzymes may not remove all O-linked oligosaccharides, but should remove many common oligosaccharide structures under native conditions. Since denatured DMBT1 lost inhibition of twitching motility (Figure 3.1A), denatured de-O-glycosylation could not be used to completely remove O-linked glycans. Nevertheless, the results suggest that simple O-glycosylation is not involved in DMBT1 inhibition of *P. aeruginosa* twitching motility.

To study if complex DMBT1 O-glycosylation could be involved in twitching motility inhibition, DMBT1 was digested with neuraminidase, $\beta$1-4 galactosidase, or $\beta$-N-acetylglucosaminidase in a different (more optimal) digestion buffer (50 mM sodium acetate, 0.5 mM CaCl2, pH 5.5). However, none of these complex de-O-glycosylation treatments of DMBT1 had a significant effect on its ability to inhibit twitching motility, although $\beta$1-4 galactosidase appeared to have some effect (Figure 3.7C). Thus, the data suggest that complex O-glycosylation of DMBT1 was also not required for inhibition of twitching motility.

Purified DMBT1 was digested with PNGase F as well in order to remove N-linked glycans in native buffer. De-N-glycosylation enzyme treatment of DMBT1 significantly reduced its ability to inhibit *P. aeruginosa* twitching motility compared to DMBT1 (Figure 3.8A, B). Examination of colony size data at 24 h indicated that de-N-glycosylation of DMBT1 reduced its ability to inhibit twitching motility by ~57% (Figure 3.6B). Thus, the extent to which DMBT1 de-N-glycosylation reduced twitching motility inhibitory activity versus untreated DMBT1 was similar to, if not greater than, that observed with non-specific deglycosylation (Figure 3.6A, B). Thus, these

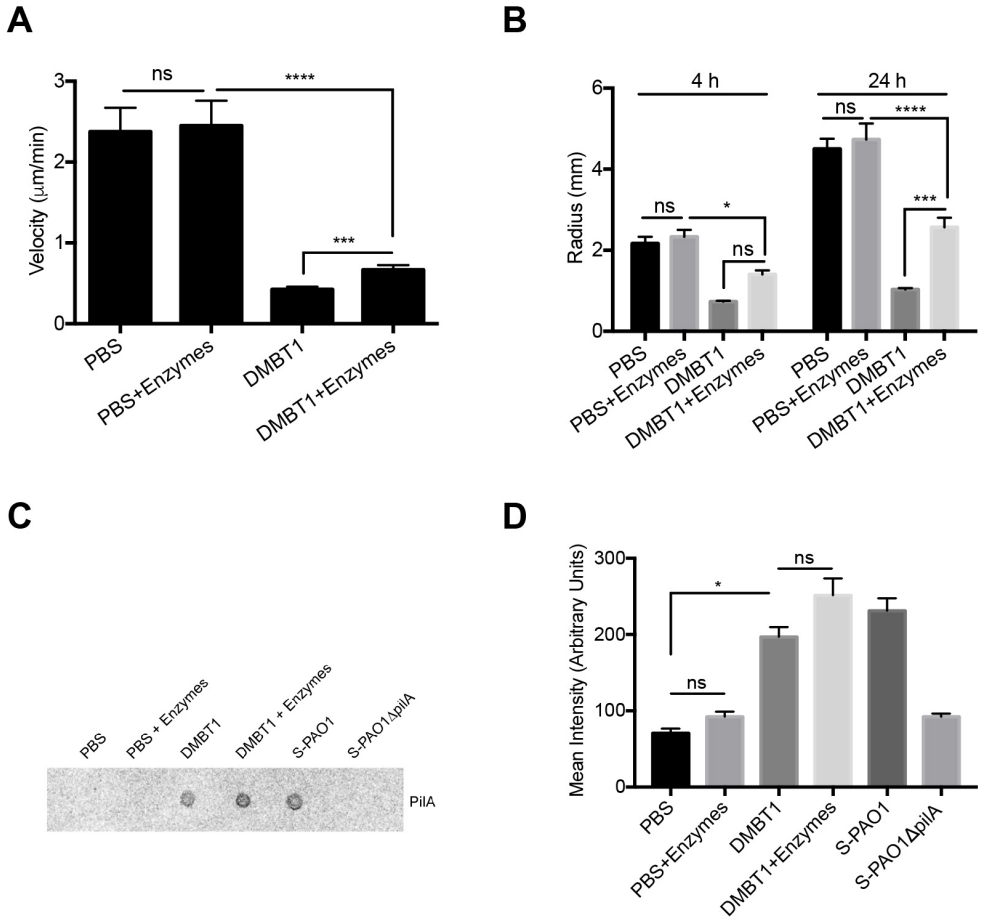


**Figure 3.6:** DMBT1 glycosylation is involved in inhibition of *P. aeruginosa* twitching motility. Effect of DMBT1 digested by deglycosylation enzymes on (A) twitching velocity of *P. aeruginosa* PAO1 after 4 h, and (B) colony size of *P. aeruginosa* PAO1 after 4 h and 24 h. Data are shown as the mean ± SEM per sample from three independent experiments. Significance was determined using one-way ANOVA (panel A) or two-way ANOVA (panel B) each with Tukey's multiple comparisons, ****, $P < 0.0001$; ***, $P < 0.001$; *, $P < 0.05$; ns, not significant. (C) Dot-immunoblot assay with anti-PilA antibody shows continued binding of PAO1 pili to DMBT1 after deglycosylation digestion. Pili extracts from PAO1 (S-PAO1), extracts from the pilA mutant (S-PAO1-pilA::Tn), both diluted 1 in 500 in PBS were used as controls, along with PBS alone. (D) Quantification of dot-intensity using ImageJ from the dot-immunoblot assay shown in panel C. Data are shown as the mean ± SEM of duplicate measurements from each sample. Significance determined used Kruskal-Wallis test with Dunn's multiple comparisons, *, $P < 0.01$; ns, not significant.

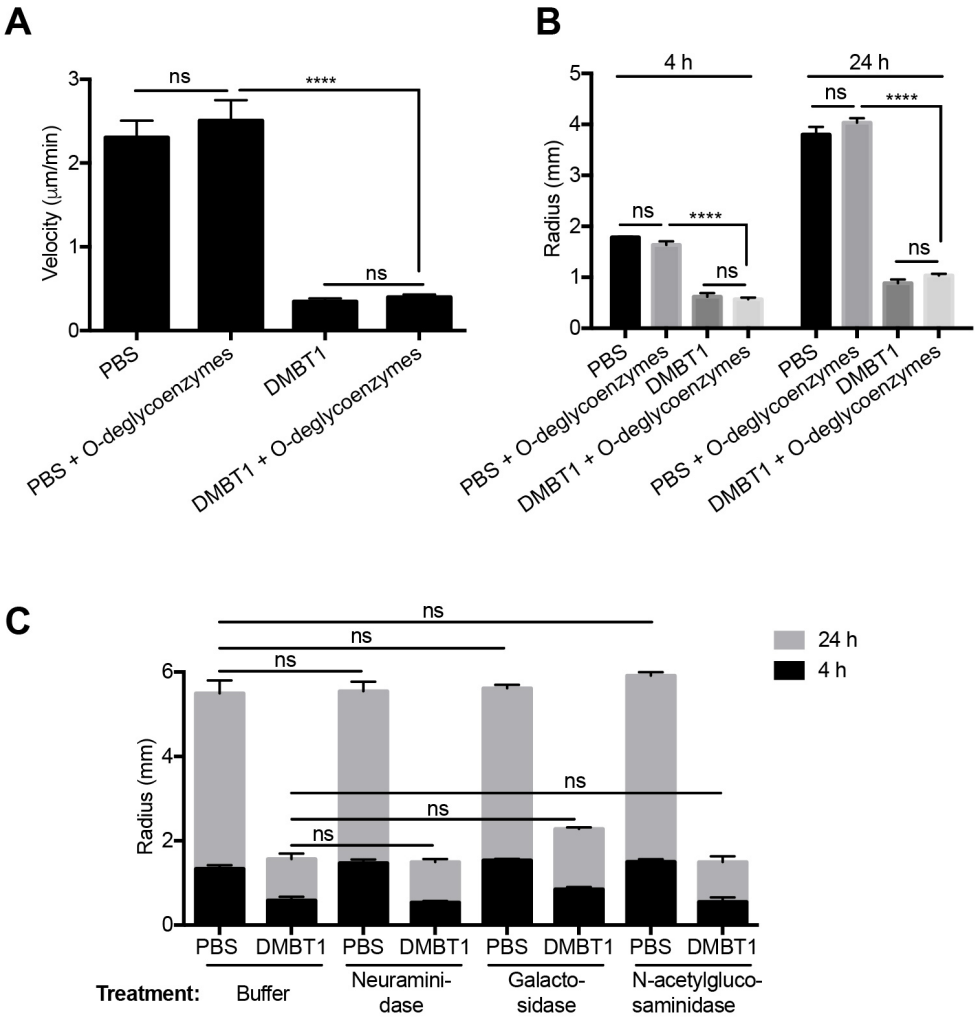


**Figure 3.7:** O-Glycosylation of DMBT1 does not contribute to inhibition of bacterial twitching motility. (A) Effect of DMBT1 digested by an O-deglycosylation enzyme mix on twitching velocity of *P. aeruginosa* PAO1 after 4 h. DMBT1 (100 ng/$\mu$L) was digested by a mixture of O-deglycosylation enzymes (O-glycosidase, Neuraminidase, Galactosidase and N-acetyl-glucosaminidase) at 37°C for 2 days in native glycobuffer (50 mM sodium phosphate, pH 7.5) to remove complex O-glycosylation of DMBT1. PBS and DMBT1 diluted with same volume of glycobuffer served as controls. (B) Effects of DMBT1 digested by the O-deglycosylation enzyme mix on colony size of *P. aeruginosa* PAO1 after 4 h and 24 h. (C) Effects of differently digested DMBT1 on colony size of P. aeruginosa PAO1 after 4 h and 24 h. DMBT1 (100 ng/$\mu$L) was digested by Neuraminidase (desialylation glycosidase), Galactosidase or N-acetylglucosaminidase (both exoglycosidases) at 37°C for 2 h in glycobuffer (50 mM sodium acetate, 0.5 mM $CaCl_2$, pH 5.5) to remove sialic acid residues and other complex glycosylation of DMBT1. PBS and DMBT1 diluted with same volume of glycobuffer served as controls. Data shown as the mean ± SEM per sample from three independent experiments. Significance was determined using one-way ANOVA (panel A) or two-way ANOVA (panel B) each with with Tukey's multiple comparisons, ****, $P < 0.0001$; ns, not significant.

data suggest that N-glycosylation of DMBT1 is involved in the inhibition of twitching motility. However, de-N-glycosylated DMBT1 still showed a significant inhibition of twitching motility compared to PBS-enzyme controls (Figure 3.8A, B), suggesting that N-glycosylation of DMBT1 is only partly involved in twitching inhibitory activity, and other molecular characteristics are also

required. Furthermore, de-N-glycosylated DMBT1 still bound to pili similarly to native DMBT1 (Figure 3.8C, D), suggesting that factors additional to, or instead of, direct pilus interaction are needed.

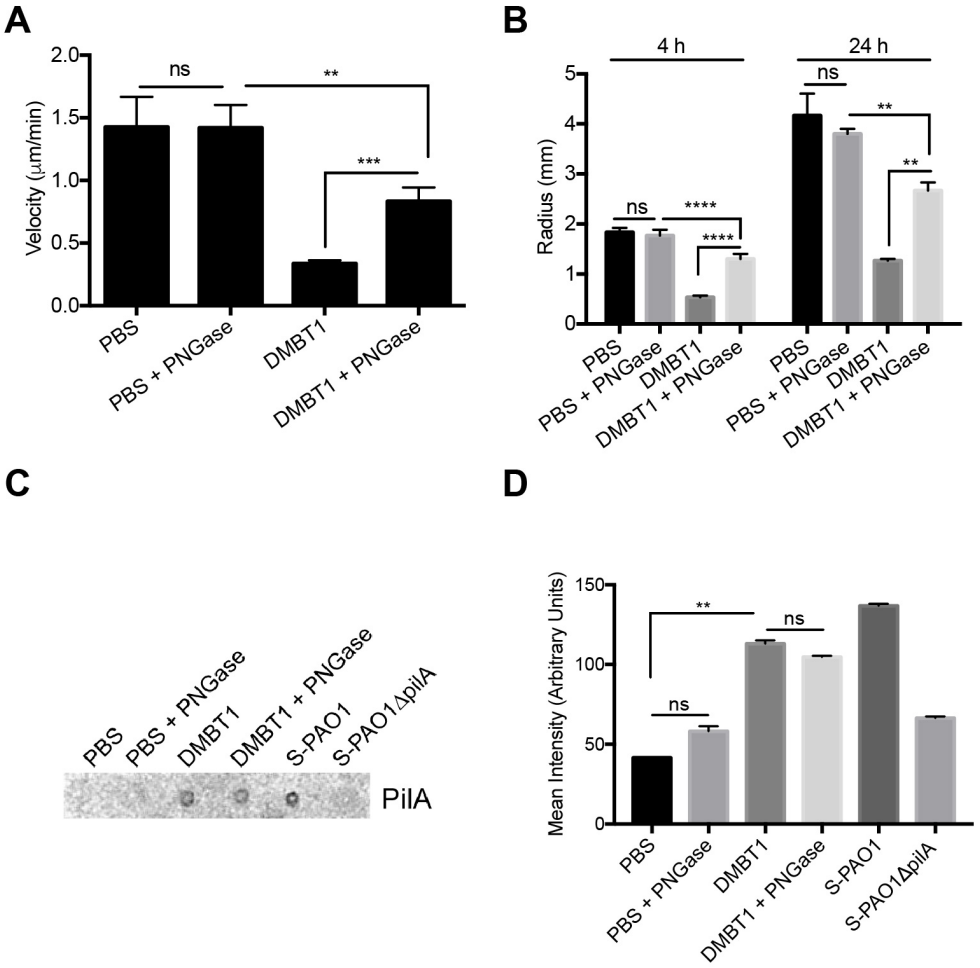


**Figure 3.8:** DMBT1 inhibition of *P. aeruginosa* twitching motility involves its N-Glycosylation. DMBT1 (100 ng/$\mu$L) was digested by PNGase F (glycerol-free) at 37°C for 2 days in native glycobuffer (50 mM sodium phosphate, pH 7.5) to remove N-glycosylation of DMBT1. PBS and DMBT1 diluted with same volume of native glycobuffer, and PBS treated with same volume of PNGase served as controls. (A) Effect of DMBT1 digested by PNGase F on twitching velocity of *P. aeruginosa* PAO1 after 4 h. (B) Effects of DMBT1 digested by PNGase F on colony size of *P. aeruginosa* PAO1 after 4 h and 24 h. Data are shown as the mean ± SEM per sample from three independent experiments. Significance was determined using one-way ANOVA (panel A) or two-way ANOVA (panel B) each with Tukey's multiple comparisons, ****, $P < 0.0001$; ***, $P < 0.001$; **, $P < 0.01$; ns, not significant. (C) Dot-immunoblot assay using anti-PilA antibody showing the binding of PAO1 pili to DMBT even after PNGase F digestion. Pili extracts from PAO1 (S-PAO1), extracts from the pilA mutant (S-PAO1-pilA::Tn), both diluted 1 in 500 in PBS were used as controls, along with PBS alone. (D) Quantification of dot-intensity using ImageJ from the dot-immunoblot assay shown in panel C. Data are shown as the mean ± SEM of duplicate measurements from each sample. Significance determined used Kruskal-Wallis test with Dunn's multiple comparisons, **, $P < 0.01$; ns, not significant.

## 3.5 Discussion

Previously, we showed that the glycoprotein DMBT1 in human tear fluid, and purified from human saliva, inhibited twitching motility of *P. aeruginosa* and consequently prevented bacterial traversal through human corneal epithelial cells in vitro, and reduced disease in a murine model of corneal infection (Li et al., 2017). Here, we focused on determining how salivary DMBT1 (DMBT1$^{SAG}$) inhibited twitching motility using structure-function studies. Results showed that the ability of salivary DMBT1 to inhibit twitching motility was removed by heat denaturation, correlating with a reduction in binding to purified pili. Results also showed that Lys-C digestion of DMBT1 had no effect on twitching inhibition, the activity residing in high molecular-weight fractions after Lys-C digestion. Moreover, no effect on twitching inhibition was observed for custom-synthesized individual or pooled SRCR derived peptides, recombinant N-terminal DMBT1, nor the SRCR-SID rich glycoprotein CD163. However, experiments using enzymatic deglycosylation of DMBT1 showed that the inhibition of twitching motility was partially, but significantly, associated with N-glycosylation, but not O-glycosylation, and that loss of inhibitory activity after de-N-glycosylation did not correlate with a reduction in binding to purified pili.

The finding that heat denatured salivary DMBT lost its ability to inhibit *P. aeruginosa* twitching motility suggests that structural conformation is important for this activity. Indeed, the result is consistent with our previous results with tear fluid containing DMBT1, which also lost its inhibitory effects on twitching motility heat denaturation (Li et al., 2017). In addition to loss of structural conformation, loss of inhibitory activity after heat denaturation could include the compromise of DMBT1 moieties that normally bind bacterial ligands. Indeed, heat denaturation did cause reduced DMBT1 binding to pili extracts from *P. aeruginosa*. Heat denaturation may also cause a loss of DMBT1-associated molecules that mediate, or help-mediate, twitching inhibition. However, in our previous study, mass spectrometry analysis of purified salivary DMBT1 did not reveal any known DMBT1-associated innate defense molecules (Li et al., 2017), suggesting this possibility is less likely.

Digestion of saliva-purified DMBT1 with Lys-C followed by size exclusion chromatography, suggested that the SRCR/SID domains of salivary DMBT1 were essential for the inhibition of *P. aeruginosa* twitching motility, i.e. high-Mw fragments of the N-terminal (aa 1-1812). That result would be consistent with a previous study in which Lys-C digestion of salivary DMBT1 revealed that binding of *Streptococcus mutans* was associated with SRCR/SID domains 19. In that study, and a subsequent study, a series of custom-synthesized peptides that together span the 109 amino acid consensus sequence of the SRCR domains of salivary DMBT1 were used to identify specific bacterial binding regions. SRCR-mediated DMBT1 binding of *S. mutans* and many other bacteria, e.g. *Staphylococcus aureus*, *Escherichia coli*, and *Helicobacter pylori*, was specifically localized to a 16 amino acid peptide designated SRCRP2 (Bikker et al., 2002; 2004). In our study, however, SRCRP2 did not inhibit *P. aeruginosa* twitching motility, nor did it bind pili extracts. Controls also confirmed that SRCRP2 could agglutinate *Streptococcus* spp. as previously shown (Bikker et al., 2002; Wu et al., 2006), but not *P. aeruginosa*. Moreover, none of the other

SRCR peptides representing other regions of the SRCR domain consensus sequence had any effect either individually or pooled. Of course, these findings do not preclude involvement of the SRCR domains in DMBT1-mediated inhibition of *P. aeruginosa* twitching motility, e.g. use of peptides with a different sequence from the SRCR domain consensus sequence may be needed. Alternatively, SID domains may be required by themselves, or to bridge a series of SRCR domains. For example, a region of the N-terminal domain of DMBT1 containing one SRCR and half of its neighboring SID binds HIV-1 gp-120 to exert antiviral effects(Wu et al., 2006). Moreover, similar molecules to DMBT1 with multiple, connected SRCR domains, e.g. CD163 expressed on tissue macrophages, also bind multiple different bacteria triggering release of proinflammatory mediators (Fabriek et al., 2009). However, neither recombinant N-terminal DMBT1 (aa 1- 220) nor recombinant CD163 had any effect on *P. aeruginosa* twitching, nor did they bind pili extracts. Again, this does not preclude an involvement of the N-terminal domain of DMBT1 with multiple SRCR domains and their respective SIDs, in the inhibition of *P. aeruginosa* twitching motility, but does suggest that it involves DMBT1-bacterial cell interaction(s) that differ from those reported for numerous other Gram-positive and Gram-negative bacteria.

It is also possible that the activity of high-Mw fractions of Lys-C digested DMBT1 reflect the presence of residual undigested DMBT1, since it is very difficult to separate undigested native DMBT1 from other high-Mw fragments, and heat denaturation removes its twitching inhibitory activity. Even if residual DMBT1 were present, however, that would not change the above conclusion that the mechanism(s) of twitching motility inhibition likely involve a different type of DMBT1 interaction with *P. aeruginosa* than reported for other bacteria. Moreover, lack of activity of smaller-Mw fractions of Lys-C digested DMBT1 does show that the C-terminal fragments generated by Lys-C digestion were, by themselves, insufficient for twitching inhibition. That finding, in turn, suggests that twitching inhibition does not involve the two CUB domains and ZP domain of DMBT1.

Enzymatic deglycosylation of salivary DMBT1 did result in a partial reduction in twitching motility, which appeared to be specifically associated with the removal of N-glycosylated residues (~46% reduction in DMBT1 effects on bacterial twitching velocity, and a ~57% reduction in effects on bacterial colony size). While only a partial reduction in twitching inhibitory effects, the data show that N-glycosylation of DMBT1 is important for inhibition of *P. aeruginosa* twitching motility. N-linked glycosylation is known to be critical for general protein stability and dynamics (Daniels et al., 2003; Li et al., 2016; Petrescu et al., 2004). Indeed, the precise location of N-glycans are significant for activity (Li et al., 2016). This could help to explain why CD163, a SRCR/SID containing bacterial receptor protein very similar to DMBT1 with many N-glycans, did not inhibit twitching of *P. aeruginosa*. For respiratory mucosal fluid-derived DMBT1 (gp-340) there are 14 potential sites of N-linked glycosylation 22, only 4 of which reside within the N-terminal fragment of DMBT1 formed after Lys-C digestion. However, despite our data implicating SRCR/SID domains of DMBT1 (aa 1-1812) in twitching motility inhibition, and the absence of effects of C-terminal DMBT1 fractions obtained after Lys-C digestion (Figure 3.2), it remains possible that C-terminal N-glycosylation (9 sites between aa 1813-2413) could also play a role. Interestingly, while not specific to DMBT1, N-glycans of tear proteins have been implicated in mediating their binding to clinical ocular isolates of *P. aeruginosa* (Kautto et al.,

2016). As such, further investigation is warranted to determine which DMBT1 N-glycosylation site(s) is/are important for the twitching inhibitory phenotype.

While glycosylation differences (e.g. in sialyl-Le [Lewis] antigens) have been noted between different isoforms of DMBT1 (gp-304) from tear fluid, saliva, and respiratory fluid (Eriksson et al., 2007; SCHULZ et al., 2002), we previously noted that sialyl-Le (Lewis) antigen differences between DMBT1 isoforms would unlikely be involved since both tear fluid and salivary DMBT1 inhibit twitching motility, but express different sialyl-Le antigens (Li et al., 2017). Moreover, sialyl-Le antigens are attached to tear fluid and salivary DMBT1 by O-glycosylation (Issa et al., 2010; SCHULZ et al., 2002), and in the present study, enzymatic de-O-glycosylation of DMBT1 did not impact its inhibition of *P. aeruginosa* twitching motility.

While de-N-glycosylation reduced DMBT1's ability to inhibit twitching, there remained a significant inhibition versus to PBS indicating that other components of DMBT1 also contribute to twitching inhibition. Since heat denaturation of DMBT1 resulted in a complete loss of activity (Figure 3.1), these other mechanisms are also heat-sensitive. However, given the similarity of inhibition levels between de-N-glycosylation and general deglycosylation (Figure 3.8B versus Figure 3.6B), and the lack of effect of specific de-O-glycosylation (Figure 3.7B), suggest that these other mechanisms of twitching inhibition relate to other aspects of DMBT1 molecular structure.

In our previous study, the ability of DMBT1 to inhibit twitching motility correlated with binding to extracted bacterial pili suggesting involvement in the inhibitory mechanism (Li et al., 2017). In the present study, however, this correlation was weakened by two observations; 1) that heat-denatured DMBT1 retained pili binding (~60% after denaturation) despite the complete loss of activity, and 2) that de-N-glycosylation had no effect on pili binding, yet inhibitory activity was reduced by ~57%. Thus, DMBT1 can bind *P. aeruginosa* pili without inhibiting twitching motility. Previous studies have shown that DMBT1 (gp-340) can bind bacterial pili with various outcomes. For example, pili-mediated binding of Group A *Streptococci* to gp-340 was associated with bacterial aggregation and defense against bacterial adhesion (Edwards et al., 2008). In contrast, pili-mediated binding of Group B *Streptococci* to surface immobilized gp-340 was proposed as a host colonization mechanism, while bacterial aggregation by fluid-phase gp-340, a likely host defense, was pili independent (Brittan and Nobbs, 2015). Thus, our findings do not preclude an involvement of pili binding in DMBT1-mediated inhibition of twitching motility as a host defense, but suggest that this activity may not be fully accomplished by binding to pili alone. Alternatively, DMBT1 binding to *P. aeruginosa* pili may serve an entirely separate function from host defense, or could mediate multiple events in the host. Other potential mechanisms for DMBT1 inhibition of *P. aeruginosa* twitching motility could involve the deregulation of gene expression in the Pil-Chp pathway that controls type IV pilus production and twitching motility (Fulcher et al., 2010; Moulton and Montie, 1979). While our previous study showed that genes *cyaB, chpB*, and *pilK* were not necessary for DMBT1-mediated twitching inhibition (Li et al., 2017), other genes in this pathway could still be affected. DMBT1 could also interact with other proteins involved in pilus extension or retraction (e.g. ATPases PilB, PilT and PilU or chemosensory protein PilJ) (Bertrand et al., 2010; Chiang et al., 2008; DeLange et al., 2007) which could compromise twitching motility. Thus, the role of DMBT1-pili interactions in inhibition of *P. aeruginosa* twitching motility may be complex, and understanding may require significant

further study.

In conclusion, the results of this study add to our understanding of DMBT1-mediated inhibition of *P. aeruginosa* twitching motility, a contribution to mucosal fluid defense of surface epithelia that would help prevent bacteria from traversing mucosal epithelia, forming surface-associated biofilms, and causing disease pathology. The data show that the inhibitory mechanism of human salivary DMBT1 (DMBT1$^{SAG}$) is heat-sensitive, suggesting that molecular conformation is important, and that DMBT1 N-glycosylation, but not O-glycosylation, contributes to ~50% or more of twitching inhibitory activity. The results also show that salivary DMBT1 can bind *P. aeruginosa* pili without inhibiting twitching motility, suggesting that if pili binding is involved, additional mechanisms are likely to play a role. Nevertheless, the lack of twitching inhibitory activity of consensus sequence-based peptides of salivary DMBT1, and presence of twitching inhibitory activity despite enzymatic de-O-glycosylation, suggest that the mechanism(s) involved differ from those demonstrated for DMBT1-mediated defense against other bacterial pathogens.

## 3.6 Acknowledgements

The work done in this chapter was done in equal contribution with Dr. Jianfang Li. This work was supported by the National Institutes of Health (EY024060, SMJF), and an International Postdoctoral Exchange Program Fellowship from the China Postdoctoral Council (20140085, JL). *P. aeruginosa* PAO1 and its mutants were obtained from the University of Washington *P. aeruginosa* mutant collection supported by the National Institutes of Health (P30 DK089507). Many thanks to Dr. Joanne Engel (University of California, San Francisco) for providing the antibody to PilA, and to Dr. Chris Jeans (University of California, Berkeley) for help with protein purification.

# Chapter 4

# Role of transient receptor potential ion channels in corneal defense against bacteria

## 4.1 Abstract

The normal healthy cornea is free from bacterial colonization despite being constantly in contact with the environment. Several factors have been identified that contribute to the epithelial barrier function of the cornea such as tear fluid, antimicrobial peptides, tight junctions and innate immune signaling pathways. However, the role of corneal nerves and their receptors in regards to bacterial defense is not well understood. The neuro and immune systems have traditionally been thought to be separate mechanisms that serve different functions. However, it is becoming increasingly clear that neuro-immune cross talk plays a significant role in maintaining homeostasis and following tissue damage. The cornea is the most innervated tissue in the body with polymodal nociceptors expressed on the majority of the sensory nerve fibers. Nociceptors are activated by a wide range of stimuli and can initiate events to protect the organism. Here, we explored the role of polymodal nociceptors transient receptor potential ankyrin 1 (TRPA1) and transient receptor potential vanilloid 1 (TRPV1) in defense against bacterial colonization on the murine cornea. We used TRPA1$^{-/-}$/TRPV1$^{-/-}$ mice to show that mice lacking these ion channels have increased bacterial adherence on the cornea. While wild-type mice normally elicit an influx of immune cells (CD45+) in response to *Pseudomonas aeruginosa* challenge, TRPA1$^{-/-}$/TRPV1$^{-/-}$ mice lacked this response. Further, mice with selective ablation of TRPA1 and TRPV1 ion channels also had a reduction in CD11c+ cell infiltration post inoculation. This study demonstrates a role for TRPA1 and TRPV1 ion channels in protecting the cornea from bacterial colonization and emphasizes the interconnectedness of the neuro and immune systems.

## 4.2 Introduction

The healthy cornea is an expert at preventing bacterial infections. In fact, despite being constantly exposed to the environment and therefore a multitude of debris, pathogens, and allergens, the cornea is relatively free of bacterial colonization (Wan et al., 2018). Previous studies have revealed various factors involved in epithelial barrier function that protect the cornea from colonization. These include tear fluid components, mucins, antimicrobial peptides, tight junctions, MyD88-dependent factors, immune cell surveillance, and many others (Alarcon et al., 2011; Augustin et al., 2011; Fleiszig et al., 1994; Kwong et al., 2007; Li et al., 2017; McNamara et al., 1999; Metruccio et al., 2017; Sullivan et al., 2015; Tam et al., 2012; Wan et al., 2018; Yi et al., 2000). Of particular interest, our laboratory's recent work has demonstrated the role of CD11c+ cells in sensing and responding to *P. aeruginosa* on the cornea which only occurs *in vivo* and happens as early as 4 h (Metruccio et al., 2017).

Recently, more evidence suggests the intertwining of the nervous and immune system. Indeed, it has even been shown that dendritic cells and corneal nerves are structurally interdependent (Gao et al., 2016). Microbial infection has also been associated with an increase in number of infiltrating immune cells and reduced subbasal nerves in the central cornea (Cruzat et al., 2011). While it was once thought that inflammatory pain and immune cell infiltration was due to immune-derived factors, it has now been shown that bacteria can directly activate sensory nerve fibers that also modulate innate immune activation (Chiu et al., 2013). It is also interesting that *in vitro*, *P. aeruginosa* can easily invade and kill human epithelial cells (Fleiszig et al., 1995; Kroken et al., 2018) while *in vivo*, thick pastes of inoculum are quickly cleared from the epithelial surface (Mun et al., 2009; Wan et al., 2018). One factor that is obviously missing from *in vitro* experiments using cell culture systems are nerves.

The role of corneal nerves and their receptors in regards to bacterial defense in the cornea is not well understood. The cornea is the most innervated tissue in the body, supplied by the ophthalmic division of the trigeminal nerve and terminates as free nerve endings in the epithelium (Cruzat et al., 2010; Laura Oliveira-soto, 2001; Shaheen et al., 2014). The majority of the nerve fibers (70%) in the corneal epithelium are polymodal, meaning they respond to a variety of stimuli. Of interest, are transient receptor potential (TRP) cation channels, which play important roles for sensory transduction in the cornea (Belmonte et al., 2017). These ion channels have been shown to release neuropeptides such as substance P and calcitonin gene-related peptide (CGRP) in response to tissue injury which initiates and mediates an inflammatory reaction (Belmonte et al., 2017). TRP channels have also been found to respond specifically to microbial ligands in tissues and their ability to respond within milliseconds makes them an ideal first line of defense against pathogens (Chiu et al., 2013; Pinho-Ribeiro et al., 2017) . Additionally, immune cells, including dendritic cells and neutrophils, express receptors for neuromodulators allowing them to respond to nociceptor signals (Pinho-Ribeiro et al., 2018).

Here, we tested the hypothesis that transient receptor potential ankyrin 1 (TRPA1) and transient receptor potential vanilloid 1 (TRPV1) play a role in corneal defense against bacterial colonization. TRPV1 was first identified as the receptor for capsaicin (i.e. heat) but has been

shown to be activated by several stimuli to sense and withdraw from noxious environmental elements. TRPA1 also is activated by noxious stimuli and is primarily known for its thermosensitivity to cold (Belmonte et al., 2017; Okada et al., 2015; Reinach et al., 2015). Both TRPV1 and TRPA1 expression has been identified in the corneal epithelium (Alamri et al., 2015; Okada et al., 2015; Zhang et al., 2007). The role of TRPA1 and TRPV1 channels in corneal defense has not been previously explored. The results from this study demonstrated that TRPV1 and TRPA1 nociceptors contribute to epithelial barrier function against both inoculated pathogens and environmental bacteria which was associated with the regulation of immune cell infiltration. We found that TRPV1 alone does not contribute to bacterial defense and that TRP channels associated with neuronal activation were primarily responsible for preventing bacterial colonization.

## 4.3 Experimental Procedures

### 4.3.1 Bacteria

*Pseudomonas aeruginosa* (strain PAO1) expressing d-Tomato on plasmid p67T1 (PAO1-dtom) was used throughout (Singer et al., 2010). Inocula were prepared from overnight cultures grown on tryptic soy agar (TSA) plates supplemented with carbenicillin 400 μg/mL at 37°C for ~16 h. Bacteria were suspended in Dulbecco's Modified Eagle's Medium (DMEM) (Lonsa, Walkersville,MD) to a concentration of ~$10^{11}$ CFU/mL.

### 4.3.2 *In vivo* Bacterial Adhesion Model

All procedures were carried out in accordance with a protocol approved by the Animal Care and Use Committee, University of California, Berkeley. Six to 12 week old male or female TRPA1$^{-/-}$/TRPV1$^{-/-}$ double knockout mice and TRPV1$^{-/-}$ single knockout mice were provided by Dr. Diana Bautista (University of California, Berkeley) and age and sex-matched wild-type (C57BL/6, bred in house) were used. The *in vivo* model was used as described previously (Metruccio et al., 2017). Mice were anesthetized by intraperitoneal injection of ketamine (80-100 mg/Kg) and dexmedetomide (0.25-0.5 mg/Kg). Corneas were rinsed with PBS to wash away tear fluid. In one group one cornea was subjected to blotting with a Kimwipe™ tissue paper to enable bacterial adhesion. Eyes were inoculated with 5 $\mu$L of *P. aeruginosa* (~$10^{11}$ CFU/mL) once every hour. After 4 h, animals were euthanized, eyes enucleated, rinsed with PBS, and fixed in 2% paraformaldehyde (PFA) overnight at 4°C, then imaged using confocal microscopy with a 60x water-dipping objective. Bacteria were identified and quantified by ImageJ on maximum intensity projections (reducing a 3D image into a 2D image by projecting the maximum intensity of each pixel to the z plane).

### 4.3.3 Fluorescence *in Situ* Hybridization

Labeling of bacterial on corneas without any prior manipulation was performed as previously described (Wan et al., 2018). Mice were euthanized by intraperitoneal injection of ketamine (80-100 mg/Kg) and xylazine (5-10mg/Kg) followed by cervical dislocation. Whole eyes were enucleated and fixed in 2% PFA for 1 h on rotator at room temperature (RT). Fixed eyes were then washed in 80% EtOH, 95% EtOH, and then PBS for 10 min each at RT. Eyes were placed in hybridization buffer solution [NaCl (0.9 M), Tris-HCl (20mM, PH 7.2) and SDS (0.01%)] and incubated at 55°C for 30 min and then 16S rRNA gene probe was added to final concetration of 100nM and incubated at 55°C overnight. Bacterial hybridization was performed using a universal 16S rRNA gene [Alexa488]- GCTGCCTCCCGTAGGAGT-[Alexa488] (Eurofins Genomics) (Mark Welch et al., 2016; Vaishnava et al., 2011). Eyes were then transferred to wash buffer solution [NaCl (0.9 M) and Tris-HCl (20mM, PH 7.2)] and washed three times for 10 min each at RT before imaging on confocal microscope using a 60x water-dipping objective. Bacteria were identified and quantified by ImageJ on maximum intensity projections.

### 4.3.4 Wheat Germ Agglutinin Staining

Mice were anesthetized and one eye inoculated with bacteria as described above. After 4 h, mice were euthanized, eyes enucleated and rinsed in PBS. Eyes were then transferred to Alex Fluor® 647 conjugate of wheat germ agglutinin solution (10 $\mu$g/mL, Invitrogen™) for 5 min at RT then washed 3 times with PBS. Eyes were then fixed in 2% PFA overnight at 4°C before imaging using confocal microscopy with a 60x water-dipping objective. Mean fluorescence intensity and area covered on maximum intensity projections were quantified using ImageJ.

### 4.3.5 Fluorescein Staining

After induction of anesthesia as described above, eyes were rinsed with PBS and stained with fluorescein as previously described (Wan et al., 2018). Briefly, for wild-type mice, one eye was blotted with a Kimwipe™ tissue paper as a positive control. A drop (5 $\mu$L) of fluorescein solution (0.02%) was then added to the ocular surface and corneal epithelial integrity was examined using a slit lamp and confocal microscopy with a 60x water-dipping objective. Mean fluorescence intensity and area covered on maximum intensity projections were quantified using ImageJ.

### 4.3.6 Antimicrobial Activity of Corneal Lysates

The antimicrobial activity of murine corneal lysates was assessed as previously described with some modifications (Sullivan et al., 2015; Wan et al., 2018). Corneas of wild-type or TRPA1$^{-/-}$/TRPV1$^{-/-}$ mice were extracted and homogenized in distilled water (two corneas per 350 $\mu$L of water) and centrifuged at 14,000 x g for 2 min to remove cell debris. Protein concentration of crude lysates were quantified with a bicinchoninic acid (BCA) assay kid (Pierce Biotechnology, Inc., Thermo Fisher Scientific, Rockford, IL, United States). Lysates were diluted

to 100 $\mu$g/mL final concentration and inoculated with *P. aeruginosa* ($10^9$ CFU) in a 96-well plate (100 $\mu$L total volume). Optical density at 540nm (OD540) were read every 15 min on a BioTek Synergy HTX plate reader warmed to 37°C with shaking between readings.

### 4.3.7 Whole Mount Cornea Immunohistochemistry

Staining protocol was adapted from (Hill et al., 2018). Briefly, mice were euthanized and corneas extracted then fixed overnight in 2% PFA overnight at 4°C. Corneas were rinsed three times in PBS, 10 min each, then washed with 0.3% Triton X-100 in PBS (PBST) for 4-6 h, changing solution every 1.5-2 h. Primary antibody (1:100) was applied in blocking solution (75% PBST, 20% chilled DMSO, 5% goat serum) and incubated overnight at 4°C on rotator. Corneas again were rinsed three times in PBS (10 min) then washed with PBST for 6-8 h, changing solution every 1.5-2 h. Secondary antibody (1:400) was applied in blocking solution and incubated overnight at 4°C on rotator. Next, Corneas were washed three times in PBS then PBST for 4-6 before mounting on slide and imaging with confocal microscopy using a 20x water-dipping objective. For CD45+ cell staining, primary CD45 monoclonal antibody (30-F11, eBioscience™) was used with secondary goat anti-rat IgG, Alex Fluor 647 secondary antibody (Invitrogen™). CD45+ cells were quantified in a 20 $\mu$M maximum intensity projection in the corneal stroma using ImageJ.

### 4.3.8 TRPA1 and TRPV1 Depletion

TRPA1 and TRPV1 expressing cells were selectively ablated using subcutaneous chronic application of resiniferatoxin (RTX) as previously described (Caudle et al., 2003; Pecze et al., 2009). CD11c-yfp transgenic mice were used for these experiments to determine the presence of CD11c+ cells in response to PAO1 inoculation. One mg of RTX was dissolved in 500 µL 96% ethanol and diluted in sterile PBS. Mice were anesthetized with isoflurane and then RTX injected into the scruff of the neck at 20 $\mu$g/kg body weight daily for 3 days. Control mice were injected with PBS. To confirm ablation of TRPA1 and TRPV1 in the cornea, the eye wipe test was performed in lightly anesthetized animals. 100 µM capsaicin solution was dropped into the eye and the number of defensive wiping movements for 1 min was counted. To image presence of CD11c+ cells, a 20x water-dipping objective was used and images quantified with ImageJ.

### 4.3.9 Corneal Nerve Block

To suppress neuronal activation in the cornea, 0.5% bupivacaine solution (Habib et al., 1993; Jinks et al., 2018) was injected (5 $\mu$L) subconjuntivally in anesthetized mice with a Hamilton small volume syringe and small hub 33 gauge needle. Then, 5 $\mu$L was topically applied onto the cornea. After 20 min, corneas were washed with PBS and bacterial inoculation of PAO1 was done as described above.

### 4.3.10 Confocal Microscopy

Murine eyeballs were imaged *ex vivo* as previously described (Tam et al., 2011). Eyes were fixed to a 12 mm glass coverslip with cyanoacrylate glue with cornea facing upward. The coverslip with eyeball was placed in 46 mm Petri dish and filled with PBS to cover the eyeball completely. Confocal imaging was performed using an Olympus FV1000 confocal microscope [Olympus BX615Wi upright microscope with Olympus FluoView 1000 detection system equipped with Laser Diodes (LD) 405, 440, 559, 635 and an Argon Laser 488/515]. The 405 nm laser was used for detection of DAPI, 488 nm laser used for detection of bacteria labeled with FISH or corneas stained with fluorescein, the 559 nm laser used for detection of red-fluorescent bacteria (PAO1-dtom) or red fluorescent cell membranes, and the 635 nM laser was used for corneas stained with WGA or CD45+ antibody. In instances where red-fluorescent cell membrane mice were not used, ocular surface reflectance (excitation and emission at same wavelength) was obtained. For 60x images, four or more randomly chosen fields of each eye were imaged from the corneal surface. For 20x images, three or more randomly chosen fields of each eye were imaged from the corneal surface. Three-dimensional images were reconstructed from z-stacks using IMARIS software (Bitplane).

### 4.3.11 Statistical Analysis

Statistical analysis was performed using Prism (GraphPad Software, Inc.). Data were expressed as mean ± standard error of the mean (SEM). Statistical significance of differences between means was determined using Student's t-Test for two group comparison or two-way ANOVA with Tukey's multiple comparison test for three or more groups. For nonparametric data, Mann-Whitney or Kruskal-wallis tests were used. P-values less than 0.05 were considered significant.

## 4.4 Results

### 4.4.1 TRPA1 and TRPV1 ion channels contribute to the epithelial barrier against bacteria

The normal healthy cornea is incredibly resistant to bacterial colonization. Indeed, the murine cornea quickly clears away both inoculated pathogenic and commensal bacteria (Mun et al., 2009; Wan et al., 2018). To investigate the role of TRPA1 and TRPV1 channels in in corneal defense against bacteria during health, we challenged wild-type and TRPA1$^{-/-}$/TRPV1$^{-/-}$ mouse corneas with *P. aeruginosa in vivo* as previously described (Metruccio et al., 2017). TRPA1$^{-/-}$/TRPV1$^{-/-}$ corneas showed a significant increase in bacterial adhesion compared to wild-type (28.4 ± 5.9 bacteria/field compared to 13.0 ± 3.5 bacteria/field, respectively) (Figure 4.1A,B). Bacteria only adhered to the superficial epithelium and did not penetrate beyond the surface (Figure 4.1C).

Next, eyes were superficially injured by gently blotting the epithelium with a KimWipe™ which has been shown to increase bacterial adhesion and disruption to the epithelial integrity (Jolly et al., 2017; Metruccio et al., 2017; Tam et al., 2011). With blotting, TRPA1$^{-/-}$/TRPV1$^{-/-}$ corneas still had significantly more bacterial adhesion compared to wild-type (103.1 ± 25.1 bacteria/field of view compared to 33.8 ± 5.7 bacteria/field of view respectively) (Figure 4.1A,B). Still, bacteria did not penetrate into the corneal epithelium and only remained surface associated (Figure 4.1C).

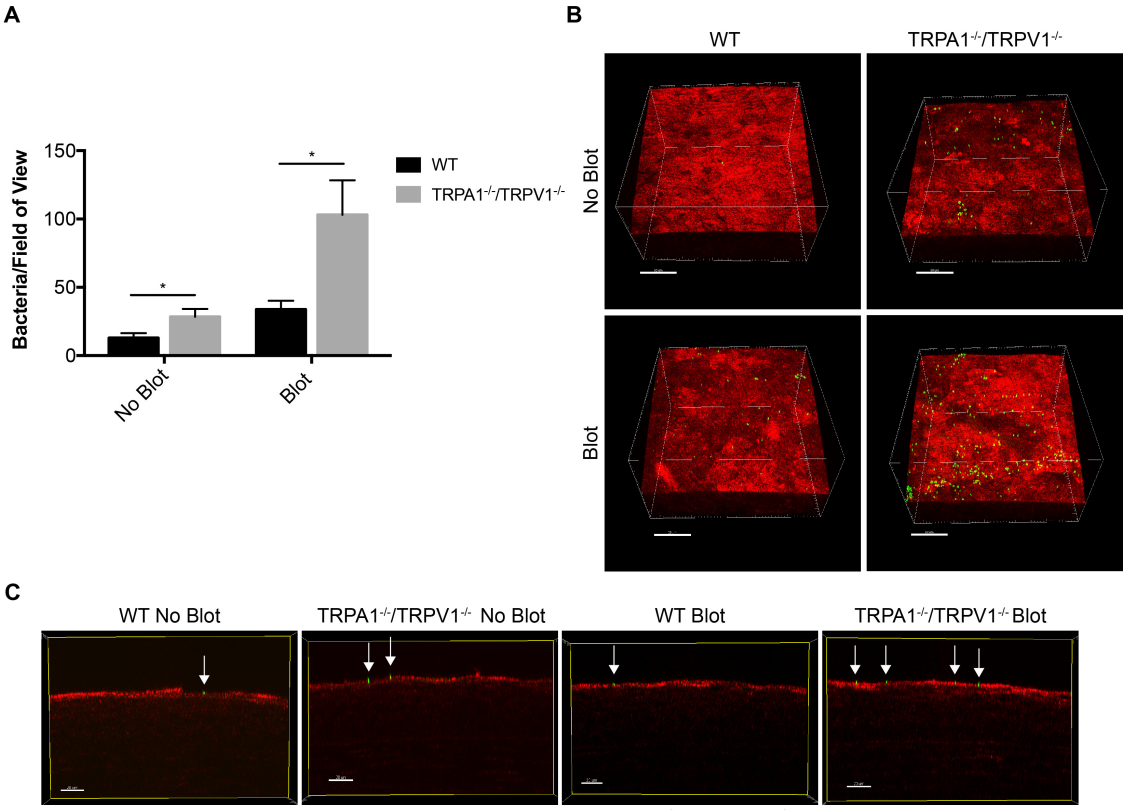


**Figure 4.1:** Inoculated *P. aeruginosa* adheres significantly more to TRPA1$^{-/-}$/TRPV1$^{-/-}$ corneas *in vivo* compared to wild-type (WT) corneas. (A) Quantification of number of bacteria sticking to cornea per field of view after inoculation of 1x10$^{11}$ CFUs/mL every hour for 4 h on untreated and blotted corneas. On a normal WT cornea, 13.0 ± 3.5 bacteria/field of view adhered to the cornea compared to 28.4 ± 5.9 bacteria/field of view on untreated TRPA1$^{-/-}$/TRPV1$^{-/-}$ corneas. More bacteria adhered when corneas were blotted (33.8 ± 5.7 bacteri/field of view on WT corneas compared to 103.1 ± 25.1 bacteria/field of view on TRPA1V1$^{-/-}$/TRPV1$^{-/-}$ blotted corneas). * = $P < 0.05$, Two-way ANOVA. (B) Example images of *P. aeruginosa* (green) adhering to the cornea (red) in each condition. (C) Slice of XZ axis showing that bacteria remained surface associated (green, arrows) and did not penetrate into the corneal epithelium (red).

The normal healthy cornea lacks a stable microbiome and is considered to be relatively sterile, despite being constantly exposed to the environment (Wan et al., 2018). Thus, after we established that TRPA1/V1 ion channels contributes to the defense against inoculated *P. aeruginosa*, we next wanted to assess if they also play a role in preventing a corneal microbiome (i.e. environmental bacteria colonization). FISH labeling for universal bacterial 16S rRNA gene (Mark Welch et al., 2016; Vaishnava et al., 2011) revealed that several more environmental bacteria

inhabited the corneas of TRPA1$^{-/-}$/TRPV1$^{-/-}$ (8.0 ± 2.0 bacteria/field) compared to wild-type mouse corneas (1.9 ± 0.6 bacteria/field) (Figure 4.2). These results suggest that TRPA1 and TRPV1 ion channels also are important for constitutive defense against bacteria and contribute to keeping the cornea free of bacteria.

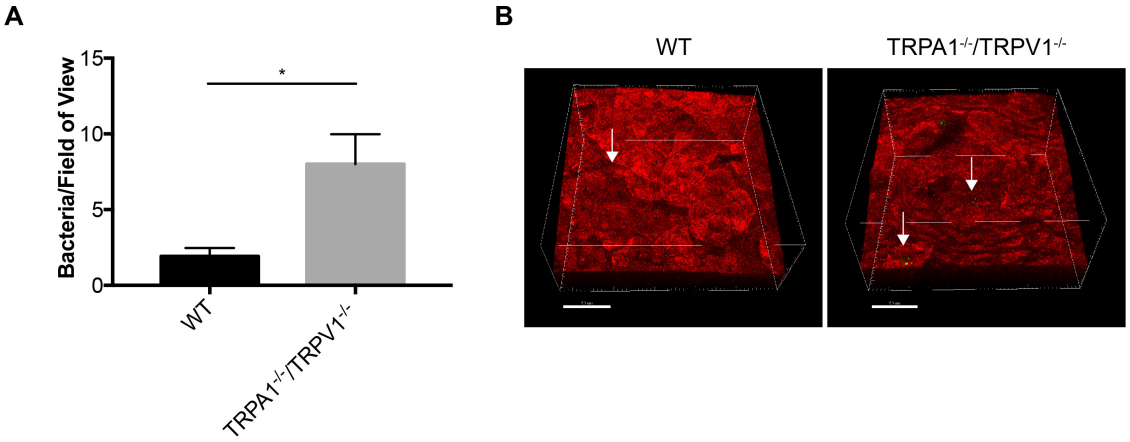


**Figure 4.2:** FISH labeling reveals increased colonization of environmental bacteria on TRPA1$^{-/-}$/TRPV1$^{-/-}$ corneas compared to wild-type (WT). (A) Quantification of number of bacteria detected on corneas of WT (1.9 ± 0.6 bacteria/field of view) and TRPA1$^{-/-}$/TRPV1$^{-/-}$ (8.0 ± 2.0 bacteria/field of view) without any prior treatment using FISH. * = P < 0.05, Student's T-test. (B) Representative images showing FISH labeling (green, arrows) of environmental bacteria detected on on WT and TRPA1$^{-/-}$/TRPV1$^{-/-}$ corneas (red).

### 4.4.2 TRPA1$^{-/-}$/TRPV1$^{-/-}$ corneas have normal innate constitutive defense mechanisms

The cornea has several lines of defenses to prevent bacterial colonization which could lead to sight-threatening keratitis. Here, we wanted to determine how TRPA1 and TRPV1 ion channels regulate epithelial barriers. Since, tears were washed away in our adhesion experiments we bypassed this set of defenses and first looked at the glycocalyx, a membrane-associated mucin barrier that protects the epithelium from pathogen penetration (Blalock et al., 2007; Fleiszig et al., 1994; Linden et al., 2008; Mantelli and Argüeso, 2008). To do this, we used fluorescent-conjugated wheat germ agglutinin (WGA) which specifically binds to N-acetyl glycosamine and N-acetyl neuraminic acid, components of the ocular surface glycocalyx (Mochizuki et al., 2010). WGA revealed that staining patterns were very similar on untreated wild-type corneas compared to TRPA1$^{-/-}$/TRPV1$^{-/-}$ corneas (Figure 4.3A). Quantification of mean fluorescence intensity and area covered confirmed these findings (Figure 4.3B). Next, we determined if *P. aeruginosa* challenge altered WGA staining on the cornea. Overall wild-type and TRPA1$^{-/-}$/TRPV1$^{-/-}$ had similar staining patterns in response to bacteria on the cornea (Figure 4.3A,B). Wild-type corneas did show a decrease in fluorescence intensity of WGA staining after PAO1 inoculation compared to TRPA1$^{-/-}$/TRPV1$^{-/-}$, however this was not statistically significant (Figure 4.3B). Furthermore, no differences in amount of stained area (Figure 4.3B) occurred indicating that overall, TRPA1$^{-/-}$/TRPV1$^{-/-}$ corneas had similar responses compared to wild-type.

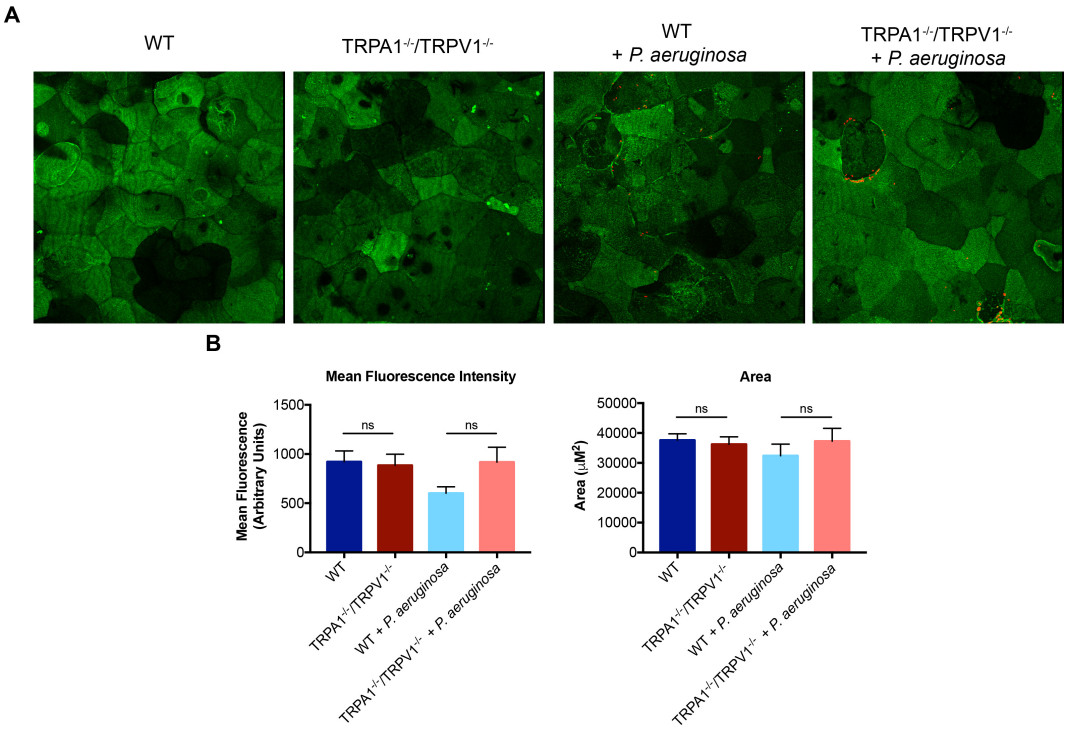


**Figure 4.3:** TRPA1$^{-/-}$/TRPV1$^{-/-}$ corneas have an intact glycocalyx. (A) Representative maximum intensity projections of wheat germ agglutinin (WGA) staining and *P. aeruginosa* adhesion on wild-type (WT) and TRPA1$^{-/-}$/TRPV1$^{-/-}$ corneas. (B) Quantification of WGA mean fluorescence intensity and area of WGA staining. No differences in WT or TRPA1$^{-/-}$/TRPV1$^{-/-}$ was observed indicating a normal glycocalyx and response to *P. aeruginosa*. Ns = no significance. ANOVA with Tukey's multiple comparison test.

We then looked at epithelial integrity of TRPA1$^{-/-}$/TRPV1$^{-/-}$ corneas using fluorescein staining. Disruption of epithelial junctions reduces epithelial barrier function and loss of cell polarity enabling increased bacterial adhesion (Alarcon et al., 2011; Fleiszig et al., 1997; Tam et al., 2011). To explore this possibility, wild-type corneas were superficially injured with a Kimwip™ to disrupt the epithelial integrity (Jolly et al., 2017) and compared to uninjured wild-type corneas and TRPA1$^{-/-}$/TRPV1$^{-/-}$ corneas. Fluorescein staining visualized under the slit lamp was clearly observed in the superficially injured wild-type corneas but not in uninjured TRPA1$^{-/-}$/TRPV1$^{-/-}$ corneas, similar to uninjured wild-type controls (Figure 4.4A). Furthermore, confocal imaging revealed no fluorescein penetration in the uninjured wild-type and TRPA1$^{-/-}$/TRPV1$^{-/-}$ corneas unlike in the blotted wild-type mice (Figure 4.4A,B). This indicates intact epithelial tight junctions in TRPA1$^{-/-}$/TRPV1$^{-/-}$ corneas. Interestingly, quantification of fluorescence intensity of fluorescein in confocal images revealed a significant difference in wild-type and TRPA1$^{-/-}$/TRPV1$^{-/-}$ corneas (Figure 4.4B). However, this showed that TRPA1$^{-/-}$/TRPV1$^{-/-}$ corneas had even less fluorescein staining, suggesting that the mutant corneas are even less susceptible to small molecule penetration compared to wild-type.

Lastly, antimicrobial activity of corneal lysates was assessed. Previously, our lab has shown that MyD88$^{-/-}$ and IL-1R$^{-/-}$ corneas have increased bacterial adhesion similar to the results

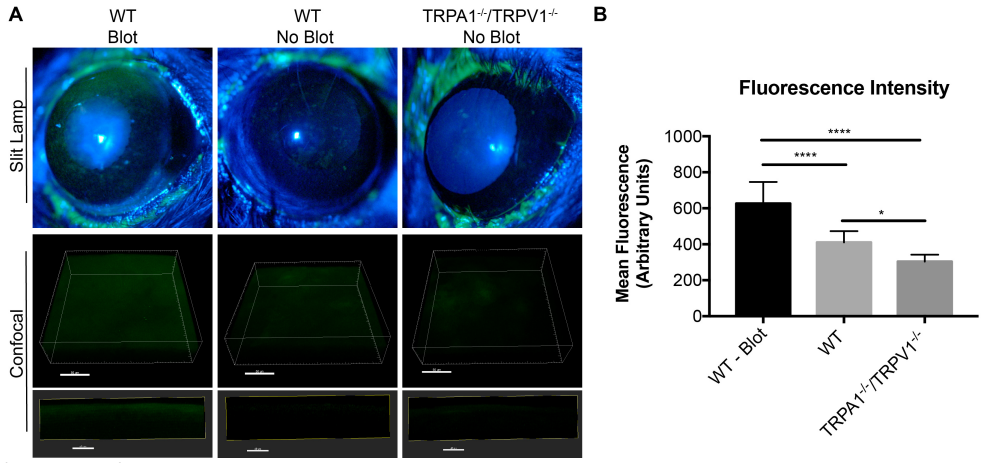


**Figure 4.4:** TRPA1$^{-/-}$/TRPV1$^{-/-}$ corneas do not stain with fluorescein. (A) Fluorescein under the slit lamp (upper panels) reveals staining in blotted wild-type (WT) corneas but lower levels in WT and TRPA1$^{-/-}$/TRPV1$^{-/-}$ corneas under no blot conditions. Confocal images (lower panels) also shows that TRPA1$^{-/-}$/TRPV1$^{-/-}$ corneas have little staining and no penetration of fluorescein demonstrating good epithelial integrity. Upper confocal panel images are 3D reconstructions of corneal images and lower confocal panel images are 10 µM XZ stacks. (B) Quantification of mean fluorescence intensity of fluorescein staining in Z-projection of confocal images. **** = P < 0.0001, * = P < 0.05. One-way ANOVA with Tukey's multiple comparisons test.

shown in this study on TRPA1$^{-/-}$/TRPV1$^{-/-}$ corneas (Metruccio et al., 2017; Sullivan et al., 2015; Wan et al., 2018). Further research showed that that MyD88-/- and IL-1R-/- corneas were less antimicrobial than wild-type corneas suggesting that this pathway regulates antimicrobials expressed in the cornea (Sullivan et al., 2015; Wan et al., 2018). Here, we tested the inhibition of *P. aeruginosa* growth in wild-type compared to TRPA1$^{-/-}$/TRPV1$^{-/-}$ corneal lysates. We found that both lysates inhibited growth compared to TSB only controls (Figure 4.5). No significant differences occurred at any time point in wild-type compared to TRPA1$^{-/-}$/TRPV1$^{-/-}$. Although not statistically significant, lysates from TRPA1$^{-/-}$/TRPV1$^{-/-}$ corneas seemed to inhibit the growth of *P. aeruginosa* even more than wild-type after 11 h of incubation.

### 4.4.3 CD45+ cell infiltration is reduced in TRPA1$^{-/-}$/TRPV1$^{-/-}$ corneal stromas compared to wild-type

Not only does an influx of immune cells occur during ocular infection (Huang et al., 2006; Pearlman et al., 2013; Sun et al., 2010) but resident myeloid cells also respond to noxious stimuli during corneal health. For example, corneal CD11c+ cells sense and respond to *P. aeruginosa* challenge after 4h *in vivo* (Metruccio et al., 2017). Furthermore, nociceptors can directly sense bacterial components and release immune mediators that modulate macrophages, dendritic cells, T cells, and other innate lymphoid cells (Baral et al.; Chiu et al., 2013; Pinho-Ribeiro et al., 2017). Given these observations, we next wanted to explore the role of TRPA1 and TRPV1 and immune cell responses during corneal health. Wild-type and TRPA1$^{-/-}$/TRPV1$^{-/-}$ mice were used and eyes challenged with *P. aeruginosa* as in experiments above, then labeled for CD45+ cells, a marker for all differentiated hematopoietic cells. Consistent with previous findings, wild-type corneas had an increase in stromal CD45+ cells after P. aeruginosa challenge

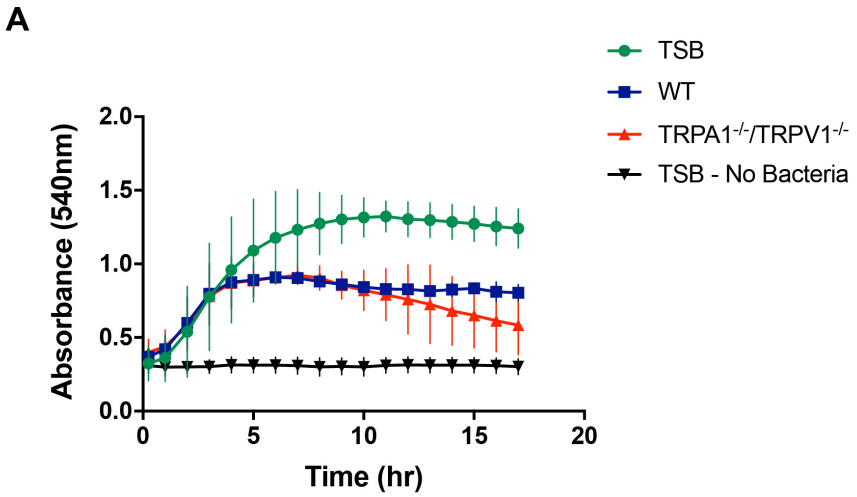


**Figure 4.5:** TRPA1$^{-/-}$/TRPV1$^{-/-}$ and wild-type (WT) corneal lysates have similar antimicrobial activity. (A) Growth curves of *P. aeruginosa* grown in corneal lysates of WT or TRPA1$^{-/-}$/TRPV1$^{-/-}$ corneas. Both corneal lysates show an increase in antimicrobial activity compared to TSB control. No significant differences occurred at any time point in WT lysates compared to TRPA1$^{-/-}$/TRPV1$^{-/-}$ lysates (Student's T-test).

(Figure 4.6A,B). This observation occurred after just 4 h. TRPA1$^{-/-}$/TRPV1$^{-/-}$ mouse corneas had similar basal levels of CD45+ cells compared to wild-type. However, after inoculation of *P. aeruginosa*, TRPA1$^{-/-}$/TRPV1$^{-/-}$ corneas lacked CD45+ cell infiltration (Figure 4.6A,B), indicating that TRPA1/TRPV1 ion channels play a role in immune cell recruitment in response to bacteria.

### 4.4.4 Mice depleted of TRPA1 and TRPV1 channels lack CD11c+ cell influx in response to *P. aeruginosa* inoculation on the cornea

Given the quick timing of immune cell infiltration (4 h), the known response of CD11c+ cells to *P. aeruginosa* challenge (Metruccio et al., 2017), and that dendritic cells and corneal nerves are interdependent (Gao et al., 2016), we hypothesized that TRPA1/TRPV1 channels regulate dendritic cell responses in the healthy cornea. To test this hypothesis, resiniferatoxin (RTX) was used to deplete TRPA1 and TRPV1 ion channels (Caudle et al., 2003; Pecze et al., 2009) in CD11c+-yfp transgenic mice, then CD11c+ cells in the cornea were quantified after *P. aeruginosa* inoculation on the cornea. The capsaicin eye wipe test demonstrated ablation of the ion channels after treatment and fluorescein staining showed that the RTX treatment does not interfere with corneal epithelail integrity (Supplementary Figure 1). At baseline levels, the number of CD11c+ cells identified in the cornea were similar in the vehicle control mice compared to RTX treated mice (Figure 4.7A,B). After *P. aeruginosa* inoculation for 4h, an increase in CD11c+ cells was

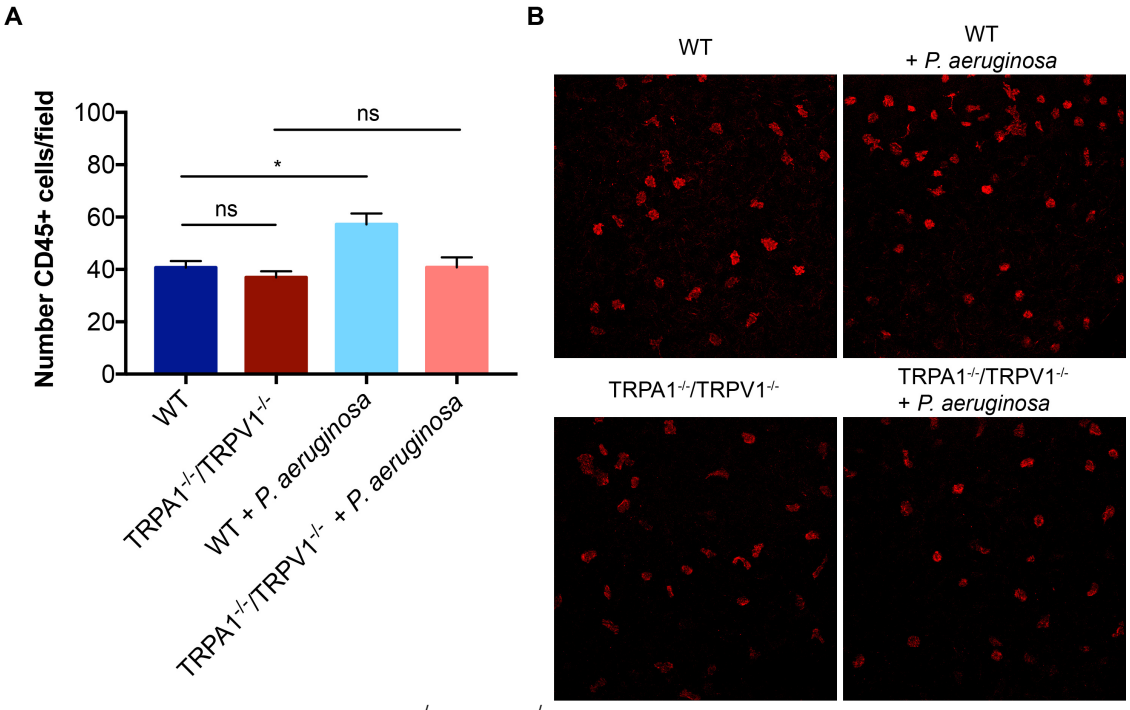


**Figure 4.6:** CD45+ cells did not infiltrate TRPA1$^{-/-}$/TRPV1$^{-/-}$ corneal stroma after *P. aeruginosa* challenge. (A) Quantification of number of CD45+ cells in corneal stroma in untreated conditions and after 4 hr PAO1 inoculation. Increased numbers of CD45+ cells were detected in inoculated WT stromas (57.18 ± 4.21 cells) compared to untreated WT (40.7 ± 2.48 cells). No differences occurred in inoculated TRPA1$^{-/-}$/TRPV1$^{-/-}$ corneas (40.81 ± 3.83 cells) compared to untreated KOs (36.93 ± 2.383). No significant differences (ns) were found in baseline levels in WT compared to TRPA1$^{-/-}$/TRPV1$^{-/-}$, ANOVA with Tukey's multiple comparisons test. (B) Representative images of CD45* staining (maximum intensity projections) in the stroma in each condition.

observed in control mice, similar to previously published results (Metruccio et al., 2017) but no significant increase in CD11c+ cells was seen in RTX treated mice (Figure 4.7A,B) suggesting that TRPA1/TRPV1 ion channels and dendritic cells communicate to prevent bacterial adherence on the cornea. Interestingly, the CD11c+ cells in control mice were also morphologically different after inoculation (Figure 4.7C). These cells tended to have an increase in perimeter measurements which indicates less circularity and therefore more dendrites suggesting activation of the cells. RTX treated mice had no significant difference in CD11c+ cellular morphology before and after *P. aeruginosa* challenge (Figure 4.7C). Importantly, mice treated with RTX also still showed an increase in *P. aeruginosa* adherence (Figure 4.7D,E), similar to the phenotype observed with TRPA1$^{-/-}$/TRPV1$^{-/-}$ mice in Figure 1.

### 4.4.5 Receptors expressed on neurons are important for preventing bacterial adhesion

Since TRP channels are expressed on neurons and thought to be expressed on epithelial and immune cells (Belmonte et al., 2017), we wanted to determine which tissue location for these channels is important for corneal defense. *Ex vivo* experiments, in which the eye was

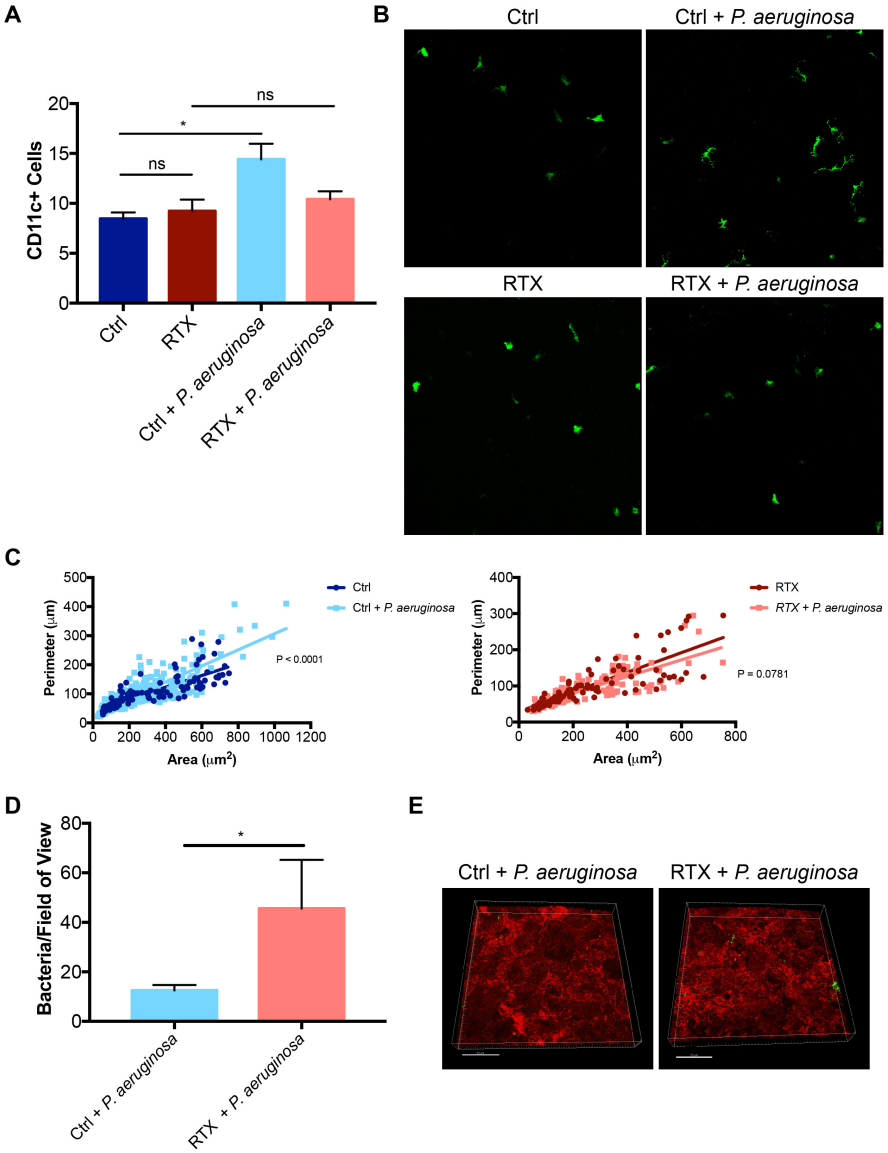


**Figure 4.7:** Mice treated with RTX to deplete TRPA1 and TRPV1 channels have less CD11c+ cell infiltration compared to untreated vehicle controls. (A) Quantification of number of CD11c+ cells in cornea in untreated vehicle control (ctrl) and RTX corneas and after *P. aeruginosa* challenge. A significant increase in CD11c+ cells was observed after *P. aeruginosa* inoculation control mice (14.4 ± 1.6 cells compared to 8.5 ± 0.6 cells at baseline, $P < 0.05$). No difference was observed after *P. aeruginosa* inoculation in RTX treated mice (10.4 ± 0.8 cells compared to 9.2 ± 1.2 cell at baseline, NS). ANOVA with Tukey's multiple comparisons test. (B) Representative images (maximum intensity projections) of CD11c+ cells in cornea in each condition. (C) Morphological analysis of CD11c+ cells using MorpholibJ tools for 3D segmentation in ImageJ and parameters related to z-projections used (perimeter and area). Graphs show distribution of individual cells based on area and perimeter with a linear regression fit. The left panels shows two significantly different curves ($P < 0.0001$) in the control mice whereas the right panel shows no significant difference in curves ($P = 0.078$) in RTX treated mice. (D) Quantification of number of bacteria adhered to control (12.5 ± 2.8 bacteria/field of view) and RTX treated (45.6 ± 19.7 bacteria/field of view) mouse corneas after 4h of *P. aeruginosa* (PAO1) inoculation. * = $P < 0.05$, Mann-Whitney test. E. Example images of *P. aeruginosa* (green) adhering to the cornea (red) in control and RTX treated mice.

enucleated and then incubated in *P. aeruginosa* for 4 h, revealed equal numbers of bacterial adhesion between wild-type and TRPA1$^{-/-}$/TRPV1$^{-/-}$ corneas in both the untreated and blotted conditions (Figure 4.8). Because the eye was *ex vivo*, the optic nerve was severed and thus nerve stimulation should no longer be able to occur. Thus, the finding that TRPA1$^{-/-}$/TRPV1$^{-/-}$ corneas no longer have an increase in bacterial adhesion compared to wild-type suggests that ion channels present on the nerves are important for preventing adhesion since the receptors on the epithelial and immune cells are not creating a difference in the bacteria's ability to adhere to the cornea.

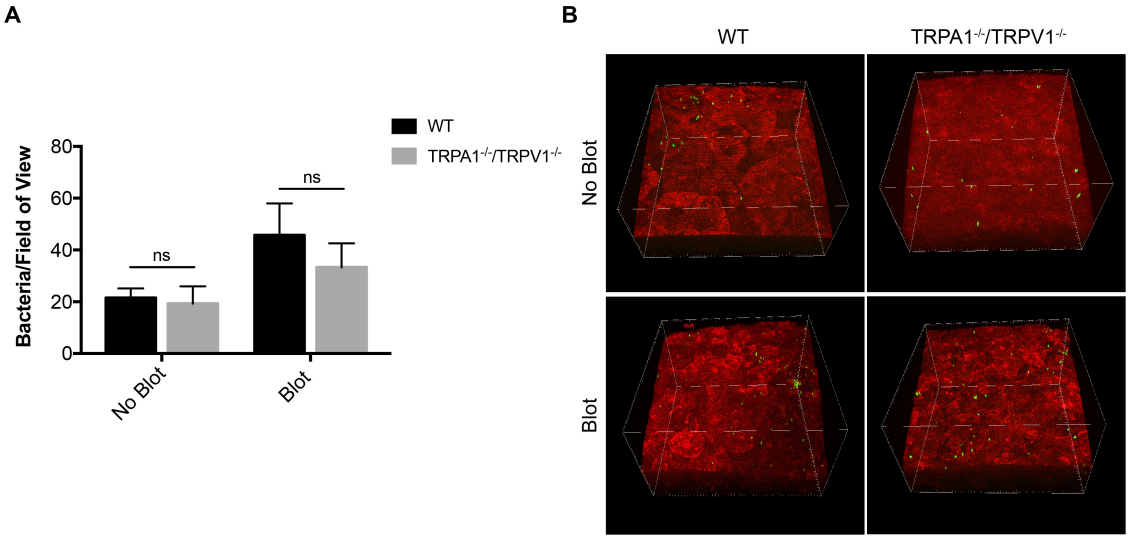


**Figure 4.8:** Equal amounts of *P. aeruginosa* adhere to *ex vivo* TRPA1$^{-/-}$/TRPV1$^{-/-}$ corneas compared to wild-type (WT). (A) Quantification of number of bacteria sticking to the cornea per field of view after inoculation of 1x10$^{11}$ CFUs/mL on untreated and blotted corneas *ex vivo*. On a normal WT cornea, 21.5 ± 3.6 bacteria/field of view adhered to the cornea compared to 19.3 ± 6.7 bacteria/field of view on untreated Equal amounts of *P. aeruginosa* adhere to *x vivo* TRPA1$^{-/-}$/TRPV1$^{-/-}$ corneas compared to WT corneas. More bacteria adhered when corneas were blotted but still in similar amounts (45.7 ± 12.3 bacteria/field of view on WT corneas compared to 33.313 ± 9.3 bacteria/field of view on Equal amounts of *P. aeruginosa* adhere to *ex vivo* TRPA1$^{-/-}$/TRPV1$^{-/-}$ corneas compared to WT blotted corneas). Ns = not significant, Two-way ANOVA. (B) Example images of *P. aeruginosa* (green) adhering to the cornea (red) in each condition.

To confirm this finding, corneal nerve stimulation was blocked by a subconjunctival injection of 0.5% bupivacaine hydrochloride, a local anesthetic that prevents depolarization and thus nerve signaling. Then, corneas were challenged *in vivo* with *P. aeruginosa* for 4 h and compared to corneas that were not treated with bupivacaine. Indeed, corneas treated with bupivacaine were found to have an increased amount of adhesion of *P. aeruginosa* (76.5 ± 16.8 bacteria/field of view) compared to untreated control corneas (21.5 ± 6.5 bacteria/field of view) (Figure 4.9). This, along with our *ex vivo* results suggest that receptors located on corneal nerves contribute to defending corneas against bacterial adhesion.

### 4.4.6 TRPA1 prevents bacterial adherence on the mouse cornea

Finally, we wanted to determine the contribution of TRPA1 versus TRPV1 nociceptors. First, we used TRPV1$^{-/-}$ due to its known ability to respond to bacteria and regulation of dendritic

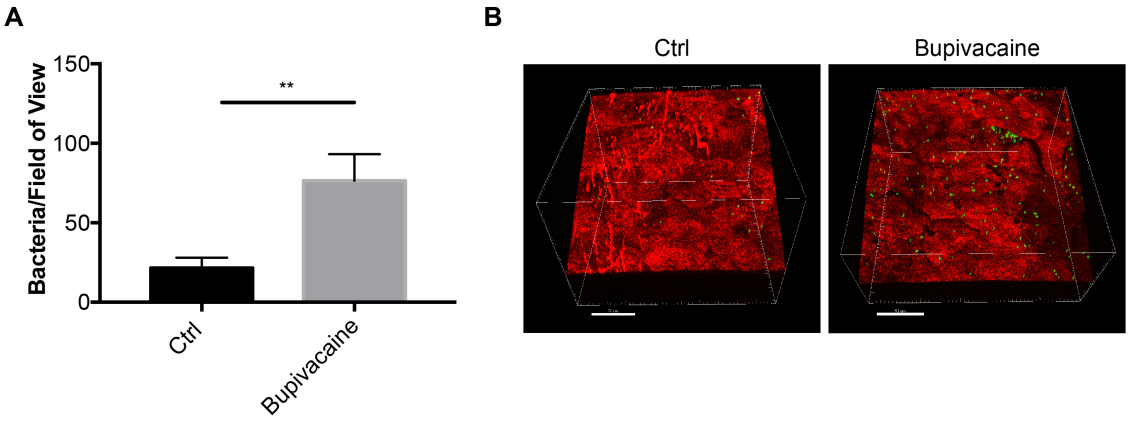


**Figure 4.9:** Corneal nerve block increases adherence of inoculated *P. aeruginosa* to the cornea. (A) Quantification of number of bacteria sticking to cornea per field of view after inoculation of $1x10^{11}$ CFUs/mL every hour for 4 h on untreated controls and bupivacaine corneas. On a control corneas, 21.5 ± 6.5 bacteria/field of view adhered to the cornea compared to 76.5 ± 16.8 bacteria/field of view on bupivacaine treated corneas. ** = P , 0.01, Student's T-test. (B) Example images of *P. aeruginosa* (green) adhering to the cornea (red) in each condition

cells to prevent infection (Baral et al.; Chiu et al., 2013). To do this, TRPV1$^{-/-}$ mice were used and challenged with *P. aeruginosa* to determine if increased bacteria adhesion occurs, similar to the double knock-out mice. Interestingly, no significant differences in bacterial adhesion was observed in either the no blot or blotted conditions (Figure 4.10), suggesting that either TRPA1 contributes to defense against bacterial colonization or both TRPA1 and TRPV1 are necessary components. Thus, single knockout mice for TRPA1 were then used. Indeed, TRPA1$^{-/-}$ mice had significant increases in bacterial adhesion after *P. aeruginosa* inoculation compared to wild-type in both the no blotted and blotted conditions (Figure 4.11). These results mirrored those of the TRPA1$^{-/-}$/TRPV1$^{-/-}$ results, indicating that TRPA1 contributes to defense against bacterial adhesion on the cornea.

## 4.5 Discussion

Overall, the results of this study demonstrate that TRPA1 nociceptors present on the corneal sensory nerve endings play a role in the defense against bacteria. Normal constitutive defenses such as the glycocalyx, epithelial integrity and antimicrobial activity were similar in wild-type and TRPA1$^{-/-}$/TRPV1$^{-/-}$. However, the lack of immune cell infiltration (CD45+ cells and CD11c+ cells) in response to *P. aeruginosa* challenge indicates TRPA1 and TRPV1 are involved in immune cell regulation.

TRPA1$^{-/-}$/TRPV1$^{-/-}$ mice had an increase in *P. aeruginosa* adherence after a 4h inoculation condition compared to wild-type in both untreated and blotted conditions (Figure 4.1). This phenotype was upheld when RTX was used to selectively ablate both TRPA1 and TRPV1 nociceptors (Figure 4.7). Furthermore, TRPA1$^{-/-}$/TRPV1$^{-/-}$ mice also had an increase in environmental bacteria colonizing the cornea compared to wild-type as indicated using FISH labeling of bacterial 16s rRNA genes (Figure 4.2). Together, this data provides strong evidence that TRPA1 and TRPV1

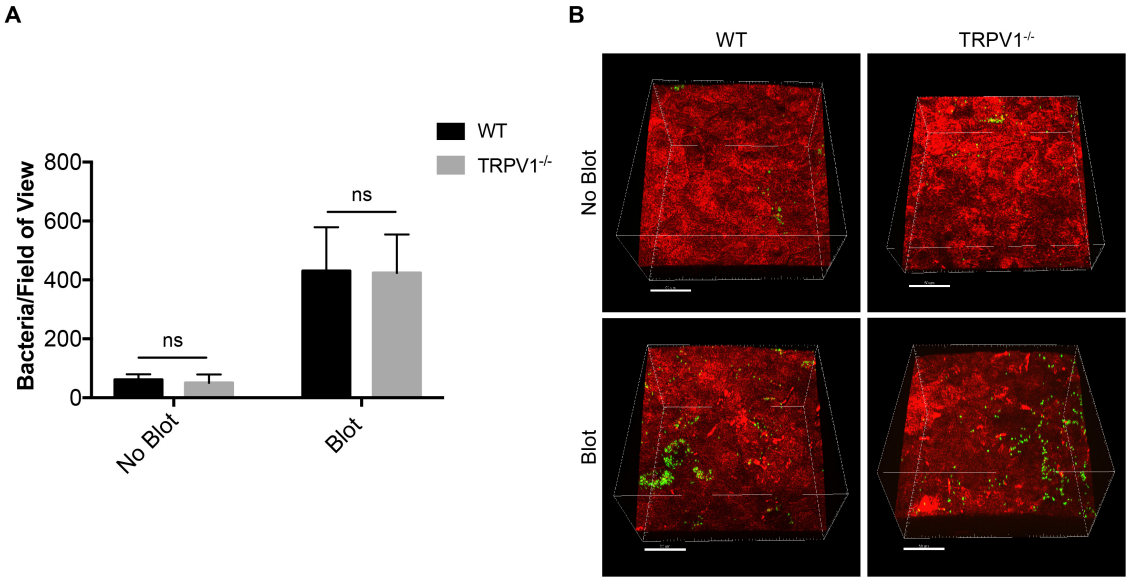


**Figure 4.10:** Equal amounts of inoculated *P. aeruginosa* adheres to TRPV1$^{-/-}$ corneas *in vivo* compared to wild-type (WT) corneas. (A) Quantification of number of bacteria sticking to the cornea per field of view after inoculation of 1x10$^{11}$ CFUs/mL every hour for 4 h on untreated and blotted corneas. On a normal WT corneas, 61.0 ± 18.7 bacteria/field of view adhered to the cornea compared to 50.0 ± 29.0 bacteria/field of view on untreated TRPV1 KO corneas. More bacteria adhered when corneas were blotted but at similar amounts (430.4 ± 148.6 bacteria/field of view on WT corneas compared to 423.6 ± 131.1 bacteria/field of view on TRPV1$^{-/-}$ blotted corneas). Ns = not significant, two-way ANOVA. (B) Example images of *P. aeruginosa* (green) adhering to the cornea (red) in each condition

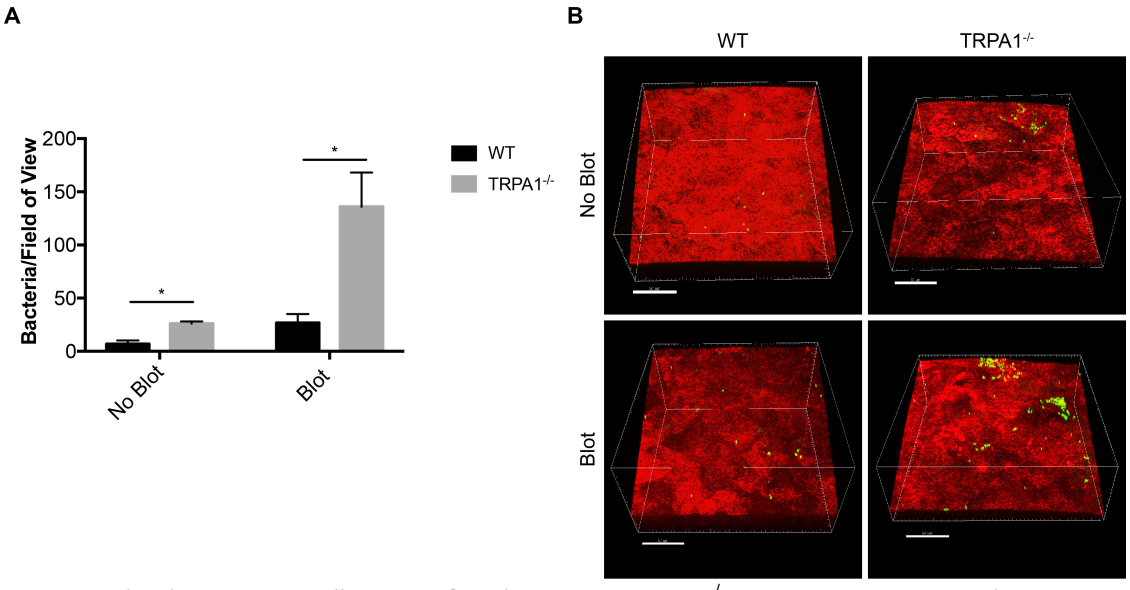


**Figure 4.11:** Inoculated *P. aeruginosa* adheres significantly more to to TRPA1$^{-/-}$ corneas *in vivo* compared to WT corneas. (A) Quantification of number of bacteria sticking to the cornea per field of view after inoculation of 1x10$^{11}$ CFUs/mL every hour for 4 h on untreated and blotted corneas. On a normal WT corneas, 6.8 ± 3.3 bacteria/field of view adhered to the cornea compared to 26.1 ± 1.9 bacteria/field of view on untreated TRPA1$^{-/-}$ corneas. The results were magnified when corneas were blotted (26.8 ± 8.3 bacteria/field of view on WT corneas compared to 135.7 ± 32.33 bacteria/field of view on TRPV1$^{-/-}$ blotted corneas). * = $P < 0.05$, Two-way ANOVA (B) Example images of PAO1-dtom (green) adhering to the cornea (red) in each condition

ion channels play an important role in preventing bacteria (both pathogens and commensal bacteria) from adhering and thus, colonizing the cornea.

To further understand how these nociceptors regulate defense against bacteria in the cornea we first explored normal constitutive defenses of the cornea. First, we looked to see if TRPA1$^{-/-}$/TRPV1$^{-/-}$ mice had a difference in mucin composition which could lead to an increase in bacterial adherence. Mucins are concentrated on the tips of apical cells and form a dense glycocalyx that prevents microbes from gaining access to host cells (Mantelli and Argüeso, 2008). Removing mucins from the ocular surface has previously been associated with an increase in bacterial adhesion (Fleiszig et al., 1994). To assess differences in the glycocalyx of wild-type and TRPA1$^{-/-}$/TRPV1$^{-/-}$ mice, wheat germ agglutinin (WGA) was used which binds to components of the corneal glycocyalx. No differences were observed in WGA staining in wild-type compared to TRPA1$^{-/-}$/TRPV1$^{-/-}$ mice both before and after bacterial inoculation (Figure 4.3).

Next, epithelial barrier integrity was assessed. Junctional complexes are present throughout the corneal epithelial and make it extremely difficult for small particles to gain access and penetrate the cornea (Mantelli and Argüeso, 2008). Disruption to epithelial junctions has been shown to cause an increase in bacterial adhesion (Alarcon et al., 2011; Tam et al., 2011). Epithelial integrity was assessed using fluorescein staining both macroscopically using a slit lamp and at high magnification with confocal imaging. Compared to the blotted control, known to have altered epithelial integrity (Tam et al., 2010), TRPA1$^{-/-}$/TRPV1$^{-/-}$ mice did not have significant fluorescein staining or penetration (Figure 4.4). In fact, the TRPA1$^{-/-}$/TRPV1$^{-/-}$ mice had even less fluorescein staining compared to wild-type. It remains a possibility that these mice upregulate other defenses in compensation for lacking TRPA1 and TRPV1 ion channels to prevent infection from occurring.

We then determined if antimicrobial activity of the cornea was altered in TRPA1$^{-/-}$/TRPV1$^{-/-}$ mice. Antimicrobial peptides are an important component of corneal defense against bacteria (Huang et al., 2007; Maltseva et al., 2007; McNamara et al., 1999; Tam et al., 2012). Previous studies have also shown that mice lacking innate regulatory signaling molecules MyD88 and IL-1R also have an increased susceptibility to bacterial adhesion (both inoculated and commensal) which is correlated with a decrease in antimicrobial activity (Sullivan et al., 2015; Wan et al., 2018). Thus, we explored if this also remained true in TRPA1$^{-/-}$/TRPV1$^{-/-}$ mice. Interestingly, no differences in bacterial growth was observed in TRPA1$^{-/-}$/TRPV1$^{-/-}$ corneal lysates compared to wild-type suggesting that TRPA1 and TRPV1 do not regulate antimicrobial peptides in the cornea (Figure 4.5). However, in these experiments whole corneal lysates were used. It could be interesting to determine if corneal epithelium alone lacks antimicrobial capabilities. It is interesting that many phenotypes in regards to bacterial adhesion are identical in the TRPA1$^{-/-}$/TRPV1$^{-/-}$ mice compared to IL-1R$^{-/-}$ and MyD88$^{-/-}$ mice but here we see a difference. The cornea must have several pathways and mechanisms in place to defend itself and prevent bacterial attachment.

Immune cell responses are another vastly important component in corneal defense. Dendritic cells have been shown to sense and respond to bacteria inoculated onto the mouse cornea within 4 hours (Metruccio et al., 2017), and the stimulation of macrophages and neutrophils have also been demonstrated to be important for bacterial killing in the cornea (Akpek and Gottsch, 2003; Karmakar et al., 2012; Pearlman et al., 2013; Sun et al., 2010). Thus, we utilized

fluorescent staining of CD45+ cells, a marker for all differentiated hematopoietic cells which include both myeloid and lymphoid derived cells. At baseline, with no treatment, wild-type and TRPA1$^{-/-}$/TRPV1$^{-/-}$ corneas had similar numbers of CD45+ cells present in the cornea (Figure 4.7). However, after inoculation of *P. aeruginosa*, wild-type corneas showed an increase in CD45+ cells as expected but TRPA1$^{-/-}$/TRPV1$^{-/-}$ corneas lacked this response (Figure 4.7). This data indicates that TRPA1 and TRPV1 receptors are associated with immune cell recruitment in response to bacterial challenge. Indeed, it has formerly been shown that nociceptor neurons regulate immune cell infiltration and function. For example, nociceptors respond to harmful stimuli by releasing neuropeptides, such as substance P and CGRP, which can lead to an influx and activation of immune cells (Chiu et al., 2012; Hosoi et al., 1993; Mantelli et al., 2010; Reilly et al., 2005).

We next wanted to decipher specific immune cell types that TRPA1 and TRPV1 regulate in the context of bacterial inoculation. Due to the quick timing of the influx of immune cells (4 h), and published results demonstrating CD11c+ cells (i.e. dendritic cells) also respond to bacteria within this time frame (Metruccio et al., 2017), we investigated the effects of TRPA1 and TRPV1 on CD11c+ cell recruitment. To do this, resiniferatoxin (RTX) was used to selectively ablate TRPA1 and TRPV1 channels in mice expressing CD11c-yfp cells. Without any bacterial inoculation, control and RTX treated mice had similar numbers of CD11c+ cells present in the cornea. After *P. aeruginosa* inoculation an increase in the number of CD11c+ cells was observed in control mice but not RTX treated mice. Thus, we suggest that specifically, TRPA1 and TRPV1 nociceptors are involved with dendritic cell recruitment in response to bacterial adherence on the cornea. It is important to note, that this response is being observed during homeostasis, when the cornea is healthy. Under an infection or inflammatory states, it remains a viable possibility that alternative responses and signals occur. However, these results also suggest that TRP ion channels may have two levels of regulation of barrier function: 1.) at a constitutive level which helps to clear commensal bacteria as evidenced by an increase in colonization of environmental bacteria on TRPA1$^{-/-}$/TRPV1$^{-/-}$ corneas but no differences in immune cells (Figure 4.6; 4.7) and 2.) as a response to large amounts and potentially more harmful bacteria as shown by an increase in adherence of inoculated *P. aeruginosa* (Figure 4.1) and a lack of immune cell infiltration (Figure 4.6; 4.7). This immune cell response observed post-inoculation could be due to an increase in amount of bacteria present on the cornea or perhaps due to the pathogenicity of *P. aeruginosa* compared to commensal bacteria.

Given that TRPA1 and TRPV1 channels are claimed to be present on epithelial cells and immune cells, in addition to sensory nerve endings (Belmonte et al., 2017), we aimed to determine the receptors on which cell type was important for preventing bacterial adhesion on the cornea. Thus, *P. aeruginosa* adherence experiments were repeated *ex vivo* in which the eye is enucleated and the optic nerve is severed. No differences in the number of bacteria adhered to the cornea was observed (Figure 4.8). To confirm this finding, corneal nerve blocks were utilized via subconjunctival injection of bupivacaine, an anesthetic that prevents nerve firing with long lasting effects. Mice treated with bupivacaine still had a significant increase in *P. aeruginosa* adhered to the cornea compared to control mice (Figure 4.9). These results indicate that neuron-associated TRP channels are important for keeping the cornea free of bacterial colonization. This also is in

line with the opinion of the neurobiology field which believe that in actuality, TRP channels are only expressed on neurons and not on other cell types.

Interestingly, TRPV1$^{-/-}$ had similar amounts of bacteria adhering to the cornea post- inoculation compared to wild-type (Figure 4.10) suggesting that either TRPA1 alone or both TRPA1 and TRPV1 channels are important for bacterial defense in the cornea. Thus single-knockout mice for TRPA1 were tested. TRPA1$^{-/-}$ recapitulated the results using the double-knockout mice indicating that TRPA1 is important for preventing bacterial adherence on the cornea. Indeed, TRPA1 has been shown to be directly activated by bacterial components such as LPS (Meseguer et al., 2014). Additionally, ion channel TRPA1 has also previously been shown to mediate inflammation in other tissues such as in models of dermatitis, colitis, and asthma (Caceres et al., 2009; Engel et al., 2011; Liu et al., 2013). TRPA1 is also associated with superficial neurons which would correspond with their ability to respond to surface associated bacteria.

Overall, this study demonstrates that transient receptor potential ion channels (TRP channels) are an important component of corneal defense and contribute towards keeping the healthy cornea bacteria-free. These ion channels are neuron-associated and are involved in immune cell recruitment in the cornea. This is the first study to demonstrate the role of sensory neurons in defense against bacteria on the cornea. Further, this data adds to our understanding of neurogenic inflammation and emphasizes the important role of nerves in epithelial defense. Not only are corneal nerves critical for sensory induction and structural support, but they also play a large role in signal transduction regarding immune activation and corneal resistance to bacteria. Our current model hypothesizes that TRP ion channels, specifically TRPA1, located on sensory nerve endings quickly respond to bacteria present on the corneal epithelium and initiates a signaling cascade to promote dendritic cell infiltration and activation to clear the threatening microbes. Further studies are warranted to differentiate between the roles of TRPA1 and TRPV1 as well as identify other nociceptor contributions to corneal defense. The exact molecular underpinnings of this phenomenon (i.e. if release of substance P or CGRP is involved) also need to be clarified. However, this study furthers our understanding of the mechanisms in place and a role of sensory nerves during homeostasis to keep a cornea free of bacteria.

## 4.6 Acknowledgements

This work was supported by the National Institutes of Health EY011211 (SMJF). Our many thanks to Dr. Dara Frank (Medical College of Wisconsin) for the *P. aeruginosa* (PAO1-dtom) strain. A huge thank you to Dr. Diana Bautista (UC Berkeley) and Rose Hill for their advice and consultation with this project.

## 4.7 Supplementary Material

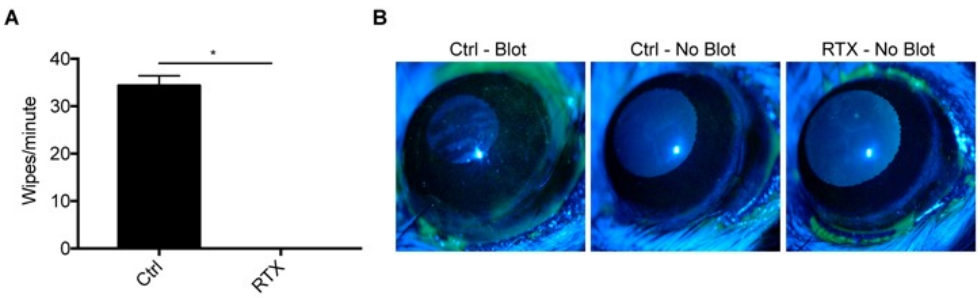


**Figure 4.12:** A. Capsaicin eye wipe test. 100μM capsaicin was dropped onto lightly anesthetized control and RTX treated mice and number of eye wipes for 1 min counted. RTX treated mice did not wipe eyes after capsaicin application whereas control mice had an average of 34 wipes/minute. B. Fluorescein under the slit lamp reveals staining in blotted control corneas but no staining in no blot controls or RTX treated corneas indicating normal epithelial integrity.

# Chapter 5

# Experimentally induced dry eye disease does not increase murine corneal susceptibility to environmental bacterial colonization

## 5.1 Abstract

Microbiomes play an important role in host homeostasis. Disturbances in either abundance or diversity of the bacterial constituents is often associated with disease. Remarkably, unlike other exposed mucosal tissues, the cornea is devoid of a microbiome. The cornea harnesses a slew of defense mechanisms to prevent bacterial colonization, which could lead to inflammation and sight threatening infections. Dry eye disease is a multifactorial disease associated with discomfort and inflammation of the ocular surface that can drastically affect the quality of life of patients. The role of bacteria during dry eye disease has been often questioned but has not been fully characterized. Given that dry eye also reduces several corneal defenses, we hypothesized that dry eye disease makes the cornea susceptible to bacterial colonization which could contribute to the accompanying pain and inflammation. This was studied using bacterial imaging techniques on mice with experimentally-induced dry eye disease to overcome obstacles and limitations of 16s rRNA sequencing and standard culture methods. Interestingly, we found that dry eye disease does not enable environmental colonization of the cornea. Similarly, no changes in the conjunctiva were observed. These data suggest that the associated irritation and inflammation of dry eye disease occurs without disruption to mechanisms that normally prevent colonization of the mouse cornea.

## 5.2 Introduction

Microbial communities exist in most mucosal surfaces and play an important role in maintaining homeostasis. Remarkably, the cornea is devoid of a bacterial microbiome despite being constantly exposed to the environment (Wan et al., 2018). Its neighboring tissue, the conjunctiva does support a small population of resident bacteria however, in much fewer numbers compared to other mucosal surfaces (Doan et al., 2016; Dong et al., 2011; St Leger et al., 2017; Wan et al., 2018). The inherent resistance to microbial colonization of the ocular surface and primarily the cornea, is due to the several defenses employed including: washing effects of tears and blinking (Selinger et al., 1979), antimicrobial properties of tear fluid(Akpek and Gottsch, 2003; Fleiszig et al., 2003; McClellan, 1997), antimicrobial peptides expressed at the ocular surface (McDermott, 2009; McNamara et al., 1999; Tam et al., 2012), epithelial barrier function(Alarcon et al., 2011) and innate immunity signaling pathways(Metruccio et al., 2017; Sullivan et al., 2015). These defenses are critical to prevent opportunistic bacterial colonization which could lead to sight-threatening infections.

Dry eye is a multifactorial disease of the ocular surface characterized by loss of tear film leading to symptoms of discomfort, inflammation and damage to the ocular surface (Craig et al., 2017). Dry eye disease (DED) is associated with several factors that suggests a compromise in defenses against microbial colonize such as altered tear film composition, decrease in antimicrobial factors (Caffery et al., 2008; Narayanan et al., 2003), loss of conjunctival goblet cells which secret MUC5A known to trap and clear bacteria (Argüeso et al., 2002; Fleiszig et al., 1994), and poor epithelial integrity (Beardsley et al., 2008). However, it is not well characterized if any of these changes associated with DED enable colonization of environmental bacteria. It remains a possibility that the presence of bacteria contribute to the ocular surface damage and inflammation observed during DED. Indeed, oral antibiotics have been used as a therapy and shown to improve dry eye symptoms which could correlate to a reduction in bacteria (Dougherty et al., 1991). Additionally, TLR-4, which responds to lipopolysaccharide, a component of the cell wall of Gram-negative bacteria, is upregulated during DED and contributes to the inflammatory response (Lee et al., 2012). These studies underpinned the hypothesis that bacteria, not normally present on the healthy eye, could play a role in the pathogenesis of this debilitating disease.

Few studies have looked at the presence of bacteria in association with dry eye disease. Graham et al., used culture and 16S rRNA gene sequencing to look at the posterior lid margin and lower conjunctival sac of patients with DED compared to healthy controls. Conventional culture methods resulted in a slight increase in overall number of bacteria present in DED, including a significant difference in the mean bacterial count of the control group compared to a severe DED group (Graham et al., 2007). However, there was no statistically significant difference in number of positive PCR swabs in normal and DED subjects (Graham et al., 2007). Another group also assessed differences in the ocular surface microbiome using 16s rRNA gene sequencing methods of conjunctival swabs in patients with Sjögren Syndrome. No differences in bacterial constituents was found between the DED and control group (De Paiva et al., 2016). However, both of these studies only assessed the conjunctiva and it has previously been established that

the cornea and conjunctiva have differences in their microbial constituents during health (Wan et al., 2018).

Here, we tested the hypothesis that experimentally induced dry eye disease (EDE) would alter corneal susceptibility to environmental bacterial colonization. To investigate this, we employed alkyne-functionalized D-alanine (alkDala) to label metabolically active bacteria and fluorescent in situ hybridization (FISH) of a universal bacterial 16S rRNA gene probe to detect bacteria independent of peptidoglycan metabolism on the ocular surface. Our results showed the EDE mouse corneas remain devoid of bacteria.

## 5.3 Experimental Procedures

### 5.3.1 Mice

All procedures were carried out in accordance with a protocol approved by the Animal Care and Use Committee, University of California, Berkeley and adhered to the ARVO Statement for the use of Animals in Ophthalmic Vision Research. Six to twelve week old wild-type female C57/BL6 mice were used. In some studies, transgenic mice with fluorescent red cell membranes (*mT/mG* knock-in mice) (Muzumdar et al., 2007) mice were used. These studies only used females because females have a higher incidence and severity of the disease (Gao et al., 2015; Schaumberg et al., 2013) and males did not tolerate the treatment well. After the course of treatment was completed, mice were euthanized by intraperitoneal injection of ketamine (80-100mg/kg) and xylazine (5-10 mg/kg) followed by cervical dislocation.

### 5.3.2 Experimentally-Induced Dry Eye (EDE) Murine Model

EDE was induced in mice as previously described (Gao et al., 2015; Heimer et al., 2013). Mice were given subcutaneous injections of scopolamine hydrobromide (0.1mL of 10 mg/mL for first three days and then 0.1mL of 5mg/mL for next 4-7 days) three times daily, alternating between right and left flanks for a total of five or ten days. Animals were housed in mesh-sided cages and exposed to continuous fan-generated air drafts with low humidity (35-40%). Litter matched controls were housed in normal conditions. Aqueous tear production was assessed by placing a phenol red cotton thread (Zone-Quick; FCI Ophthalmics) in the lateral canthus for 1 min and reported as millimeters of wetted thread. Mean corneal epithelial cell area and density were calculated as previously described (Beardsley et al., 2008). Corneal epithelia area was measured by outlining 20 individual cells per image using Image J and computing the average for each group. After the mean cell area was calculated, the cell density was determined by dividing by the known image field area and then standardized to cells per square millimeter. Fluorescein staining was done as previously described (Wan et al., 2018). Eyes were rinsed with PBS after induction of anesthesia. A drop (5 $\mu$L) of fluorescein solution (0.02%) was then added to the ocular surface, and corneal epithelial integrity examined using a slit lamp.

### 5.3.3 Fluorescence *In situ* Hybridization (FISH)

Whole enucleated mouse eyes were fixed in paraformaldehyde (2%) for 1 h with shaking at RT. Bacterial hybridization was performed using a universal 16S rRNA gene [Alexa488]-GCTGCCTCCCGTAGGAGT-[Alexa488] (Eurofins Genomics) as previously described (Mark Welch et al., 2016; Vaishnava et al., 2011). Briefly, fixed lenses and eyes were washed in 80% EtOH, 95% EtOH, and then PBS for 10 min each with shaking at RT. Lenses and eyes were then placed in a hybridization buffer solution [NaCl (0.9 M), Tris-HCl (20 mM, pH 7.2) and SDS (0.01%)] and incubated at 55°C for 30 min. The probe was added to final concentration of 100 nM and incubated at 55°C overnight. Eyes were then transferred to wash buffer solution [NaCl (0.9 M) and Tris-HCl (20 mM, pH 7.2)] and washed 3 times for 10 min each with shaking at RT.

### 5.3.4 Alkyne Functionalized D-alanine Labeling (alkDala)

Labeling of live bacteria using an alkyne functionalized D-alanine (alkDala) bioorthogonal probe (Shieh et al., 2014; Siegrist et al., 2013) on the ocular surface was done as previously described (Wan et al., 2018). Enucleated eyes were incubated in a solution of alkDala (10 mM) in Dulbecco's Modified Eagle Medium (DMEM) at 37°C for 2 h. Eyes were then transferred to pre-chilled 70% EtOH and fixed for 20 min at -20°C. After rinsing, eyes were permeabilized in PBS containing Triton-X100 (0.5%) for 10 min with shaking at room temperature (RT), then washed 3 times for 5 min each in PBS containing Triton-X100 (0.1%) and BSA (3%) with shaking at RT. Eyes were then transferred to the Click-labeling cocktail [in PBS, TBTA (100 $\mu$M), CuSO4 (1 mM), sodium ascorbate (2 mM), 488 nm azide fluorophore (10 $\mu$M), BSA (0.1 mg/mL)] for 1 h with shaking at RT.

### 5.3.5 Confocal Microscopy

Murine eyeballs were imaged *ex vivo* as previously described (Tam et al., 2011). Briefly, eyes were fixed to a 12 mm glass coverslip with cyanoacrylate glue. The coverslip with eyeball was placed in a 47 mm Petri dish and filled with PBS to cover the eyeball completely. Confocal imaging was performed using an Olympus FV1000 confocal microscope. A 488 nm laser was used for detection of bacteria labeled with alkDala or FISH, or corneas stained with fluorescein and a 559 nm laser used for detection of red-fluorescent cellular membranes when appropriate, and a 635 nm laser used to obtain corneal reflectance (excitation and emission at same wavelength) when mice without fluorescent membranes were used. At least four fields of each eye (~0.04 $mm^2$) were imaged from the corneal surface through the entire epithelium in 0.5 $\mu$m steps. Three-dimensional images were reconstructed from z-stacks using IMARIS software (Bitplane) which was also used to quantify detected bacteria.

### 5.3.6 Statistical Analysis

Data were expressed as mean ± standard error of the mean (SEM). Statistical significance of differences between means of two groups was determined using an unpaired Student's t-Test or Mann–Whitney *U*-test for non-parametric groups. For three or more groups, ANOVA with Tukey's multiple comparison test for post hoc analysis or the Kruskal–Wallis test was used with Dunn's multiple comparison test for *post hoc* analysis for non-parametric tests. P-values < 0.05 were considered significant.

## 5.4 Results

### 5.4.1 Induction of experimental dry eye disease does not affect gross ocular morphology

Mice were given a five or ten-day regimen of scopolamine injections and housed in dehumidified conditions to induce dry eye disease. After five or ten days, aqueous tear production was assessed using a phenol red thread tear test. Treated mice had about a 60% decrease in tear production compared to control mice (1.94 ± 0.26mm thread wetness in controls compared to 0.63 ± 0.13mm thread wetness at 5 days and 0.788 ± 0.09mm thread wetness at 10 days., P < 0.0001, ANOVA with Tukey's multiple comparisons test) (Figure 5.1A). Mice exhibited no gross morphological corneal defects but increased fluorescein staining in treated mice confirmed the induction of dry eye (Figure 5.1B).

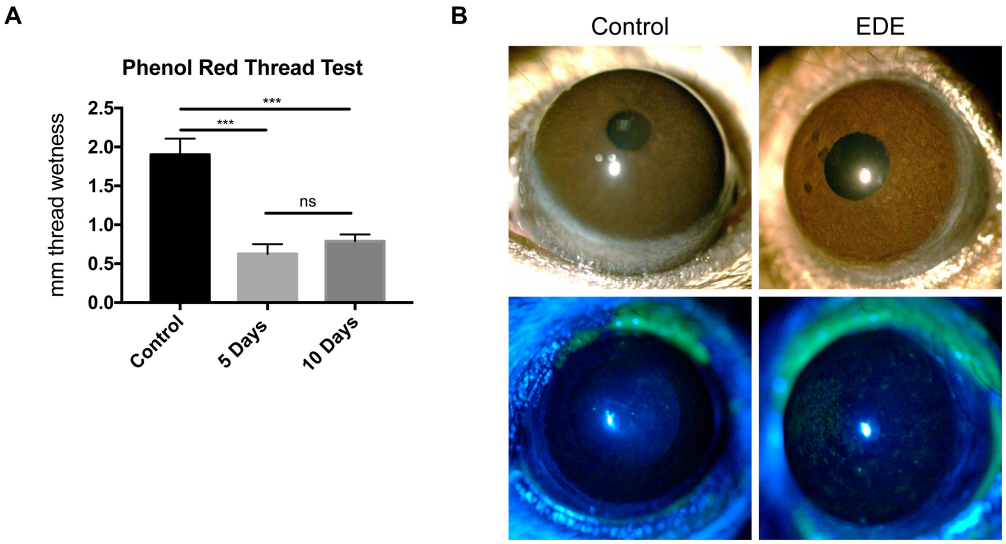


**Figure 5.1:** Induction of experimental dry eye. (A) Tear volumes in the eyes of C57/BL6 mice under dry eye (EDE) conditions verses normal controls were measured using the phenol red thread tear test. EDE resulted in a significant decrease in tear volume after 5 and 10 days of treatment. Tears were collected from the lateral canthus using a cotton thread and reported as millimeters of wetted thread. Data expressed as mean ± SEM. *** = P < 0.001, ANOVA with Tukey's multiple comparisons test. (B) After induction of dry eye, photographs taken with a slit lamp demonstrate that no overt changes to the ocular surface occurred (upper panels). However, increased fluorescein staining in EDE mice (lower panels) demonstrate reduced epithelial integrity.

To investigate this further on a cellular level, mice with red-fluorescent cell membranes were utilized (Muzumdar et al., 2007). After the course of treatment, mice were euthanized and live enucleated eyes were imaged using laser-scanning confocal microscopy. Snapshots of each corneal layer are shown in Figure 5.2A. No morphological changes in the cornea stood out in EDE mice. Furthermore, no significant differences were observed in mean epithelial cell area or density in EDE corneas compared to controls (Figure 5.2). This corresponds to a significant paradox in dry eye disease in which many patients complain of several symptoms of dry eye disease yet have no overt signs of disease.

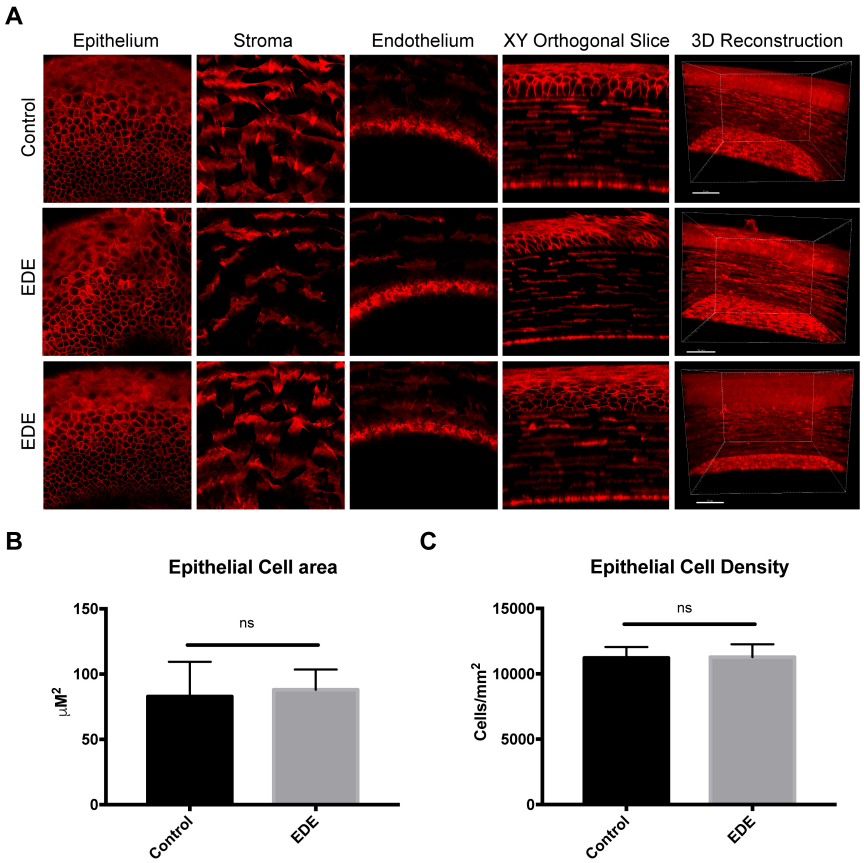


**Figure 5.2:** Confocal imaging of corneas in EDE versus control mice. (A) Transgenic C57/BL6 mice with red fluorescent cell membranes were sacrificed, then eyes enucleated and glued onto glass cover slip and covered in DMEM to keep alive. Eyes were imaged at 0.5 $\mu$M stacks through the entire cornea. No differences in corneal morphology was detected between EDE and control corneas. Snapshots of the epithelium, stroma, endothelium, XY orthogonal slice and 3D reconstruction are shown (B) Epithelial cell area in EDE mice (88.77 ± 10.65 $\mu M^2$) did not differ significantly from control mice (90.78 ± 6.69 $\mu M^2$). (C) Similarly, no significant differences were observed in corneal epithelial cell density in EDE mice (11,224 ± 825.3 cells/mm$^2$) compared to controls (11,280 ± 978.4 cells/mm$^2$).

### 5.4.2 EDE does not alter mouse corneas to be susceptible to environmental bacteria

Since dry eye disease is associated with a reduction of defense mechanisms at the ocular surface we hypothesized that this would enable bacterial colonization on the otherwise sterile tissue. To test this, mouse eyes with EDE were subjected to alkDala labeling which detects metabolically active bacteria (Figure 5.3). EDE corneas rarely had any live bacteria identified (0.42 ± 0.30 bacteria/field of view at 5 days treatment and 0.67 ± 0.67 bacteria/field of view at 10 days treatment) which was similar to control mouse corneas (0.81 ± 0.52 bacteria/field of view).

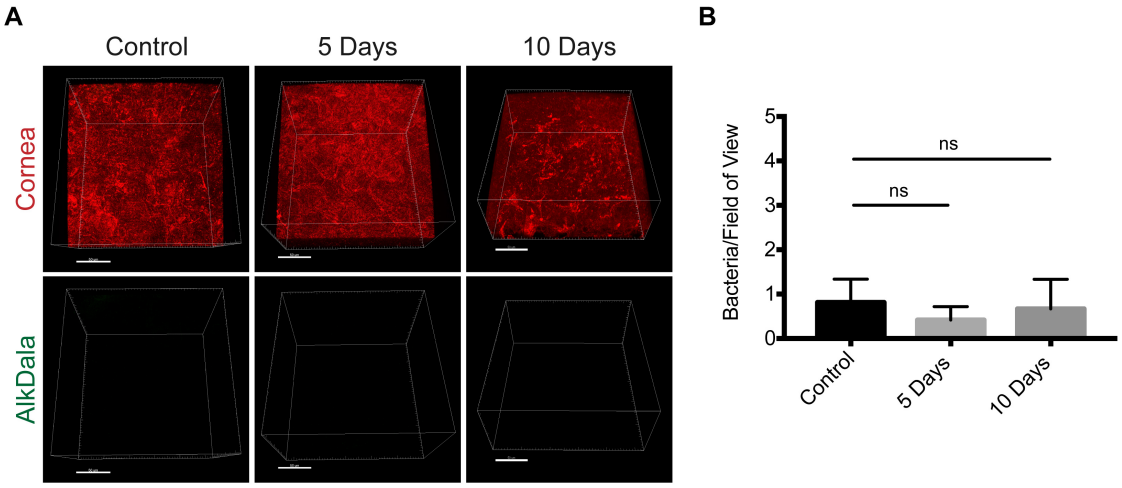


**Figure 5.3:** EDE mouse corneas do not host live bacteria. (A) Confocal images of mouse corneas (upper panels) and alkDala labeling (lower panels, same image as above with red channel removed) in control and EDE corneas after 5 and 10 days of treatment. Bacteria were rarely identified on corneas in either group. (B) Quantification of number of bacteria detected/field of view expressed as mean ± SEM. AlkDala labeling detected 0.81 ± 0.52 bacteria/field of view in control mice compared to 0.42 ± 0.30 bacteria/field of view and 0.67 ± 0.67 bacteria/field of view in 5 and 10 days of treatment respectively. NS, no significance, Kruskal-Wallis test with Dunn's multiple comparisons.

To confirm that bacteria were not present on the mouse cornea, FISH labeling against a universal bacterial 16S rRNA gene was utilized (Figure 5.4). This data corroborated our previous results in that bacteria were rarely detected on EDE mice compared to controls. FISH labeling detected 0.65 ± 0.65 bacteria/field of view in control mice compared to 0.25 ± 0.25 bacteria/field of view in 5 day EDE mice and 1.11 ± 1.11 bacteria/field of view in 10 day EDE mice corneas.

### 5.4.3 EDE does not alter the conjunctival microbiome

Because bacteria were rarely detected in the mouse cornea during dry eye disease we thought that this could be due to the inhospitable environment that dry eye disease induces. Bacteria thrive in moist and nutrient rich environments which a dry eye is clearly not. Previous studies using 16s rRNA sequencing methods may not have found differences in bacterial components due to detecting nucleic acids and not live microbes. Similarly, standard culture methods have several

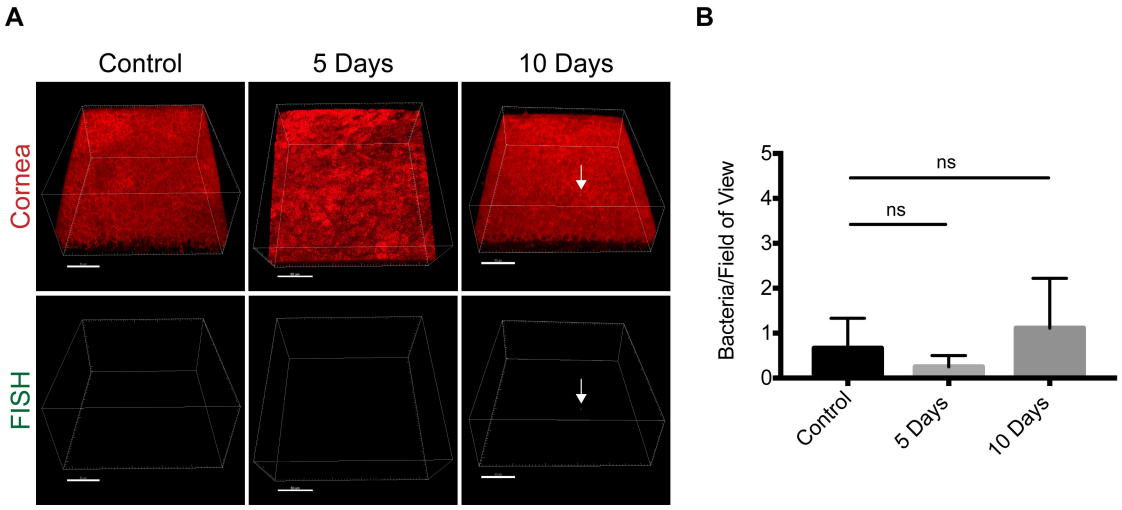


**Figure 5.4:** FISH labeling rarely detected bacteria on EDE mice (A) 3D reconstructions of mouse corneas (upper panels) and FISH labeling (lower panels, same image as above with red channel removed) showing that bacterial detection was infrequent. White arrow points to detected bacteria. FISH labeling confirms that dry eye disease does not enable environmental bacterial colonization on the mouse cornea. (B) Quantification of number of bacteria detected/field of view expressed as mean ± SEM. FISH labeling detected 0.65 ± 0.65 bacteria/field of view in control mice compared to 0.25 ± 0.25 bacteria/field of view in 5 day EDE mice and 1.11 ± 1.11 bacteria/field of view in 10 day EDE mice corneas. NS, no significance, Kruskal-Wallis test with Dunn's multiple comparisons.

limitations in the number and type of bacteria detected. Therefore, we looked to determine if the presence of metabolically active bacteria, particularly the filamentous bacteria identified previously in the conjunctiva (Wan et al., 2018) differed in EDE mice compared to controls. To test for this, alkDala labeling was employed. Numerous metabolically active filamentous bacteria were still detected in the conjunctiva in EDE mice, similar to control mice (Figure 5.5). Overall, these results indicate that dry eye disease does not diminish bacterial defenses on the ocular surface. However, whether the same mechanisms compared to homeostasis remain in place or if other defenses are upregulated to compensate remains to be determined.

## 5.5 Discussion

In this study, we addressed the possibility that commensal bacteria could inhabit the cornea after the induction of dry eye disease. To do this, we utilized alkDala, a metabolic label of peptidoglycan and FISH against universal 16s rRNA to directly visualize viable bacteria on the mouse cornea using confocal imaging. Dry eye disease is associated with a myriad of changes to the ocular environment including several associated with a decrease in defense against bacterial colonization. Despite this, our results suggest that dry eye disease does not alter the bacterial landscape (or lack there-of) on the ocular surface.

After the induction of experimentally induced dry eye disease, corneal morphology was assessed. As expected, tear production decreased and fluorescein staining increased. These hallmarks of dry eye confirmed that we successfully induced dry eye disease in our murine

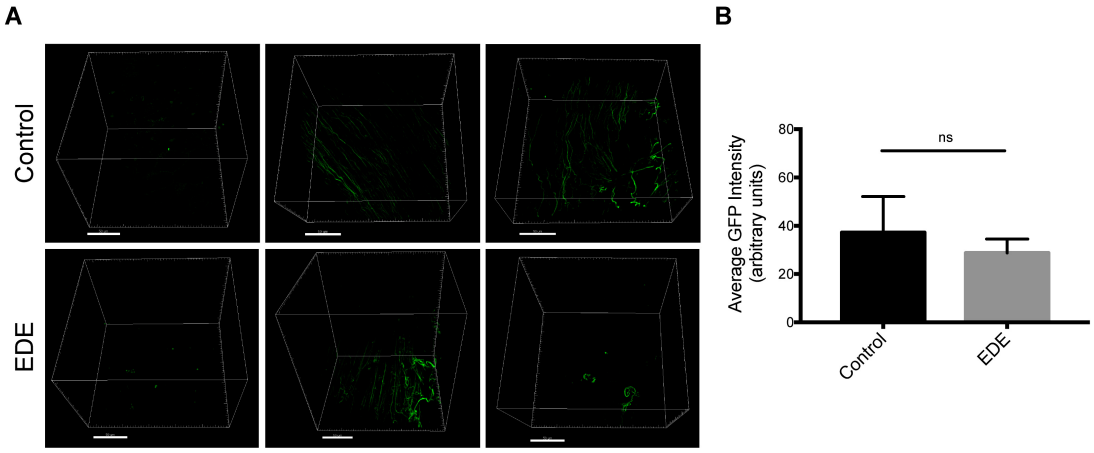


**Figure 5.5:** EDE does not alter filamentous bacteria identified on the mouse conjunctiva. Unlike the cornea, the mouse conjunctiva hosts bacteria including filamentous bacteria. (A) Confocal images show that EDE does not alter the ability to identify these filamentous bacteria on the conjunctiva. (B) No significant differences were detected in the conjunctiva of controls compared to EDE mice in terms of alkDala labeling measured as average GFP intensity (37.22 ± 14.88 average GFP intensity in controls vs. 28.74 ± 5.78 average GFP intensity in DED mice). NS, no significance, Mann-Whitney test.

model. Interestingly, utilizing transgenic mice with red fluorescent cell membranes indicated that no major alterations to the corneal cells occurs. No changes in epithelial cell area or density were detected. This observation differed to what previously was reported which identified a decrease in epithelial cell area and density after EDE (Beardsley et al., 2008). Perhaps this mirrors the variability observed with dry eye in human patients. While some patients express apparent ocular signs of dry eye, others do not. But both groups can still experience debilitating symptoms.

Once induction of EDE was confirmed, mouse eyes were subjected to either alkDala or FISH labeling to detect bacteria *in situ* on the ocular surface. Bacteria were rarely detected on the mouse cornea after both five and ten days of treatment using both labeling methods. Furthermore, similar amounts of bacteria were also detected on the conjunctiva in EDE mice compared to control mice. This result supports previous studies identifying bacteria on the conjunctiva during dry eye (De Paiva et al., 2016; Graham et al., 2007) suggesting that EDE overall does not alter the bacterial landscape on the conjunctiva nor allow bacteria to colonize the cornea.

While our finding showing that commensal bacteria do not inhabit the cornea after EDE was the opposite of our initial hypothesis, our results are in line with a previous study that deliberately inoculated *Pseudomonas aeruginosa* onto the cornea (Heimer et al., 2013). Mice with EDE were still able to clear the bacteria, similar to controls. Together, these results indicate that dry eye does not inhibit defenses of the cornea to enable either environmental or pathogenic colonization. Interestingly, this same study also showed that EDE mice had an increase of expression of surfactant protein-D (SP-D) in ocular washes compared to controls (Heimer et al., 2013). Previously, SP-D has been shown to play a role in defending the cornea against *P. aeruginosa* (Mun et al., 2009). It then remains a distinct possibility that rather than no changes to corneal defenses occurring, dry eye disease may cause an upregulation of other defense mechanisms that

then keep the cornea free of bacteria. Further studies are necessary to determine this distinction.

Overall, these results indicate that dry eye disease does not render the ocular surface to be susceptible to increased bacterial colonization. It then seems that local bacteria on the ocular surface are unlikely to play a role in the pathogenesis of dry eye disease. However, this study only looked at the presence or absence of live bacteria on the cornea or conjunctiva. It is possible that dry eye disease results in changes to the species of bacteria present on the conjunctiva, as well as the surrounding lid margins. Additionally, microbial components may also induce inflammatory responses. Whether these types of changes occur and do indeed affect the pathogenesis of dry eye disease remains to be understood.

## 5.6 Acknowledgements

This research was supported by the National Institute of Health EY011211 (SMJF). Our many thanks to Drs. Karsten Gronert and Becca Flitter (University of California, Berkeley) for assistance in EDE model set-up and to Dr. Carolyn Bertozzi (Stanford University) for reagents for alkDala labeling

# Chapter 6

# A novel murine model for contact lens wear reveals clandestine IL-1R dependent corneal parainflammation and susceptibility to microbial keratitis upon inoculation with *Pseudomonas aeruginosa*

## 6.1 Abstract

This Chapter is a full reprint of Metruccio et al., *The Ocular Surface* (2018), in which I was a primary author. The work is included with permission from authors.

**Relevant Publication:**
Metruccio, M.M.E., Wan, S.J., Horneman, H., Kroken, A.R., Sullivan, A.B., Truong, T.N., Mun, J.J., Tam, C.K.P., Frith, R., Welsh, L., et al. (2018). A novel murine model for contact lens wear reveals clandestine IL-1R dependent corneal parainflammation and susceptibility to microbial keratitis upon inoculation with *Pseudomonas aeruginosa*. The Ocular Surface.

*Purpose*: Contact lens wear carries a risk of complications, including corneal infection. Solving these compli- cations has been hindered by limitations of existing animal models. Here, we report development of a new murine model of contact lens wear.
*Methods*: C57BL/6 mice were fitted with custom-made silicone-hydrogel contact lenses with or without prior inoculation with *Pseudomonas aeruginosa* (PAO1-GFP). Contralateral eyes served as controls. Corneas were monitored for pathology, and examined *ex vivo* using high-magnification, time-lapse imaging. Fluorescent reporter mice allowed visualization of host cell membranes and immune cells. Lens-colonizing bacteria were detected by viable counts and FISH. Direct-colony PCR was used for bacterial identification.

*Results*: Without deliberate inoculation, lens-wearing corneas remained free of visible pathology, and retained a clarity similar to non-lens wearing controls. CD11c-YFP reporter mice revealed altered numbers, and distribu- tion, of CD11c-positive cells in lens-wearing corneas after 24 h. Worn lenses showed bacterial colonization, primarily by known conjunctival or skin commensals. Corneal epithelial cells showed vacuolization during lens wear, and after 5 days, cells with phagocyte morphology appeared in the stroma that actively migrated over resident keratocytes that showed altered morphology. Immunofluorescence confirmed stromal Ly6G-positive cells after 5 days of lens wear, but not in MyD88 or IL-1R gene-knockout mice. *P. aeruginosa*-contaminated lenses caused infectious pathology in most mice from 1 to 13 days.
*Conclusions*: This murine model of contact lens wear appears to faithfully mimic events occurring during human lens wear, and could be valuable for experiments, not possible in humans, that help solve the pathogenesis of lens-related complications.

## 6.2 Introduction

Contact lenses represent a common form of vision correction with over 40 million wearers in the USA 1. (Cope et al., 2015), and estimates of over 140 million wearers worldwide (Stapleton et al., 2007; Nichols et al., 2013). Lens-wear is expected to rise dramatically over the next decade due to an ongoing myopia epidemic (Wu et al., 2016), the use of lenses for drug delivery (El Shaer et al., 2014;Ciolino et al., 2014), development of lenses with biosensing electronics (health monitoring) (Phan et al., 2016; Farandos et al., 2015), and their potential use for augmented reality (Park et al., 2018).

It is well established, however, that contact lens wear can predispose the human cornea to various complications. The most serious is microbial keratitis (Stapleton et al., 2007; Willcox and Holden, 2001) for which there are multiple risk factors; including microbial contamination of lenses and lens cases, over- night or extended wear, potential failure of lens care solutions, and poor hygienic practices (Stapleton and Carnt, 2011; Wu et al., 2015; Lim et al., 2016; Schein et al., 1994; Stapleton et al., 2008). Contact lenses also carry the risk of other corneal and ocular complications, including acute and chronic inflammatory events, dryness, and overall discomfort (Stapleton et al., 2007; Nichols et al., 2013; Sorbara et al., 2009). Unfortunately, despite considerable progress in contact lens design (e.g., development of silicone hydrogel lenses with high oxygen transmissibility), the incidence of microbial keratitis has not changed (Stapleton et al., 2013). User non-compliant practices remain widespread, often under-reported, and may exacerbate the risk of adverse events (Lim et al., 2016; Chalmers et al., 2012; Dumbleton et al., 2013; Robertson, 2011). The etiology and pathogenesis of infections, and other complications, remain unresolved.

Human studies, such as those cited above, are of considerable value in determining the epidemiology of contact lens-related complications, and risk factors involved. However, our progress in understanding these complications at a molecular, cellular, and tissue level has been hindered by the limitations of experiments that can be performed on human subjects.

Several studies have reported the use of contact lens-wearing animal models to investigate the pathogenesis of lens-associated microbial keratitis. Examples include cytokine and chemokine profiles of *P. aeruginosa*-challenged corneas in a lens-wearing rat model (Szliter et al., 2002; Zhang et al., 2008), the association of contact lens-associated biofilms/bacterial adaptations in development of *P. aeruginosa* keratitis in a lens-wearing rat model (Tam et al., 2010), the relationship between neutrophil infiltration and severity of *P. aeruginosa* keratitis in a rabbit model (Wei et al., 2014), and the role of lens colonization and microbial antigens in lens-induced infiltrative events in a guinea pig model (Vijay et al., 2009). However, these previous lens-wearing models have been limited by one or more factors: 1) limited lens supply (Tam et al., 2010), 2) use of a larger animal (e.g. rabbit) for which eyelid closure or nictitating membrane surgery is required for lens retention (Wei et al., 2014; Lawin-Brüssel et al., 1993), 3) infiltrative, inflammatory events that occur but do not lead to microbial keratitis (e.g. guinea pig) (Vijay et al., 2009), 4) microbial keratitis that does not occur or is evident at a low level despite repeated bacterial inoculation (e.g. rat) (Szliter et al., 2002; Zhang et al., 2008). All of these models are also limited by availability of research tools suitable for the animals involved, such as methods for genetic manipulation and analysis, antibodies for protein detection, purification, or imaging, given that many modern reagents are designed for use only in mice.

In the absence of a mouse contact lens, researchers interested in understanding the pathogenesis of contact lens-induced infection have had to use surrogate models to ask relevant questions, including *in vitro* cell culture models. Other researchers have used *in vivo* mouse models in which scarification, healing after scarification, or intrastromal injection are used to induce infection. The latter have enormously advanced our understanding of the immune and inflammatory response to microbes (Hazlett, 2004; Hazlett and Hendricks, 2010; Willcox, 2007), and the role of bacterial virulence factors (Lee et al., 2003; Zolfaghar et al., 2006; Choy et al., 2008; Evans and Fleiszig, 2013; Sullivan et al., 2015), once infection has already initiated. However, while full-thickness epithelial injury is a common predisposing factor for corneal infection in non-lens wearers (Lin et al., 2012; Somabhai Katara et al., 2013), there is little evidence to support the idea that contact lens wearers are predisposed to microbial keratitis in this way. Thus, such injury-based models are not ideal for exploring host and microbial factors involved in initiating infection of a previously healthy cornea in the context of contact lens wear.

Dendritic (or Langerhans) cell recruitment in the central cornea and conjunctiva has been reported as a response to contact lens wear in humans, regardless of material, solution type or lens wear modality (Alzahrani et al., 2016; Alzahrani et al., 2017; Sindt et al., 2012). Even though the cornea is normally devoid of resident viable bacteria (Wan et al., 2018), commensal microbe accumulation on human lenses during wear without resulting infection has also been well established (Willcox, 2013a). Here, we report development of a novel contact lens-wearing murine model which faithfully reproduces both of these human events. Moreover, aligning with the known risk of infection with opportunistic microbes during human lens wear, corneas of mice wearing lenses became susceptible to infection with *P. aeruginosa*, an opportunist unable to infect healthy corneas in the absence of lens wear. Using reagents available for mice but not humans, we additionally show that uninoculated contact lens wear can induce parainflammation consisting of neutrophil recruitment in otherwise healthy-appearing corneas. This phenomenon

was found dependent on MyD88 and IL-1R, well known for their role in host innate defense, and as we have previously shown, regulate multiple relevant phenomena in the healthy cornea including its lack of a viable bacterial microbiome, its glycosylation, and epithelial defenses against microbial adhesion and penetration (Wan et al., 2018; Jolly et al., 2017; Metruccio et al., 2017). This model allows us to further our understanding of lens-associated events at the ocular surface, and their role in susceptibility to infection. Such in-depth biochemical, tissue and cellular experiments involving use of molecular markers would not be possible in humans.

## 6.3 Methods

### 6.3.1 Murine Contact Lenses

The contact lenses used in this study were fabricated by CooperVision, Inc. (Pleasanton, CA) and were provided without compensation under a material transfer agreement between CooperVision, Inc. and the University of California, Berkeley. The lenses were custom-designed with parameters suited to fit the eyes of C57BL/6 mice, a challenging task due to the steep curvature of murine eyes, e.g. measurements of 6 weeks old C57BL/6 mice indicated a corneal diameter of 3.2 mm and SAG (Sagittal Depth) of 1.5 mm. The lens design was based upon fitting mouse corneas with those dimensions. Success of the design was shown by the excellent fit observed (see results). The mouse lenses are ~20% of the average diameter of a human contact lens with a similar center thickness (e.g. maximum 0.70 mm). The lens material is the same as that of a currently marketed silicone hydrogel lens. However, these lenses are investigational devices, and may not be re- presentative of, nor comparable to, any commercial contact lens pro- duct sold by CooperVision, Inc.

### 6.3.2 Murine Model of Lens Wear

All procedures involving animals were carried out in accordance with standards established by the Association for the Research in Vision and Ophthalmology, under the protocol AUP-2016-08-9021 approved by the Animal Care and Use Committee, University of California Berkeley, an AAALAC accredited institution. The protocol adheres to PHS policy on the humane care and use of laboratory animals, and the guide for the care and use of laboratory animals. Wild-type C57BL/6 mice were used along with gene knockouts in MyD88 (-/-) or IL-1R (-/-). For imaging purposes, some experiments utilized mice with CD11c-YFP (CD11c-positive cells, e.g. dendritic cells, yellow), td-tomato or mT/mG (all cell membranes, red), or LysMcre (Lyz2-positive cells, myeloid-derived, green). Male and female mice were used, and all mice were obtained from the Jackson Laboratory (Bar Harbor, ME) except for F1 derived from the cross of mT/mG with either CD11c-YFP or LysMcre. The custom-made silicon hydrogel contact lenses were removed from their packaging solution and placed in sterile phosphate buffered saline (PBS) for 1 h. A contact lens was then fitted to one eye of each mouse. A Handi-Vac suction pen (Edmund Optics, Barrington, NJ) with a 3/32" probe was used for contact lens handling and fitting (Sup-

plemental Video S1) which was performed under isoflurane anesthesia (1.5–2%) delivered using a precision vaporizer (VetEquip Inc., Pleasanton, CA). After lens application, mice were fitted with Elizabethan collars (Kent Scientific), then single-housed without enrichments to prevent lens removal using Pure-o'Cel paper bedding (The Andersons Inc., Maumee OH) to reduce dust levels. Mice were monitored daily for the retention of lenses, and evidence of pathology, e.g. discharge or corneal opacity, was recorded via stereomicroscope ex- amination (Zeiss, Stemi 2000-C) with attached Canon EOS T5i camera while mice were under short-term (~20 min) isoflurane anesthesia. At the end of each experiment, or if mice presented with excessive weight loss, distress or signs of keratitis, euthanasia was performed using $CO_2$ asphyxia followed by cervical dislocation. Eyes were then enucleated for further experiments. Supplementary data related to this article can be found at https:// doi.org/10.1016/j.jtos.2018.11.006.

### 6.3.3 Confocal Imaging

Freshly enucleated eyes were washed once in PBS, mounted upright on acrylamide adhesive and immersed in clear DMEM. Confocal imaging was performed using a 60x/1.00 NA or a 20x/0.56 NA water-dipping objective, and an upright Olympus Fluoview FV1000 Confocal Microscope. Eyes were imaged using 559 nm (td-tomato membrane), 515 nm (CD11c-YFP), and 488 nm (PAO1-GFP or Lyz2+-GFP) laser lines. Z stacks (0.5 or 1 $\mu$m steps) were collected from 4 or more random fields per sample. In some experiments, Z-stacks over time were collected to capture moving cells. 3-D and 4-D image reconstruction, cell morphology analysis and movie generation were performed using Image-J (MorpholibJ tools collection) and Imaris (Bitplane). Maximum intensity projection (reducing a 3-D image into 2-D by projecting the maximum intensity of each pixel in a specific channel to the z plane) was used where indicated to visualize Lyz2+ or CD11c+ cell number and morphology, and to reduce 4D acquisition (xyz over time) in 2D movies (xy over time) to lower image complexity and better appreciate cell movement.

### 6.3.4 Immunofluorescence Imaging

Freshly enucleated eyes were fixed in 2% paraformaldehyde in PBS at 4°C for ~16 h. Fixed eyes were then protected by immersion in sucrose (15% for 4 h, then 30% for an additional 4 h) at room temperature. Cryo-protected eyes were embedded in OCT (Tissue Tek), flash frozen in liquid nitrogen and stored at -80°C. Embedded eyes were sectioned at 10 $\mu$m thickness using a Leica CM 1900 cryostat, placed on a glass slide and stored at 80°C. Corneal sections were stained for Ly6G-positive cells using rat NIMP-R14 antibody (10 $\mu$g/mL, ThermoFisher) and Alexa 647-conjugated goat anti-rat antibody (5 $\mu$g/ mL, Life Technology). Samples were counter-stained with DAPI (12.5 $\mu$g/mL, ThermoFisher) and, in the case of sections from IL-1R (-/-) and MyD88 (-/-) mice, ActiGreen (Phalloidin, 1:10, ThermoFisher). Frozen sections were rinsed with PBS, blocked with 2% BSA blocking buffer for 1 h, followed by primary antibody incubation for 1 h (both at room temperature). The sections were rinsed with PBS then incubated with secondary antibody for 1h (also at room temperature), then rinsed with PBS, and mounted on a coverslip with Prolong Diamond (ThermoFisher). Sections were allowed to set for a minimum of 30 min

before imaging using a Nikon Ti-E inverted wide- field fluorescence microscope equipped with Lumencor SpectraX illumination source, and CFI Plan APO VC 20x/0.75 NA objective. Neutrophil quantification was performed by manual counting Ly6G+ cells in at least 4 fields per sample, and at least 3 samples per condition

### 6.3.5 Bacteria

*Pseudomonas aeruginosa* strain PAO1 was used throughout. For many imaging experiments, PAO1 transformed with plasmid pSMC2 expres- sing enhanced GFP was used (Bloemberg and O'Toole, 1997). Bacteria were grown on tryptic soy agar (TSA) plates at 37°C for ~16 h. TSA was supplemented with carbenicillin 300 $\mu$g/mL for growing PAO1-GFP. Inocula were prepared by suspending bacteria in PBS to a concentration of ~$10^7$ CFU/mL (confirmed by viable counts). New contact lenses were then placed in the bacterial suspension for ~16 h at room temperature before fitting on the murine corneas. To ascertain the typical inoculum under these conditions, control experiments were performed in which new murine contact lenses were inoculated with *P. aeruginosa* as above, and after ~16 h incubation at room temperature, viable counts were performed on lens homogenates. These inoculum preparation conditions reliably produced ~$10^5$ CFU/lens.

### 6.3.6 Bacterial Isolation and Identification

To culture bacteria from worn murine contact lenses, lenses were removed with sterile forceps, cut in half with a sterile scalpel, and placed in 500 $\mu$L of PBS in tubes containing 2.8 mm ceramic beads (Omni International). Samples were homogenized, plated onto TSA, and incubated at 37°C in both aerobic and anaerobic conditions for up to 7 days. Isolated bacterial colonies were then identified by direct colony PCR of the 16S ribosomal RNA gene using universal primers P11P (5'-GAGGAAGGTGGGGATGACGT-3' and P13P (5'-AGGCCCGGG AACGTATTCAC-3' (James, 2010). Reaction mixes (50 $\mu$L) were set up as follows: 1X Q5 Reaction Buffer (New England BioLabs), 1X Q5 High GC En- hancer, 200 $\mu$M dNTPs, 0.5 $\mu$M Forward Primer, 0.5 $\mu$M Reverse Primer, and 0.02 U/$\mu$L Q5 High-Fidelity DNA Polymerase. A sterile toothpick was used to touch a bacterial colony on an agar plate and inserted directly into the PCR reaction tube. The reaction mixtures were subjected to the following thermal cycling sequence on a Bio-Rad Thermal Cycler: 98°C or 3 min followed by 30 cycles of 98°C for 10 s, 63°C for 20 s, 72°C for 45 s, followed by a final extension of 72°C for 2 min. Molecular grade water was included as a negative control, and a known strain of *P. aeruginosa* (PAO1) used as a positive control. Following amplification, samples were examined by electrophoresis in 1% agarose gels in 1X TBE buffer. Amplicons were purified using Pure-LinkTM PCR Purification Kit (Invitrogen), and sequenced at the UC Berkeley DNA Sequencing Facility. Sequences were identified with BLAST (https://blast.ncbi.nlm.nih.gov).

### 6.3.7 Fluorescence *In Situ* Hybridization

Contact lenses removed from the mouse eye, cut in half with a sterile scalpel, and fixed in paraformaldehyde (2%) for 1 h with shaking at RT. Bacterial hybridization was performed using a universal 16S rRNA gene probe [Alexa488]-GCTGCCTCCCGTAGGAGT-[Alexa488] (Eurofins Genomics) as previously described (Mark Welch et al., 2016; Vaishnava et al., 2011). Briefly, fixed lenses and eyes were washed in 80% EtOH, 95% EtOH, and then PBS for 10 min each with shaking at RT. Lenses and eyes were then placed in a hybridization buffer solution [NaCl (0.9 M), Tris-HCl (20 mM, pH 7.2) and SDS (0.01%)] and incubated at 55°C for 30 min. The probe was added to a final concentration of 100 nM and incubated at 55°C overnight. Lenses and eyes were then transferred to wash buffer solution [NaCl (0.9 M) and Tris-HCl (20 mM, pH 7.2)] and washed 3 times for 10 min each with shaking at RT. Lenses were mounted on slides and imaged using an Olympus FV1000 confocal microscope. A 488 nm laser was used for the detection of bacteria labeled by FISH, and a 635 nm laser was used to obtain contact lens reflections (excitation and emis- sion at the same wavelength). Three or more random fields per sample were imaged in 0.5 $\mu$m steps, and 3D images were reconstructed from z- stacks using IMARIS software (Bitplane).

### 6.3.8 Statistical Analysis

Quantitative data were expressed as a mean ± standard deviation or median with upper and lower quartiles. The Student's t-test was used to compare two groups. The Kruskal-Wallis test or two-way ANOVA with Sidak's multiple comparison test were used to compare three or more groups. Survival curves were analyzed using Log-rank Mantel-Cox test. Prism was used for linear regression analysis, curve fitting, and the above statistical tests. P values $< 0.05$ were considered significant.

## 6.4 Results

### 6.4.1 Biomicroscopic and OCT evaluation of the murine contact lens and lens-wearing eye *in vivo*

A dissecting microscope was used to evaluate the parameters surrounding fit of the contact lens on the murine eye. After placement on the eye (mice aged 5–12 weeks) (see Supplemental Video S1), the lenses were found to cover most of the cornea with the lens periphery in close proximity to the limbus *in vivo* and *ex vivo* (Figure 6.1a). Ocular Coherence Tomography (OCT) imaging of the lens in-situ showed a seamless fit over the corneal surface (Figure 6.1b). After lens placement, mice were single-housed and fitted with an Elizabethan collar to prevent mice removing the lenses through grooming. Since reduced grooming caused dust and some discharge to build up on the conjunctiva, an alternate form of paper bedding was used that vastly improved ocular surface cleanliness. The contact lens retention rate *in vivo* was 63–73% over 2 days, becoming 47% after 7 days (Figure 6.1c, left panel). Of the several actors investigated, only body

weight had a significant effect on lens retention (Figure 6.1c, right panel). Smaller body weights of 19 g or less were associated with a 57% retention rate after 7 days, compared to body weights over 19 g showing a 30% retention rate over the same period ($p < 0.05$, Log-rank Mantel-Cox test).

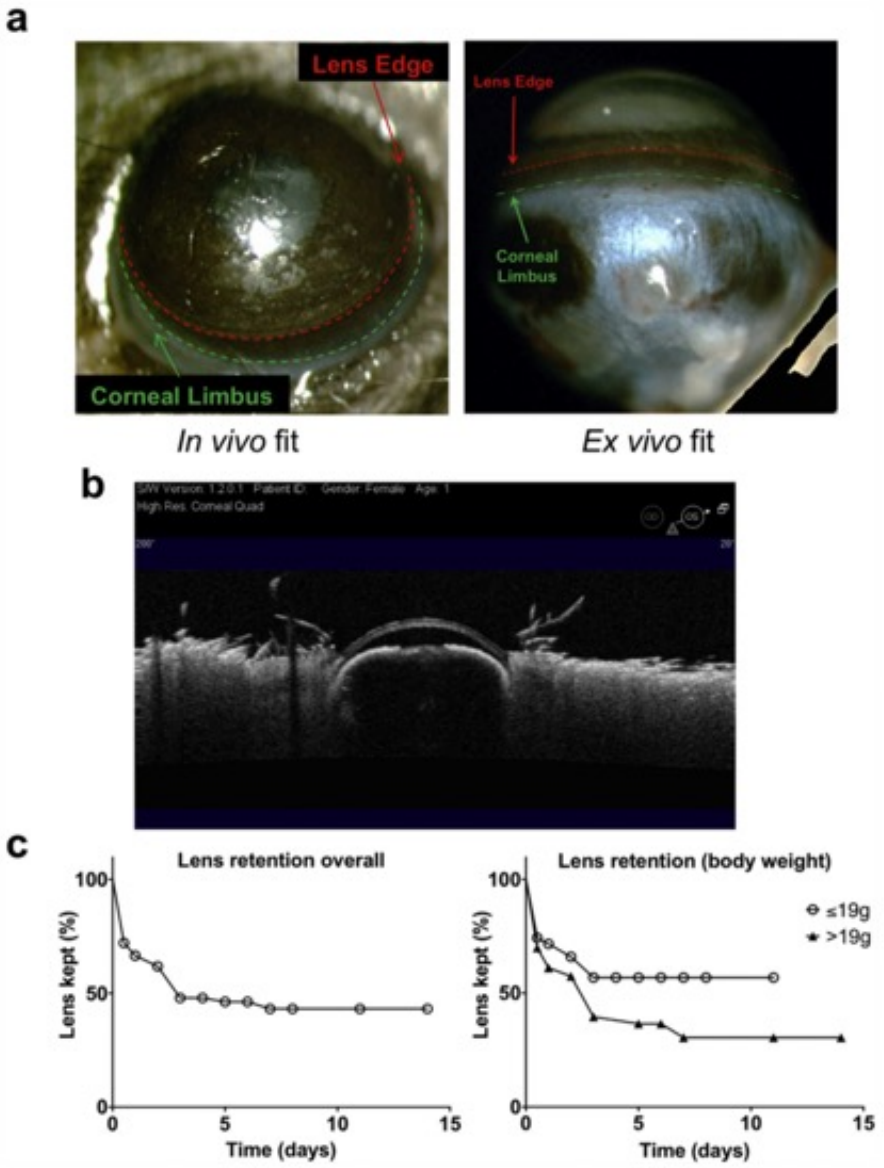


**Figure 6.1:** Fitting of custom-made contact lenses in 6–12 weeks old C57BL/6 mice. (a) Dissecting microscope images (acquired *in vivo* and *ex vivo*) showing the contact lens covering most of the murine cornea excluding the limbus and conjunctiva. (b) Optical coherence tomography (OCT) image showing close alignment of the contact lens to the murine cornea over its entire surface. (c) Overall contact lens retention rate (left panel, n°147 subjects), and retention rates according to body weight (right panel, n°74 ≤ 19 g and n°73 > 19 g). Mice with a body weight of ≤ 19 g showed a significantly different retention curve compared to those with a body weight of > 19 g ($p < 0.05$, Log-rank Mantel-Cox test).

After fitting, lens-wearing eyes were compared to non-lens wearing contralateral controls daily using a dissecting microscope over a period of 2–14 days of lens wear. Corneas appeared

healthy without visible signs of inflammation, injury, or opacity as compared to contralateral control eyes (Figure 6.2). Worn lenses appeared relatively clear and remained hydrated as shown by their reflective wet front surface (Figure 6.2, lower row), which was confirmed after removal.

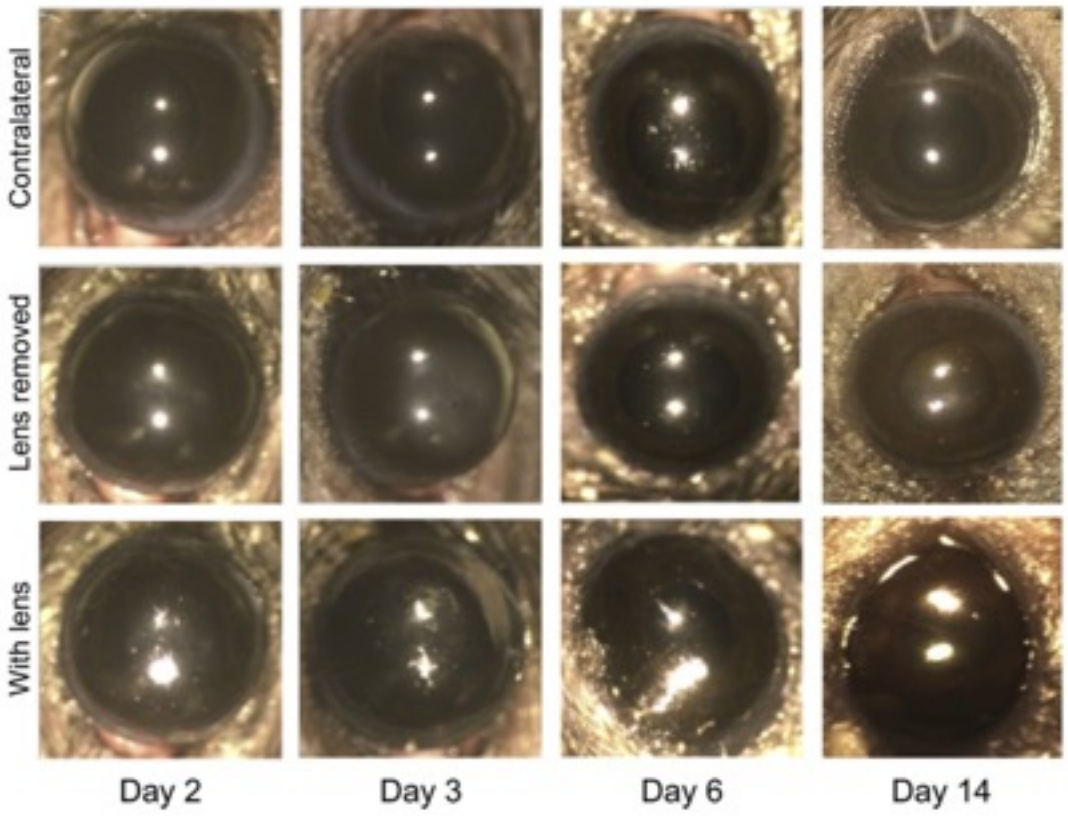


**Figure 6.2:** *In vivo* images of mouse eyes wearing a contact lens (bottom row), after removing the contact lens (central row) and con- tralateral controls (top row) were taken using a dissecting microscope at indicated time-points. Although some alteration in the reflective properties and smoothness of the contact lens could be observed in some cases, all corneas appeared healthy and transparent with no signs of opacity or scratches at all time-points, and only minimal debris accumulation on the contact lenses (bottom row).

### 6.4.2 Use of a membrane reporter mouse reveals multiple changes to corneal morphology during lens wear

To obtain more detail about the impact of lens wear, we used mice expressing membrane-localized td-tomato to compare lens wearing corneas to contralateral non-lens wearing corneas by high-resolution confocal microscopy. To account for the possibility that there might be effects on the contralateral eye induced by lens wear, or by Elizabethan collar use, we also included mice that were not fitted with lenses, with and without the use of collars, in the study. Corneas of contralateral control eyes of lens-wearing mice showed typical morphology, i.e., an intact multilayered epithelium above a stroma containing healthy interconnected keratocytes

(Figure 6.3a). These corneas were indistinguishable from those of non-lens-wearing mice with or without the Elizabethan collar (data not shown). However, significant alterations in the corneal epithelium and stroma were observed for lens-wearing eyes compared to contralateral controls. As seen in Figure 3 (and Supplemental Video S2), after 14 days of continuous lens wear, small round vesicles (1-4 $\mu$m diameter) were visible in the most external layers of the corneal epithelium and were not present in controls. In the stroma, keratocyte morphology was visibly altered, with cell edges appearing jagged compared to the smooth profile of the keratocytes in contralateral eye controls (Figure 3a and Supplemental Video S2). Moreover, the stroma contained numerous small cells not normally present. These cells appeared to be actively motile, seen trafficking along and over the surfaces of the stromal keratocytes, altering their position between image collection time intervals while acquiring high-resolution confocal z-stacks (pseudo time-lapse Supplemental Video S2). Real time-lapse video microscopy used over 30 min confirmed the presence of numerous highly motile round cells throughout the stroma (Figure 6.3b and Supplemental Video S3). These cells were found as early as 5 days after initiation of lens wear. Supplementary data related to this article can be found at https://doi.org/10.1016/j.jtos.2018.11.006.

### 6.4.3 Murine contact lens wear is associated with neutrophil recruitment into the corneal stroma dependent on IL-1R and MyD88

To investigate if the infiltrating cells seen with lens wear were myeloid-derived, we employed the CRE recombinase expressed in LysMcre mice, and crossed them with mT/mG mice harboring a CRE cassette that mediates the switch in expression from td-tomato to GFP (see Methods) to obtain a murine strain expressing membrane-localized GFP in granulocytes, mature macrophages and partially in dendritic cells (CD11c-positive) (Clausen et al., 1999), and td-tomato in all other cell types. After 7 days of lens wear, morphological observations and shape measurements (area [A], perimeter [P] and circularity [C]), in z-projections of Figure 6.4a (and Supplemental Video S4), allowed 4 types of cells expressing GFP (i.e. myeloid-derived) to be distinguished in the contralateral non-lens-wearing eyes. Based upon their appearance, cells were assigned to one of the following created categories: small round cells (#1, resembling neutrophils, A = 234 $\mu m^2$, P = 63 $\mu$m, Circ. = 0.740), large lobulated (#2, resembling macrophages, A = 861 $\mu m^2$, P = 195 $\mu$m, Circ. = 0.283), thin dendriform (#3, resembling dendritic cells, A = 390 $\mu m^2$, P = 358 $\mu$m, Circ. = 0.038) and extremely elongated (#4, resembling oligodendrocytes, A = 2294 $\mu m^2$, P = 804 $\mu$m, Circ. = 0.045). After 7 days of lens wear, a clear increase in the total number of cells was apparent in lens-fitted eyes (Figure 6.4a and c [left panel], and Supplemental Video S4) that was absent in contralateral controls and naïve eyes (Figure 6.4c, left panel). Indeed, both controls showed similar Lyz2-positive cell numbers indicating that lens-induced effects were specific to the fitted eyes. Morphological analysis (Figure 6.4b and c [middle and right panels]) revealed a shift in cell shape after lens wear, indicated by an increase in area and decrease in perimeter (Figure 6.4c, middle panel). Additionally, we measured an increase in the frequency of cells with higher circularity (Figure 6.4b and c [right panel]). Fast-moving cells

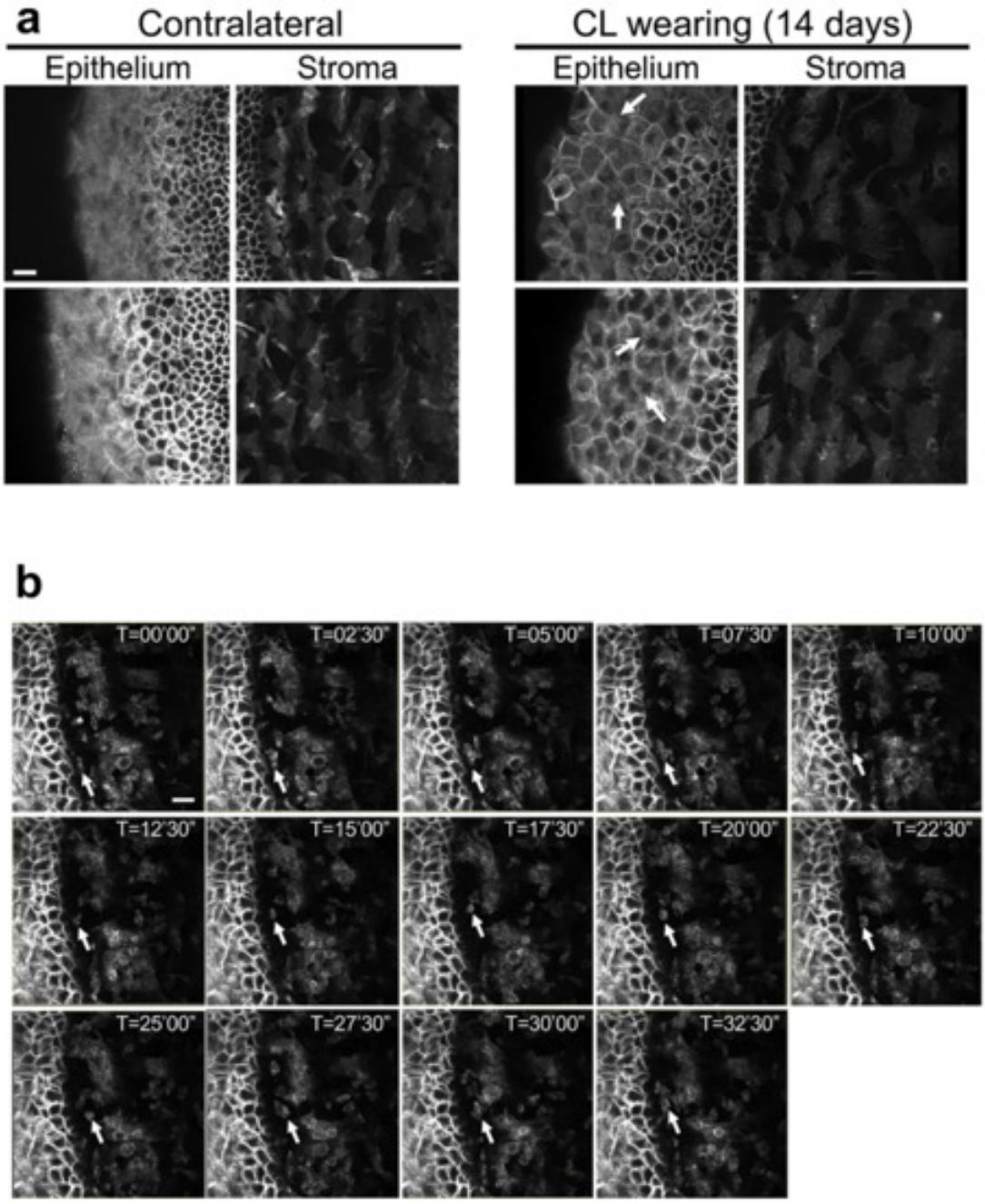


**Figure 6.3:** Confocal imaging of murine corneas after 14 days contact lens wear. Mice expressing td-tomato protein in all cell membranes were used. (a) Confocal optical sections showing the presence of multiple small vesicles (arrows) in the epithelium of lens-wearing corneas, absent in contralateral eyes. Stromal keratocytes of lens-wearing eyes showed altered morphology with most showing jagged cell edges compared to the smoother profile of keratocytes in control corneas. (b) Time-lapse images showing multiple small round cells moving across the keratocytes in the stroma of contact lens wearing eyes (arrow shows one example) over a 32 min, 30 s time-span. White bar = 20 $\mu$m.

appeared to belong to the small round cell category #1) as evident in time-lapse in Figure 6.4d and Supplemental Videos S4 and S5. Supplementary data related to this article can be found at https://doi.org/10.1016/j.jtos.2018.11.006.

The appearance and motility of these additional cells in the corneal stroma of lens-wearing eyes suggested infiltration of neutrophils, which are not usually present in the cornea. To test that hypothesis, we performed immunofluorescence imaging of corneal cryo-sections using antibodies against Ly6G, a neutrophil marker. The results confirmed the presence of a significant number of Ly6G-positive cells (suggesting neutrophils) that were not detected in contralateral control eyes (Figure 6.5a). Quantification of Ly6G-positive cells after 6 days (Figure 6.5c, left panel) confirmed these observations, while time-course studies indicated that Ly6G-positive cell recruitment required a minimum of 5 days of continuous lens-wear (Figure 6.5c, right panel), and it was maintained at a similar level for up to 14 days thereafter (data not shown).

To gain insights into the mechanisms for Ly6G-positive cell recruitment, and to begin to understand its significance, we also fitted MyD88 (-/-) and IL-1R (-/-) mice with lenses. The Ly6G-positive cell response to contact lens wear was found lacking in the corneas of these mice (Figure 6.5b). Ly6G-positive cells were found in the limbal and conjunctival regions of wild-type, MyD88 (-/-) and IL-1R (-/-) mice with and without lens-wear for 6 days (Supplemental Figure S1) with no significant difference between control and lens-wearing eyes in any group. While limbal and conjunctival regions of IL-1R (-/-) eyes showed a reduction in Ly6G-positive cells versus wild-type controls, the reduction was similar for control and lens-wearing eyes IL-1R (-/-) eyes, and was not observed in eyes of MyD88 (-/-) mice. Thus, these data suggest that the lack of Ly6G-positive cell recruitment into the corneas of lens-wearing MyD88 (-/-) or IL-1R (-/-) mice after 6 days (Figure 6.5) involves defective recruitment from the limbus/con- junctiva.

The immunohistological images also allowed for examination of the impact of lens wear on corneal structure. They showed that the corneal epithelium and the remainder of the cornea remained intact despite the Ly6G-positive (neutrophil) response.

### 6.4.4 Lens wear altered CD11c-positive cell distribution in the central cornea

In human subjects, it has been shown that contact lens wear can alter the distribution of dendritic cells within the cornea even after only a few hours of wear (Alzahrani et al., 2016; Alzahrani et al., 2017; (Sindt et al., 2012). Dendritic cells, which can be distinguished by their expression of CD11c, are known to be sentinel cells in mucosae and epithelia (Veres et al., 2011; Arques et al., 2009; (Seyed-Razavi et al., 2013). Indeed, we previously showed that CD11c-positive cells play important roles in early recognition of, and response to, *P. aeruginosa* at the ocular surface at 4 h (Metruccio et al., 2017). Thus, we investigated CD11c-positive cell responses to contact lens wear using mice expressing YFP under control of the CD11c promoter. Contact lens wear was found to recruit CD11c-positive (dendritic) cells to the central cornea by 24 h (Figure 6.6a and c [left panel]) with no further increase at later time points up to 6 days (Figure 6.6a). As above (Figure 6.4c, left panel), contralateral controls and naïve eyes showed no change in

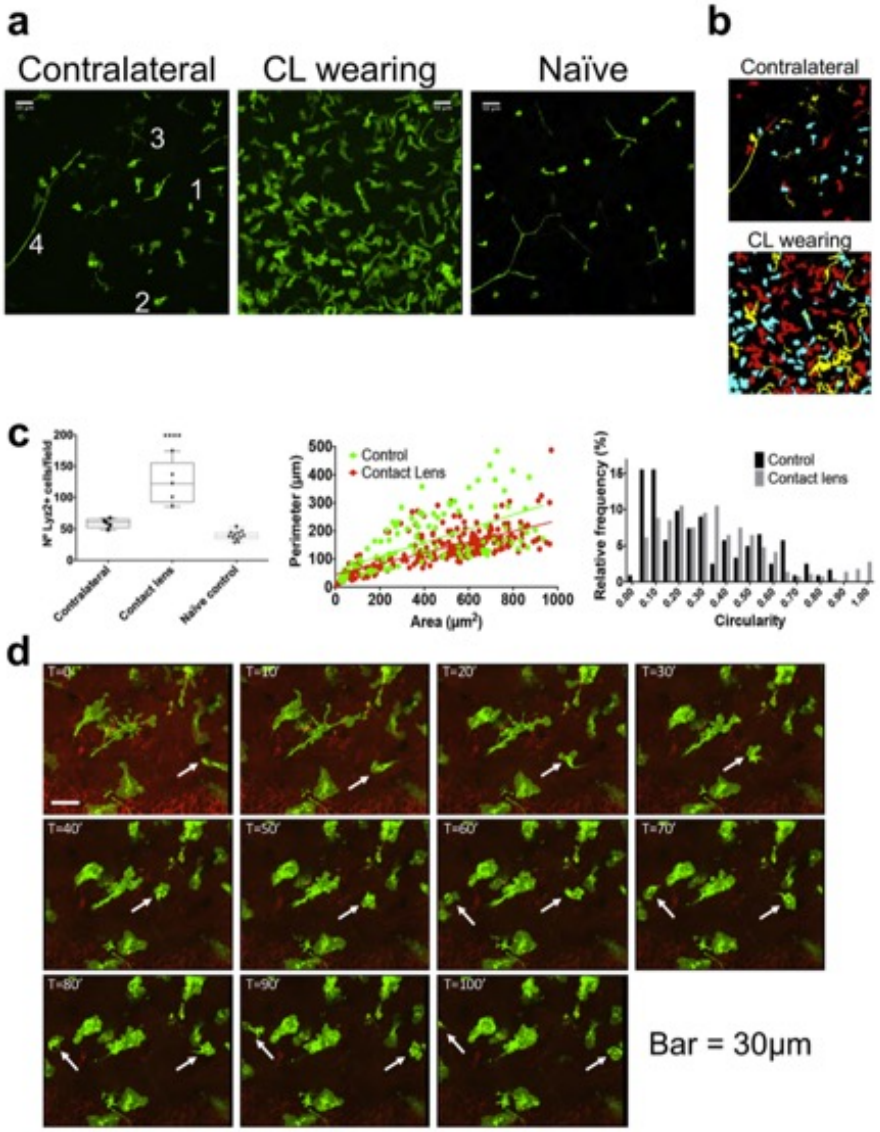


**Figure 6.4:** Multiple Lyz2+ (myeloid-derived) cells respond to contact lens wear. (a) Z-projections of the GFP channel (all Lyz2+ cells projected into one plane) in the central cornea of a mT/mG-LysMcre hybrid mouse (see Methods) after 7 days of continuous lens wear compared to the contralateral control and a naïve eye. Numbers indicate the different myeloid-derived cell types observed based on morphology (see Results). Scale bar = 50 $\mu$m. (b) Same field as in (a) for contralateral control and lens-wearing eyes after Morpholib morphological segmentation (see Methods) and color-coding based on circularity arbitrarily divided in 3 groups, each accounting for a third of the total cell number (yellow $\leq 0.1$, red $0.1 < > 0.3$ and cyan $\geq 0.3$. (c) Left panel shows quantification of Lyz2+ cells per field of view in contact lens-wearing corneas versus contralateral controls and naïve eyes (****$p < 0.0001$, Kruskal-Wallis test). Middle and right panels show the quantification of morphological parameters of Lyz2+ cells from contact lens-wearing corneas versus contralateral controls. Image analysis was performed using MorpholibJ tools for 3D segmentation in ImageJ and parameters related to z-projections used (perimeter, area and circularity) to exclude artifacts due to lower z resolution. The middle panel shows the corneal distribution of individual cells based on area and perimeter with a linear regression fit indicating two significantly different curves ($p = 0.0325$). The right panel shows the relative frequency distribution based on Lyz2+ cell circularity. (d) Time-lapse images showing multiple Lyz2+ cells in the corneal stroma of a contact lens-wearing eye with two small round cells moving at considerable speed (arrows) over a 100 min time-span. White bar = 20 $\mu$m.

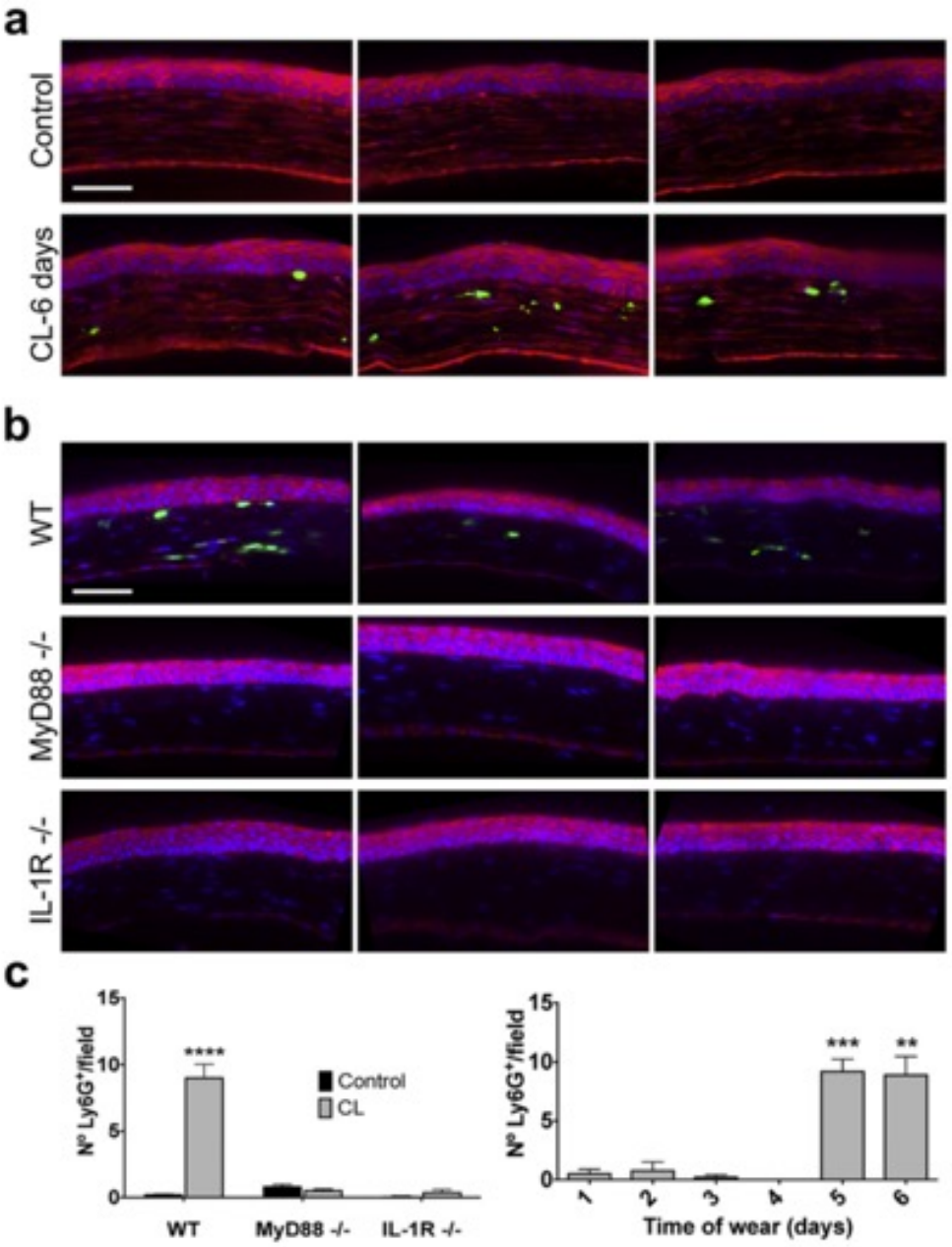


**Figure 6.5:** Immunofluorescence imaging showing neutrophil infiltration of contact lens wearing murine corneas after 6 days that requires MyD88 and IL-1R. (a) Cryo- sections of mT/mG mouse corneas (red, membrane) stained with DAPI (blue, nuclei) and Ly6G-antibody (green) showing Ly6G+ cell (neutrophil) recruitment in the corneal stroma of lens-wearing eyes (6 days of continuous wear) compared to contralateral controls (3 different corneas are shown per group). (b) Cryo-sections of wild-type (WT), MyD88 (-/-), or IL-1R (-/-) murine corneas after 6 days of contact lens wear, stained with phalloidin (magenta, actin), DAPI (blue, nuclei) and Ly6G-antibody (green) showing the absence of Ly6G-positive cells (neutrophils) in the gene-knockout corneas (3 different corneas shown per group). Scale bar = 50 $\mu$m. (c) Quantification of Ly6G+ cells (neutrophils) (number of Ly6G+ cells per field of view) in WT versus MyD88 (-/-) and IL-1R (-/-) contact lens-wearing corneas versus controls (6 days lens wear) (left panel), and in WT mice at different time points after lens fitting (right panel). Ly6G+ cell recruitment required 5 days of lens wear (****$p < 0.0001$, ***$p < 0.001$, **$p < 0.01$, Kruskal-Wallis test).

CD11c-positive cell numbers, and were similar to each other (Fig. 6c, left panel). Some CD11c-positive cells were found at the basal lamina with processes in the stroma and extending into the epithelium (Figure 6.6b). However, the bimodal distribution of CD11c-positive cells within the central cornea was altered in lens-wearing mice after 24 h with their localization closer to the epithelial surface and the posterior corneal endothelium than in contralateral control eyes (Figure 6.6c, center panel). An increase in corneal thickness was also observed in lens-wearing eyes after 24 h that was statistically significant (Figure 6.6c, right panel). Increased thickness involved changes to both the stroma (control 62.2 ± 1.8 $\mu$m versus lens-wear 71.8 ± 5.0 $\mu$m) and the epithelium (control 40.4 ± 1.6 $\mu$m versus lens-wear 44.1 ± 2.3 $\mu$m). However, each of these individual increases in thickness was not statistically significant.

### 6.4.5 Worn mouse contact lenses harbor commensal-type microbes

Previous studies in our laboratory showed that the healthy murine cornea contrasts with the adjacent conjunctiva in that it does not harbor a viable bacterial microbiome, a phenomenon dependent on IL-1R (Wan et al., 2018). Even when extremely large quantities of bacteria (either pathogenic or commensals) are inoculated onto healthy non-lens wearing mouse eyes, the cornea uses IL-1R dependent strategies to clear them within 24 h (Wan et al., 2018). Nevertheless, studies have shown that during human lens wear, the contact lens is often contaminated with microbes that are com- mensals of the adjacent conjunctiva and skin (Willcox, 2013a). Here, we explored if worn mouse lenses also harbor microbes.

Lenses were removed from mice after 1–11 days of wear using sterile forceps, and lens homogenates examined for viable bacteria using standard techniques (see methods). The results revealed that culturable bacteria were present on 13 of 14 lenses, with Corynebacterium spp. being the most commonly identified (Table 6.1). Given that not all bacteria can be cultured, we also used FISH with a universal 16S rRNA gene probe on a subset of worn lenses to visualize bacteria. FISH demonstrated the presence of bacteria on both anterior and posterior sides of worn lenses with significantly more bacteria detected on posterior versus anterior surfaces, the latter showing no colonization for several lenses (Figure 6.7a and b). Colonization was ob- served on each day of lens wear, with a small increase in bacterial numbers observed over the first 3 days, although this increase was not statistically significant (Figure 6.7b).

A subgroup of 5 mice that had worn a lens for at least 5 days were studied for Ly6G-positive cell infiltration in addition to the identity and quantity of lens-colonizing bacteria using culture methods. As expected, Ly6G-positive cell infiltration was seen in lens-wearing corneas of all 5 mice. Of the 5 lenses removed from these eyes, 4 harbored *Corynebacterium* spp. as the predominant lens-colonizing bacteria, but no bacteria were recovered from the remaining lens (Table 6.1).

The FISH method was also used to determine if bacteria were also present on the surface of lens-wearing corneas. Very few bacteria were detected on corneas of either contact lens wearing or contralateral controls (Figure 6.7c and d). On rare occasion, individual bacteria were detected within the corneal epithelium of contact lens-wearing eyes (example in Figure 6.7d). Importantly, the presence of commensal bacteria (including a *Pseudomonas* sp. in one instance) on mouse

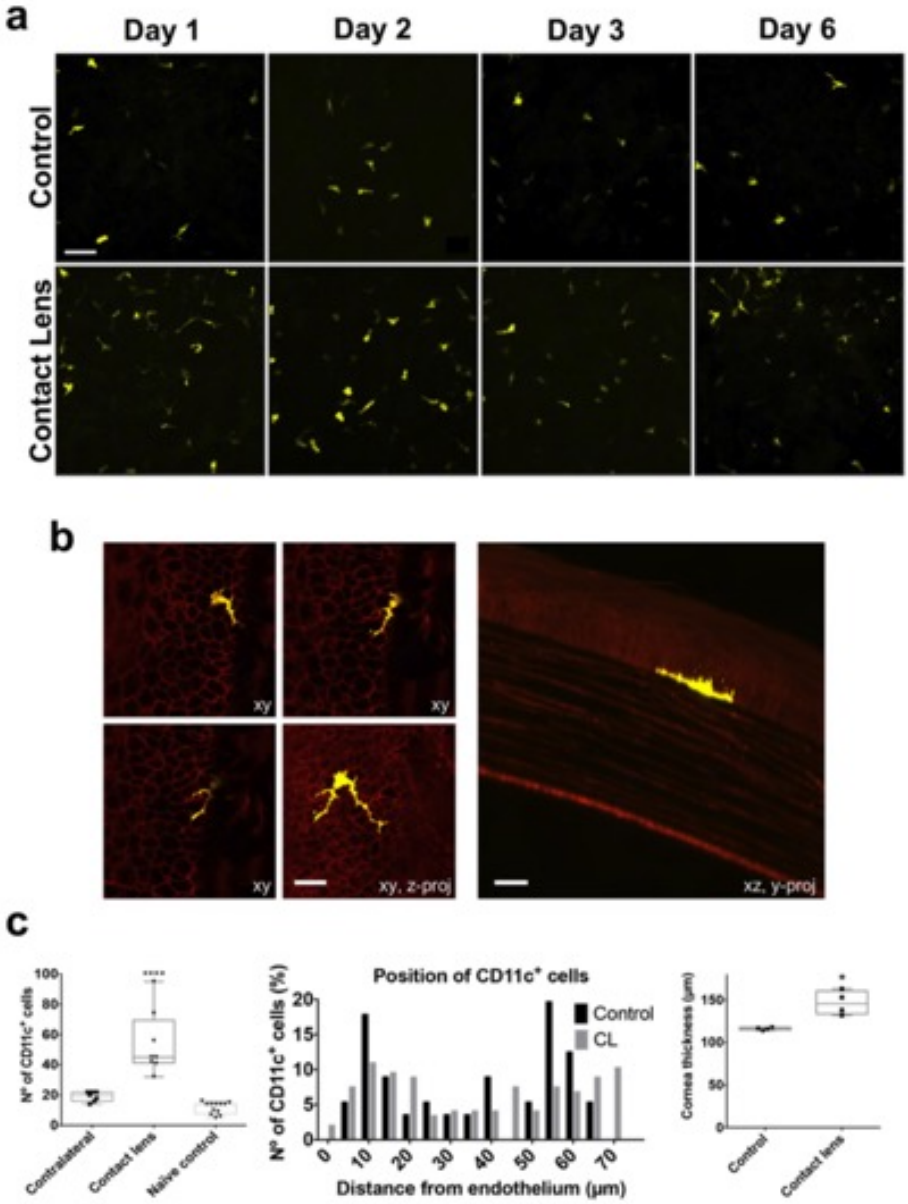


**Figure 6.6:** Early recruitment of CD11c+ cells after contact lens wear. (a) Maximum intensity z-projection of the YFP signal (all CD11c+ cells projected into one plane) in the central cornea of a contact lens-wearing eye shows an increased number of cells present versus the contralateral control at all time-points starting at 1 day. (b) Optical ortho-slicing (xy, 0.5 $\mu$m thick), maximum intensity z-projection (xy, z-proj, 24 $\mu$m thick) and maximum intensity y-projection (xz, y-proj) of a single CD11c+ cell showing localization at, and across, the basal lamina with processes extending into the corneal epithelium after 6 days of contact lens wear. (c) Quantification of the increase in CD11c+ cells in the central cornea of lens-wearing eyes versus contralateral and naïve controls after 1 day (left graph, ****p < 0.0001, Kruskal-Wallis test), along with the distribution of CD11c+ cells within the cornea (central graph) showing an increase in cell frequency closer to the endothelium and the epithelium versus contralateral controls, and increased cor- neal thickness in contact lens wearing eyes versus contralateral controls (right graph, *p < 0.05, unpaired Student's t-test).

contact lenses after wear (Table 6.1) did not result in development of microbial keratitis in any of the mice for up to 14 days of wear (Figure 6.8a and b).

**Table 6.1:** Identification and quantification of bacteria on contact lenses worn by wild-type mice

| Lens # | Days worn | CFU/lens | Bacteria identified |
|---|---|---|---|
| 1 | 1 | 10 | *Staphylococcus* spp. (CNS) |
| 2 | 1 | 10 | *Bacillus* spp. |
| 3 | 1 | 330<br>30 | *Propionibacterium* spp.<br>*Actinobacillus* spp. |
| 4 | 2 | 1935 | *Corynebacterium* spp. |
| 5 | 2 | 5120 | *Corynebacterium* spp. |
| 6 | 3 | 21500<br>370 | *Staphylococcus* spp. (CNS)<br>*Streptococcus* spp. |
| 7 | 3 | 10 | *Corynebacterium* spp. |
| 8 | 4 | 1650 | *Corynebacterium* spp. |
| 9[a] | 5 | 1500<br>10<br>10 | *Corynebacterium* spp.<br>*Staphylococcus* spp. (CNS)<br>*Actinobacillus* spp. |
| 10[a] | 6 | 0 | N/A |
| 11[a] | 7 | 41000 | *Corynebacterium* spp. |
| 12[a] | 7 | 4900 | *Corynebacterium* spp. |
| 13 | 7 | 110<br>10 | *Corynebacterium* spp.<br>*Pseudomonas* spp. |
| 14[a] | 11 | 3300 | *Corynebacterium* spp. |

[a] Corneas were also examined for and demonstrated, Ly6G-positive cell infiltration

### 6.4.6 Murine lenses predispose the cornea to infection when contaminated with *P. aeruginosa*

The opportunistic pathogen *P. aeruginosa* is the most common cause of contact lens-related infection. This bacterium does not infect the healthy mouse cornea in the absence of contact lens wear unless there is deep penetrating injury that compromises the basal lamina beneath the corneal epithelium (Lee et al., 2003; Hazlett and Berk, 1984). Previous studies using other species have shown that lens wear enhances susceptibility to *P. aeruginosa* infection in people, rats and rabbits, but not guinea pigs (Stapleton et al., 2008; Tam et al., 2010; Wei et al., 2014; Vijay et al., 2009).

To explore if lens wear enables infection in the C57BL/6 mice used in this study, we inoculated lenses with *P. aeruginosa*, then cultured the bacteria overnight to achieve a final concentration of ~$10^5$ CFU per lens prior to fitting (see Methods). Microbial keratitis occurred as early as 24h post-fitting (9% of mice, Figure 6.8b). Incidence of microbial keratitis increased with duration

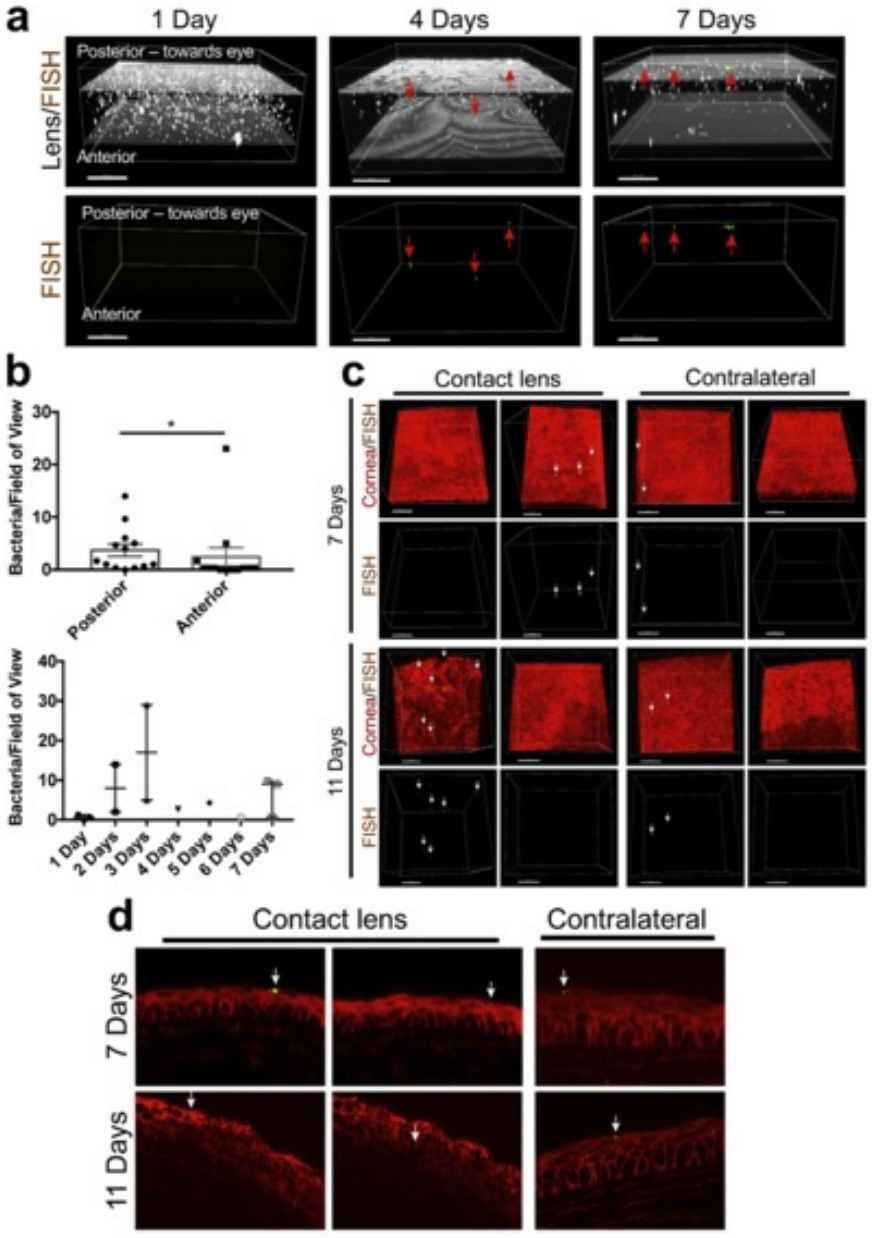


**Figure 6.7:** Colonization of murine contact lenses during wear by commensal bacteria. (a) FISH labeling using a universal bacterial 16S rRNA gene probe identified bacteria (red arrows) present on worn contact lenses at various time points. Bacteria were rarely identified on lenses worn for 1 day while several bacteria were identified on lenses at later time points. Bacteria were found on both the posterior and anterior lens surfaces. (b) Number of bacteria identified/field of view on the inside (posterior surface) of the worn contact lens compared to bacteria identified on the outside (anterior surface) (upper panel). Data expressed as a median with interquartile range. (*p = 0.03, Mann- Whitney U Test). Number of bacteria identified in a field of view on worn contact lenses over time (lower panel). c) FISH labeling using a universal bacterial 16S rRNA gene probe on murine corneas after 7 and 11 days of contact lens wear. Very few viable bacteria were detected (white arrows) in contact lens wearing eyes or contralateral controls. (d) In rare instances, bacteria were also found within the corneal epithelium after 11 days of contact lens wear.

of wear (32% of mice after 6 days, and 55% of subjects after 11 days) (Figure 6.8b). Bacteria isolated from mice with microbial keratitis (from the cornea and contact lens) were confirmed as *P. aeruginosa* from the original inoculum.

Corneas with microbial keratitis typically showed a loss of stromal organization and disruption of the basal epithelium. The remainder of the epithelium above the stroma appeared to be roughly intact, with cell membranes still attached to one another, although individual cells appeared to have altered morphology with more irregularities. In some corneas, clusters of small, round, fast-moving cells resembling the neutrophils in the stroma were seen within the corneal epithelium. In the example shown in Figure 6.8d (Supplemental Video S6) these appeared to be coming from the stroma corresponding to the presence of a small, localized, corneal opacity. *P. aeruginosa* was observed penetrating the epithelium which appeared roughly intact and multilayered, but with disorganized epithelial cell structure, sometimes without observable corneal opacity (Figure 6.8c). Within the epithelium, some cells were found to contain bacterial aggregates/microcolonies (Figure 6.8c, arrows). Supplementary data related to this article can be found at https:// doi.org/10.1016/j.jtos.2018.11.006.

However, not all eyes fitted with *P. aeruginosa*-inoculated contact lenses became infected. In some mice, *P. aeruginosa* inoculated with the contact lens was cleared at variable times, with the eye showing no residual bacteria or pathology (see Supplemental Figure S2).

## 6.5 Discussion

Contact lens wear is a widely used and a successful form of vision correction, but it carries a risk of complications, the most serious being a vision-threatening microbial keratitis. Understanding and resolving the pathogenesis of contact lens-related microbial keratitis, and other lens-related complications, requires suitable animal models that allow the effects of lens wear on corneal homeostasis to be determined at a molecular, cellular and tissue level. This depth of research investigation needed to understand and solve these problems is currently not possible using human subjects for multiple obvious reasons related to safety, ethics, and intrasubject variability.

In this study, we report development of a novel murine model of contact lens wear, enabling the many reagents and technologies available for mouse research to be utilized. Using the model, we showed it can faithfully mimic various biological phenomena occurring in human lens wear, including colonization of the lens with conjunctival and skin associated commensals (Willcox, 2013a), a rapid dendritic cell response (Alzahrani et al., 2016; Alzahrani et al., 2017; Sindt et al., 2012), and enhanced susceptibility to infection with *P. aeruginosa* (Stapleton et al., 2013; Green et al., 2008). Beyond what can be done using human subjects, we also demonstrated a Ly6G-positive cell (likely neutrophil) response in the stroma requiring IL-1R and MyD88 following 5 days of lens wear that does not disrupt the transparency of the cornea and confirmed that the earlier dendritic-shaped cell response involves CD11c-positive cells. Using a mouse with red fluorescent (tdTomato expressing) membranes, with and without deliberate inoculation with green (GFP-expressing) bacteria, we have also been able to observe changes to corneal

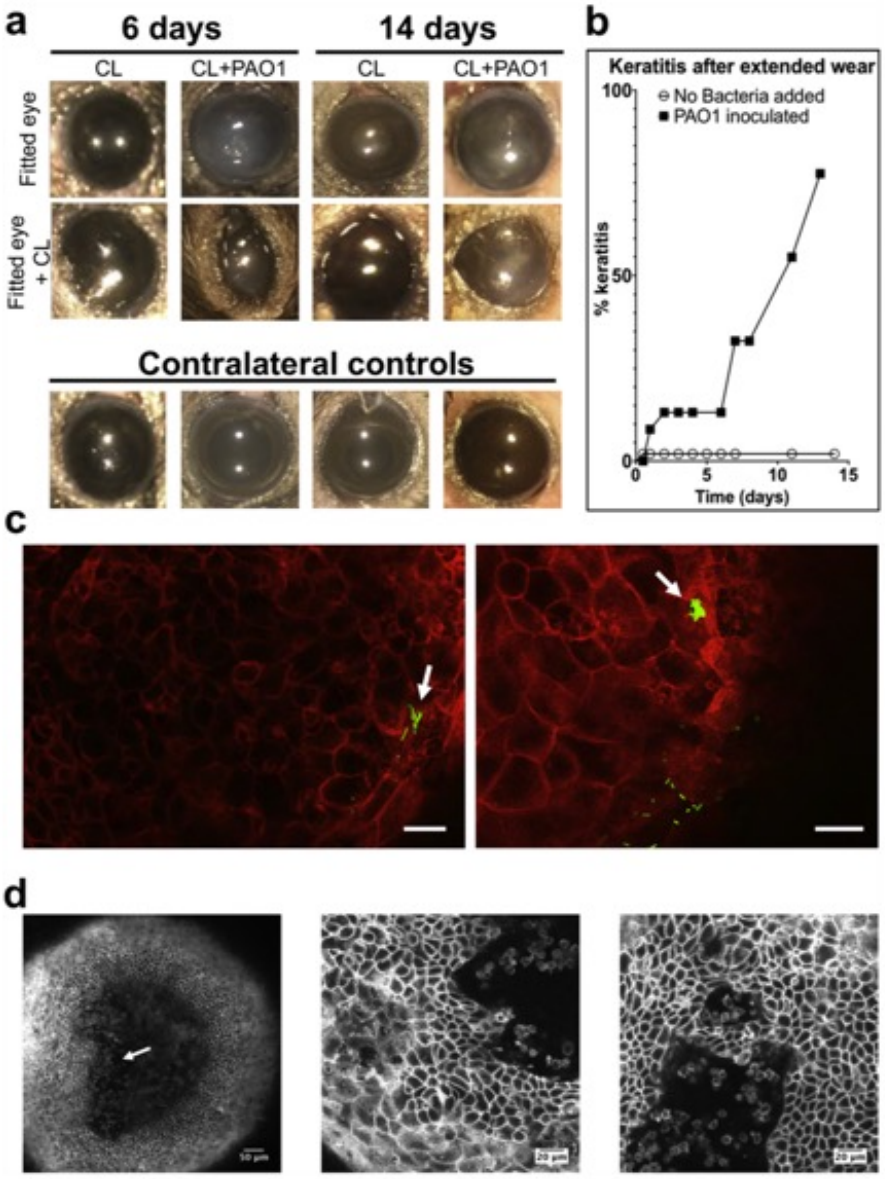


**Figure 6.8:** Development of microbial keratitis after fitting murine corneas with *P. aeruginosa* inoculated lenses. (a) *In vivo* images of mouse eyes wearing a contact lens (central row) previously inoculated with *P. aeruginosa* PAO1 (CL + PAO1) or not inoculated (CL), after removing the contact lens (top row) and contralateral controls (not fitted with a contact lens and not inoculated, bottom row) were taken using a dissecting microscope at indicated time points. Cornea opacity was present only in bacteria inoculated-contact lens wearing eyes. (b) Survival analysis showing the incidence of microbial keratitis in inoculated versus uninoculated contact lenses (keratitis was indicated by the presence of corneal opacity) ($p < 0.01$, Log-rank Mantel-Cox test). (c) Optical ortho-slicing (xy plane) of a mT/mG mouse cornea after 7 days wear of a PAO1-GFP inoculated contact lens showing an example of bacteria closely adherent to the surface, penetrating the disorganized epithelium and forming intra-tissue microcolonies (arrows). Green, bacteria and red, td-tomato cell membrane, scale bars = 20 $\mu$m. (d) Optical ortho-slicing (xy plane) of a mT/mG mouse cornea after 14 days wear of PAO1-inoculated contact lens showing an example of small round cells (resembling neutrophils) infiltrating and disrupting organization of the stroma in the central cornea (arrow, left image), and penetrating the corneal epithelium (central and right images).

cell morphology caused by lens wear with and without *P. aeruginosa* infection. Additionally, we detected *P. aeruginosa* in the process of traversing the corneal epithelium (and in some cells forming biofilm) in clear healthy-looking corneas, which is likely to be an early step in pathogenesis of lens-related infection difficult to study using injury models.

Neutrophil infiltration into the cornea generally causes collateral damage (Wei et al., 2014; Hazlett, 2004; Pearlman et al., 2013). However, the Ly6G-positive cell (neutrophil) response during mouse lens wear occurred without associated changes to corneal transparency suggesting an alternate neutrophil phenotype with reduced generation of reactive oxygen species. Recent studies have demonstrated the plasticity and heterogeneity of neutrophils in health and disease (Bird, 2010; Kolaczkowska and Kubes, 2013; Tsuda et al., 2004; (Deniset and Kubes, 2018). Indeed, neutrophils have been shown to be required for corneal wound healing in some instances (Gan et al., 1999; Li et al., 2006). Further, quiescent neutrophils were recently shown to infiltrate the lung in a murine model of sterile lung injury (Tian et al., 2017).

The changes to the cornea induced by uninoculated contact lens wear over a period of 5 days in our murine model aligns well with the definition of para-inflammation. As described by Medzhitov in 2008, para-inflammation is a tissue adaptive response intermediate between basal tissue homeostasis and classical inflammation mediated by resident macrophages (Medzhitov, 2008). While not previously described in the cornea, para-inflammation is known to occur in the aging retina and it relates to the pathogenesis of some retinal diseases (Chen and Xu, 2015; Xu et al., 2009). It is also thought to play a role in diabetes, atherosclerosis, age-related neurodegenerative diseases, obesity, and some forms of cancer (Rea et al., 2018; Aran et al., 2016). The intended purpose of para-inflammation is to restore normal function and homeostasis in response to changes in the environment, but it can also have a dark side in the face of excessive stress, when it can turn into outright inflammation. Aspects of the response to mouse contact lens wear that suggest a para-inflammatory response include the dendritic cell changes observed after 24 h that persist over time, and the later infiltration of Ly6G-positive cells (neutrophils) into the stroma without an impact on corneal transparency or the epithelial barrier.

Considering that continuous lens wear is known to increase the risk of contact lens complications in people, it was interesting that the Ly6G-positive cell response occurred only after several days of continuous wear in mice. Future studies will be required to determine the relationship between this response and the pathogenesis of these complications. Since most people wear lenses on a daily wear basis, it would also be important to ascertain if removal of the lens for part of the day, and/or regular lens replacement prevents this phenomenon from occurring over several days of lens wear.

The trigger for the para-inflammatory response during contact lens wear and its function is yet to be established. Microbial antigens are likely contributors, and small numbers of bacteria were found colonizing worn lenses in our study. While there was a lens from which we could not culture bacteria that had been in an eye undergoing the parainflammatory response, culture methods can fail to detect viable bacteria if they are in a non-culturable state, and they cannot detect microbial debris (antigens) which can still trigger immune responses. The bacteria that were detected included *Corynebacterium* spp. and coagulase-negative *Staphylococcus* spp, which are commonly identified as conjunctival and skin commensals in humans (Willcox, 2013b),

readily colonize contact lenses (Willcox, 2013a), and are each involved in protective ocular immune responses to P. aeruginosa in scarification-injury murine models of corneal infection (Kugadas et al., 2016; St Leger et al., 2017). As such, the function of the parainflammatory response may be to prevent microbes from colonizing the cornea. Indeed, we did not find bacteria colonizing the cornea despite their presence on the lens. The requirement of IL-1R for these parainflammatory responses could also indicate microbial triggers (Metruccio et al., 2017; Altmeier et al., 2016;Metruccio et al., 2016), but would not exclude other potential (non-microbial) factors asso- ciated with the lens or post-lens environment that could activate endogenous danger-associated molecular patterns, with IL-1$\alpha$ and/or IL-1$\beta$ release, and similar cellular responses (Tian et al., 2017; Takenouchi et al., 2014; Couillin et al., 2013; Rabolli et al., 2014).

Multiple mechanisms contribute to keeping the healthy cornea free of microbes when a lens is not worn. Indeed, the cornea normally lacks a microbiome despite constant exposure to microbes from the environment and adjacent colonized tissue surfaces (Wan et al., 2018). It even resists colonization by potential pathogens introduced in large numbers (Mun et al., 2009; Augustin et al., 2011), with resistance requiring IL-1R and MyD88 (Wan et al., 2018; Tam et al., 2011) of both epithelial cells and resident CD11c-positive cells (Metruccio et al., 2017), with contributions made by surfactant protein D, epithelial tight junctions, and antimicrobial peptides (Mun et al., 2009; Augustin et al., 2011; Alarcon et al., 2011; Tam et al., 2012). Antimicrobial peptide expression by the corneal epithelium can be constitutive and upregulated (McDermott et al., 2003). In the present study, the lack of corneal colonization by the commensal-type bacteria contaminating lenses, suggests mechanisms normally preventing microbiome establishment were not compromised, or that compensatory mechanisms were employed during lens wear. Whether para-inflammation plays a role in this respect is to be determined.

High magnification *ex vivo* imaging of mice expressing red fluorescent membranes showed subtle changes to cell morphology in lens-wearing corneas not observed using a dissecting microscope or immunohistochemistry. They included numerous small vesicles in epithelial cells and keratocytes appeared jagged. An increase in corneal thickness was also observed after 24h. The significance of these changes is unclear, since corneal transparency was maintained in these eyes. Maintenance of corneal transparency is a complex regulated process dependent on the fine structure and biochemistry of the stroma, and on normal function of cells within all three cellular layers. Our data suggest, therefore, that CD11c-positive cell and neutrophil responses to lens wear did not functionally disrupt physiological processes that maintain corneal transparency, and/or that compensation mechanisms were in effect. It is also difficult to ascertain if some of the tissue changes, e.g. epithelial vesicles, are typical of para-inflammation, as other body sites are less amenable to detailed high-resolution imaging.

When mouse contact lenses were contaminated with *P. aeruginosa* before placement on the eye, an aggressive infiltrative response was observed in the stroma. The large number of infiltrating cells, rounded morphology, style of motility, and the damage to surrounding stroma and the basal epithelium, suggested a classical activated phagocyte, with high levels of oxidative burst and microbicidal activity. This aligns with published findings using the scarification injury model of *P. aeruginosa* infection, with essential roles for such cells in clearing infecting bacteria,

and promoting disease resolution, but with a significant cost in collateral damage (Hazlett, 2004; Lee et al., 2003; Zolfaghar et al., 2006; Hazlett et al., 1992; Pearlman et al., 2008; Wu et al., 2011; Sun et al., 2012; Tam et al., 2007). Mechanism(s) for the apparent change in neutrophil phenotype after *P. aeruginosa* challenge via the lens include pattern recognition receptors and possibly bacterial virulence factors, such as the type three secretion system of *P. aeruginosa* that is known to modulate neutrophil migration and function (Zolfaghar et al., 2006; Sun et al., 2012; Vareechon et al., 2017; Garrity-Ryan et al., 2000). In this respect, whether underlying lens-induced para-inflammation actually contributed to development of infection when mouse lenses were contaminated with *P. aeruginosa* is another open question. Alternatively, changes to ocular surface defense and microbial adaptations to the ocular surface ((Tam et al., 2010) might drive disease initiation regardless of the presence or status of neutrophils in the cornea. Further work will be needed to delineate the respective roles of microbes and infiltrating cells in the pathogenesis of contact lens-related infection.

## 6.6 Conclusion

We have successfully developed a murine model of *in vivo* contact lens wear. The model faithfully replicates in mice several lens-associated phenomena previously reported in humans across a variety of lens materials, lenses from different manufacturers, different modalities of wear, and advances on what can be done using human subjects. Without the need to suture the eye shut to retain the lens, and its amenability to mouse-specific reagents, it also improves on existing larger animal models.

While the discovery that lens wear can cause a para-inflammatory response in mice is the first example of this type of response in the cornea, para-inflammation is known to be important in understanding health and disease at other body sites including the retina. This phenomenon might relate to multiple issues associated with contact lens wear, e.g. discomfort, inflammation and infection. For example, a recent study comparing reusable and daily disposable contact lens wear in humans revealed a positive association between lens discomfort and ratios of pro-inflammatory to anti-inflammatory tear cytokines, e.g. IL- 1$\beta$ to IL-10 (Chao et al., 2017). Prior to that study, a perspective review of contact lens research in human subjects concluded that contact lens wear is “intrinsically inflammatory”, and suggested that para-inflammatory events were a part of uncomplicated lens wear, and might have a protective role (Efron, 2017). Moreover, our data showing that *P. aeruginosa* can penetrate into the corneal epithelium during contact lens wear without injury provides important information about the role of lens wear in susceptibility to infection and is a phenomenon that cannot be demonstrated or properly studied using other mouse infection models. With the projected escalation of contact lens use due to the need for myopia correction in humans, and contact lens use as an electronic device (e.g. for health monitoring), the development and availability of this novel murine model is timely. In addition to deciphering the mechanisms and relationships between phenomena occurring during lens wear and their significance, this model could also be of value to study impact of various contact lens-wearing modalities worn by people, e.g. differences between continuous wear as used in

the present study, and daily removal with or without lens replacement. Beyond contact lens wear, this model provides another tool for researchers studying intrinsic mechanisms by which the cornea maintains health and transparency critical for vision and/or how it resists microbial colonization and infection.

Contrasting with other body sites, the cornea is ideal for imaging due to its transparency and superficial location. The response to contact lens wear in mice involves recruitment and morphological changes to multiple cell types while the cornea remains clear and amenable to high resolution intravital imaging using a standard confocal microscope. Thus, this model could also be useful for researchers outside the field of cornea research studying cellular, molecular and immunological processes in general or as they relate to other body sites.

## 6.7 Funding and Disclosures

This work was supported by the National Institutes of Health EY024060 (SMJF). The funding source was not involved in study design, data collection or analysis, decision to publish or article preparation. Authors RF, LW, and MG are paid employees of CooperVision Inc. JM, TT, and CM were former paid employees of CooperVision Inc. CM is a consultant for CooperVision Inc. JM is presently a paid employee of Johnson and Johnson Inc.

## 6.8 Acknowledgements

Our thanks to Lisa Telford, Zena Gough, and Lee Norris (each from CooperVision Inc.) for their skillful assistance in murine lens fabrication.

## 6.9 Supplementary Material

Supplementary videos to this article can be found online at
https:// doi.org/10.1016/j.jtos.2018.11.006.

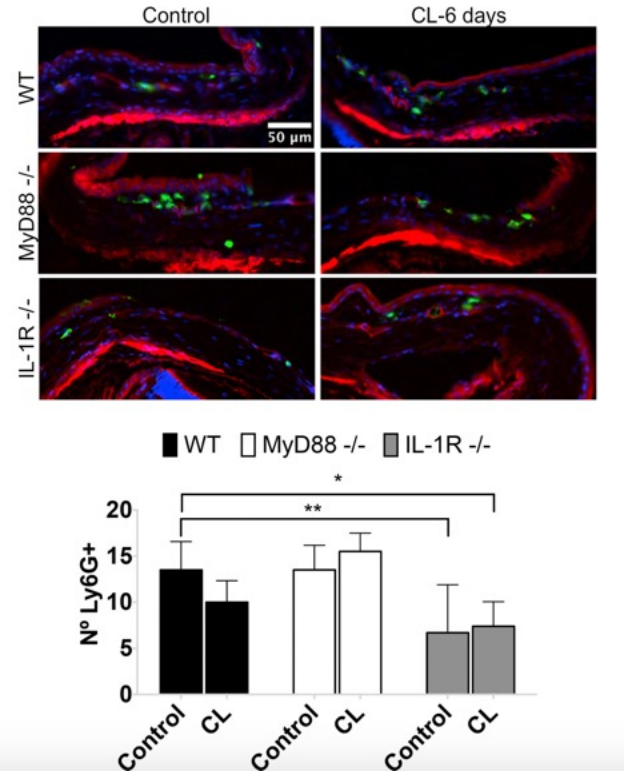


**Figure 6.9:** Supplementary Figure S1. Cryo-sections of limbal and conjunctival regions of wild-type (WT), MyD88 (-/-), or IL-1R (-/-) mice after 6 days of contact lens wear, stained with phalloidin (magenta, actin), DAPI (blue, nuclei) and Ly6G-antibody (green) showing the presence of Ly6G-positive cells (neutrophils) in all eyes. Scale bar = 50 $\mu$m. Quantification of the number of Ly6G-positive cells per field in the limbal and conjunctival regions of WT versus MyD88 (-/-) or IL-1R (-/-) mice revealed no significant difference between controls and lens-wearing eyes for any group. IL-1R (-/-) control and lens-wearing eyes showed a similar reduction in Ly6G-positive cells per field versus WT controls, but this reduction was not observed in MyD88 (-/-) eyes (* $p < 0.05$, ** $p < 0.01$, two-way ANOVA with Sidak's multiple comparison test).

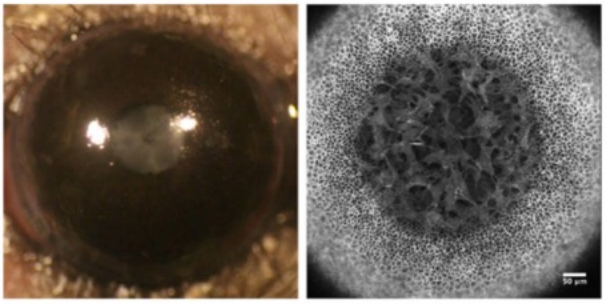

**Figure 6.10:** Supplementary Figure S2. Representative images of a murine cornea after wearing a *P. aeruginosa*-inoculated CL for 22 days without the development of bacterial keratitis. Dissecting microscope image (left) and confocal image (right).

# Chapter 7

# Conclusions

The microbial world is vast and surrounds us. Even more, communities of bacteria (microbiomes) inhabit most tissues of our bodies and play critical roles for maintaining health. While normally, we have a symbiotic relationship with these tiny organisms, alterations in the diversity or number of bacteria is often associated with disease (Turnbaugh et al., 2007). Further, insult or damage to tissues allows opportunistic bacteria access to normally protected areas causing infections and inflammatory reactions. As such, our relationship with these important microorganisms is a delicate balance.

While microbiomes associated with the body in the gut, nasal tract, respiratory tract, urogenital tract, oral cavity and skin were being popularly studied, whether a microbiome existed on the ocular surface was largely ignored. Furthermore, a debate in the field was beginning to gain traction on this very notion. Many, exclaimed that the ocular surface, a mucosal tissue similar to those that host large communities of bacteria, of course was inhabited by bacteria as it is constantly in contact with bacteria in the environment. Others, pointed out that the eye is excellent at preventing pathogenic bacteria from causing infections, thus environmental bacteria also have no chance of forming a home on the eye. As interest in this topic began to grow, it became apparent that some bacteria do in fact inhabit the conjunctiva. It then became a common claim that bacteria inhabit all of the eye, including its neighboring tissue the cornea. However, this was never explicitly proven. In general, there often is not a distinction between the conjunctiva and the cornea despite being separate tissues and several news outlets even published articles exclaiming the presence of a multitude of bacteria on the eye without the differentiation (Berne, 2019; Shaikh-Lesko, 2014).

Understanding the normal microbial environment on the eye is critical. Local bacteria often play a role in maintaining homeostasis and can help prevent infection. Alternatively, understanding differences occurring in a diseased state to allow more or different types of bacteria to inhabit an eye may also play a role in the pathogenesis of various diseases. Thus, I first set out to truly understand whether the ocular surface hosts a microbiome, particularly on the cornea.

Traditionally, identification of bacterial communities has been studied using standard laboratory culture techniques. However, this often has limitations on the types of bacteria that can be

grown (Epstein, 2013; Kawai et al., 2015; Oliver, 2005). Culture-independent techniques are now the gold standard due to advances in molecular technologies, overcoming obstacles with culture methods. This primarily is done through sequencing 16s rRNA genes, a conserved sequence in the bacterial kingdom with interspersed variable regions that identify bacteria down to the species level (Turnbaugh et al., 2007). However, this method detects nucleic acids which does not necessarily equate to viable bacteria. Furthermore, considering previous studies that explored the presence of bacteria on the conjunctiva (Doan et al., 2016), if bacteria are present on the cornea, it would be in much less abundance compared to other tissues. Having a low biomass makes it very difficult to extract the true signal from the noise using sequencing methods leading to false-positive results due to contaminants from the environment or reagents (Salter et al., 2014; Schabereiter-Gurtner et al., 2001). Neither of these methods also provide any spatial information.

To explore if the ocular surface hosts a microbiome, we used labeling techniques to be able to visualize live bacteria *in situ* on the mouse cornea to circumvent limitations with culturing and sequencing methods. Not only does this provide information about viable microbes present on the ocular surface but importantly, but the tissue location, between the cornea and the conjunctiva could also be distinguished. Using these probes, we found that the cornea is relatively sterile. This is a remarkable feat considering the eye is in constant contact with the environment and thus the surrounding microbes. It is likely then that any bacteria detected were transient microbes that have not yet succumbed to the ocular defenses. Interestingly, the conjunctiva did have several live bacteria detected on its surface including long filamentous bacteria belonging to the Corynebacterineae suborder. I suspect that one reason these bacteria can colonize the conjunctiva, but not the cornea, is due to the irregularity of the conjunctiva. The filamentous bacteria are able to grab a hold and be protected in the numerous folds of the conjunctiva whereas on the cornea, there is nowhere to hide. Furthermore, filamentous bacteria in the gut are the only bacteria found to be able to directly interact with the epithelia. Other bacteria have a 50 $\mu$M clear zone due to epithelial defenses. Being in a filamentous state is often protective and these bacteria can withstand the presence of antimicrobials (Justice et al., 2006; Vaishnava et al., 2011).

The finding that bacteria inhabit the conjunctiva is also in line with previous studies that have reliably found bacteria, including *Corynebacterium* to be present (Doan et al., 2016; Dong et al., 2011; Graham et al., 2007; St Leger et al., 2017). One study has even shown that *C. mastitidis* protects from *C. albicans* and *P. aeruginosa* infections through IL-17 responses (St Leger et al., 2017). Whether these bacteria also play a role in immune responses on the cornea remain to be determined and would be an interesting avenue to explore. The palpebral conjunctiva constantly washes over the cornea through blinking, and when eyes are closed at night it lies right on top of the cornea so it is a viable possibility that anything on the conjunctiva can also directly affect the cornea.

Not only do bacteria prevent a microbiome from forming on the cornea but the cornea can also inhibit large inocula of bacteria from adhering. This was found to be true for not only pathogenic *P. aeruginosa* but also for Gram-positive *S. aureus* and a mouse eyelid commensal, Coagulase-negative *Staphylococci* spp. To further our understanding of the mechanisms by which the cornea maintains this amicrobiomic environment, we explored the possibility that

innate immune defenses that normally detect and respond to microbes are necessary. The role of IL-1R and MyD88 were examined given that these play an important role in innate immunity at mucosal surfaces and have been shown to protect the mouse corneal epithelium against colonization and penetration of inoculated *P. aeruginosa* (Metruccio et al., 2017; Tam et al., 2011). Indeed, knockout mice lacking these important proteins harbored metabolically active bacteria on their corneas suggesting that these signaling molecules not only respond to pathogenic bacteria when in contact with the cornea, but also play a significant role in constitutively maintaining the bacteria-free state of the cornea. We further explored this mechanism and found that IL-1R$^{-/-}$ corneas have normal epithelial junction integrity similar to previously published results with MyD88$^{-/-}$ (Tam et al., 2011). However, IL-1R$^{-/-}$ mouse corneas showed reduced antimicrobial activity compared to wild-type. This result mirrored prior research demonstrating that MyD88$^{-/-}$ corneal lysates exhibited less antimicrobial activity. Several factors involved in IL-1R and MyD88 signaling have been associated with the regulation of antimicrobial peptides such as hBD2 and LL-37 (McDermott et al., 2003; Redfern et al., 2011). Given the remarkable ability for the cornea to remain relatively sterile, it is conceivable that the cornea is a minefield for undiscovered antimicrobials. These substances would also be biocompatible and could be extremely useful for the development of novel antibiotics or even preventative strategies such as coatings on contact lens cases to inhibit bacterial growth.

The cornea has a multitude of defense mechanisms to prevent bacterial adherence and traversal. Tears are one of the first substances bacteria will encounter when trying to gain entry into the corneal epithelium. Not only do tears help to provide a lubricant for the eyelids to blink and wash away unwanted debris on the eye but they also contain several antimicrobial components (Akpek and Gottsch, 2003; Fleiszig et al., 2003; McClellan, 1997). Further, tears also can inhibit bacterial growth and reduce virulence independent of antimicrobial activity. One example is DMBT1, a glycoprotein in tears and saliva, that inhibits twitching motility of *P. aeruginosa* (Li et al., 2017). Twitching is a pili-mediated surface movement that is important for host cell exit and invasion as well as traversal of corneal epithelia (Alarcon et al., 2009; Zolfaghar et al., 2003). Given the importance of twitching motility for bacterial virulence and host cell invasion, the mechanisms by which DMBT1 inhibits this was explored.

DMBT1 was first enzymatically digested with Lys-C which produces a large fragment containing the majority of the SRCR and SID domains as well as many smaller fragments. The fraction containing the large SRCR/SID domains was the only fraction to retain twitching inhibition activity. Thus, this domain was further divided using synthesized SRCR peptides, a recombinant truncated peptide with the N-terminal domain of DMBT1, and CD163 a member of the SRCR-super family to systematically determine which domain contributes to inhibiting *P. aeruginosa* twitching motility. None of these demonstrated inhibition of twitching motility, even CD163 a glycoprotein with multiple SRCR/SID regions that is very similar to DMBT1. These results suggest that it is not the SRCR nor SID domains themselves that contribute to inhibiting bacterial twitching. Thus, effects of post-translational modifications were tested. Since DMBT1 is a highly-glycosylated protein, it was hypothesized that glycosylation of DMBT1 is involved. Indeed, DMBT1 digested by a deglycosylation enzyme mix partially lost its ability to inhibit

twitching. This was further narrowed down to be due to N-glycosylation. However, unlike previous studies that suggested DMBT1-mediated twitching inhibition was due to pili binding (Li et al., 2017), the results from these studies did not demonstrate any reduction in pili binding with de-N-glycosylated DMBT1. This result indicates that additional or other mechanisms than pili binding may be involved.

Overall, this study contributes to our understanding of how DMBT1 inhibits twitching motility and thus protects epithelial tissues against *P. aeruginosa* infection. *P. aeruginosa* is an opportunistic, Gram-negative pathogen that infects compromised hosts at various mucosal tissues such as burn sites, lung epithelia in pneumonia or cystic fibrosis patients, and epithelial surfaces in contact with catheters, ventilators, and contact lenses. DMBT1 is present in multiple mucosal tissues and body fluids but can be expressed as different isoforms in various tissues due to alternative splicing and post-translation modifications (Ligtenberg et al., 2010; Madsen et al., 2010; Polley et al., 2015). Since N-glycosylation contributes to DMBT1's activity to inhibit twitching and may even be site specific, it would be of interest to determine if our findings are maintained across various isoforms of DMBT1. These findings would add to our understanding of how mucosal fluids protect themselves against pathogens, as well as offering insights for the development of novel strategies to defend and prevent bacterial infections at specific tissue sites.

The effects of DMBT1 on the ocular surface are striking. This was clearly observed in a corneal infection model in which the mouse cornea is scratched then allowed to heal for 6 h before inoculated with *P. aeruginosa* in PBS or DMBT1 (Li et al., 2017). Corneas inoculated with *P. aeruginosa* in PBS showed obvious signs of infection after day 1 that worsened after day 2. On the other hand, corneas treated with *P. aeruginosa* in DMBT1 had reduced pathology at day 1 that did not become any more severe by day 2. It would be of interest to determine how DMBT1 on the ocular surface changes as a result of disease or even in instances of dry eye or contact lens wear. Not only would it be important to determine if levels of expression are altered but also determine changes to the conformation, specifically N-glycosylation, of DMBT1. If changes do occur, it could be of use to harness DMBT1's anti-infection capabilities and add unaltered protein back into these models to determine if any effects occur to reduce or even prevent infections.

If bacteria evade defenses of the cornea such as tears or the glycocalyx and gain access to epithelial cells, they are still faced with several obstacles before they reach the stroma and wreak havoc. One important aspect of the cornea that has not been explored in terms of bacterial defense is sensory nerves. The cornea is the most innervated tissue of the body and the nerves are critical for sensory transduction and structural support. One component of our laboratory's research that has stood out is that *P. aeruginosa* easily invades human corneal epithelial cells *in vitro* (Fleiszig et al., 1995; Kroken et al., 2018) but has a difficult time even sticking to the epithelial cells *in vivo* on a mouse eye (Mun et al., 2009; Wan et al., 2018). While several factors differ in the *in vitro* versus host environment, one aspect that is clearly missing from cell lines is nerves. This along with the surge of research demonstrating neuro-immunomodulary relationships led us to wonder if corneal nerves and their receptors play a role in corneal defense. The majority of corneal nerve fibers are polymodal and often express TRPA1 and TRPV1. These ion channels are most known for signal transduction related to pain, itch, and temperature but several studies

have also shown that they respond to microbial ligands (Belmonte et al., 2017; Chiu et al., 2013; Pinho-Ribeiro et al., 2017).

Indeed, we found that inoculated *P. aeruginosa* adhered better to TRPA1$^{-/-}$/TRPV1$^{-/-}$ mouse corneas compared to wild-type. Furthermore, TRPA1$^{-/-}$/TRPV1$^{-/-}$ corneas also had an increase in environmental bacteria detected in the cornea compared to wild-type indicating that mice lacking these ion channels have a reduced ability to prevent bacterial adherence. Thus, we wanted to understand how these ion channels modulate the cornea to prevent colonization. We found that TRPA1$^{-/-}$/TRPV1$^{-/-}$ mice have normal epithelial junction integrity, glycocalyx expression, and antimicrobial activity. It is interesting that while phenotypes regarding bacterial colonization were similar to those observed with IL-1R$^{-/-}$ and MyD88$^{-/-}$ mice (Metruccio et al., 2017; Sullivan et al., 2015; Tam et al., 2011; Wan et al., 2018) , TRPA1$^{-/-}$/TRPV1$^{-/-}$ mice retained antimicrobial activity in corneal lysates while IL-1R$^{-/-}$ and MyD88$^{-/-}$ did not. Clearly, a multitude of parallel pathways and mechanisms are in place to help protect the cornea.

Because nociceptors can directly sense bacterial components and release immune mediators that modulate macrophage, dendritic cells, T cells and other immune cells (Baral et al.; Chiu et al., 2012; Pinho-Ribeiro et al., 2017), we next wanted to explore the role of TRPA1 and TRPV1 and immune cell responses. TRPA1$^{-/-}$/TRPV1$^{-/-}$ mice had similar numbers of CD45+ cells (differentiated hematopoietic cells) compared to wild-type but after inoculated with *P. aeruginosa*, wild-type mice showed an increase of CD45+ cells while TRPA1$^{-/-}$/TRPV1$^{-/-}$ did not. We wanted to then decipher specific cell types that may contribute to this. We hypothesized that dendritic cells may be involved since previously published data has shown that *P. aeruginosa* causes an influx of dendritic cells in the cornea and that nerves and dendritic cells are intimately intertwined (Gao et al., 2016; Metruccio et al., 2017). TRPA1 and TRPV1 ion channels were selectively depleted in transgenic CD11c-yfp mice then challenged with *P. aeruginosa*. As in prior studies, inoculated corneas with *P. aeruginosa* caused an infiltration of CD11c+ cells (i.e dendritic cells) in control wild-type mice (Metruccio et al., 2018), but not in TRPA1/TRPV1 depleted mice. Lastly, I found that TRPA1$^{-/-}$ mice but not TRPA1$^{-/-}$ had increased bacterial adherence on the cornea suggesting that TRPA1 is necessary to stop colonization. This aligns with other studies that have found that TRPA1 responds to LPS and modulates immune cells in other inflammatory diseases (Caceres et al., 2009; Engel et al., 2011; Liu et al., 2013; Meseguer et al., 2014). However, further studies are necessary to clearly delineate the specific roles of TRPA1 and TRPV1 in defense against bacteria on the cornea.

The signaling pathway for how bacteria are detected then consequently cleared also remains to be defined. However, given that the response of sensory nerves is within milliseconds and that dendritic cells can respond to neuromodulators released by TRP channels (Chiu et al., 2012), I postulate that when bacteria come into contact with the epithelium, TRPA1 expressing sensory nerves detect the microbes and release neuronal factors such as substance P, CGRP or GFR$\alpha$3 that in turn recruit and prime dendritic cells. The dendritic cells then may drive further immune responses such as T cell recruitment. Determining the molecular underpinnings of this sequence of events would be of value. In terms of a healthy cornea that is not yet infected, it is likely that substance P or GFR$\alpha$3 are the neuropeptides released since CGRP is expressed by nociceptors in the wing and basal layers of the cornea (Alamri et al., 2015) and here, we are looking at surface

associated bacteria. It is also important to note that this sequence of events and factors involved may differ in an infected cornea compared to a healthy cornea since they are two completely different environments. However, this important study is the first to demonstrate that corneal sensory nerves play a role in defense against bacteria.

After determining that the healthy cornea is free of colonizing bacteria and investigating some components that contribute to this resistance, I next wanted to investigate how modulations to the cornea affect its ability to withstand microbes. Dry eye disease (DED) is a common and debilitating disease characterized by loss of tear film leading to symptoms of discomfort, inflammation and damage to the ocular surface (Craig et al., 2017). The pathogenesis of DED is not well understand but is associated with several factors that compromise defenses against bacteria. It has long been questioned, if bacteria play a role in the pathogenesis of DED and the impact of DED towards bacterial keratitis has been debated (Graham et al., 2007; Narayanan et al., 2013). Thus, we utilized an experimental induced murine model of dry eye disease (EDE) and the bacterial labeling techniques from Chapter 2 to determine if environmental bacteria can colonize the eyes of mice with DED. It was found that the cornea remained free of live bacteria after induction of dry eye. Further, no changes in the amount of bacteria present on the conjunctiva was observed, similar to findings of other studies (De Paiva et al., 2016; Graham et al., 2007). This is quite interesting considering that dry eye disease has been associated with loss of tear fluid, decrease in antimicrobial activity, loss of goblet cells that secret mucins to trap and clear bacteria, and poor epithelial integrity (Argüeso et al., 2002; Beardsley et al., 2008; Caffery et al., 2008; Narayanan et al., 2003). Furthermore, a previous study even found that EDE corneas were still able to clear inoculated *P. aeruginosa* similar to controls (Heimer et al., 2013).

The cornea is still able to ward of unwanted inhabitants, both environmental and inoculated pathogenic bacteria, after the induction of dry eye. However, it is quite plausible that while some defenses of the cornea are hindered by dry eye, others are upregulated. This was exemplified in Heimer, et al., (2013), which observed an upregulation of SP-D in ocular washes after induction of DED. SP-D previously has been shown to be involved in corneal defense against infection (Heimer et al., 2013; Ni et al., 2005). I suspect then that there is a myriad of defenses that are altered both up and down during dry eye disease, but a balance is retained to still allow the cornea to defend against bacterial adhesion.

The results from this study suggest that live local bacteria on the cornea do not contribute to the pathogenesis of dry eye disease. However, here we only looked for the presence of live bacteria. It is a possibility that bacterial components could still elicit immune responses that contribute to inflammation on the eye. It also seems unlikely that bacteria on the conjunctiva play a role in the pathogenesis of dry eye considering in this study no differences in number of bacteria present was observed. Furthermore, other studies also did not detect significant differences in species of bacteria present on the conjunctiva during dry eye compared to healthy controls (De Paiva et al., 2016; Graham et al., 2007). We are fortunate that the cornea holds a wide arsenal of defenses that can be employed in different states to help protect it and preserve its clarity.

Contact lens wear is one of the most common forms of vision correction with over 140

million wearers world-wide. (Nichols et al., 2013; Stapleton et al., 2007). The use of contact lens wear is also expected to increase greatly with the rise of myopia and development of lenses for technological advancement such as drug delivery, health monitoring and augmented reality (ElShaer et al., 2014; Park et al., 2018; Phan et al., 2016; Wu et al., 2016). Contact lens wear is the highest risk factor for bacterial keratitis (Stapleton et al., 2013) and so, it paramount to gain a better understanding of how contact lenses alter the corneal environment to increase susceptibility to pathogens. Interestingly, contact lenses do not affect the gross morphology of the cornea and thus, how the bacteria gain access and cause an infection during contact lens wear is not well understood. This is largely due to limitations with human studies and a prior lack of animal models for lens wear.

Our lab developed a customized silicone-hydrogel lens to fit C57BL/6 mice. We first fit the lens (not inoculated) on the mouse eye to determine how the lens itself affects the corneal environment. Using a dissecting microscope, the eye fit with a lens looked identical to contralateral control eyes that were not exposed to lens wear. However, using mice with fluorescent cell membranes, confocal microscopy revealed a multitude of alterations to the cornea microscopically. This is the first time changes to the cornea could be observed after lens wear at a cellular level. It was found that after 24 h of lens wear, a dendritic cell response occurred which was followed by an infiltration of neutrophils after 5 days of lens wear that was MyD88 and IL-1R dependent. Not only were there a large quantity of cells but they also appeared to be highly motile and activated. Interestingly, despite this influx of immune cells the cornea remained clear and did not swell. Since these infiltrating immune cells do not cause an outright inflammatory response, we have suggested that this is a parainflammatory response. Whether this is a harmful (i.e. the first step towards a full inflammatory response) or protective, remains to be determined and is of great interest. These studies also employed continuous wear schedules. It would be interesting to determine if similar responses occurred in a daily wear regimen (removing lenses at night) or if the parainflammatory response is resolved.

We next explored if lens wear could harbor microbes given that the dendritic cell response is similar to what was previously observed with bacterial inoculation (Metruccio et al., 2017) and healthy mouse eyes use IL-1R dependent strategies to clear bacteria (Wan et al., 2018). We found that lenses removed after 1-11 days of wear did in fact harbor bacteria, with *Corynebacterium spp.* being the most commonly identified. Few bacteria were also found to be present on the epithelium with rare instances of penetration occurring. However, none of the mice developed microbial keratitis. An infection does not occur unless the lens is contaminated with *P. aeruginosa*, and this is still variable. Most of the bacteria identified on the uncontaminated contact lenses were also located on the posterior side of the lens which is in contact with the cornea. It remains to be determined if these microbes that colonize the contact lens during wear play a role in the parainflammatory response. Given what we know about the presence of bacteria on the cornea and immune cell responses, it seems likely that microbes may be a trigger.

The cornea is a remarkable and sturdy tissue equipped to stop and heal harmful insults to protect itself. As visual creatures, our sight is of the utmost importance and the ability of the cornea to go to great lengths to prevent inflammation (and therefore opacification) highlights

this. This dissertation emphasis the remarkable ability of the cornea to safeguard itself from bacteria. First, by demonstrating that the cornea refrains from hosting a microbiome, despite being constantly exposed to bacteria in the environment. This finding also underlines the importance of treating the cornea and conjunctiva as separate tissues, particularly in respect to microbiome research. However, how one influences the other is important to keep in mind. I then go on to explore mechanisms by which the cornea prevents bacterial colonization. These include tear fluid glycoprotein DMBT1, IL-1R and MyD88 dependent pathways, and nociceptors expressed on corneal nerves. The diversity of these various mechanism underscores the arsenal of defenses the cornea has to maintain its healthy state, but it is a complicated process and not simply black and white. Pathways to protect the cornea are in parallel as well as with substantial overlap, making it extremely difficult to dissect out the precise mechanisms by which the cornea defends itself against microbes. However, this dissertation adds to our understanding, and importantly uses models of health to grasp how the normal cornea prevents insult rather than infection models which are useful to determine how the cornea responds to already occurring damage. Lastly, I explored how modifications to the cornea alters its environment and ability to defend against bacteria. Dry eye disease retains its ability to withstand unwanted invaders, possibly due to an upregulation of alternate defense mechanisms not normally employed. It is striking that even in this diminished state, the cornea can still ward off bacteria. Contact lens wear however does lead to colonization on the lens that interacts with the cornea and results in a low grade inflammatory response. Still, the cornea does not normally get infected. This understanding of how the healthy cornea maintains homeostasis is critical in order to truly decipher what is going wrong during disease or how a contact lens alters the environment to increase risk of infection. However, considering the multitude of layers in place, this is not a simple task. Nevertheless, the results from this dissertation will be useful for the field to harness a greater understanding of the healthy corneal environment and interactions with bacteria. By taking a multidisciplinary approach (microbiology, immunology, and neurobiology) we can appreciate the vast complexity of this amazing tissue and garner a more expansive view of all the mechanisms in place to protect it and what could be deregulated that ultimately leads to disease.

# Chapter 8

# References

Akpek, E.K., and Gottsch, J.D. (2003). Immune defense at the ocular surface. Eye (Lond) 17, 949–956.

Alamri, A., Bron, R., Brock, J.A., and Ivanusic, J.J. (2015). Transient receptor potential cation channel subfamily V member 1 expressing corneal sensory neurons can be subdivided into at least three subpopulations. Front Neuroanat 9, 71.

Alarcon, I., Evans, D.J., and Fleiszig, S.M.J. (2009). The Role of Twitching Motility in *Pseudomonas aeruginosa* Exit from and Translocation of Corneal Epithelial Cells. Invest. Ophthalmol. Vis. Sci. 50, 2237–2244.

Alarcon, I., Tam, C., Mun, J.J., LeDue, J., Evans, D.J., and Fleiszig, S.M.J. (2011). Factors impacting corneal epithelial barrier function against *Pseudomonas aeruginosa* traversal. Invest. Ophthalmol. Vis. Sci. 52, 1368–1377.

Allentoft, M.E., Collins, M., Harker, D., Haile, J., Oskam, C.L., Hale, M.L., Campos, P.F., Samaniego, J.A., Gilbert, M.T.P., Willerslev, E., et al. (2012). The half-life of DNA in bone: measuring decay kinetics in 158 dated fossils. Proceedings of the Royal Society B: Biological Sciences 279, 4724–4733.

Altmeier, S., Toska, A., Sparber, F., Teijeira, A., Halin, C., and LeibundGut-Landmann, S. (2016). IL-1 Coordinates the Neutrophil Response to *C. albicans* in the Oral Mucosa. PLoS Pathog 12, e1005882.

Alzahrani, Y., Colorado, L.H., Pritchard, N., and EFRON, N. (2017). Longitudinal changes in Langerhans cell density of the cornea and conjunctiva in contact lens-induced dry eye. Clinical and Experimental Optometry 100, 33–40.

Alzahrani, Y., Pritchard, N., and EFRON, N. (2016). Changes in corneal Langerhans cell density during the first few hours of contact lens wear. Cont Lens Anterior Eye 39, 307–310.

Aran, D., Lasry, A., Zinger, A., Biton, M., Pikarsky, E., Hellman, A., Butte, A.J., and Ben-Neriah, Y. (2016). Widespread parainflammation in human cancer. Genome Biol. 17, 145.

Argüeso, P., Balaram, M., Spurr-Michaud, S., Keutmann, H.T., Dana, M.R., and Gipson, I.K. (2002). Decreased levels of the goblet cell mucin MUC5AC in tears of patients with Sjögren syndrome. Invest. Ophthalmol. Vis. Sci. 43, 1004–1011.

Arques, J.L., Hautefort, I., Ivory, K., Bertelli, E., Regoli, M., Clare, S., Hinton, J.C.D., and Nicoletti, C. (2009). *Salmonella* Induces Flagellin- and MyD88-Dependent Migration of Bacteria-Capturing Dendritic Cells Into the Gut Lumen. Gastroenterology 137, 579–587.e2.

Augustin, D.K., Heimer, S.R., Tam, C., Li, W.Y., Le Due, J.M., Evans, D.J., and Fleiszig, S.M.J. (2011). Role of Defensins in Corneal Epithelial Barrier Function against *Pseudomonas aeruginosa* Traversal. Infection and Immunity 79, 595–605.

Baral, P., Mills, K., Pinho-Ribeiro, F.A., microbe, I.C.C.H., 2016 Pain and itch: beneficial or harmful to antimicrobial defense? Elsevier.

Beardsley, R.M., De Paiva, C.S., Power, D.F., and Pflugfelder, S.C. (2008). Desiccating stress decreases apical corneal epithelial cell size–modulation by the metalloproteinase inhibitor doxycycline. Cornea 27, 935–940.

Belmonte, C., Nichols, J.J., Cox, S.M., Brock, J.A., Begley, C.G., Bereiter, D.A., Dartt, D.A., Galor, A., Hamrah, P., Ivanusic, J.J., et al. (2017). TFOS DEWS II pain and sensation report. Ocular Surface 15, 404–437.

Bertrand, J.J., West, J.T., and Engel, J.N. (2010). Genetic Analysis of the Regulation of Type IV Pilus Function by the Chp Chemosensory System of *Pseudomonas aeruginosa*. Journal of Bacteriology 192, 994–1010.

Bikker, F.J., End, C., Ligtenberg, A.J.M., Blaich, S., Lyer, S., Renner, M., Wittig, R., Nazmi, K., van Nieuw Amerongen, A., Poustka, A., et al. (2017). The scavenging capacity of DMBT1 is impaired by germline deletions. Immunogenetics 69, 401–407.

Bikker, F.J., Ligtenberg, A.J.M., End, C., Renner, M., Blaich, S., Lyer, S., Wittig, R., van't Hof, W., Veerman, E.C.I., Nazmi, K., et al. (2004). Bacteria binding by DMBT1/SAG/gp-340 is confined to the VEVLXXXXW motif in its scavenger receptor cysteine-rich domains. J. Biol. Chem. 279, 47699–47703.

Bikker, F.J., Ligtenberg, A.J.M., Nazmi, K., Veerman, E.C.I., van't Hof, W., Bolscher, J.G.M., Poustka, A., Nieuw Amerongen, A.V., and Mollenhauer, J. (2002). Identification of the bacteria-binding peptide domain on salivary agglutinin (gp-340/DMBT1), a member of the scavenger receptor cysteine-rich superfamily. J. Biol. Chem. 277, 32109–32115.

Bird, L. (2010). Immune regulation: Controlling neutrophil plasticity. Nature Reviews Immunology 10, 752–752.

Blalock, T.D., Spurr-Michaud, S.J., Tisdale, A.S., Heimer, S.R., Gilmore, M.S., Ramesh, V., and Gipson, I.K. (2007). Functions of MUC16 in Corneal Epithelial Cells. Invest. Ophthalmol. Vis. Sci. 48, 4509–4510.

Bloemberg, G.V., and O'Toole, G.A. (1997). Green fluorescent protein as a marker for *Pseudomonas* spp. Appl Environ Microbiol. 1997;63:4543–4551.

Brittan, J.L., and Nobbs, A.H. (2015). Group B *Streptococcus* pili mediate adherence to salivary glycoproteins. Microbes Infect. 17, 360–368.

Caceres, A.I., Brackmann, M., Elia, M.D., Bessac, B.F., del Camino, D., D'Amours, M., Witek, J.S., Fanger, C.M., Chong, J.A., Hayward, N.J., et al. (2009). A sensory neuronal ion channel essential for airway inflammation and hyperreactivity in asthma. Proc Natl Acad Sci USA 106, 9099–9104.

Caffery, B., Joyce, E., Boone, A., Slomovic, A., Simpson, T., Jones, L., and Senchyna, M. (2008). Tear lipocalin and lysozyme in Sjögren and non-Sjögren dry eye. Optometry and Vision Science 85, 661–667.

Caudle, R.M., Karai, L., Mena, N., Cooper, B.Y., Mannes, A.J., Perez, F.M., Iadarola, M.J., and Oláh, Z. (2003). Resiniferatoxin-Induced Loss of Plasma Membrane in Vanilloid Receptor Expressing Cells. NeuroToxicology 24, 895–908.

Chalmers, R.L., Keay, L., McNally, J., and Kern, J. (2012). Multicenter Case-Control Study of the Role of Lens Materials and Care Products on the Development of Corneal Infiltrates. Optometry and Vision Science 89, 316–325.

Chao, C., Stapleton, F., Willcox, M.D.P., Golebiowski, B., and Richdale, K. (2017). Preinflammatory Signs in Established Reusable and Disposable Contact Lens Wearers. Optometry and Vision Science 94, 1003–1008.

Chen, M., and Xu, H. (2015). Parainflammation, chronic inflammation, and age-related macular degeneration. Journal of Leukocyte Biology 98, 713–725.

Chiang, P., Sampaleanu, L.M., Ayers, M., Pahuta, M., Howell, P.L., and Burrows, L.L. (2008). Functional role of conserved residues in the characteristic secretion NTPase motifs of the *Pseudomonas aeruginosa* type IV pilus motor proteins PilB, PilT and PilU. Microbiology 154, 114–126.

Chiu, I.M., Heesters, B.A., Ghasemlou, N., Hehn, Von, C.A., Zhao, F., Tran, J., Wainger, B., Strominger, A., Muralidharan, S., Horswill, A.R., et al. (2013). Bacteria activate sensory neurons that modulate pain and inflammation. Nature 501, 52–57.

Choy, M.H., Stapleton, F., Willcox, M.D.P., and Zhu, H. (2008). Comparison of virulence factors in *Pseudomonas aeruginosa* strains isolated from contact lens- and non-contact lens-related keratitis. Journal of Medical Microbiology 57, 1539–1546.

Ciolino, J.B., Stefanescu, C.F., Ross, A.E., Salvador-Culla, B., Cortez, P., Ford, E.M., Wymbs, K.A., Sprague, S.L., Mascoop, D.R., Rudina, S.S., et al. (2014). *In vivo* performance of a drug-eluting contact lens to treat glaucoma for a month. Biomaterials 35, 432–439.

Clausen, B.E., Burkhardt, C., Reith, W., Renkawitz, R., and Förster, I. (1999). Conditional gene targeting in macrophages and granulocytes using LysMcre mice. Transgenic Res 8, 265–277.

Cope, J.R., Collier, S.A., Rao, M.M., Chalmers, R., Mitchell, G.L., Richdale, K., Wagner, H., Kinoshita, B.T., Lam, D.Y., Sorbara, L., et al. (2015). Contact Lens Wearer Demographics and Risk Behaviors for Contact Lens-Related Eye Infections–United States, 2014. MMWR. Morbidity and Mortality Weekly Report 64, 865–870.

Couillin, I., Gombault, A., and Baron, L. (2013). ATP release and purinergic signaling in NLRP3 inflammasome activation. Front Immunol 3.

Craig, J.P., Nichols, K.K., Akpek, E.K., Caffery, B., Dua, H.S., Joo, C.-K., Liu, Z., Nelson, J.D., Nichols, J.J., Tsubota, K., et al. (2017). TFOS DEWS II Definition and Classification Report. The Ocular Surface 15, 276–283.

Cruzat, A., Pavan-Langston, D., and Hamrah, P. (2010). *In vivo* confocal microscopy of corneal nerves: analysis and clinical correlation. Semin Ophthalmol 25, 171–177.

Cruzat, A., Witkin, D., Baniasadi, N., Zheng, L., Ciolino, J.B., Jurkunas, U.V., Chodosh, J., Pavan-Langston, D., Dana, R., and Hamrah, P. (2011). Inflammation and the Nervous System:

The Connection in the Cornea in Patients with Infectious Keratitis. Invest. Ophthalmol. Vis. Sci. 52, 5136.

Danielle M Robertson, H.D.C. (2011). Non-compliance with contact lens wear and care practices: a comparative analysis. Optometry and Vision Science : Official Publication of the American Academy of Optometry 88, 1402–1408.

Daniels, R., Kurowski, B., Johnson, A.E., and Hebert, D.N. (2003). N-linked glycans direct the cotranslational folding pathway of influenza hemagglutinin. Mol. Cell 11, 79–90.

De Paiva, C.S., Jones, D.B., Stern, M.E., Bian, F., Moore, Q.L., Corbiere, S., Streckfus, C.F., Hutchinson, D.S., Ajami, N.J., Petrosino, J.F., et al. (2016). Altered Mucosal Microbiome Diversity and Disease Severity in Sjögren Syndrome. Sci. Rep. 6, 23561.

DeLange, P.A., Collins, T.L., Pierce, G.E., and Robinson, J.B. (2007). PilJ Localizes to Cell Poles and Is Required for Type IV Pilus Extension in *Pseudomonas aeruginosa.* Curr Microbiol 55, 389–395.

Deniset, J.F., and Kubes, P. (2018). Neutrophil heterogeneity: Bona fide subsets or polarization states? Journal of Leukocyte Biology 103, 829–838.

Doan, T., Akileswaran, L., Andersen, D., Johnson, B., Ko, N., Shrestha, A., Shestopalov, V., Lee, C.S., Lee, A.Y., and Van Gelder, R.N. (2016). Paucibacterial Microbiome and Resident DNA Virome of the Healthy Conjunctiva. Invest. Ophthalmol. Vis. Sci. 57, 5116–11.

Dong, Q., Brulc, J.M., Iovieno, A., Bates, B., Garoutte, A., Miller, D., Revanna, K.V., Gao, X., Antonopoulos, D.A., Slepak, V.Z., et al. (2011). Diversity of Bacteria at Healthy Human Conjunctiva. Invest. Ophthalmol. Vis. Sci. 52, 5408–6.

Dougherty, J.M., McCulley, J.P., Silvany, R.E., and Meyer, D.R. (1991). The role of tetracycline in chronic blepharitis. Inhibition of lipase production in staphylococci. Invest. Ophthalmol. Vis. Sci. 32, 2970–2975.

Dumbleton, K., Woods, C.A., Jones, L.W., and Fonn, D. (2013). The Impact of Contemporary Contact Lenses on Contact Lens Discontinuation. Eye Contact Lens 39, 93–98.

Edwards, A.M., Manetti, A.G.O., Falugi, F., Zingaretti, C., Capo, S., Buccato, S., Bensi, G., Telford, J.L., Margarit, I., and Grandi, G. (2008). Scavenger receptor gp340 aggregates group A *Streptococci* by binding pili. Molecular Microbiology 68, 1378–1394.

Efron, N. (2017). Contact lens wear is intrinsically inflammatory. Clinical and Experimental Optometry 100, 3–19.

ElShaer, A., Ghatora, B., Mustafa, S., and Alany, R.G. (2014). Contact lenses as drug reservoirs and delivery systems: the successes and challenges. Http://Dx.Doi.org/10.4155/Tde.14.73 5, 1085–1100.

Engel, M.A., Leffler, A., Niedermirtl, F., Babes, A., Zimmermann, K., Filipović, M.R., Izydorczyk, I., Eberhardt, M., Kichko, T.I., Mueller Tribbensee, S.M., et al. (2011). TRPA1 and Substance P Mediate Colitis in Mice. Gastroenterology 141, 1346–1358.

Epstein, S.S. (2013). Science Direct The phenomenon of microbial uncultivability. Current Opinion in Microbiology 16, 636–642.

Eriksson, C., Frängsmyr, L., Niemi, L.D., Loimaranta, V., Holmskov, U., Bergman, T., Leffler, H., Jenkinson, H.F., and Strömberg, N. (2007). Variant size- and glycoforms of the scavenger receptor cysteine-rich protein gp-340 with differential bacterial aggregation. Glycoconj J 24, 131–142.

Evans, D.J., and Fleiszig, S.M.J. (2013). Why Does the Healthy Cornea Resist *Pseudomonas aeruginosa* Infection? American Journal of Ophthalmology 155, 961–970.e962.

Fabriek, B.O., van Bruggen, R., Deng, D.M., Ligtenberg, A.J.M., Nazmi, K., Schornagel, K., Vloet, R.P.M., Dijkstra, C.D., and van den Berg, T.K. (2009). The macrophage scavenger receptor CD163 functions as an innate immune sensor for bacteria. Blood 113, 887–892.

Farandos, N.M., Yetisen, A.K., Monteiro, M.J., Lowe, C.R., and Yun, S.H. (2015). Contact Lens Sensors in Ocular Diagnostics. Advanced Healthcare Materials 4, 792–810.

Fleiszig, S.M.J., Kwong, M.S.F., and Evans, D.J. (2003). Modification of *Pseudomonas aeruginosa* Interactions with Corneal Epithelial Cells by Human Tear Fluid. Infection and Immunity 71, 3866–3874.

Fleiszig, S.M., Evans, D.J., Do, N., Vallas, V., Shin, S., and Mostov, K.E. (1997). Epithelial cell polarity affects susceptibility to *Pseudomonas aeruginosa* invasion and cytotoxicity. Infection and Immunity 65, 2861–2867.

Fleiszig, S.M., Zaidi, T.S., and Pier, G.B. (1995). *Pseudomonas aeruginosa* invasion of and multiplication within corneal epithelial cells *in vitro*. Infection and Immunity 63, 4072–4077.

Fleiszig, S.M., Zaidi, T.S., Ramphal, R., and Pier, G.B. (1994). Modulation of *Pseudomonas aeruginosa* adherence to the corneal surface by mucus. Infection and Immunity 62, 1799–1804.

Fleiszig, S.M.J., and Efron, N. (1992). Conjunctival Flora in Extended Wear of Rigid Gas Permeable Contact Lenses. Optometry and Vision Science 69, 354.

Forrester, J.V., Dick, A.D., McMenamin, P.G., Roberts, F., and Pearlman, E. (2015). The Eye: basic sciences in practice (Elsevier Health Sciences).

Fulcher, N.B., Holliday, P.M., Klem, E., Cann, M.J., and Wolfgang, M.C. (2010). The *Pseudomonas aeruginosa* Chp chemosensory system regulates intracellular cAMP levels by modulating adenylate cyclase activity. Molecular Microbiology 76, 889–904.

Gan, L., Fagerholm, P., and Kim, H.J. (1999). Effect of leukocytes on corneal cellular proliferation and wound healing. Invest. Ophthalmol. Vis. Sci. 40, 575–581.

Gao, N., Lee, P., and Yu, F.-S. (2016). Intraepithelial dendritic cells and sensory nerves are structurally associated and functional interdependent in the cornea. Sci. Rep. 6, 105.

Gao, Y., Min, K., Zhang, Y., Su, J., Greenwood, M., and Gronert, K. (2015). Female-Specific Downregulation of Tissue Polymorphonuclear Neutrophils Drives Impaired Regulatory T Cell and Amplified Effector T Cell Responses in Autoimmune Dry Eye Disease. J. Immunol. 195, 3086–3099.

Garrity-Ryan, L., Kazmierczak, B., Kowal, R., Comolli, J., Hauser, A., and Engel, J.N. (2000). The Arginine Finger Domain of ExoT Contributes to Actin Cytoskeleton Disruption and Inhibition of Internalization of *Pseudomonas aeruginosa* by Epithelial Cells and Macrophages. Infection and Immunity 68, 7100–7113.

Gillan, W.D.H. (2008). Conjunctival impression cytology: a review. African Vision and Eye Health 67, 136–141.

Graham, J.E., Moore, J.E., Jiru, X., Moore, J.E., Goodall, E.A., Dooley, J.S.G., Hayes, V.E.A., Dartt, D.A., Downes, C.S., and Moore, T.C.B. (2007). Ocular Pathogen or Commensal: A PCR-Based Study of Surface Bacterial Flora in Normal and Dry Eyes. Invest. Ophthalmol. Vis. Sci. 48, 5616–5618.

Green, M., Apel, A., and Stapleton, F. (2008). A Longitudinal Study of Trends in Keratitis in Australia. Cornea 27, 33–39.

Habib, N.E., El-Kasaby, H.T., Marczak, A.M., and Hsuan, J. (1993). Subconjunctival bupivacaine versus topical amethocaine in strabismus surgery. Eye 7, 757–759.

Hamrah, P., Liu, Y., Zhang, Q., and Dana, M.R. (2003). The Corneal Stroma Is Endowed with a Significant Number of Resident Dendritic Cells. Invest. Ophthalmol. Vis. Sci. 44, 581–589.

Hamrah, P., Zhang, Q., Liu, Y., and Dana, M.R. (2002). Novel Characterization of MHC Class II–Negative Population of Resident Corneal Langerhans Cell–Type Dendritic Cells. Invest. Ophthalmol. Vis. Sci. 43, 639–646.

Hartshorn, K.L., Ligtenberg, A., White, M.R., van Eijk, M., Hartshorn, M., Pemberton, L., Holmskov, U., and Crouch, E. (2006). Salivary agglutinin and lung scavenger receptor cysteine-rich glycoprotein 340 have broad anti-influenza activities and interactions with surfactant protein D that vary according to donor source and sialylation. Biochemical Journal 393, 545–553.

Hazlett, L.D., and Berk, R.S. (1984). Effect of C3 depletion on experimental *Pseudomonas aeruginosa* ocular infection: histopathological analysis. Infection and Immunity 43, 783–790.

Hazlett, L.D., Zucker, M., and Berk, R.S. (1992). Distribution and kinetics of the inflammatory cell response to ocular challenge with *Pseudomonas aeruginosa* in susceptible versus resistant mice. Ophthalmic Res 24, 32–39.

Hazlett, L.D., and Hendricks, R.L. (2010). Reviews for Immune Privilege in the Year 2010: Immune Privilege and Infection. Ocular Immunology and Inflammation 18, 237–243.

Hazlett, L.D. (2004). Corneal response to *Pseudomonas aeruginosa* infection. Progress in Retinal and Eye Research 23, 1–30.

Heimer, S.R., Evans, D.J., Mun, J.J., Stern, M.E., and Fleiszig, S.M.J. (2013). Surfactant Protein D Contributes to Ocular Defense against *Pseudomonas aeruginosa* in a Murine Model of Dry Eye Disease. PLoS ONE 8, e65797.

Hill, R.Z., Hoffman, B.U., Morita, T., Campos, S.M., Lumpkin, E.A., Brem, R.B., and Bautista, D.M. (2018). The signaling lipid sphingosine 1-phosphate regulates mechanical pain. eLife Sciences 7, 702.

Holly, F.J. (1973). Formation and rupture of the tear film. Experimental Eye Research 15, 515–525.

Holmskov, U., Lawson, P., Teisner, B., Tornoe, I., Willis, A.C., Morgan, C., Koch, C., and Reid, K.B. (1997). Isolation and characterization of a new member of the scavenger receptor superfamily, glycoprotein-340 (gp-340), as a lung surfactant protein-D binding molecule. J. Biol. Chem. 272, 13743–13749.

Holmskov, U., Mollenhauer, J., Madsen, J., Vitved, L., Grønlund, J., Tornøe, I., Kliem, A., Reid, K.B.M., Poustka, A., and Skjødt, K. (1999). Cloning of gp-340, a putative opsonin receptor for lung surfactant protein D. Proc Natl Acad Sci USA 96, 10794–10799.

Huang, L.C., Reins, R.Y., Gallo, R.L., and McDermott, A.M. (2007). Cathelicidin-Deficient ( Cnlp-/-) Mice Show Increased Susceptibility to *Pseudomonas aeruginosa* Keratitis. Invest. Ophthalmol. Vis. Sci. 48, 4498–11.

Huang, X., Du, W., McClellan, S.A., Barrett, R.P., and Hazlett, L.D. (2006). TLR4 Is Required for Host Resistance in *Pseudomonas aeruginosa* Keratitis. Invest. Ophthalmol. Vis. Sci. 47, 4910–4917.

Issa, S., Moran, A.P., Ustinov, S.N., Lin, J.H.-H., Ligtenberg, A.J., and Karlsson, N.G. (2010). O-linked oligosaccharides from salivary agglutinin: *Helicobacter pylori* binding sialyl-Lewis x and Lewis b are terminating moieties on hyperfucosylated oligo-N-acetyllactosamine. Glycobiology 20, 1046–1057.

Jacobs, M.A., Alwood, A., Thaipisuttikul, I., Spencer, D., Haugen, E., Ernst, S., Will, O., Kaul, R., Raymond, C., Levy, R., et al. (2003). Comprehensive transposon mutant library of *Pseudomonas aeruginosa*. Proc Natl Acad Sci USA 100, 14339–14344.

James, G. (2010). Universal Bacterial Identification by PCR and DNA Sequencing of 16S rRNA Gene. In PCR for Clinical Microbiology, (Dordrecht: Springer, Dordrecht), pp. 209–214.

Jinks, M.R., Fontenot, R.L., Wills, R.W., and Betbeze, C.M. (2018). The effects of subconjunctival bupivacaine, lidocaine, and mepivacaine on corneal sensitivity in healthy horses. Vet Ophthalmol 21, 498–506.

Jolly, A.L., Agarwal, P., Metruccio, M.M.E., Spiciarich, D.R., Evans, D.J., Bertozzi, C.R., and Fleiszig, S.M.J. (2017). Corneal surface glycosylation is modulated by IL-1R and *Pseudomonas aeruginosa* challenge but is insufficient for inhibiting bacterial binding. Faseb J. fj.201601198R.

Jones, T.C., Mohr, U., and Hunt, R.D., (2011). Monographs on Pathology of Laboratory Animals. 1–181

Jumblatt, M.M., Imbert, Y., Young, W.W., Foulks, G.N., Steele, P.S., and Demuth, D.R. (2006). Glycoprotein 340 in Normal Human Ocular Surface Tissues and Tear Film. Infection and Immunity 74, 4058–4063.

Karmakar, M., Sun, Y., Hise, A.G., Rietsch, A., and Pearlman, E. (2012). Cutting Edge: IL-1$\beta$ Processing during *Pseudomonas aeruginosa* Infection Is Mediated by Neutrophil Serine Proteases and Is Independent of NLRC4 and Caspase-1. The Journal of Immunology 189, 4231–4235.

Kautto, L., Nguyen-Khuong, T., Everest-Dass, A., Leong, A., Zhao, Z., Willcox, M.D.P., PACKER, N.H., and Peterson, R. (2016). Glycan involvement in the adhesion of *Pseudomonas aeruginosa* to tears. Experimental Eye Research 145, 278–288.

Khalil, M., Alliger, K., Weidinger, C., Yerinde, C., Wirtz, S., Becker, C., and Engel, M.A. (2018). Functional Role of Transient Receptor Potential Channels in Immune Cells and Epithelia. Front Immunol 9, 174.

Kinoshita, S., Adachi, W., Sotozono, C., Nishida, K., Yokoi, N., Quantock, A.J., and Okubo, K. (2001). Characteristics of the human ocular surface epithelium. Progress in Retinal and Eye Research 20, 639–673.

Knop, E., and Knop, N. (2007). Anatomy and immunology of the ocular surface. Chem Immunol Allergy 92, 36–49.

Kolaczkowska, E., and Kubes, P. (2013). Neutrophil recruitment and function in health and inflammation. Nature Reviews Immunology 13, 159–175.

Kroken, A.R., Chen, C.K., Evans, D.J., Yahr, T.L., Fleiszig, S.M.J., and Whiteley, M. (2018). The Impact of ExoS on *Pseudomonas aeruginosa* Internalization by Epithelial Cells Is Independent of

fleQ and Correlates with Bistability of Type Three Secretion System Gene Expression. mBio 9, e00668–18.

Kugadas, A., Christiansen, S.H., Sankaranarayanan, S., Surana, N.K., Gauguet, S., Kunz, R., Fichorova, R., Vorup-Jensen, T., and Gadjeva, M. (2016). Impact of Microbiota on Resistance to Ocular *Pseudomonas aeruginosa*-Induced Keratitis. PLoS Pathog 12, e1005855–24.

Kukita, K., Kawada-Matsuo, M., Oho, T., Nagatomo, M., Oogai, Y., Hashimoto, M., Suda, Y., Tanaka, T., Komatsuzawa, H., and Bäumler, A.J. (2013). *Staphylococcus aureus* SasA Is Responsible for Binding to the Salivary Agglutinin gp340, Derived from Human Saliva. Infection and Immunity 81, 1870–1879.

Kumar, A., and Yu, F.-S.X. (2006). Toll-like receptors and corneal innate immunity. Curr. Mol. Med. 6, 327–337.

Kwong, M.S.F., Evans, D.J., Ni, M., Cowell, B.A., and Fleiszig, S.M.J. (2007). Human Tear Fluid Protects against*Pseudomonas aeruginosa* Keratitis in a Murine Experimental Model. Infection and Immunity 75, 2325–2332.

Laura Oliveira-soto, N.E. (2001). Morphology of Corneal Nerves Using Confocal Microscopy. Cornea 20, 374–384.

Lawin-Brüssel, C.A., Refojo, M.F., Leong, F.L., Hanninen, L., and Kenyon, K.R. (1993). Effect of *Pseudomonas aeruginosa* concentration in experimental contact lens-related microbial keratitis. Cornea 12, 10–18.

Lee, E.J., Cowell, B.A., Evans, D.J., and Fleiszig, S.M.J. (2003). Contribution of ExsA–Regulated Factors to Corneal Infection by Cytotoxic and Invasive *Pseudomonas aeruginosa* in a Murine Scarification Model. Invest. Ophthalmol. Vis. Sci. 44, 3892–3898.

Lee, H.S., Hattori, T., Park, E.Y., Stevenson, W., Chauhan, S.K., and Dana, R. (2012). Expression of Toll-Like Receptor 4 Contributes to Corneal Inflammation in Experimental Dry Eye Disease. Invest. Ophthalmol. Vis. Sci. 53, 5632–5640.

Leighton, T.L., Buensuceso, R.N.C., Howell, P.L., and Burrows, L.L. (2015). Biogenesis of *Pseudomonas aeruginosa* type IV pili and regulation of their function. Environmental Microbiology 17, 4148–4163.

Li, J., Metruccio, M.M.E., Evans, D.J., and Fleiszig, S.M.J. (2017). Mucosal fluid glycoprotein DMBT1 suppresses twitching motility and virulence of the opportunistic pathogen *Pseudomonas aeruginosa*. PLoS Pathog 13, e1006392.

Li, J.-H., Huang, W., Lin, P., Wu, B., Fu, Z.-G., Shen, H.-M., Jing, L., Liu, Z.-Y., Zhou, Y., Meng, Y., et al. (2016). N-linked glycosylation at Asn152 on CD147 affects protein folding and stability: promoting tumour metastasis in hepatocellular carcinoma. Sci. Rep. 6, 35210.

Li, Z., Burns, A.R., and Smith, C.W. (2006). Two Waves of Neutrophil Emigration in Response to Corneal Epithelial Abrasion: Distinct Adhesion Molecule Requirements. Invest. Ophthalmol. Vis. Sci. 47, 1947–1955.

Ligtenberg, A.J.M., Karlsson, N.G., and Veerman, E.C.I. (2010). Deleted in Malignant Brain Tumors-1 Protein (DMBT1): A Pattern Recognition Receptor with Multiple Binding Sites. International Journal of Molecular Sciences 2010, Vol. 11, Pages 5212-5233 11, 5212–5233.

Ligtenberg, A.J.M., Veerman, E.C.I., Nieuw Amerongen, A.V., and Mollenhauer, J. Salivary agglutinin/glycoprotein-340/DMBT1: a single molecule with variable composition and with

different functions in infection, inflammation and cancer. Biological Chemistry 388, 35.

Lim, C.H.L., Carnt, N.A., Farook, M., Lam, J., Tan, D.T., Mehta, J.S., and Stapleton, F. (2016). Risk factors for contact lens-related microbial keratitis in Singapore. Eye 30, 447–455.

Lin, C.C., Prajna, L., Srinivasan, M., Prajna, N.V., McLeod, S.D., Acharya, N.R., Lietman, T.M., and Porco, T.C. (2012). Seasonal trends of microbial keratitis in south India. Cornea 31, 1123–1127.

Linden, S.K., Sutton, P., Karlsson, N.G., Korolik, V., and McGuckin, M.A. (2008). Mucins in the mucosal barrier to infection. Mucosal Immunol 1, 183–197.

Liu, B., Escalera, J., Balakrishna, S., Fan, L., Caceres, A.I., Robinson, E., Sui, A., McKay, M.C., McAlexander, M.A., Herrick, C.A., et al. (2013). TRPA1 controls inflammation and pruritogen responses in allergic contact dermatitis. The FASEB Journal 27, 3549–3563.

Loimaranta, V., Jakubovics, N.S., Hytönen, J., Finne, J., Jenkinson, H.F., and Strömberg, N. (2005). Fluid- or Surface-Phase Human Salivary Scavenger Protein gp340 Exposes Different Bacterial Recognition Properties. Infection and Immunity 73, 2245–2252.

Madsen, J., Mollenhauer, J., and Holmskov, U. (2010). Review: Gp-340/DMBT1 in mucosal innate immunity. Innate Immun 16, 160–167.

Maltseva, I.A., Fleiszig, S.M.J., Evans, D.J., Kerr, S., Sidhu, S.S., McNamara, N.A., and Basbaum, C. (2007). Exposure of human corneal epithelial cells to contact lenses in vitro suppresses the upregulation of human $\beta$-defensin-2 in response to antigens of *Pseudomonas aeruginosa*. Experimental Eye Research 85, 142–153.

Mantelli, F., and Argüeso, P. (2008). Functions of ocular surface mucins in health and disease. Current Opinion in Allergy and Clinical Immunology 8, 477–483.

Mark Welch, J.L., Rossetti, B.J., Rieken, C.W., Dewhirst, F.E., and Borisy, G.G. (2016). Biogeography of a human oral microbiome at the micron scale. Proc Natl Acad Sci USA 113, E791–E800.

Martin, M.U., and Wesche, H. (2002). Summary and comparison of the signaling mechanisms of the Toll/interleukin-1 receptor family. Biochimica Et Biophysica Acta (BBA) - Molecular Cell Research 1592, 265–280.

Mattick, J.S. (2003). Type IV Pili and Twitching Motility. Http://Dx.Doi.org/10.1146/Annurev.Micro.56.012302.160938 56, 289–314.

McClellan, K.A. (1997). Mucosal defense of the outer eye. Surv Ophthalmol 42, 233–246.
McDermott, A.M. (2009). The Role of Antimicrobial Peptides at the Ocular Surface. Ophthalmic Res 41, 60–75.

McDermott, A.M., Redfern, R.L., Zhang, B., Pei, Y., Huang, L., and Proske, R.J. (2003). Defensin Expression by the Cornea: Multiple Signalling Pathways Mediate IL-1$\beta$ Stimulation of hBD-2 Expression by Human Corneal Epithelial Cells. Invest. Ophthalmol. Vis. Sci. 44, 1859–1865.

McNamara, N.A., VAN, R., Tuchin, O.S., and Fleiszig, S.M.J. (1999). Ocular Surface Epithelia Express mRNA for Human Beta Defensin-2. Experimental Eye Research 69, 483–490.

MD, D.W.D., and MD, T.K. (2011). Anatomy and physiology of the cornea. Journal of Cataract and Refractive Surgery 37, 588–598.

Medzhitov, R. (2008). Origin and physiological roles of inflammation. Nature 454, 428–435.

Meseguer, V., Alpizar, Y.A., Luis, E., Tajada, S., Denlinger, B., Fajardo, O., Manenschijn, J.-A., Fernández-Peña, C., Talavera, A., Kichko, T., et al. (2014). TRPA1 channels mediate acute neurogenic inflammation and pain produced by bacterial endotoxins. Nat Commun 5, 3125.

Metruccio, M.M.E., Evans, D.J., Gabriel, M.M., Kadurugamuwa, J.L., and Fleiszig, S.M.J. (2016). *Pseudomonas aeruginosa* Outer Membrane Vesicles Triggered by Human Mucosal Fluid and Lysozyme Can Prime Host Tissue Surfaces for Bacterial Adhesion. Front. Microbiol. 7, 871–19.

Metruccio, M.M.E., Tam, C., Evans, D.J., Xie, A.L., Stern, M.E., and Fleiszig, S.M.J. (2017). Contributions of MyD88-dependent receptors and CD11c-positive cells to corneal epithelial barrier function against *Pseudomonas aeruginosa*. Sci. Rep. 7, 13829.

Metruccio, M.M.E., Wan, S.J., Horneman, H., Kroken, A.R., Sullivan, A.B., Truong, T.N., Mun, J.J., Tam, C.K.P., Frith, R., Welsh, L., et al. (2018). A novel murine model for contact lens wear reveals clandestine IL-1R dependent corneal parainflammation and susceptibility to microbial keratitis upon inoculation with *Pseudomonas aeruginosa*. The Ocular Surface.

Mochizuki, H., Fukui, M., Hatou, S., Yamada, M., and Tsubota, K. (2010). Evaluation of ocular surface glycocalyx using lectin-conjugated fluorescein. Clinical Ophthalmology (Auckland, N.Z.) 4, 925–930.

Moulton, R.C., and Montie, T.C. (1979). Chemotaxis by *Pseudomonas aeruginosa*. Journal of Bacteriology 137, 274–280.

Mun, J.J., Tam, C., Kowbel, D., Hawgood, S., Barnett, M.J., Evans, D.J., and Fleiszig, S.M.J. (2009). Clearance of *Pseudomonas aeruginosa* from a Healthy Ocular Surface Involves Surfactant Protein D and Is Compromised by Bacterial Elastase in a Murine Null-Infection Model. Infection and Immunity 77, 2392–2398.

Mun, J.J., Tam, C., Evans, D.J., and Fleiszig, S.M.J. (2011). Modulation of epithelial immunity by mucosal fluid. Sci. Rep. 1, 1–7.

Muzumdar, M.D., Tasic, B., Miyamichi, K., Li, L., and Luo, L. (2007). A global double-fluorescent Cre reporter mouse. Genesis 45, 593–605.

Narayanan, S., Miller, W.L., and McDermott, A.M. (2003). Expression of human beta-defensins in conjunctival epithelium: relevance to dry eye disease. Invest. Ophthalmol. Vis. Sci. 44, 3795–3801.

Nichols, J.J., Willcox, M.D.P., Bron, A.J., Belmonte, C., Ciolino, J.B., Craig, J.P., Dogru, M., Foulks, G.N., Jones, L., Nelson, J.D., et al. (2013). The TFOS International Workshop on Contact Lens Discomfort: Executive Summary. Invest. Ophthalmol. Vis. Sci. 54, TFOS7–TFOS13.

Oho, T., Yu, H., Yamashita, Y., and Koga, T. (1998). Binding of Salivary Glycoprotein-Secretory Immunoglobulin A Complex to the Surface Protein Antigen of *Streptococcus mutans*. Infection and Immunity 66, 115–121.

Okada, Y., Reinach, P.S., Shirai, K., Kitano-Izutani, A., Miyajima, M., Yamanaka, O., Sumioka, T., and Saika, S. (2015). Transient Receptor Potential Channels and Corneal Stromal Inflammation. Cornea 34 Suppl 11, S136–S141.

Park, J., Kim, J., Kim, S.-Y., Cheong, W.H., Jang, J., Park, Y.-G., Na, K., Kim, Y.-T., Heo, J.H., Lee, C.Y., et al. (2018). Soft, smart contact lenses with integrations of wireless circuits, glucose sensors, and displays. Sci Adv 4, eaap9841.

Pearlman, E., Johnson, A., Adhikary, G., Sun, Y., Chinnery, H.R., Fox, T., Kester, M., and McMenamin, P.G. (2008). Toll-like Receptors at the Ocular Surface. The Ocular Surface 6, 108–116.

Pearlman, E., Sun, Y., Roy, S., Karmakar, M., Hise, A.G., Szczotka-Flynn, L., Ghannoum, M., Chinnery, H.R., McMenamin, P.G., and Rietsch, A. (2013). Host Defense at the Ocular Surface. International Reviews of Immunology 32, 4–18.

Pecze, L., Pelsőczi, P., Kecskés, M., Winter, Z., Papp, A., Kaszás, K., Letoha, T., Vizler, C., and Oláh, Z. (2009). Resiniferatoxin Mediated Ablation of TRPV1+ Neurons Removes TRPA1 as Well. Canadian Journal of Neurological Sciences 36, 234–241.

Persat, A., Inclan, Y.F., Engel, J.N., Stone, H.A., and Gitai, Z. (2015). Type IV pili mechanochemically regulate virulence factors in *Pseudomonas aeruginosa*. Proc Natl Acad Sci USA 112, 201502025–201507568.

Petrescu, A.-J., Milac, A.-L., Petrescu, S.M., Dwek, R.A., and Wormald, M.R. (2004). Statistical analysis of the protein environment of N-glycosylation sites: implications for occupancy, structure, and folding. Glycobiology 14, 103–114.

Phan, C.-M., Subbaraman, L., and Jones, L.W. (2016). The Use of Contact Lenses as Biosensors. Optometry and Vision Science 93, 419–425.

Pinho-Ribeiro, F.A., Baddal, B., Haarsma, R., O'Seaghdha, M., Yang, N.J., Blake, K.J., Portley, M., Verri, W.A., Dale, J.B., Wessels, M.R., et al. (2018). Blocking Neuronal Signaling to Immune Cells Treats *Streptococcal* Invasive Infection. Cell.

Pinho-Ribeiro, F.A., Verri, W.A., and Chiu, I.M. (2017). Nociceptor Sensory Neuron-Immune Interactions in Pain and Inflammation. Trends Immunol. 38, 5–19.

Polley, S., Louzada, S., Forni, D., Sironi, M., Balaskas, T., Hains, D.S., Yang, F., and Hollox, E.J. (2015). Evolution of the rapidly mutating human salivary agglutinin gene (DMBT1) and population subsistence strategy. Proc Natl Acad Sci USA 112, 5105–5110.

Poretsky, R., Rodriguez-R, L.M., Luo, C., Tsementzi, D., and Konstantinidis, K.T. (2014). Strengths and Limitations of 16S rRNA Gene Amplicon Sequencing in Revealing Temporal Microbial Community Dynamics. PLoS ONE 9, e93827–12.

Prakobphol, A., Xu, F., Hoang, V.M., Larsson, T., Bergstrom, J., Johansson, I., Frängsmyr, L., Holmskov, U., Leffler, H., Nilsson, C., et al. (2000). Salivary agglutinin, which binds *Streptococcus mutans* and *Helicobacter pylori*, is the lung scavenger receptor cysteine-rich protein gp-340. J. Biol. Chem. 275, 39860–39866.

Rabolli, V., Badissi, A.A., Devosse, R., Uwambayinema, F., Yakoub, Y., Palmai-Pallag, M., Lebrun, A., De Gussem, V., COUILLIN, I., Ryffel, B., et al. (2014). The alarmin IL-1$\alpha$ is a master cytokine in acute lung inflammation induced by silica micro- and nanoparticles. Particle and Fibre Toxicology 2014 11:1 11, 69.

Rea, I.M., Gibson, D.S., McGilligan, V., McNerlan, S.E., Alexander, H.D., and Ross, O.A. (2018). Age and Age-Related Diseases: Role of Inflammation Triggers and Cytokines. Front Immunol 9, 1111e.

Redfern, R.L., Reins, R.Y., and McDermott, A.M. (2011). Toll-like receptor activation modulates antimicrobial peptide expression by ocular surface cells. Experimental Eye Research.

Redfern, R.L., and McDermott, A.M. (2010). Toll-like receptors in ocular surface disease. Experimental Eye Research 90, 679–687.

Reinach, P.S., Mergler, S., Okada, Y., and Saika, S. (2015). Ocular transient receptor potential channel function in health and disease. BMC Ophthalmol 15 Suppl 1, 153.

Schaumberg, D.A., Uchino, M., Christen, W.G., Semba, R.D., Buring, J.E., and Li, J.Z. (2013). Patient Reported Differences in Dry Eye Disease between Men and Women: Impact, Management, and Patient Satisfaction. PLoS ONE 8, e76121.

Schein, O.D., Buehler, P.O., Stamler, J.F., Verdier, D.D., and Katz, J. (1994). The Impact of Overnight Wear on the Risk of Contact Lens—Associated Ulcerative Keratitis. Arch Ophthalmol 112, 186–190.

Schulz, B.L., Oxley, D., Packer, N.H., and Karlsson, N.G. (2002). Identification of two highly sialylated human tear-fluid DMBT1 isoforms: the major high-molecular-mass glycoproteins in human tears. Biochemical Journal 366, 511–520.

Selinger, D.S., Selinger, R.C., and Reed, W.P. (1979). Resistance to infection of the external eye: the role of tears. Surv Ophthalmol 24, 33–38.

Sender, R., Fuchs, S., and Milo, R. (2016). Revised Estimates for the Number of Human and Bacteria Cells in the Body. PLoS Biol. 14, e1002533.

Seyed-Razavi, Y., Hickey, M.J., cell, L.K.I.A., 2013 Membrane nanotubes in myeloid cells in the adult mouse cornea represent a novel mode of immune cell interaction. Nature.com.

Shaheen, B.S., Bakir, M., and Jain, S. (2014). Corneal nerves in health and disease. Surv Ophthalmol 59, 263–285.

Shieh, P., Siegrist, M.S., Cullen, A.J., and Bertozzi, C.R. (2014). Imaging bacterial peptidoglycan with near-infrared fluorogenic azide probes. Proc Natl Acad Sci USA 111, 5456–5461.

Shirai, K., Okada, Y., Cheon, D.-J., Miyajima, M., Behringer, R.R., Yamanaka, O., and Saika, S. (2014). Effects of the Loss of Conjunctival Muc16 on Corneal Epithelium and Stroma in Mice. Invest. Ophthalmol. Vis. Sci. 55, 3626–3637.

Siegrist, M.S., Whiteside, S., Jewett, J.C., Aditham, A., Cava, F., and Bertozzi, C.R. (2013). d-Amino Acid Chemical Reporters Reveal Peptidoglycan Dynamics of an Intracellular Pathogen. ACS Chem. Biol. 8, 500–505.

Sindt, C.W., Grout, T.K., Critser, D.B., Kern, J.R., and Meadows, D.L. (2012). Dendritic immune cell densities in the central cornea associated with soft contact lens types and lens care solution types: a pilot study. Clinical Ophthalmology (Auckland, N.Z.) 6, 511–519.

Singer, J.T., Phennicie, R.T., Sullivan, M.J., Porter, L.A., Shaffer, V.J., and Kim, C.H. (2010). Broad-host-range plasmids for red fluorescent protein labeling of gram-negative bacteria for use in the zebrafish model system. Applied and Environmental Microbiology 76, 3467–3474.

Somabhai Katara, R., Dhanjibhai Patel, N., and Sinha, M. (2013). A clinical microbiological study of corneal ulcer patients at western Gujarat, India. Acta Med Iran 51, 399–403.

Sorbara, L., Jones, L., and Williams-Lyn, D. (2009). Contact lens induced papillary conjunctivitis with silicone hydrogel lenses. Contact Lens and Anterior Eye 32, 93–96.

St Leger, A.J., Desai, J.V., Drummond, R.A., Kugadas, A., Almaghrabi, F., Silver, P., Raychaudhuri, K., Gadjeva, M., Iwakura, Y., Lionakis, M.S., et al. (2017). An Ocular Commensal Protects against Corneal Infection by Driving an Interleukin-17 Response from Mucosal $\delta$ $\gamma$ T Cells. Immunity 47, 148–158.e5.

Stapleton, F., and Carnt, N. (2011). Contact lens-related microbial keratitis: how have epidemiology and genetics helped us with pathogenesis and prophylaxis. Eye 26, 185–193.

Stapleton, F., Keay, L., Edwards, K., and Holden, B. (2013). The Epidemiology of Microbial Keratitis With Silicone Hydrogel Contact Lenses. Eye Contact Lens 39, 79–84.

Stapleton, F., Keay, L., Edwards, K., Naduvilath, T., Dart, J.K.G., Brian, G., and Holden, B.A. (2008). The incidence of contact lens-related microbial keratitis in Australia. Ophthalmology 115, 1655–1662.

Stapleton, F., Keay, L., Jalbert, I., and Cole, N. (2007). The epidemiology of contact lens related infiltrates. Optometry and Vision Science 84, 257–272.

Sullivan, A.B., Tam, K.P.C., Metruccio, M.M.E., Evans, D.J., and Fleiszig, S.M.J. (2015). The Importance of the *Pseudomonas aeruginosa* Type III Secretion System in Epithelium Traversal Depends upon Conditions of Host Susceptibility. Infection and Immunity 83, 1629–1640.

Sun, Y., Karmakar, M., Roy, S., Ramadan, R.T., Williams, S.R., Howell, S., Shive, C.L., Han, Y., Stopford, C.M., Rietsch, A., et al. (2010). TLR4 and TLR5 on Corneal Macrophages Regulate *Pseudomonas aeruginosa* Keratitis by Signaling through MyD88-Dependent and -Independent Pathways. The Journal of Immunology 185, 4272–4283.

Sun, Y., Karmakar, M., Taylor, P.R., Rietsch, A., and Pearlman, E. (2012). ExoS and ExoT ADP ribosyltransferase activities mediate *Pseudomonas aeruginosa* keratitis by promoting neutrophil apoptosis and bacterial survival. J. Immunol. 188, 1884–1895.

Szliter, E.A., Morris, C.A., Carney, F., Gabriel, M.M., and Hazlett, L.D. (2002). Development of a New Extended-Wear Contact Lens Model in the Rat. Eye Contact Lens 28, 119.

Takenouchi, T., Tsukimoto, M., Hashimoto, M., Inflammasome, H.K., 2014 Inflammasome activation by danger signals: extracellular ATP and pH. Degruyter.com.

Tam, C., Lewis, S.E., Li, W.Y., Lee, E., Evans, D.J., and Fleiszig, S.M.J. (2007). Mutation of the phospholipase catalytic domain of the *Pseudomonas aeruginosa* cytotoxin ExoU abolishes colonization promoting activity and reduces corneal disease severity. Experimental Eye Research 85, 799–805.

Tam, C., LeDue, J., Mun, J.J., Herzmark, P., Robey, E.A., Evans, D.J., and Fleiszig, S.M.J. (2011). 3D Quantitative Imaging of Unprocessed Live Tissue Reveals Epithelial Defense against Bacterial Adhesion and Subsequent Traversal Requires MyD88. PLoS ONE 6, e24008–e24012.

Tam, C., Mun, J.J., Evans, D.J., and Fleiszig, S.M.J. (2010). The Impact of Inoculation Parameters on the Pathogenesis of Contact Lens–Related Infectious Keratitis. Invest. Ophthalmol. Vis. Sci. 51, 3100–3107.

Tam, C., Mun, J.J., Evans, D.J., and Fleiszig, S.M.J. (2012). Cytokeratins mediate epithelial innate defense through their antimicrobial properties. J. Clin. Invest. 122, 3665–3677.

Tian, X., Sun, H., Casbon, A.-J., Lim, E., Francis, K.P., Hellman, J., and Prakash, A. (2017). NLRP3 Inflammasome Mediates Dormant Neutrophil Recruitment following Sterile Lung Injury and Protects against Subsequent Bacterial Pneumonia in Mice. Front Immunol 8, 1391.

Tsubota, K., Tseng, S.C.G., and Nordlund, M.L. (2002). Anatomy and Physiology of the Ocular Surface. In Ocular Surface Disease Medical and Surgical Management, (New York: Springer, New York, NY), pp. 3–15.

Tsuda, Y., Takahashi, H., Kobayashi, M., Hanafusa, T., Herndon, D.N., and Suzuki, F. (2004). Three different neutrophil subsets exhibited in mice with different susceptibilities to infection by methicillin-resistant *Staphylococcus aureus*. Immunity 21, 215–226.

Turnbaugh, P.J., Ley, R.E., Hamady, M., Fraser-Liggett, C.M., Knight, R., and Gordon, J.I. (2007). The Human Microbiome Project. Nature 449, 804–810.

Turnbull, L., and Whitchurch, C.B. (2014). Motility assay: twitching motility. Methods Mol. Biol. 1149, 73–86.

Vaishnava, S., Yamamoto, M., Severson, K.M., Ruhn, K.A., Yu, X., Koren, O., Ley, R., Wakeland, E.K., and Hooper, L.V. (2011). The antibacterial lectin RegIIIgamma promotes the spatial segregation of microbiota and host in the intestine. Science 334, 255–258.

Vareechon, C., Zmina, S.E., Karmakar, M., Pearlman, E., and Rietsch, A. (2017). *Pseudomonas aeruginosa* Effector ExoS Inhibits ROS Production in Human Neutrophils. Cell Host and Microbe 21, 611–618.e615.

Veres, T.Z., Zoltán Veres, T., Voedisch, S., Spies, E., Tschernig, T., and Braun, A. (2011). Spatiotemporal and functional behavior of airway dendritic cells visualized by two-photon microscopy. Am. J. Pathol. 179, 603–609.

Vijay, A.K., Sankaridurg, P., Zhu, H., and Willcox, M.D.P. (2009). Guinea Pig Models of Acute Keratitis Responses. Cornea 28, 1153–1159.

Wan, S.J., Sullivan, A.B., Shieh, P., Metruccio, M.M.E., Evans, D.J., Bertozzi, C.R., and Fleiszig, S.M.J. (2018). IL-1R and MyD88 Contribute to the Absence of a Bacterial Microbiome on the Healthy Murine Cornea. Front. Microbiol. 9, 1368.

Wei, C., Zhu, M., Petroll, W.M., and Robertson, D.M. (2014). *Pseudomonas aeruginosa* Infectious Keratitis in a High Oxygen Transmissible Rigid Contact Lens Rabbit Model. Invest. Ophthalmol. Vis. Sci. 55, 5890–5899.

Willcox, M.D.P., and Holden, B.A. (2001). Contact Lens Related Corneal Infections. Bioscience Reports 21, 445–461.

Willcox, M.D.P. (2007). *Pseudomonas aeruginosa* Infection and Inflammation During Contact Lens Wear: A Review. Optometry and Vision Science 84, 273–278.

Willcox, M.D.P. (2013a). Characterization of the normal microbiota of the ocular surface. Experimental Eye Research 117, 99–105.

Willcox, M.D.P. (2013b). Microbial Adhesion to Silicone Hydrogel Lenses: A Review. Eye Contact Lens 39, 61–65.

Wu, M., Peng, A., Sun, M., Deng, Q., Hazlett, L.D., Yuan, J., Liu, X., Gao, Q., Feng, L., He, J., et al. (2011). TREM-1 Amplifies Corneal Inflammation after *Pseudomonas aeruginosa* Infection by Modulating Toll-Like Receptor Signaling and Th1/Th2-Type Immune Responses. Infection and Immunity 79, 2709–2716.

Wu, P.-C., Huang, H.-M., Yu, H.-J., Fang, P.-C., and Chen, C.-T. (2016). Epidemiology of Myopia. The Asia-Pacific Journal of Ophthalmology 5, 386–393.

Wu, Y.T.-Y., Willcox, M., Zhu, H., and Stapleton, F. (2015). Contact lens hygiene compliance and lens case contamination: A review. Contact Lens and Anterior Eye 38, 307–316.

Wu, Z., Lee, S., Abrams, W., Weissman, D., and Malamud, D. (2006). The N-Terminal SRCR-SID Domain of gp-340 Interacts with HIV Type 1 gp120 Sequences and Inhibits Viral Infection. Https://Home.Liebertpub.com/Aid 22, 508–515.

Xu, H., Chen, M., and Forrester, J.V. (2009). Para-inflammation in the aging retina. Progress in Retinal and Eye Research 28, 348–368.

Yi, X., Wang, Y., and Yu, F.S. (2000). Corneal epithelial tight junctions and their response to lipopolysaccharide challenge. Invest. Ophthalmol. Vis. Sci. 41, 4093–4100.

Zhang, F., Yang, H., Wang, Z., Mergler, S., Liu, H., Kawakita, T., Tachado, S.D., Pan, Z., Capó-Aponte, J.E., Pleyer, U., et al. (2007). Transient receptor potential vanilloid 1 activation induces inflammatory cytokine release in corneal epithelium through MAPK signaling. J. Cell. Physiol. 213, 730–739.

Zhang, Y., Gabriel, M.M., Mowrey-McKee, M.F., Barrett, R.P., McClellan, S., and Hazlett, L.D. (2008). Rat Silicone Hydrogel Contact Lens Model: Effects of High vs. Low Dk Lens Wear. Eye Contact Lens 34, 306–311.

Zolfaghar, I., Evans, D.J., and Fleiszig, S.M.J. (2003). Twitching Motility Contributes to the Role of Pili in Corneal Infection Caused by *Pseudomonas aeruginosa*. Infection and Immunity 71, 5389–5393.

Zolfaghar, I., Evans, D.J., Ronaghi, R., and Fleiszig, S.M.J. (2006). Type III Secretion-Dependent Modulation of Innate Immunity as One of Multiple Factors Regulated by *Pseudomonas aeruginosa* RetS. Infection and Immunity 74, 3880–3889.